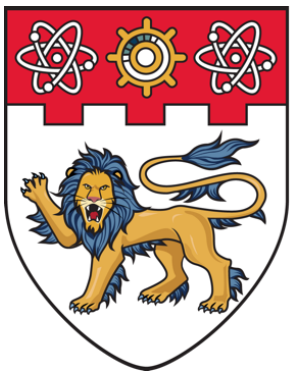

NANYANG TECHNOLOGICAL UNIVERSITY
SINGAPORE

Age-dependent transcriptional and epigenetic alterations in mouse hepatocytes

ANKUR SHARMA

SCHOOL OF BIOLOGICAL SCIENCES

2021

Age-dependent transcriptional and epigenetic alterations in mouse hepatocytes

ANKUR SHARMA

SCHOOL OF BIOLOGICAL SCIENCES

A thesis submitted to the Nanyang Technological University in partial fulfilment of the requirement for the degree of Doctor of Philosophy

2021

Statement of Originality

I hereby certify that the work embodied in this thesis is the result of original research done by me except where otherwise stated in this thesis. The thesis work has not been submitted for a degree or professional qualification to any other university or institution. I declare that this thesis is written by myself and is free of plagiarism and of sufficient grammatical clarity to be examined. I confirm that the investigations were conducted in accord with the ethics policies and integrity standards of Nanyang Technological University and that the research data are presented honestly and without prejudice.

27th Dec 2021

. . . . . .

Date

. . . . . .

Ankur Sharma

Supervisor Declaration Statement

I have reviewed the content and presentation style of this thesis and declare it of sufficient grammatical clarity to be examined. To the best of my knowledge, the thesis is free of plagiarism and the research and writing are those of the candidate's except as acknowledged in the Author Attribution Statement. I confirm that the investigations were conducted in accord with the ethics policies and integrity standards of Nanyang Technological University and that the research data are presented honestly and without prejudice.

27th Dec 2021

. . . . . .
Date

Amartya Sanyal

. . . . . .
Amartya Sanyal

Authorship Attribution Statement

This thesis contains material that was presented in a poster in the following conference in which I am listed as the first author.

Part of chapter 2 was presented in a poster titled “Significance of hepatocyte polyploidization in liver physiology and pathology” in Cell symposia “Transcriptional regulation in evolution, development and disease” at Chicago, USA in Oct 2019. Authors of this poster are Ankur Sharma, Agnes Ong, Torsten Wuestefeld and Amartya Sanyal.

The contributions of the co-authors are as follows:

- Dr. Amartya Sanyal and Dr. Torsten Wuestefeld supervised the study, guided the analysis and interpretation of results, and revised the poster.
- Agnes Ong and I carried out mouse liver perfusion
- I sorted the cells, extracted RNA and send samples for sequencing
- I analyzed the FACS profiles, RNA-seq data, and public datasets, interpreted the results and prepared the poster.

27th Dec 2021

. . . . . .

Date

. . . . . .

Ankur Sharma

Acknowledgements

I would like to express my gratitude to Dr Amartya Sanyal and Dr Torsten Wuestefeld for their patient guidance throughout my candidature. I am thankful for the opportunity to work on this project, and the time spent at the labs in NTU and GIS. I believe the time and the process has forged me into a better person and has equipped me with the skills to be a better scientist.

I would like to thank my current and past thesis advisory committee members- Dr Lu Lei (SBS), Dr Torsten Wuestefeld (GIS), and Dr Katsutomo Okamura (TLL). I am grateful to Dr Koh Cheng Gee for ensuring I finish my PhD after some dark phases in life. I am thankful to May in general office for helping me in several ways from claiming part-time salary to giving valuable suggestions. I would also like to thank NTU for the scholarship that supported me and providing me with the resources to complete my PhD.

I am thankful to my past lab members, Aravinda, Vijay, Rawaidah, Jacklyn, Jonavan, and other FYPs to their efforts in ensuring a healthy work environment in lab. I am also thankful to my lab members in GIS: Agnes, Jonathan, Vika, Anna and others for helping me in various ways. Analysing data without a proper training was most challenging task for me during all these years and therefore I am extremely grateful to Costerwell and Yao for uncountable data analysis troubleshooting even beyond office hours. I am grateful to many scientists, researchers, and acquaintances who took time and efforts to reply to my bioinformatics queries at various online platforms.

I am lucky to have a support system of my friends- Suki, Sushant, Anshuman, and Abhinay. My PhD life would have been miserable without you people. Thank you for providing me with all memories and a life outside lab all these years.

My biggest pillar has been my family. We faced many difficulties over last few years and yet we supported each other to get through each challenge. It was my father’s wish that I persue a doctorate degree and the biggest reason that I persisted despite so many setbacks. I hope I did some justice to his wish.

This thesis is dedicated to my late father Mr.

Bhupendra Sharma.

He was and will continue to be my greatest

motivation.

"*Your memory is my keepsake with which I'll never part, God has you in his arms,*

and I have you in my heart"

Contents

Abbreviations 8

Abstract 10

Short Abstract 13

Chapter 1: Introduction 14

1.1 Physiological aging 14

1.2 Theories of aging 14

1.3 Hallmarks of aging 17

1.3.1 Genomic instability 17
1.3.2 Telomere attrition 18
1.3.3 Epigenetic Alterations 18
1.3.4 Loss of proteostasis 30
1.3.5 Mitochondrial dysfunction 31
1.3.6 Cellular senescence 31
1.3.7 Deregulated nutrient-sensing 32
1.3.8 Stem cell exhaustion 35
1.3.9 Altered intercellular communication 36

1.4 The obstacles of current aging research 37

1.5 Liver as an aging model 39

1.6 Effect of aging on liver 40

1.6.1 Hepatic stellate cells (HepSCs) 41
1.6.2 Liver Endothelial Sinusoidal Cells (LESCs) 41
1.6.3 Küpffer cells 42
1.6.4 Hepatocytes 42

1.7 Polyploidy in liver 44

1.8 Scope of this thesis 45

Chapter 2 Liver polyploidy 47

2.1 Introduction to polyploidy 47

2.2 Mechanisms of polyploidization 47

2.3 Polyploidy in the liver 48

2.4 Molecular mechanisms of hepatocyte polyploidization 50

2.5 Significance of hepatocyte polyploidization 52

2.5.1 Relationship between polyploidization, proliferation and aging 53
2.5.2 Polyploidy changes gene expression in hepatocytes 55
2.5.3 Polyploidy and liver cancer 56
2.5.4 Polyploidization as a mediator for genetic diversity 57
2.5.5 Polyploidization during fatty liver disease 58

2.6 Hypothesis and objectives: 59

2.7 Materials and Methods: 60

2.7.1 Liver perfusion and hepatocyte isolation 60
2.7.2 Removal of red blood cells (RBCs) 61
2.7.3 Hepatocyte staining for sorting based on ploidy 61
2.7.4 Sorting of hepatocytes 62
2.7.5 RNA extraction 62
2.7.6 RNA sequencing 63

2.7.7 RNA-seq data analysis *64*
2.7.8 Ploidy profile analysis of diet-induced NASH mice *67*
2.7.9 Ploidy specific gene expression analysis of NAFLD associated genes *68*
2.8.1 Hepatocyte ploidy profile changes with age *69*
2.8.2 Hepatocytes with different ploidy have different gene signatures *72*
2.8.3 Average gene expression between different ploidy hepatocytes *75*
2.8.4 Hepatocytes of different ploidy are enriched in different signalling/molecular pathways *76*
2.8.4 Differential gene expression analysis between different ploidy hepatocytes *86*
2.8.5 Age is a major driver of gene expression *88*
2.8.6 Liver polyploidy and fatty liver disease *89*

2.9 Discussion **92**

2.10 Work contribution **94**

Chapter 3: Age-dependent transcriptional and epigenetic changes in mouse hepatocytes **95**

3.1 Introduction **95**

3.1.1 Age-dependent transcriptional changes in the liver **95**

3.1.2 DNA repair in aging liver **96**

3.1.3 Age-dependent alteration in liver chromatin **97**

3.1.4 Liver regeneration and aging **98**

3.1.5 Aging and liver diseases **99**
3.1.5.1 Aging and non-alcoholic fatty liver disease (NAFLD) *99*
3.1.5.2 Aging and alcoholic liver disease *99*
3.1.5.3 Aging and chronic viral hepatitis C *100*

3.1.6 Hypothesis and objectives **100**

3.2 Materials and Methods **102**

3.2.1 Liver perfusion and hepatocyte isolation **102**

3.2.2 RNA extraction **102**

3.2.3 RNA sequencing **103**

3.2.4 RNA-seq data analysis **103**
3.2.4.1 The k-means clustering *103*
3.2.4.2 Pathway analysis *104*

3.2.5 Formaldehyde fixation for chromatin immunoprecipitation sequencing (ChIP-seq) **105**

3.2.6 Chromatin Immunoprecipitation sequencing (ChIP-seq) **105**
3.2.6.1 Lysis of crosslinked cells *106*
3.2.6.2 Chromatin fragmentation by sonication *106*
3.2.6.4 Chromatin Immunoprecipitation *107*
3.2.6.5 Washing *108*
3.2.6.6 Desalting *108*
3.2.6.7 Purification using AMPure beads *109*
3.2.6.8 NGS paired-end library preparation for Illumina sequencing *109*

3.2.7 ChIP-seq data analysis **112**

3.2.8 Chromosome conformation capture (3C)-sequencing of mouse hepatocytes isolated from different age groups **113**

3.2.9 3C-seq data analysis **117**

3.3 Results **121**

3.3.1 Hepatocyte transcriptome changes with age **121**

3.3.2 Average gene expression changes with age in mouse hepatocytes **123**

3.3.3 Differential gene expression analysis identified age-related gene expression differences in hepatocytes **124**

3.3.4 Hepatocytes have differential molecular pathways enriched in each age group **125**

3.3.4.1 The k-means clustering of RNA-seq datasets revealed age-dependent gene signatures ***125***

3.3.4.2 Pathway analysis revealed comprehensive molecular pathways signature for each age group ***128***

3.3.5 Age-dependent changes in histone PTMs **134**

3.3.6 Three-dimensional chromatin organization of 8-week and 32-week mouse hepatocytes **151**

3.3.6.1 Compartment analysis between 8-week and 32-week hepatocytes ***154***

3.4 Discussion **157**

3.5 Work contributions **161**

Chapter 4: Conclusion and future work **162**

Appendix 1: Reactome pathways identified by GSEA **171**

Appendix 2: NAFLD associated genes passing filter cutoff and their Log_2RPKM values in ploidy samples. **181**

Appendix 3: GSEA and CPDB pathways upregulated in 8-week, 32-week and 94-week hepatocytes **184**

References **200**

List of Tables:

Table 1.1: Biological theories of aging: Brief summaries of major stochastic and non-stochastic theories of aging 15

Table1.2: Histone modifications positions, writers, readers and erasers and functions 28

Table 2.1: Age-dependent changes in ploidy profiles of mouse hepatocytes. 71

Table 2.2: Read statistics of RNA-seq samples 73

Table 3.1: Read statistics of RNA-seq samples of total hepatocytes isolated from different age groups 122

Table 3.2: Important pathways identified using GSEA and CPDB in 8-week, 32-week, and 94-week hepatocytes 129

Table 3.3: Read statistics of ChIP-seq experiments showing the total number of paired-end reads obtained and read alignment for each ChIP experiment and corresponding input sample 135

Table 3.4: Summary of genome-wide and genic region impact in active and inactive histone PTMs alterations in 32-week hepatocytes compared to 8-week hepatocytes 150

Table 3.5: 3C-seq read statistics obtained from hiclib output 151

List of Figures:

Figure 1.1: Hierarchical organization of chromatin in the Interphase nucleus 19

Figure.1.2: Epigenetic regulation by DNA methylation, histone acetylation and histone methylation 24

Figure 2.1: Polyploidization during postnatal liver growth 50

Figure 2.2: Strategy to isolate different ploidy mouse hepatocytes and study their gene expression using RNA-seq 59

Figure 2.3 Hepatocytes ploidy changes with age 70

Figure 2.4: Histogram showing ploidy dynamics at different age mouse hepatocytes 71

Figure 2.5: FACS profiles of two biological replicates of 8-week and 32-week-old mouse hepatocytes 73

Figure 2.6: Gene expression profiles between different ploidy hepatocytes are different 74

Figure 2.7: Bean plots of gene expression values of different ploidy hepatocytes in 8-week and 32-week mouse hepatocytes 76

Figure 2.8: Reactome pathways enriched in polyploid hepatocytes compared to diploid hepatocytes 77

Figure 2.9: Pathways upregulated in diploid hepatocytes compared to polyploid hepatocytes 81

Figure 2.10: Pathways enriched in 4N compared to 8N Hepatocytes 83

Figure 2.11: Pathways enriched in 8N compared to 4N Hepatocytes 85

Figure 2.12: DEGs between different ploidy populations across 8-week-old and 32-week-old mice 87

Figure 2.13: PCA of different ploidy samples from 8-week-old and 32-week-old hepatocytes analysed together taking average of replicates for each age group. 89

Figure 2.14: NASH model development and ploidy profiles 90

Figure 2.15: Gene expression of NAFLD associated genes- 91

Hierarchical clustering of orthologs of NAFLD-associated genes in 2N, 4N and 8N hepatocyte RNA-seq samples generated in this study from 8-week and 32-week wild-type hepatocytes

Figure 3.1: Strategy to isolate hepatocytes and study their gene expression and epigenetic regulation in different ages 101

Figure 3.2: PCA of RNA-seq data of total mouse hepatocytes isolated from three different age groups, viz. 8-week, 32-week and 94-week 122

Figure 3.3 Beanplot showing the gene expression values of mouse hepatocytes at 8-week, 32-week and 94-week age 123

Figure 3.4: Differentially expressed genes between different age groups hepatocytes 125

Figure 3.5: A k-means clustering of RNA-seq samples of different ages 128

Figure 3.6: Pathways upregulated specifically in 8-week, 32-week and 94-week hepatocytes as identified by GSEA and CPDB 130

Figure 3.7: UCSC genome browser snapshot for H3K27ac signals across Chr 1, chr2 and chr4 in 8-week and 32-week hepatocytes 137

Figure 3.8: H3K27ac signals in 8-week and 32-week hepatocytes 138

Figure 3.9: Gene expression levels of different HDACs in 8-week and 32-week hepatocytes 139

Figure 3.10: UCSC genome browser snapshots of H3K4me3 ChIP signals across chr12, chr9 and chr13 in 8-week and 32-week hepatocytes 140

Figure 3.11: H3K4me3 signals in 8-week and 32-week hepatocytes 141

Figure 3.12: UCSC genome browser snapshots of H3K9me3 ChIP signals across chr1, chr2 and chr9 in 8-week and 32-week hepatocytes 143

Figure 3.13: H3K9me3 signals in 8-week and 32-week hepatocytes 143

Figure 3.14: UCSC genome browser snapshots of H3K27me3ChIP signals across chr1, chr15 and chr8 of 8-week and 32-week hepatocytes 145

Figure 3.15: UCSC genome browser snapshots of 8-week H3K27me3 signal, 32-week H3K9me3 signal and 32-week H3K27me3 signal across chr1, chr15 and chr8 145

Figure 3.16: H3K27me3 signals in 8-week and 32-week hepatocytes 148

Figure 3.17: Can PRC2 complex genes explain H3K27me3 signals in 8-week and 32-week hepatocytes? 148

Figure 3.18: H3K27me3 signals are reduced at genic region of 32-week upregulated genes 149

Figure 3.19 Beanplot showing the gene expression levels in hepatocytes at 8-week and 32-week age 150

Figure 3.20 Genome-wide chromatin contact heatmaps (bin size = 1 Mb) of 8-week and 32-week hepatocytes 153

Figure 3.21 (A) Correlation between PC1 eigenvectors and histone ChIP-seq signals (bin size = 1Mb; left panel) in 8-week and 32-week hepatocytes 156

Figure 3.22: The A/B compartment analysis between 8-week and 32-week hepatocytes 157

Abbreviations

cDNA	Complementary DNA
ChIP-seq	Chromatin immunoprecipitation sequencing
DEN	Diethylnitrosamine
DNA	Deoxyribonucleic acid
FACS	Flouresecence activated cell sorting
HCC	Hepatocellular carcinoma
miRNA	MicroRNA
NAFLD	Non-alcoholic fatty liver disease
NASH	Non-alcoholic steatohepatitis
NGS	Next-generation sequencing
PCR	Polymerase chain reaction
qPCR	Quantitative polymerase chain reaction
RBC	Red blood cell
RNA	Ribonucleic acid
RNA-seq	RNA sequencing
TF	Transcription factor
WBCs	White blood cells
ROS	Reactive oxygen species
CIN	Chromosome instability
GCR	Gross chromosome rearrangement
CNV	Copy number variation
TAD	Topologically associating domain
3C	Chromosome conformation capture
CTCF	CCCTC- binding factor

HGPS	Hutchinson Gilford progeria syndrome
HAT	Histone acetyltransferase
HDAC	Histone deacytylase
HMT	Histone methyltransferase
HDM	Histone demethylase
PRC	Polycomb repressive complex
PTM	Posttranslational modification
DNMT	DNA methyltransferase
SASP	Senescence associated secretory phenotype
GH	Growth hormone
IIS	Insulin and IGF-1 signalling
mTOR	Mechanistic target of rapamycin
ESC	Embryonic stem cell
HSC	Hematopoietic stem cell
HepSC	Hepatic stellate cell
LSEC	Liver sinusoidal endothelial cell
CDK	Cyclin dependent kinase
DEGs	Differentially expressed genes
PCA	Principal component analysis
GSEA	Gene set enrichment analysis
CDHFD	Choline deficient high fat diet

Abstract

Aging can be defined as a gradual loss of function at the cellular, tissue, and organismal level with time. Aging is one of the most prominent risk factors for many diseases including metabolic disorders. Several metabolic conditions involve the liver which is a complex organ essential for whole-body homeostasis via regulation of energy, xenobiotic and endobiotic clearance, and molecular biosynthesis of amino acids, hormones, enzymes, cholesterol, bile, etc. Most of these functions are performed by hepatocytes, which constitute more than 70% of the total liver cell population. The liver is constantly facing various kinds of stress. As a result, with age, the hepatocytes develop an impaired ability to respond to hepatic insults, which leads to increased incidences of liver disease in the elderly. Therefore, it is essential to investigate the age-related changes in hepatocytes. In this thesis, we investigated age-related changes in mouse hepatocytes at the DNA (ploidy), RNA (gene expression), epigenetics (histone modifications), and 3D chromatin organization levels. Chapter 1 is introduced with a concise account of physiological aging followed by a summary of different theories proposed for cellular aging. Next, we narrated different hallmarks of aging, including transcriptomic and chromatin-level changes, which provide the necessary foundational knowledge which forms an essential background for understanding the work presented in this thesis. Then, we provided the facts which establish the liver as an interesting model for studying aging and described different cell types of the liver and their age-dependent changes. We also narrated salient features of hepatocytes, including polyploidy, and explained the impact of aging at cellular and molecular levels. This information laid the groundwork of our hypothesis to study hepatocyte gene expression and its regulation.

In chapter 2, we studied gene expression profiles of hepatocytes of different ploidy to test the hypothesis if they have different functional roles. Although many hypotheses have been proposed for the significance and presence of polyploidy in hepatocytes, there is scarce evidence to support them. To address this important question, we performed RNA sequencing of 2N (diploid), 4N (tetraploid) and 8N (octoploid) hepatocytes isolated by liver perfusion of 8-week and 32-week-old mice followed by flow-cytometry based cell sorting based on their DNA content. We observed that the gene expression profile of diploid cells is different from polyploid hepatocytes. Additionally, we noted a general trend of higher average gene expression in polyploid hepatocytes compared to diploids. Moreover, we identified differentially regulated molecular pathways in different ploidy populations based on their gene signatures. Subsequently, we showed an increment in hepatocyte polyploidization in diet-induced NASH (non-alcoholic steatohepatitis) mouse model as reported earlier. We manually curated a set of genes that are associated with NAFLD (non-alcoholic fatty liver disease) from published literature which were identified by meta-analysis of patient data. We observed that the orthologues of these genes are differentially expressed in different ploidy populations of mouse hepatocytes. Finally, we established that age imparts a stronger influence on hepatocyte gene expression compared to the effects of their ploidy level.

In chapter 3, we investigated the epigenetic regulation of age-dependent gene regulation in hepatocytes. For that, we first used RNA sequencing data of total hepatocytes from different age groups and identified differentially expressed genes and molecular pathways associated with aging. To understand the regulatory mechanisms of hepatocyte gene expression, we performed ChIP-sequencing of active as well as repressed histone post-translational modifications in 8-week and 32-week-

old mouse hepatocytes. We observed a drastic increase in genome-wide histone H3K27me3 signal with age, which signifies Polycomb-mediated chromatin repression. Intriguingly, we noticed a general decrease of H3K27me3 signal in genic regions, which might explain our observation that 32-week hepatocytes have an overall higher average gene expression compared to 8-week hepatocytes. Contrastingly, chromosome conformation capture (3C)-sequencing revealed that the spatial genome organization of hepatocytes remains largely invariant at the A/B compartment level in these two age groups suggesting the robustness of genome organization at the megabase scale despite profound age-associated alterations at the transcriptome and histone modification levels.

In the last chapter of this thesis, we discussed the outcome of our study in the context of previous findings on liver polyploidy and aging. We also provided accounts of the study limitations and future perspectives that could possibly address the gap of the present study and help to explain or resolve some of the unanswered questions borne out of this study.

Short Abstract

Aging is associated with declining body function and heightened risks of various diseases. The liver is the largest solid internal organ responsible for functions ranging from metabolism to detoxification. Hepatocytes perform most liver functions and hepatocyte polyploidization is a characteristic feature of adult liver. This thesis presents the first integrative study of age-dependent transcriptomic changes in mouse hepatocytes and their epigenetic regulation. Using purified mouse hepatocytes of different ploidy, we first established differences in their gene expression patterns by RNA sequencing. Similarly, we identified age-associated molecular signatures in hepatocytes of different age groups. ChIP-sequencing of multiple histone post-translational modifications revealed a differential signal pattern of H3K27me3 at genic and non-genic regions in 8-week and 32-week hepatocytes which may be key in age-associated gene regulation. Moreover, we observed that A/B chromatin compartment is largely invariant suggesting the robustness of spatial genome organisation at Mb-scale in these age groups

Chapter 1: Introduction

1.1 Physiological aging

Aging exhibits a time-related decline of the physiological functions necessary for survival and fertility in organisms [1]. Aging in humans is usually associated with a few visible changes in appearance (like wrinkling of the skin, greying and/or loss of hair, etc.) and some non-visible changes (such as the decline in sensory and cognitive function, decline in mobility and body co-ordination, increased susceptibility to diseases, etc.). Aging is the most significant risk factor for diseases like cancer, neurodegenerative and cardiovascular diseases, metabolic disorders, etc. [2]. All these diseases are manifestations of changes at the cellular level. Therefore, understanding the molecular basis of aging is of both clinical as well as fundamental biological significance. For centuries, humans have been trying to find answers about aging, such as when we start to age, why do we age, how long we can live, etc. Despite the development of new technologies and advances in science, the knowledge of the processes underlying aging is far from complete. As a result, many theories have been proposed to explain the process of aging in organisms. In the next section, I will briefly discuss some of the major theories of aging.

1.2 Theories of aging

Several theories have been proposed to describe the aging phenomenon. These theories can be broadly categorized as stochastic and non-stochastic theories of aging. The stochastic aging theories claim aging occurs due to the accumulation of random somatic damages. The nature of these damages includes mutations, aggregated protein products, and increased reactive oxygen species (ROS), etc. [3-5]. On the

other hand, the non-stochastic aging theories suggest aging as an organized evolutionary process that leads to the death of older cells/individuals and prevents population overgrowth. The process of programmed cell death or apoptosis is considered as one of the pieces of evidence of programmed aging theories [6]. I have summarized the major aging theories in Table1.1.

Table 1.1: Biological theories of aging: Brief summaries of major stochastic and non-stochastic theories of aging

Biological Theories of Aging	
Stochastic theories	**Explanation**
Cross-linking theory (or glycosylation theory) by Johan Bjorksten in 1942[7]	It hypothesizes that some proteins become increasingly cross-linked with glucose (simple sugars) with age, which in turn inhibits the metabolic processes by hindering the transportation of nutrients and waste between cell and environment. This excessive cross-linkage leads to a decline in tissue function.
Free radical theory by Denham Harman MD in 1956 [8, 9]	Free radicals are by-products of metabolic activities. When left unchecked, the free radicals can react with unsaturated lipids in membranes of mitochondria, nuclei, lysosomes and cell membranes. Free radicals can also cause mutations in genetic material. As a result, cells could no longer function optimally.
Wear and tear theory by August Weismann in 1882 [10]	This theory assumes that the body is comparable to a machine, which loses function when its parts wear out due to repeated usage those results in aging.
DNA damage theory by P Alexander in 1967 [10]	This theory suggests that aging is caused by the build-up of naturally occurring DNA damages that are not repaired.
Non-stochastic theories	**Explanation**
Programmed longevity theory by Mladen Davidovic in 2010 [11]	This theory assumes that aging is the consequence of a sequential switching on and off particular genes.
Immunological theory by E Cornelius in 1972 [12].	This theory claims that there is a decline in immunity in the elderly, which leads to an increased vulnerability to infectious disease and thus aging and death. For example,

	antibodies lose their potency as people age, and the body can resist fewer new illnesses successfully, resulting in cellular stress and death.
Biological clock theory [13]	It claims that each cell has a genetically programmed aging code stored in DNA. Some genes trigger accelerated aging and some genes support youth.
Neuroendocrine theory [14].	According to this theory, functional disturbances in the hypothalamic-pituitary-adrenal axis, both in neural regulation and endocrine output, are thought to be the cause of aging. The actions of numerous endocrine glands and their target organs are disrupted because of these disturbances.
Metabolic theory [15].	It proposes that all organisms have a finite lifespan and associates a higher metabolic rate with a shorter lifespan. Additionally, caloric restriction increases the lifespan and delays age-related diseases.
Telomere theory [16].	As normal cell loses a part of telomeres with each cell division, this theory claims that lifespan in regulated by telomeres as cancer cells with telomerase activity have infinite dividing potential and thus never die.

From Table 1.1, it can be concluded that there are many overlapping factors, which are believed to be driving or responsible for aging in organisms. So far, there is no single aging theory that is applicable universally. This is because some parts of a specific theory may be true while other parts do not fit in with our current scientific knowledge. With improvements in technologies in the last few decades and in-depth studies of various model organisms and physiological functions, our knowledge of the aging process has improved considerably. We now understand that aging has few common molecular roadmaps irrespective of organism or tissue. These processes are termed as hallmarks of aging and I will share the current understanding of these hallmarks briefly in the next section.

1.3 Hallmarks of aging

In a landmark study, Carlos et al. identified 9 primary processes responsible for aging based on three criteria: the process should be apparent during the normal aging, its experimental reduction should expedite, and conversely, its increment should delay aging [17]. These nine hallmarks are - genomic instability, telomere attrition, epigenetic alterations, loss of proteostasis, mitochondrial dysfunction, cellular senescence, deregulated nutrient sensing, stem cell exhaustion, and altered intercellular communication.

1.3.1 Genomic instability

Genomic instability is an increased tendency of genome alterations during cell division [18]. It can result in several possibilities based on the mechanisms: a) change in chromosome number or chromosome instability (CIN) (due to failures in the chromosome segregation machinery or the mitotic checkpoint), b) accumulation of mutations due to error-prone DNA synthesis or defective DNA repair machinery and, c) miscellaneous genetic modifications such as DNA copy number variants (CNVs), loss of heterozygosity (LOH), gross chromosomal rearrangements (GCRs) and hyper-recombination [19]. Any of the above factors can result in abnormalities in nuclear DNA [20, 21], mitochondrial DNA [22-24], and nuclear architecture [25, 26] which can lead to accelerated aging. Numerous reports have shown that not only genomic damages are accumulated during a lifetime but also their experimental introduction can induce augmented aging and vice versa [24, 27-32]. For example, overexpression of *BubR1* (important for faithful chromosomal segregation) can extend longevity in mice [29], while reducing prelamin A (a nuclear lamina protein) level can delay premature aging in mice [30, 32].

1.3.2 Telomere attrition

DNA polymerase cannot replicate the terminal ends of DNA molecules. An enzyme, telomerase can maintain telomere length by adding species-dependent telomere repeat sequence to the end of telomeres. However, most somatic cells lack telomerase. This results in progressive and cumulative erosion of telomere-protective sequences from chromosome end with each replication cycle [33, 34]. A multiprotein complex called shelterin binds the telomeres. The shelterin complex represses the major DNA-damage-signaling pathway (ATM-ATR kinase pathway) [35]. When telomere sequences are shortened, shelterin complex cannot bind to them resulting in induction of senescence and/or apoptosis [36, 37]. Telomere attrition accompanies normal aging in mammals [38, 39]. The absence of telomerase and/or mutations in shelterin proteins hastens aging in mice and humans [40-42]. On the other hand, the experimental addition of telomerase and/or increasing the length of telomeres can lead to increased lifespan [43-46].

1.3.3 Epigenetic Alterations

In the eukaryotic nucleus, many changes take place with aging. These changes can happen in one or more levels of the three-dimensional (3D) chromatin organization, chromatin remodelling, histone post-translational modifications, and DNA methylation. I will describe various epigenetic processes and their aging-associated alterations briefly in the next sections.

1.3.3.1 3D genome organization

The genome is hierarchically packed inside the nucleus of eukaryotes. The 3D chromatin organization controls biological processes like DNA replication, transcription, and cell division, all of which play important roles in cell differentiation

and animal development. Taking advantage of cutting-edge microscopic and chromosome conformation capture (3C)-based techniques, we now know that inside an interphase nucleus, the genome is hierarchically organized into multiscale structural units of chromosome territories (> 1 Mb), A/B compartments (100-1000s of kb), topologically associating domains (TADs) (10s of kb) and chromatin loops (few kb) (**Figure 1.1**)

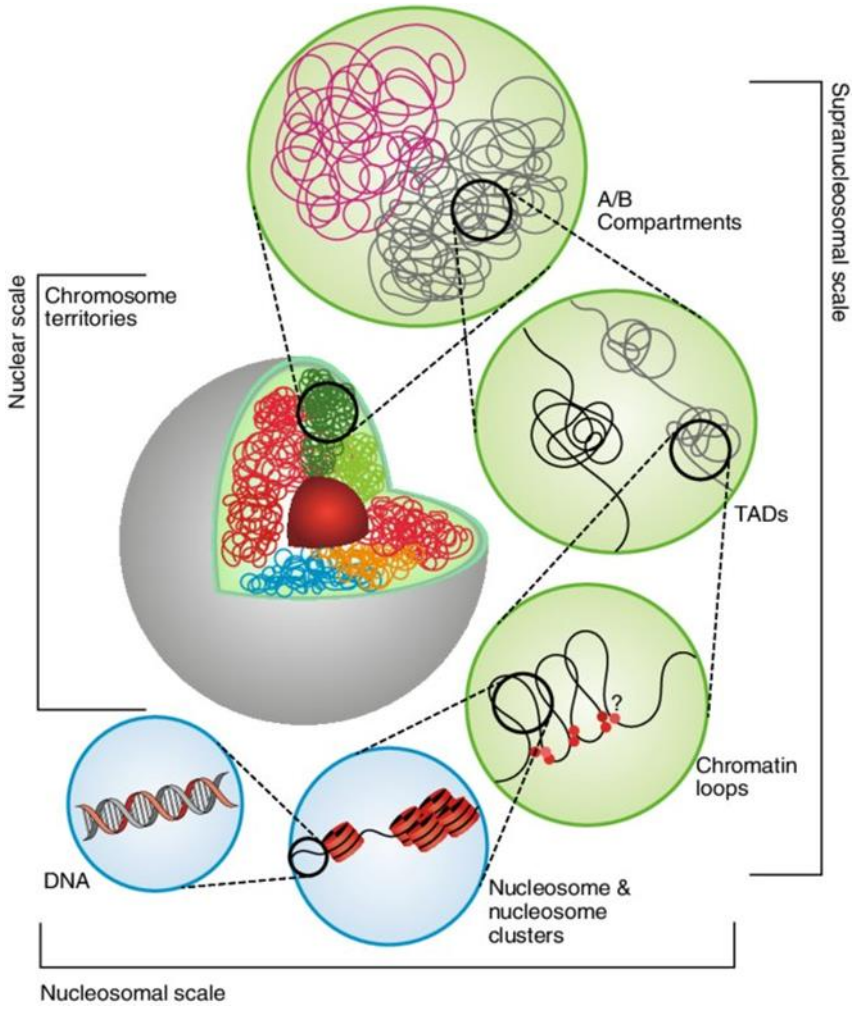

Figure 1.1: Hierarchical organization of chromatin in the interphase nucleus. The largest organisation are chromosome territories and is nucleosome. This figure was taken from the published article [47]. The permission to reuse the figure was granted by Springer Nature.

The chromosome territories are up to a few micrometres wide distinct regions inside the vertebrate interphase nucleus which are preferentially occupied by a particular chromosome [48]. Inside chromosome territories, there are two megabase-scale

spatial chromatin compartments: A and B as revealed by Hi-C. Compartment A is associated with open chromatin with enriched active histone marks and highly transcribed genes, while compartment B is linked with closed chromatin that is enriched in repressive histone modifications and inactive genes [49]. Chromosome compartments can be subdivided into smaller domains, called topologically associating domains (TADs), which form the fundamental unit of chromatin 3D organization. TADs are closed, sub-megabase, and self-interacting structures, which are separated from their neighbours by TAD boundaries [50]. TADs are highly conserved among different cell types and even across species in syntenic regions and they remain largely unchanged during many biological processes like cell differentiation and senescence [51, 52]. TADs are involved in the coordination of gene expression by facilitating regulatory element (enhancer or repressor)-promoter interactions located inside the same TAD [51, 53, 54]. TADs can be subdivided into smaller hierarchical units called sub-TADs using high-resolution Hi-C data [55, 56]. TAD insulation occurs mainly at boundary regions, which are enriched in housekeeping genes, tRNAs, and most notably, in the CCCTC-binding factor (CTCF) binding. The chromatin looping interactions are shielded by TAD boundaries so the majority of such long-range interactions occur within TADs. CTCF-mediated loops usually show a constitutive nature and are highly conserved between cell types and during differentiation whereas CTCF-independent loops are dynamic and linked to interactions that are directly associated with the transcriptional process, such as enhancer-promoter or polycomb-mediated contacts [56, 57]. Understanding of accurate interplay between all hierarchical orders of 3D chromatin organization is crucial to understand its genomic role and to assess its contributions in cell homeostasis and developmental processes.

As discussed in detail in section 1.3.6, cellular senescence is a hallmark of aging. Senescent cells show alterations in chromatin organization [58-60]. The Hutchinson-Gilford progeria syndrome (HGPS) is a premature aging disease and normal cell nuclei from old individuals acquire defects similar to those of HGPS patient cells [61]. Hi-C on skin fibroblasts from HGPS patients revealed that senescent cells have profoundly different nuclear architecture when compared to proliferating and quiescent cells [60]. The compartmentalization between euchromatic A compartments and repressive B compartments was considerably lost in late passages of HGPS fibroblasts. A subset (12%) that could still be assigned to a specific compartment exhibits compartment switching where compartment association was changed as compared to normal cells [60]. In a similar study using human lung fibroblast in proliferating, quiescent, and senescent stages, the authors found that between the three situations, the overall organization of chromatin into active (A) and repressive (B) compartments as well as TADs remains conserved, although a subset of TADs switches between compartments [62]. Additionally, a global increase of short-range interactions and a decline of long-range interactions were observed in senescent cells [62]. Thus, changes in 3D chromatin organization have been shown to affect aging and other aging-related hallmarks.

1.3.3.2 Chromatin remodelling

The DNA is packaged inside the cell in a highly condensed structure called chromatin. To carry out processes such as DNA replication, transcription and DNA damage repair, chromatin needs to be remodelled into an open conformation so that protein/enzyme complexes can access DNA. Chromatin remodelling refers to a measured alteration in the chromatin or nucleosome structure, making it shortly permissive/occlusive, to enhance/obscure binding of factors requiring DNA as a template. The chromatin

remodelling can be performed by either 1) ATP-dependent chromatin remodelling complexes by moving, ejecting or restructuring nucleosomes, or 2) histone modifiers like histone acetyltransferases (HATs), histone deacetylases (HDACs), histone methyltransferases (HMTs), histone demethylases (HDMs), kinases, etc [63-65]. The ATP-dependent chromatin remodelling complexes use ATP hydrolysis to loosen the DNA-histone interactions resulting in nucleosome sliding/repositioning, nucleosome eviction and specific histone replacement/incorporation [66]. The presence of other domains apart from ATPase domain is the basis of their categorization in subfamilies: switch/sucrose non-fermentable (SWI/SNF), chromodomain helicase DNA-binding (CHD), INO80, and imitation switch (ISWI). Many of these chromatin remodellers are altered during aging. Deletion of *ISW2* or mutation which deactivates Isw2 enzyme complex increased replicative lifespan in the budding yeast, *Saccharomyces cerevisiae* [67]. Similarly, in response to multiple stresses, the expression of *isw1* gene was found to be upregulated in *Caenorhabditis elegans*. Moreover, the depletion of *isw1* using RNAi resulted in reduced lifespan hinting ISW1 regulates longevity in worms [68]. In *C. elegans,* SWI/SNF and DAF16 co-localize at DAF16/FOXO target promoters to initiate transcription of genes associated with stress resistance and longevity [69]. In humans, the ATPases of SWI/SNF complex, BRM (SMARCA2), and BRG1 (SMARCA4) are involved in telomere structure and function maintenance and hence longevity [70, 71].

1.3.3.3 Histone modifications

Histones are basic proteins that help in packing negatively charged DNA into nucleosomes inside the nucleus of eukaryotic organisms. A nucleosomal core particle composed of 146-147 bp DNA wrapped around histone octamer of four core histones (H2A, H2B, H3, and H4) [72-74]. Histone H1 binds to the nucleosome core particle to

make a complete chromatosome [72, 75]. The N-terminal tails of histones undergo different types of post-translational modifications (PTMs) which can lead to changes in chromatin compaction depending upon the position and type of histone modification [76]. Three types of protein complexes are associated with histone modifications colloquially referred to as “writers”, “erasers”, and “readers” as shown in figure 1.2. The writers add chemical groups to histones, for example, histone acetyltransferases (HATs) and histone methyltransferases (HMTs), while the erasers remove these chemical groups, for example, histone deacetylases (HDACs), histone demethylase (HDMs). The readers, on the other hand, recognize these chemical groups, for example, acetylated lysine (AcK) residues can be recognized by bromodomain-containing proteins and methylated lysines (MeKs) can be recognized by chromodomain-containing proteins. There are several kinds of histone modifications such as acetylation, methylation, phosphorylation, ubiquitylation, sumoylation, biotinylation, etc. However, I will discuss only histone acetylation and methylation, which are relevant to my study below.

Histone acetylation: It is a reversible reaction that occurs generally on the lysine residues of the histone N-terminal tail. HATs catalyze the transfer of an acetyl group from acetyl coenzyme A, whereas HDACs remove the acetyl group. Histone acetylation reduces electrostatic interactions between histones and DNA, as each acetate group added to histone residue reduces its net positive charge by 1 and thus decreases its affinity towards DNA [77, 78]. As a result, the chromatin becomes more accessible to various protein complexes leading to transcriptional regulation [79-84]. Changes in histone acetylation at specific residue have been observed in several aging tissues and age-associated diseases like neurodegeneration, cancer, etc. [85-87]. For example, histone H3 lysine 27 acetylation (H3K27ac) has been shown to play

important roles in the timing and level of gene expression at DNA regulatory regions in many human and mouse cell types [88, 89]. H3K27ac is present at both active promoters and distal enhancers. The changes in the H3K27ac signal have been found with aging in different scenarios. For example, there is a significant reduction in the number of H3K27ac peaks in old (65-75 years old) human hematopoietic stem cells compared to young (18-30 years) ones [90]. Contrastingly, H3K27ac marks were found to be increased in aged human skeletal muscle tissues [90]. These reports indicate that the H3K27ac signal changes differently in different tissues with age.

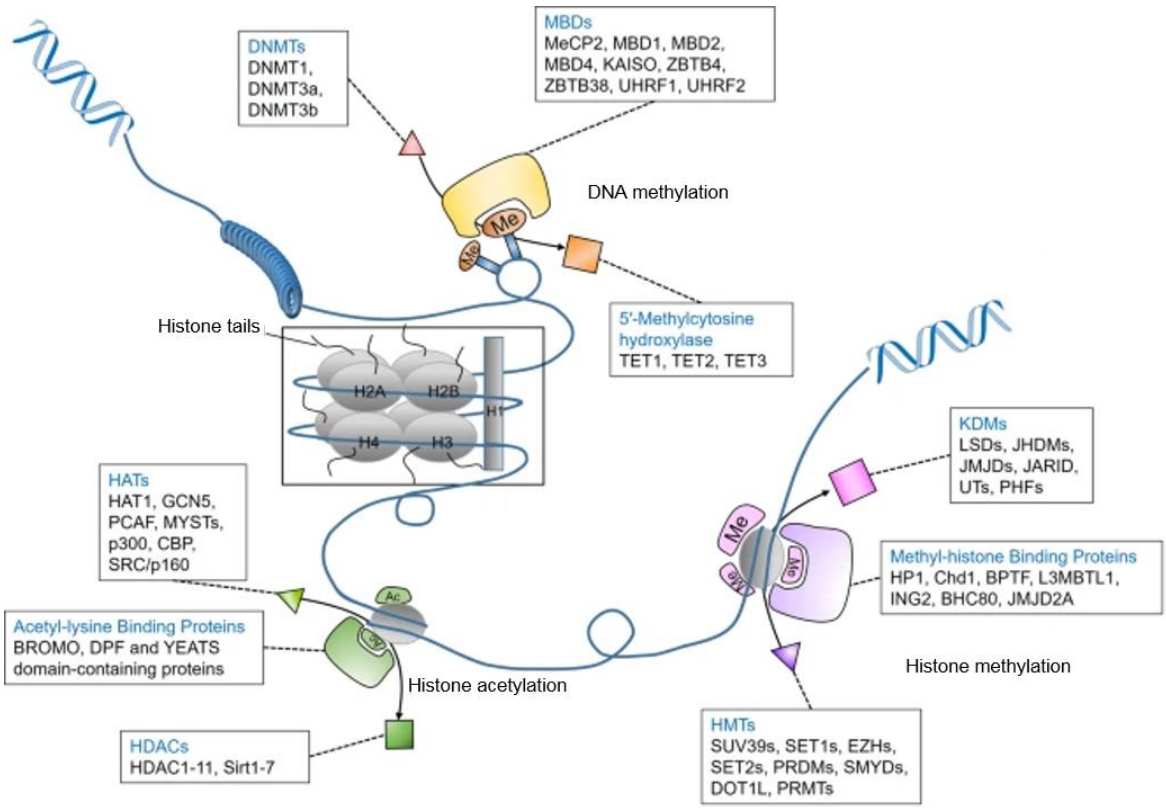

Figure.1.2: Epigenetic regulation by DNA methylation, histone acetylation and histone methylation. Different histone (grey) and DNA (blue) modifying proteins are indicated in boxes. This figure was taken from the published article [91]. The permission to reuse the figure was granted by Springer Nature

Histone methylation: When methyl group(s) is/are transferred to the basic residues of histones in a nucleosome it is termed histone methylation. Based on the level of

methylation and position of the histone residue modified, histone methylation can lead to either transcriptional activation or repression. Histone lysine methylation is widely studied in transcription. For example, di- and tri-methylation at H3K79, H3K4 and H3K36 are generally gene-activating where H3K79 and H3K36 methylation mostly happen over gene bodies [92, 93]. Similarly, H3K4me1 is generally observed at active enhancers while H3K4me3 marks the active promoters [94-97]. On the other hand, H3K9 and H3K27 methylations are mostly gene-repressive but play different roles [95, 97]. H3K9me2 is generally observed at silent or lowly expressed genes in euchromatin, H3K9me3 is strictly associated with heterochromatin and H3K27me3 is linked with suppression of dynamically regulated genes whose expression changes with developmental signals [98-101]. The process of histone methylation is dynamic as methyl marks can be added by histone methyltransferases and removed by histone demethylases [102]. Other proteins (readers) can identify and bind the methylated histone residues to alter chromatin compaction and bring about a phenotypic change [103]. In the following section, I am going to briefly discuss few important histone marks, *viz.* H3K27me3, H3K9me3 and H3K4me3, and their association with aging.

H3K27me3: Methylation at lysine 27 residue of histone H3 is catalyzed by polycomb repressive complex-2 (PRC2) [104]. In mammals, the functional PRC2 complex consists of EZH2/1 (enhancer of zeste 2/1), EED (embryonic ectoderm development), SUZ12, RBBP4/RbAp48 (or RBBP7/RbAp46) and other subunits [105-107]. EZH2 is the main catalytic subunit of PRC2 for methylating H3K27 and needs EED and SUZ12 for its activity [108-110]. Once H3K27 is trimethylated, EED binds to H3K27me3 leading to a change in conformation of EZH2, which results in allosteric activation (or increased catalytic activity) of EZH2 [111]. This process helps PRC2 to spread to neighbouring nucleosomes and deposit H3K27me3 marks [112-114]. Other core

PRC2 subunits like SUZ12 serves as stabilizing factor for PRC2 while RBBP4 and RBBP7 are essential for binding of PRC2 to unmodified nucleosomes and its proper methyltransferase activity [115-117]. Another polycomb repressive complex, PRC1 catalysis promotes PRC2 occupancy and H3K27me3 deposition, whereas PRC1 removal dramatically reduces PRC2 binding and H3K27me3 at Polycomb target sites [118-121]. The catalytic core of the PRC1 complexes, RING1A/B, binds exclusively with one of six Polycomb group RING finger (PCGF) proteins in a hierarchical fashion [122] Because of its interaction with certain PCGF proteins, PRC1 may be separated into six distinct groups, each with its own set of related proteins and distinct modes of action [122]. PRC1 is a transcription repressor that compressed local chromatin and deposited mono-ubiquitylation of histone H2A at lysine 119 (H2AK119ub1) [122].

H3K27me3 changes dynamically during aging. For example, in *Drosophila,* reduction in H3K27me3 level by CRISPR/Cas9 (clustered regularly interspaced short palindromic repeats/CRISPR-associated protein 9) mediated deletion of PRC2 and PRC1 complex genes promotes healthy lifespan [123], while increased H3K27me3 levels were observed during aging in killifish brain and mouse muscle stem cells [124, 125]. Such examples hint towards a positive relationship between H3K27me3 levels and aging. However, some contrary reports were also noted. For example, reduced H3K27me3 and increased UTX-1 (histone demethylase) levels were observed during aging in *Caenorhabditis elegans* and humans [126, 127]. Thus, H3K27me3 levels change differently with age in different organisms.

H3K9me3: Histone H3 lysine 9 trimethylation is widely associated with constitutive heterochromatin and the repression of repetitive DNA elements during evolutionary history [128-136]. H3K9me3 modification is catalyzed by specific SET domain-containing histone methyltransferases such as SETDB1, SUV39H1 and SUV39H2

[137, 138]. H3K9me3 is recognized by heterochromatin protein 1 (HP1), which ensures compaction, spreading, and inheritance of heterochromatin through self-oligomerization and interaction with other repressive modifications [139]. In fly, deletion of *Kdm4A* (an H3K9me3 demethylase) results in a shorter lifespan in males hinting that Kdm4A is important for longevity [140]. In mouse and human hematopoietic stem cells, expression of *SUV39H1* was reduced with age via miR-125b resulting in global depletion of H3K9me3 level and defective heterochromatin function [141].

H3K4me3: Histone H3 lysine 4 trimethylation is most widely present around transcription start sites (TSS) of active promoters [102]. The enzymes required for lysine methyltransferases (KMT) which catalyze H3K4 methylation contains SET domain and are found in a complex with other accessory proteins that are vital for their methyltransferase activity. These enzymes are conserved from yeast to humans [142]. The Trithorax complex, the Trithorax-related complex and the COMPASS complex are three key complexes responsible for creating H3K4me3 marks [143, 144]. Reduced H3K4me3 global level is associated with increased lifespan while their increased level is linked with reduced lifespan in worms [145]. Likewise, increased H3K4me3 levels in flies are associated with decreased lifespan [146].

Taken together, the above-mentioned observations suggest that several histone PTMs change with age. However, their variation levels are different across evolutionary lines and tissues as they do not exhibit a common theme. Thus, it is important to study age-dependent alterations in histone modifications in the context of specific tissue and organism and learn how these modifications affect chromatin structure and gene expression.

We have summarized the major histone modification marks, their writers, readers and erasers along with their function in Table 1.2.

Table1.2: Major histone modifications positions, writers, readers and erasers and functions.

Histone Mark	Writer Name	Erasers name	Reader name	Functions	References
H3K4	SET1A/KMT 2E	LSD1/KDM1A	CHD1	Chromatin remodeler	[147]
	SET1B/KMT 2F	LSD2/KDM1B	BPTF	NURF complex subunit	[148]
	MLL1/KMT2 A	NO66/MAPJD	TAF3	TFIID complex subunit	[149]
	MLL2/KMT2 B	JARID1A/KDM5A	Sgf29	Crosstalk between H3K4me2/3 and H3 acetylation	[150]
	MLL3/KMT2 C	JARID1B/KDM5B	ING4	G/M cell cycle arrest	[151]
	MLL4/KMT2 D	JARID1C/KDM5 C	CFP1	Binds to unmethylated CpG	[152]
	SMYD1/KMT 3D	JARID1D/KDM5 D	PHF2/KDM7C	Oxygen sensor in normoxia	[153]
	SMYD2/KMT 3C		SPIN1	Senescence and apoptosis	[154]
	SET7/9/KMT 7		PHF23	Autophagy	[155]
	PRDM9/KMT 8B		PYGO2	Self-renewal of mammary progenitor cells	[156]
H3K9	SUV39H/KM T1A–B	JHDM2A/KDM3A	HP1α/β	Heterochromatin formation	[139]
	G9a/KMT1C	JHDM2B/KDM3B	HP1γ	Transcription elongation	[157]
	GLP/KMT1D	JHDM2C/KDM3C	UHRF1	DNA methylation	[158]
	SETDB1/KM T1E	JHDM3A/KDM4A			
	PRDM family	JHDM3B/KDM4B			
		JHDM3C/KDM4C			
		JHDM3D/KDM4D			
		PHF8/KDM7B			
		PHF2/KDM7C			
H3K27	EZH1/KMT6 B	UTX/KDM6A	CBX7	Transcriptional depression of PRC complex target gene	[159]
	EZH2/KMT6 A	UTY/KDM6C	EED	Spreads H3K27 methylation	[114]
		JMJD3/KDM6B	BAHD1	Facultative heterochromatin formation	[160]
		KIAA1718/KDM7 A	NSD2	Transcriptional elongation	[161]
		PHF8/KDM7B			
H3K36	SETD2/KMT 3A	JHDM1A/KDM2A	DNMT3A	DNA methylation	[162]
	NSD1/KMT3 B	JHDM1B/KDM2B	LEDGF	DNA repair (HR)	[163]
	NSD2/KMT3 G	JHDM3A/KDM4A	NBS1	DNA repair (NHEJ)	[164]
	NSD3/KMT3 F	JHDM3B/KDM4B	Ku70	DNA repair (NHEJ)	[164]
	SMYD2/KMT 3C	JHDM3C/KDM4C	MRG15	RNA splicing	[165]
	ASH1L/KMT 2H	JHDM3D/KDM4D	ZMYND11	RNA splicing	[166]
	SETD3				

	SETMAR				
H3K79	DOT1L/KMT4		TP53BP1	DNA damage response	[167]
H4K20	SET8/KMT5A	PHF8/KDM7B	TP53BP1	DNA damage response	[168]
	SUV4-20H1/KMT5B	PHF2/KDM7C	L3MBTL1	Chromatin compaction	[169]
	SUV4-20H2/KMT5C	LSD1n	ORC1	Replication	[170], [171]
			ORCA	Replication	[171]
			Pdp1	Chromatin localization of H4K20 methyltransferase	[172]
H3KXac	p300/pCAF	HDAC1, HDAC2, HDAC3, HDAC4, HDAC5, HDAC9, SIR2	Bromodomain family and Tandem-PHD family		[173], [174], [175], [176], [177]

1.3.3.4 DNA methylation

In eukaryotes, a covalent transfer of methyl group to the C-5 position of cytosine base of DNA takes place during DNA methylation mediated by DNA methyltransferases (DNMTs) [178]. The methylation of the adenine base is also possible but uncommon. The extent of DNA methylation can vary according to cell types. For example, in somatic cells, about 98% of DNA methylation happens at the CpG dinucleotide whereas, in embryonic stem cells, almost 25% of DNA methylation appears at non-CpG sites [179]. In one of the earliest studies, DNA methylation was found to progressively decrease with age in mice across several tissues such as the liver, brain and small intestine [180]. Similarly, a global DNA hypomethylation has been linked with aging in humpback salmon [181], cows [182] and humans [183, 184]. However, not all genomic locations undergo DNA hypomethylation with age. A progressive increase in CpG island methylation at the promoter region of the estrogen receptor (ER) gene was observed in human colorectal mucosa [185]. Such studies spark interest that whether it is possible to predict the age of individuals based on methylation patterns of a specific set of genes. Steve Horvath used about 8000

samples from various healthy tissues and cell types of humans and identified 353 CpG sites that showed differential DNA methylation patterns with age and could serve as the epigenetic clock of tissue aging [186]. Similarly, DNA methylation quantification at the age-related CpGs in promoter regions of aging-related genes *ITGA2B, ASPA* and *PDE4C* in human blood DNA was successful in reliable age prediction [187].

1.3.4 Loss of proteostasis

Protein homeostasis or 'proteostasis' is the process that regulates proteins within the cell to maintain the composition of cellular proteome and the overall health of the organism. Proteostasis is maintained by the protein network, which involves pathways that control biogenesis, folding, trafficking, aggregation, disaggregation and degradation of proteins [188, 189]. The faulty proteostasis has been linked with aging and experimental manipulation of proteostasis has been shown to reduce aging-associated diseases. For example, overexpression of the heat shock protein 16 (*hsp-16)* and heat-induced expression of hsp70 resulted in lifespan extension in *C. elegans* and *D. melanogaster* respectively [190, 191]. The mouse strain with *Pit1* mutation is long-lived and exhibits an increased amount of heat shock protein mRNAs in liver, kidney, and heart. Likewise, deletion of ubiquitin ligase/cochaperone carboxyl terminus of Hsp70-interacting protein (CHIP), resulted in reduced lifespan and accelerated age-related pathophysiological phenotypes [192, 193]. The two major protein quality control proteolytic systems are the autophagy-lysosomal system and the ubiquitin-proteasome system. Autophagy is a regulatory mechanism in cell that removes needless or dysfunctional components and allow recycling of cellular components [194-196]. Mutants with missing components of autophagy machinery have reduced lifespan in yeast, worm, and fly [197-200], whereas increased autophagy delays aging and extend longevity in fly and worms [200, 201]. Similarly, in

mice, podocyte-specific deletion of *Atg5* resulted in age-dependent late-onset glomerulosclerosis [202-205], while overexpression of autophagic machinery genes resulted in reduced aging-associated phenotypes and extended lifespan [206, 207]. Moreover, reduction in proteasomal activity results in age-related phenotypes and endorses the development of metabolic abnormalities in various organisms and cell types [208-211].

1.3.5 Mitochondrial dysfunction

Mitochondria are actively involved in different functions like modulators of stem cell activity, intracellular signaling, regulators of innate immunity and generation of energy [212]. A decay in mitochondrial quality and activity has been linked with aging and age-related pathologies. In the early 1960s, Rockstein and colleagues reported an age-dependent decline in mitochondrial function in houseflies [213]. Increased frequency of mutations was observed in the mitochondrial DNA (mtDNA) of old rodents [214]. Moreover, mice expressing a proof-reading-deficient version of mitochondrial DNA polymerase (PolgA) showed a premature aging phenotype [215, 216]. Increased mtDNA mutations were also observed in aged human heart muscle and brain [217].

1.3.6 Cellular senescence

Cellular senescence can be defined as a permanent cell cycle arrest of a cell in response to endogenous and exogenous stresses, including telomere dysfunction, oncogene activation and persistent DNA damage [218-220]. In 1961, Hayflick et al. showed that normal cultured human fibroblasts exhibit a limited capacity for cell division before entering a permanent growth-arrest state called replicative senescence [221]. As a result, Hayflick proposed that tissue aging is the consequence of the gradual decline in the proliferative capabilities of cells [222]. BubR1 is a part of the

mitotic checkpoint apparatus to guarantee the correct segregation of chromosomes. Mice with low BubR1 levels have a shorter lifespan and other progeroid features [223]. Moreover, several tissues from these models exhibited high expression of p16 and other senescence-associated features and on reducing the expression of p16 in these mice, the age-related deterioration was diminished [224, 225]. Additionally, modest improvement of the senescence-inducing tumor suppressor pathways has been shown to extend longevity [226, 227]. The senescent cells exhibit dramatic changes in their secretome which are enriched particularly in pro-inflammatory cytokines and matrix metalloproteinases, called senescence-associated secretory phenotype (SASP) [218, 228]. Further, the pro-inflammatory secretome may contribute to aging [229].

1.3.7 Deregulated nutrient-sensing

Nutrients are organic compounds involved in biochemical reactions that produce energy or are constituents of cellular biomass [230]. A cell's capability to identify and respond to nutrients is called nutrient sensing. Many nutrient-sensing pathways are compromised during aging such as IGF1/PI3K/AKT/mTOR, and AMPK/Sirtuin/PGC1α. These pathways are involved in many vital processes like cell cycle, protein synthesis, glucose homeostasis, autophagy, stress response, etc. [231]. I am going to briefly discuss how some of the most important nutrient-sensing pathways change with aging in the next section.

1.3.7.1 The Insulin- and IGF-1-signaling pathways

In response to growth hormone (GH) from the pituitary gland, many cells (such as hepatocytes) produce insulin-like growth factor 1 (IGF-1), as a secondary mediator. The downstream signaling of IGF-1 and insulin is common and hence these pathways are often referred to as "insulin and IGF-1 signaling" (IIS) pathways. The IIS is the most conserved aging regulating pathway in evolution with many downstream targets

such as the mTOR complexes and the FOXO transcription factor family which are highly conserved and involved in aging phenotypes [232-234]. Down regulation of the IIS pathway genes resulted in up to 300% increment in lifespan while stimulation of this pathway led to a decline in lifespan in nematodes [235, 236]. Similarly, a mutation in the *chico* gene, which encodes insulin receptor substrate in *D. melanogaster,* resulted in a longer lifespan by 48% in homozygotes and 36% in heterozygotes [237, 238]. In vertebrates, tissue-specific effects of IIS pathway perturbations were observed. Therefore, many mouse models have been developed to study the impact of IIS on aging. For example, Snell and Ames mice have a mutation in *Pit1* and *Prop1* genes respectively, lack GH, prolactin and thyroid-stimulating hormone (TSH) and have 42–70% increment in longevity than wild-type mice [239-242]. Correspondingly, GH-deficient [241], GH-releasing hormone-knockout [243], and GH-receptor-knockout mice [244] have increased lifespan.

1.3.7.2 The mTOR, AMPK, and Sirtuins

Apart from IIS, three other nutrient signaling mechanisms widely studied in aging are 1) the mechanistic target of rapamycin (mTOR) pathway which senses high amino acid concentrations, 2) adenosine monophosphate-activated protein kinase (AMPK) pathway which senses low-energy states (AMP/ATP ratio) by detecting high AMP levels and, 3) sirtuins which sense low-energy states by detecting high NAD+ levels [245]. The mTOR pathway includes two multi-protein complexes, mTORC1 and mTORC2, that control almost all aspects of anabolic metabolism [246]. Down regulation of mTORC1 activity in yeast, worms, and flies prolongs longevity [247]. Two mutant mouse models, one with low mTORC1 but normal mTORC2 activities and the other with S6K1 (mTORC1 substrate) deficiency have increased lifespan [248, 249]. Harrison et al. treated mice with rapamycin and observed extended longevity [250].

Yang et al. found that hypothalamic neurons of the aged mouse have higher mTOR activity which was blocked by direct infusion of rapamycin into the hypothalamus [251]. AMPK signals nutrient scarcity and catabolism and their up-regulation supports healthy aging. AMPK activation results in mTORC1 repression [252]. Moreover, AMPK activation can exert pro-longevity effects in several species, for example, activation of AMPK in the gastrointestinal tract increased the *D. melanogaster's* lifespan by 30% [253]. Similarly, AMPK activation helps in the lifespan extension of worms [254, 255]. Increasing APMK activity reduces CREB-regulated transcriptional coactivator–1 (CRTC-1) and CREB homologue-1 (CRH-1) activities leading to increased lifespan in *C. elegans* [256]. In rats, AMPK activation induced by caloric restriction is found to protect old kidneys against senescence by increasing autophagy and reducing oxidative damage [257].

Found originally in *S. cerevisiae*, sirtuins are evolutionarily conserved from bacteria to humans [258, 259]. In humans, seven members (SIRT1-7) of the sirtuin family are documented which possess either mono-ADP ribosyltransferase or deacetylase activity. Variation of sirtuin activity is linked with processes like DNA repair, gene expression, cell cycle, immune response, cell metabolism, neuroprotection and development [260]. Overexpression of Sir2 (silent mating-type information regulation 2) or its orthologues was linked to increased lifespan in yeast, worm (sir-2.1) and fly (dSir2) [261-263]. Mice with SIRT6 deficiency displayed accelerated aging while mutant mice with SIRT6 overexpression exhibit a longer lifespan than controls [264, 265]. Moreover, Nathan et al. showed that SIRT1 is required for AMPK activation in mouse skeletal muscles [266].

Thus, mTOR and IIS pathways are generally associated with pro-aging phenotypes while AMPK and sirtuins are associated with pro-longevity.

1.3.8 Stem cell exhaustion

Stem cells are cells with two essential features- self-renewal and the ability to differentiate into one or more specific adult cell types. Based on their ability to produce types of cells, stem cells can be pluripotent or multipotent. Examples of pluripotent stem cells include embryonic stem cells (ESCs- from inner cell mass of blastocyst stage), perinatal stem cells (from umbilical cord blood), and induced pluripotent stem cells (iPSCs- adult cells reprogrammed artificially to behave like ESCs). Examples of multipotent stem cells are hematopoietic stem cells (HSCs which form blood cells), mesenchymal stem cells (MSCs).

The decay in the regenerative abilities of tissues is commonly associated with aging and this curtailment in tissue homeostasis is believed to be caused by a reduction in stem cell number and/or function [267-270]. For example, age-linked changes in hematopoietic stem cells (HSCs) differentiation result in reduced production of adaptive immune cells leading to anemia and myeloid malignancies [271]. Similar reports were found in other types of adult stem cells in mouse including the forebrain, bone, and muscle fibers [267-269]. Rossi et al. documented that the cell division frequency is decreased in old mouse HSCs compared to young mouse HSCs [272]. This reduction in the cell cycle was linked with the accumulation of DNA damage and up-regulation of cell-cycle inhibitory proteins (like p16INK4a) with age in mouse [272] [273].]. Moreover, INK4a−/− HSCs in old mice displayed improved engraftment ability and better cell-cycle activity compared to HSCs of wild-type controls [273]. Additionally, in many mouse tissues, one of the major reasons for stem cell reduction with aging was telomere shortening [274, 275]. Consequently, it is proposed that stem cell rejuvenation might reverse the aging phenotype at the organismal level [276].

1.3.9 Altered intercellular communication

Aging has been linked to alterations in intercellular communication at endocrine, neuronal or neuroendocrine levels [246, 276-278]. Aging and age-related diseases have common paths that many a time congregate on inflammation. A chronic, sterile (without any infection), low-grade inflammation develops during aging known as inflammaging [279]. Inflammaging is one of the most noticeable aging-associated variations in intercellular communication in mammals [280]. Salminen et al. documented various causes of inflammaging such as failure of the dysfunctional immune system to effectively clear pathogens and non-functional host cells, secretion of proinflammatory cytokines by senescent cells, enriched activation of the NF-κB transcription factor, defective autophagy response, accumulation of proinflammatory tissue damages, etc. All these changes lead to stimulation of NLRP3 inflammasome and other pro-inflammatory pathways which result in increased production of IL-1β, tumor necrosis factor, and interferons [280, 281]. Overactivation of the NF-κB pathway is one of the transcriptional signatures of aging and inhibition of NF-κB signaling stops age-associated features in different mouse models of accelerated aging [282-284]. Additionally, in mice, the hypothalamus is linked to the moderation of systemic aging by incorporating NF-kB-driven inflammatory responses with GnRH-mediated neuroendocrine effects [278]. Similarly, the mRNA decay factor AUF1 helps in degrading the cytokine mRNA to reduce inflammation [285]. Additionally, AUF1-deficient mice displayed increased cellular senescence and premature aging phenotype that can be rescued by its re-expression [285]. Moreover, AUF1 binds and strongly activates the transcription for telomerase catalytic subunit Tert and contributes to maintaining telomere length [285]. SIRT1, SIRT2 and SIRT6 may also

down-regulate the inflammatory response through deacetylation of NF-kB subunits and transcriptional suppression of their target genes [286-288].

In summary, as stated above, various studies using a variety of model organisms and tissues have led to a significant understanding of the various processes, pathways, proteins and genes involved in the aging process. However, we also observed that even the hallmarks of aging are not displayed to the same extent and manner at organismal, tissue, or cellular levels. Therefore, even though few common hallmarks of aging have been described, it appears that aging does not follow a common roadmap universally. As a result, it becomes important to understand the aging mechanism in a species- and tissue/cell-type- dependent manner. Recent studies showed tissue-specific changes during aging in the same model organism [289-295]. This highlights the importance of studying the aging process in specific cell types as each cell type is performing different roles even within the same organ.

1.4 The obstacles of current aging research

The most obvious limitation of current aging research is the lack of exact understanding about what is called “normal” or physiological aging. There is no indication so far that a common roadmap of aging exists, making it difficult to standardize the normal aging process. Aging is a complex and interconnected process. Individuals (or tissues) accumulate different kinds of insults over time and sometimes a vital process like DNA integrity, mitochondrial function, etc., is irreparably affected which may destabilize the entire homeostasis. Due to this, other connected processes may get disturbed and this cycle might begin a chain reaction, which can lead to the total collapse of the biological system. Thus, aging can occur very differently in each individual at molecular and phenotypic levels. This can be easily observed in our

surroundings where few older individuals are healthy and fit while even younger individuals are affected by age-associated afflictions, such as physical frailties or diseases like cancer or neurodegenerative diseases. In most aging studies, distinct exhibitions of aging are investigated (for example, knockdown of a specific gene and studying its impact on the age of an organism) making it difficult to compare study results.

Next, even if we compare results from the same species, tissues, time points, etc., it is challenging to ascertain if individuals, that are used as samples for one certain age group in a classic healthy age group comparison experiment, are good replicates or not. That is if aging has affected or damaged the same molecular functions to a comparable extent. Another challenge appears in cross-sectional study designs, where different individuals are sampled to obtain data on the age-depended changes in the function of one specific organ, making it difficult to track the actual course of molecular changes over time. This is a case where we are taking discontinuous data and treating them as continuous events to study changes over time. However, the accumulation of molecular damage and subsequent dysfunction remains random and hard to interpolate between different individuals. This is because a lot of important information is lost since all animals within the respective study can be examined only once. This leads to increased stochasticity of the obtained data, making it difficult to deduce results. Thus, aging research faces many issues currently and some of which may be solved in the future with a better (invasive and non-invasive) sampling of vital tissues/cells. However, despite these challenges, we can still draw many valuable insights about aging from the current tools and techniques. In the present study, we aim to understand the age-dependent transcriptomic and epigenetic changes using the mouse liver as a model. We tried to minimize animal to animal variation by using

liver from inbred genetically homogeneous mouse strain. Moreover, we choose to study only female mice to avoid gender bias. In the next section, I am going to discuss the importance of the liver and why we chose the mouse liver as a model to study aging.

1.5 Liver as an aging model

The liver was considered as the seat of life, soul, and intelligence by the ancient Greeks in mythologies [296]. The liver has many remarkable properties which make it one of the important organs in the body. The liver is the largest solid organ and accounts for 2% of total body weight in humans and 5% of mice [297]. The liver is responsible for an extraordinary spectrum of functions that are essential for maintaining whole-body homeostasis via regulation of energy metabolism, xenobiotic and endobiotic clearance, and molecular biosynthesis. Moreover, the liver is a moderator of systemic and local innate immunity and an important site of immune regulation [298, 299]. The liver is constantly under different kinds of stress. For example, the production of ROS due to various metabolic activities and exposure to alcohol, drugs, environmental pollutants, radiation and other xenobiotics lead to the generation of oxidative, genotoxic and xenobiotic stress in the liver. The tremendous stress levels can lead to various liver diseases, for example, oxidative stress plays a central role in the development of non-alcoholic fatty liver diseases (NAFLD), and exposure to drugs, alcohol and other xenobiotics can lead to chemical-induced liver diseases like hepatitis (acute, chronic, granulomatous), cholestasis (with bile duct injury, with or without hepatitis), steatohepatitis, vascular disorders and liver cancer. Additionally, the mammalian liver has characteristic polyploidy, a property widely associated with genomic instability and cancers. Taken together, the extremity of liver diseases varies from minor non-specific changes in hepatic structure and function to

acute liver failure, cirrhosis and liver cancer. Thus, during aging, the liver encounters higher exogenous and endogenous assaults compared to common aging-associated insults that every organ experiences. Surprisingly, despite all these extreme conditions, the liver possesses unique abilities of regeneration and its main functional constituent cells, hepatocytes, are one of the longest living cells of the human body [300-303]. This makes the liver a very interesting model to study aging. In the next section, I will briefly discuss the current understanding of aging processes in the liver and its parenchymal and non-parenchymal cells.

1.6 Effect of aging on liver

With age, several degenerative modifications transpire in the liver where its structure and function are witnessed to decline. Therefore, the elderly are more susceptible to liver disorders and more vulnerable to the consequences of liver diseases [304-306]. Studies using ultrasound revealed a 20–40% reduction in the liver volume with age [307-309]. Such changes are attributed to the aging-associated decline in the blood flow in the liver. Compared to < 40-year-old humans, there is a 35% decrease in the blood volume of humans above 65 years of age [310, 311]. However, radioisotopic scanning of the liver revealed a reduction in the liver mass but not in volume [312]. Additionally, high-density lipoprotein (HDL) cholesterol, total cholesterol, triglycerides, γ-glutamyltransferase and alkaline phosphatase gradually increase over time while the metabolism of the low-density lipoprotein (LDL) cholesterol decreases by 35% with age in humans [313]. Liver regeneration and repair are driven by a complex system of mitogenic growth factors, transcription factors, non-mitogenic cytokines, and paracrine mediators [314]. There is a reduction in liver regeneration following partial hepatectomy in older mice [315]. The build-up of oxidative stress inhibits the activation

of progenitor liver cells and promotes the depletion of hepatocytes and liver mass [316]. Aging impacts various types of liver cells, such as hepatic stellate cells (HepSCs), liver sinusoidal endothelial cells (LSECs), Küpffer cells (KCs) and hepatocytes, to different extents. In the following paragraph, I will discuss age-related changes in different types of liver cells.

1.6.1 Hepatic stellate cells (HepSCs)

HepSCs, also known as perisinusoidal cells or Ito cells, are pericytes found in the space of Disse of the liver. HepSCs help in the storage of lipid and vitamin A, regulate extracellular matrix metabolism and possibly influence sinusoidal blood flow via contractile properties. In the case of liver damage, HepSCs get activated and lose the fat-filled vesicles to produce collagen which is a key process for the progress of hepatic fibrosis and cirrhosis [317]. The markers of HepSCs activation and collagen deposition (αSMA, collagen 1α1 and 1α2 and phosphorylated Moesin), platelet-derived growth factor receptor-β (PDGFR- β) and desmin protein were found to be upregulated in aging rat liver [318]. With age, the HepSCs in mice and non-human primates increase in number and size, protrude into the sinusoidal lumen and become visible by light microscopy. Moreover, there is a marked increase in the number and size of lipid droplets with age in rodent HepSCs [319, 320].

1.6.2 Liver Endothelial Sinusoidal Cells (LESCs)

LESCs are endothelial cells that line the hepatic sinusoids and perform many functions like endocytosis of circulating proteins, bidirectional transfer of substrates between blood and hepatocytes, regulation of immunotolerance, and maintaining sinusoidal microenvironment. Research in mice, rats, non-human primates, humans, and models of premature aging revealed morphological changes that happen in LESCs with old age and are termed as pseudocapillarization. These changes include altered

expression of antigens (such as von Willebrand factor, CD31 and collagen), thickening of the endothelium, deposition of basal lamina and collagen, increased perisinusoidal staining with Masson's Trichome and Sirius Red, reduction in the number and size of fenestrations, etc [319, 321, 322].

1.6.3 Küpffer cells

Küpffer cells are a type of macrophages within the lumen of the liver sinusoids. They produce IL-6 and TNFα as an innate immune response against pathogens and phagocytose large macromolecules. Using light microscopy, Hilmer et al. found an increased number of KCs from the perfused liver of aged rats over a fixed area. They also reported decreased microspheres recovery from aged rat's liver and observed increased KCs phagocytic activity with age [323]. Similarly, Singh et al. identified a change in liver macrophage distribution with aging, where old mice had more F4/80+ macrophages located in large lymphoid structures (also containing T-cells and B-cells), and a reduction in the number of spindle-shaped macrophages throughout the parenchyma [324].

1.6.4 Hepatocytes

Hepatocytes are the most abundant cells in the liver and perform a majority of liver functions such as synthesis of fibrinogen, albumin, and lipoproteins, regulation of carbohydrate and fatty acid metabolism, synthesis of bile salts and cholesterol. They are also involved in xenobiotic and drug metabolism and regulation of liver growth and repair. These processes are controlled by targeted gene transcription, protein synthesis, mitochondrial respiratory processes and autophagy [269, 271-273]. Hepatocytes experience several changes with age such as increased polyploidization (discussed in next section), accumulation of lipofuscin in the cytoplasm, increase in nuclear DNA lesions, and decline in the number of mitochondria [325]. The

hepatocytes of older mice increase in size and their chromatin get condensed with age [277]. The decreased expression of Sirtuin1 and peroxisome proliferator-activated receptor-gamma coactivator (PGC-1α), along with a decline in nicotinamide adenine dinucleotide (NAD+) concentration lead to dysregulation of glycolysis, triglyceride synthesis, and lipid metabolism in aged mouse hepatocytes [278]. Reduced mitochondrial enzymes (mitochondrial nitric oxide synthase, manganese superoxide dismutase, complexes I and IV) were documented in aged hepatocytes [279]. The decline in hepatocyte mitochondrial function has been suggested to enhance the vulnerability of aged livers to acute liver injury and to cause delays in liver regeneration [280]. Mitochondrial dysfunction has been observed in a premature aging mouse model, which lacks an important component of DNA repair Ercc1, which manifests in impaired mitochondrial membrane potential, abnormal mitochondrial morphology, reduced oxygen consumption and proton leakage leading to high oxidative stress [281]. The reduced number of hepatocytes with autophagic vesicles and the decline in the rate of autophagy-mediated proteolysis in old rodent hepatocytes suggest that autophagy is suppressed in aging [282, 283]. Using the progeroid mouse model, Mariño et al. suggested that this decline in autophagy is promoted by alterations in energy-sensing pathways [284]. Chaperone-mediated autophagy and macroautophagy were compromised in aged rodent hepatocytes leading to a gradual decline of proteostasis, raised levels of oxidized proteins and lipid peroxidation, protein misfolding, and aggregation [159, 285-289]. The aggregation of proteins such as lipofuscins can increase ROS production that additionally inhibits autophagy [286, 287]. Besides, aging mouse livers are known to accumulate a multiprotein chromatin-modifying complex (C/EBPalpha-Brm-HDAC1) that silences E2F-dependent promoters, thereby reducing the proliferation and regenerative capacity of hepatocytes

[290]. The reduction in proliferation of aged hepatocytes may also be related to an increase in senescent cells with aging. There is dysregulation of senescence-associated signalling pathways such as p16, p21 and p53 in aged mouse hepatocytes [291]. The senescent hepatocytes also show metabolic changes, such as increased transport of conjugated bilirubin into the hepatic sinusoids, insulin resistance through dysregulated glucose transporter expression and Akt signalling among others [292]. Moreover, senescent hepatocytes produce cytokines like interleukin 6 (IL-6), tumor necrosis factor 1-α (TNFα) and interleukin 8 (IL-8) which are associated with age-related inflammation [293, 294]. Age-dependent DNA hypermethylation in 18S and 28S ribosomal RNA genes was reported in mouse liver DNA [297]. Hepatic glucokinase (GCK) is a key enzyme in glucose utilization and its downregulation is associated with insulin resistance and type 2 diabetes mellitus. Jiang et al. observed an age-linked increment in DNA methylation and decrement in Gck expression in rats suggesting that hepatic insulin resistance and diabetes susceptibility with age could involve DNA methylation [298].

1.7 Polyploidy in liver

The majority of liver functions are performed by hepatocytes which account for 70-80% of liver volume and approximately 70% of all liver cells [326]. One of the characteristic features of mammalian hepatocytes is polyploidy. The extent of polyploidization varies with species and age [327-331]. For example, hepatocytes are reported to be ~90% polyploid in adult mice and around 30% in adult humans [332-338]. Polyploidy is developmentally regulated in mammalian hepatocytes. All neonatal rodent hepatocytes are diploid with high proliferation rates [339]. The rate of cell division is observed to decline with age in rodents [340, 341]. The senescent markers (p16ink4α, p21 and p53) were expressed at high levels in 18-month-old mouse hepatocytes of

different ploidy (diploid-2N, tetraploid-4N and octoploid-8N) compared to 2N, 4N and 8N hepatocytes of 2-month-old mouse [342]. Jun Wang et al. correlated increased polyploid hepatocytes in older mice with senescence and proposed that polyploidy may induce senescence-type changes during aging [342]. I will discuss the hepatocyte polyploidy in detail in Chapter 2.

1.8 Scope of this thesis

Apart from aging-associated changes in hepatocytes ploidy, altered hepatocyte polyploidy has been associated with many liver diseases hinting towards its role in maintaining hemostasis. Moreover, the ratio of different ploidy populations is maintained as explained by the ploidy conveyor model [343]. This preservation of ploidy ratio in the adult liver hints towards a ploidy-specific functional role of hepatocytes. However, there is no consensus about the significance of hepatocytes ploidy in the liver but many hypotheses have been proposed. We hypothesized that polyploidy has a functional role in mouse hepatocytes. To test our hypothesis, we sorted mouse hepatocytes based on their DNA content (ploidy) and performed genome-wide trancriptomic profiling (RNA sequencing) to investigate gene expression signatures in different ploidy populations.

There is an increase in the aging population throughout the world. By 2030, every 1 out of 8 individuals will be 65 years or older and by 2050, the elderly (≥60 years) will outnumber the children (0-14 years) [344, 345]. Aging predisposes the elderly to various chronic diseases. Understanding the fundamental changes occurring in cells/tissues can help in developing therapeutic interventions to delay aging and aging-associated disease risks and increase health span. It is widely established that aging is genetically and epigenetically driven in a cell-dependent manner. Hepatocytes have an average lifespan of 200-400 days which is amongst the longest in rodents [303,

346, 347]. Having such a long lifespan despite encountering tremendous metabolic, oxidative, xenobiotic and genotoxic stress makes hepatocytes a great model system to understand aging. Therefore, we investigated the age-associated transcriptomic changes between 8-week, 32-week and 94-week-old female C57/BL6 mouse hepatocytes. Taking cues from transcriptomic study, we performed genome-wide ChIP-sequencing of specific histone modifications. Moreover, we investigated age-associated changes at 3D chromatin organization level in 8-week and 32-week hepatocytes. This study reveals how 3D genome organization, histone modifications and gene expression is regulated in hepatocytes during normal aging.

The rest of the thesis is structured as follows- Chapter 2 presents gene expression differences between different ploidy populations of hepatocytes isolated from two different age-groups. Chapter 3 describes the transcriptional and histone alterations as well as 3D chromatin organization changes in mouse hepatocytes with age. Chapter 4 concludes the research work presented in this thesis and discusses future research directions.

Chapter 2 Liver polyploidy

2.1 Introduction to polyploidy

A cell or an organism containing a single set of chromosomes is termed as haploid (N). Polyploidy is a state in which a cell or an organism possesses more than two complete sets of the haploid genome (e.g. 3N, 4N, …, etc.). This multiplication of genome can occur within a single cell nucleus (nuclear ploidy) or inside the same cell but in two or more nuclei (cellular ploidy). Organism-level polyploidy is common in plants and lower organisms [348-352] but rare in mammals [353-355]. The polyploidization in mammals is generally limited to specific cells, for example, acinar cells of pancreas (4N), trophoblast giant cells of placenta (8N to 64N), megakaryocytes of the bone marrow cells (16N to 128N), cardiomyocytes (4N), and hepatocytes (4N to 32N) [356-360].

2.2 Mechanisms of polyploidization

Many mechanisms have been implicated for polyploidization of cells such as cell fusion, endoreplication, and cytokinesis failure which are briefly described in the subsequent sections.

Cell fusion: This process necessitates cell-cell adhesion in the plasma membranes of the two cells, accompanied by destabilization of opposing lipid bilayers, which leads to fusion [361]. Cell fusion is the only mechanism that can lead to polyploidization without the involvement of the cell cycle and generally results in multi-nuclear polyploid cells. Cell fusion-mediated polyploidization has been found in both physiological (such as in muscle fibre formation) [362] and pathological conditions (such as in viral infection) [363]. Cell fusion plays a key role in tissue regeneration and wound healing. For example, during tissue injury, bone marrow-derived cells have been found to fuse with differentiated cells leading to the formation of hybrids with regenerative abilities.

Cell fusion is also documented in intestinal muscle cells, retina, brain, and liver [364-368].

Endoreplication: In this process, polyploid cells are produced either by endocycling (repeated G and S phases of the cell cycle without cell division) or by endomitosis (aborted mitosis by skipping metaphase, anaphase, and cytokinesis) [369-371]. Endocycling takes place by the combination of S phase cyclin-dependent kinase (S-CDK) oscillation and mitotic entry impediment, either via cyclin B proteolysis or M phase cyclin-dependent kinase (M-CDK) inhibition. Endomitosis, also known as mitotic slippage, is caused due to faulty mitosis. This process allows the cell to enter the G1 phase of the cell cycle by overriding mitotic phase. The most studied example of endoreplication in mammals is the differentiation of trophoblast stem cells into trophoblast giant cells [372, 373]. Endoreplication results in mono-nucleated polyploid cells.

Cytokinesis failure: Cytokinesis is the last step in the cell division which results in division of the parental cell into two daughter cells. Cytokinesis failure can happen at any stage of the four complex processes, such as positioning of the division plane, ingression of the cleavage furrow, formation of the midbody, and abscission [374, 375]. This process is well documented in polyploidization of heart, bone marrow and liver cells [376-378]. Cytokinesis failure leads to many diseases such as cancer, Fanconi anaemia, Wiskott–Aldrich syndrome, X-linked neutropenia, age-related macular degeneration, type II neurofibromatosis and Lowe syndrome [358, 379, 380].

2.3 Polyploidy in the liver

Polyploidy is one of the characteristic features of adult mammalian hepatocytes. To start with, all neonatal rodent hepatocytes are diploid with a high proliferation rate [339]. However, their rate of cell division declines with age [340, 341]. In rodents,

hepatocyte polyploidization begins at the initial few weeks after birth. During this period, one diploid (2N) hepatocyte can either undergo a normal cell cycle and form two diploid daughter hepatocytes (2N, 2N) or alternately, a diploid hepatocyte can undergo karyokinesis without cytokinesis to form one binucleated tetraploid hepatocyte (4N = 2N X 2) (**Figure 2.1**) [340, 381-384]. This binucleated tetraploid hepatocyte can undergo DNA replication doubling its DNA content (8N = 4N X 2) and complete the karyokinesis. Following successful cytokinesis, this cell can give rise to two mono-nucleated tetraploid hepatocytes (4N, 4N). A binucleated octoploid hepatocyte (8N = 4N X 2) will emerge in the event of cytokinesis failure [340]. This cycle may continue to maintain and establish higher polyploidization in hepatocytes. Lack of actinomyosin ring formation has been attributed as the cause of cytokinesis failure in male Wistar rats [383]. During postnatal growth in rodents, cytokinesis failure is first observed around the weaning period [383] which is also marked with important changes in metabolic pathways, feeding behavior and hormone concentration [385]. This sucking-to-weaning transition stage marks the first wave of hepatocytes polyploidization. Interestingly, the proportions of different ploidy populations are preserved following this rapid post-natal rise in polyploidization events (plateau phase) [386, 387]. For example, the percentage of polyploid hepatocytes remains almost invariant in mice between 2 to 6 months of age [387]. A similar trend is also documented in human livers where percentage of polyploid hepatocytes remain stable (14%-17%) between 20 to 50 years of age [388]. After this plateau phase, the second wave of polyploidization takes place in an aging-dependent manner [387-389]. The percentage of octoploid hepatocytes in mice changes from ~17% at 2-month age to around 34% at 18-month age [342]. Similarly, the percentage of polyploid hepatocytes in humans increases sharply after 50 years of age and reaches up to 42% in the 86 to

92-year-old age group [388]. Several molecular pathways have been implicated for the polyploidization process in liver which will be discussed in the next section.

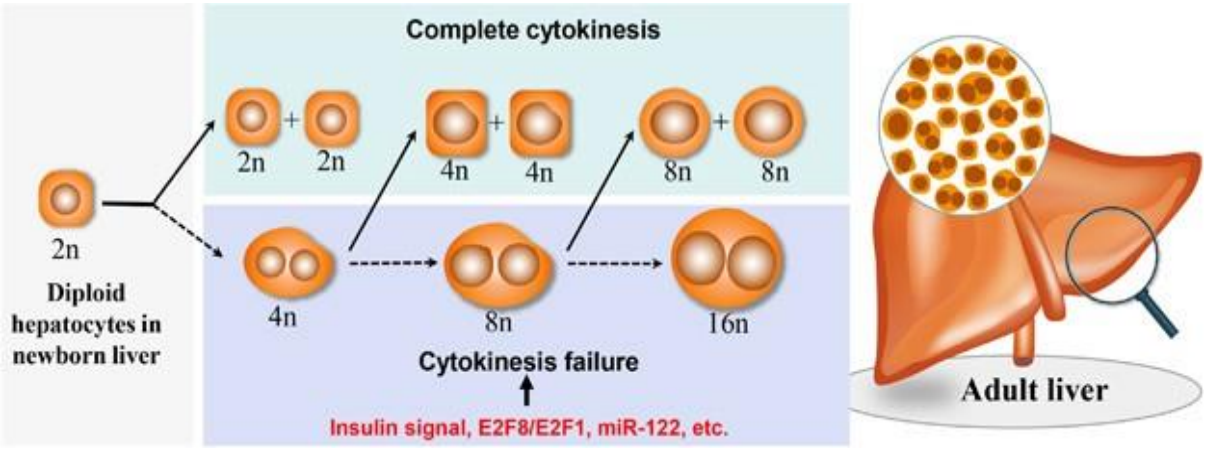

Figure 2.1: Polyploidization during postnatal liver growth. Cytokinesis failure lead to generation of higher ploidy hepatocyte while complete cytokinesis results in hepatocytes of same ploidy. This figure was taken from the published article [390]. The permission to reuse the figure was granted by Springer Nature.

2.4 Molecular mechanisms of hepatocyte polyploidization

During the postnatal liver growth, hepatocyte polyploidization is mainly caused by cytokinesis failure due to defective actinomyosin ring formation [383, 391]. In brief, the microtubules fail to touch the cortex and molecular signals necessary for cleavage plane specification (like polo-like kinase 1 (PLK1) and aurora B) do not reach properly. As a result, active RhoA (Ras homologue gene family member A) cannot accumulate at the site of division and the contractile rings fail to form [392].

Insulin signalling is one of the key factors for hepatocyte polyploidization as well as in the emergence of binucleated hepatocytes [393]. In rodents, a reduction in the insulin pathway dramatically reduces binucleated hepatocytes while repeated insulin injections increase polyploid hepatocytes [394, 395]. There is an 88% decline in binucleated 4N hepatocytes when rats were treated with Streptozotocin (STZ, a drug that specifically kills pancreatic cells) to lower circulating insulin levels before weaning. Contrastingly, around 32% higher binucleated 4N hepatocytes were observed when rats were injected with insulin during the suckling-to-weaning transition. The PI3K/AKT

(phosphatidyl inositol/AK-strain transforming) pathway is the major downstream pathway that intervenes the impact of insulin in these settings. It is known that actin cytoskeleton polarization and reorganization during processes, such as cell migration and invasion, are controlled by PI3K–AKT [396]. The inhibition of AKT in proliferating hepatocytes promotes accurate actin reorganization and precise RhoA localization at the division site resulting in successful cytokinesis [397, 398]. E2F transcription factors, a family of cell cycle master regulators, also regulate cell proliferation by controlling AKT activation in a cell cycle-dependent manner [399]. Moreover, E2F transcription factors are also linked to polyploidization of hepatocytes. This family includes activators (E2F1, E2F2, and E2F3) as well as repressors (E2F4, E2F5, E2F6, E2F7, and E2F8) in mammals [400, 401]. In mice, *E2f1 to E2f6* express at low level in liver throughout life [381], while *E2f7* and *E2f8* levels change dramatically with negligible expression at the time of birth to a maximum level at 3-5 weeks of age, a period when polyploidization begins [381, 402]. Several studies have shown that there is a reduction in binucleated polyploid hepatocytes and increase in diploid hepatocytes in *E2f7* and *E2f8* double-knockout mouse livers [334, 403-406]. Several transcripts deregulated in these double-knockout mice livers are involved in cytokinesis, such as *Ect2*, *Mklp1* and *Racgap1*. Moreover, during the hepatocytes polyploidization, activities of ECT2, MKLP1 and RACGAP1 are reduced which hinder the transfer of information from spindle to cortex. This prevents the formation of functional contractile actinomyosin ring and inhibits cytokinesis [391]. Moreover, inhibition of several cell cycle genes, *viz*. *Cdk1*, *Trp53*, *cMyc*, *Tgfb1*, *Cdkn1a*, *Birc5*, *Rb1*, *Ccne*, etc., have been shown to influence cellular or nuclear ploidy in several mouse models [386, 407-416]. The PIDDosome (signaling platform essential for caspase-2 stimulation) is used by E2F family members to control hepatocyte ploidy during liver development [417].

By directly regulating numerous downstream effectors, *Trp53* plays an important role in regulating hepatic polyploidy levels [386]. The PIDDosome-p53 axis have been shown to regulate hepatocyte ploidy during postnatal liver growth [417].

Many microRNAs (miRNAs) are linked to polyploidization and found to be expressed in an age-dependent manner in mouse liver. For example, mir-122 is differentially expressed during postnatal liver development and regulates polyploidization by antagonizing pro-cytokinesis targets [418]. A 60-70% reduction in the proportion of polyploid hepatocytes was observed in mir-122-knockout mouse liver which can be restored following the overexpression of mir-122, suggesting a critical role of this miRNA in hepatocyte polyploidization [418].

2.5 Significance of hepatocyte polyploidization

Several hypotheses have been put forward over the years to explain the occurrence of polyploidy in hepatocytes. These hypotheses can be broadly divided into three main categories. First, polyploidy is linked to the stressful environment of the liver. The liver produces a variety of metabolites and performs xenobiotic transformations which contribute to metabolic and toxic stresses to hepatocytes. During metabolism, a copious amount of free radicals is generated which can produce reactive oxygen species (ROS) and induce oxidative stress in hepatocytes [419]. For example, C to T transitions are the most common mutations caused by ROS-induced DNA damage [420]. Additionally, 8OHdG is the most common oxidative DNA lesion. The 8OHdG is highly mutagenic due to mispairing with adenine during DNA replication [421]. Multiple sets of chromosomes in polyploid cells could protect the genome against the effects of gene-inactivating mutations caused by DNA damaging agents like ROS.

The second hypothesis postulates that polyploidy increases the copy number of genes which in theory can increase the transcriptional output of the liver to meet their high

metabolic demand. The liver which performs a plethora of functions could have increased its cell number as a possible solution to address the high metabolic needs, however, that might require additional energy and resources. Instead, by increasing their genome content (polyploidy), the hepatocytes may have devised an alternate strategy and achieved an equivalent level of function [422, 423].

The third hypothesis links hepatic polyploidy to liver zonation and hepatocyte maturity [424]. Histologically, the liver is divided into lobules. The central vein runs across the lobule's centre. Portal triads are found on the lobule's periphery. The liver can be separated into three functional zones depending on oxygen availability. Zone 1 surrounds the portal tracts, which receive oxygenated blood from the hepatic arteries. Zone 3 is a low-oxygen zone that surrounds the central veins. Zone 2 is situated in the middle region between zone 1 and 2. It is known that hepatocytes mature as they travel from the periportal to the pericentral regions. According to this hypothesis, diploid hepatocytes are found in the periportal zone, whereas the pericentral zone contains mature hepatocytes with higher ploidy.

Thus, many hypotheses have been proposed but they are yet to be validated. In the next section, I will summarize the different roles of hepatocyte polyploidization based on experimental findings.

2.5.1 Relationship between polyploidization, proliferation and aging

Polyploid hepatocytes have been explored for their proliferative potential and repopulation abilities in various mouse models. Some studies have linked polyploidy with terminal differentiation while other studies could not find such differences between different ploidy hepatocytes [425-431]. One study showed that there is no substantial gap in regenerative capability between *E2f8*−/− mouse liver (with predominantly diploid hepatocytes) and wild-type liver (predominantly polyploid hepatocytes) [405].

Moreover, when diploid and octoploid hepatocytes isolated from 8-week-old mice were transplanted in *Fah*−/− (fumarylacetoacetate hydrolase) mice, their proliferative abilities are comparable [432]. These observations suggest that polyploidy does not affect the proliferation or cell division rate of hepatocytes as compared to their diploid counterparts [334, 432-435]. In contrast, several other observations indicate otherwise. For example, Ganem et al. showed that cytokinesis failure during postnatal murine liver development activates the Hippo–LATS2–p53 pathway, which plays an anti-proliferative role and restricts 4N hepatocyte growth compared to 2N hepatocytes [386, 436]. Similarly, Wilkinson et al. observed that *in vivo* and *in vitro* proliferation of liver-specific *E2f7* and *E2f8* double knockout (LKO) mouse hepatocytes (predominantly diploid) are faster compared to the wild-type controls (majority polyploid hepatocytes) [404]. They observed that when LKO and control hepatocytes were mixed in different proportions, the hepatocytes from LKO mice proliferate faster and outcompete control hepatocytes to repopulate *Fah*−/− mouse liver. Moreover, control 2N hepatocytes proliferate faster compared to control polyploid hepatocytes. These observations hint towards a differential cell cycle regulation for diploid and polyploid hepatocytes [404].

It is already established that hepatocyte ploidy changes with age in two waves of polyploidization separated by a plateau phase in between [61, 90, 96, 126]. As discussed in section 1.6, the rate of hepatocytes cell division decline whereas the expression of senescent markers increases with age. Consequently, some studies have explored the possible link between polyploidy, altered proliferation rates of different ploidy, and aging in hepatocytes. For example, 2N, 4N and 8N hepatocytes isolated and sorted from 2-month-old mice possess similar liver repopulation abilities when transplanted into *Fah*−/− recipients and nominally express senescence-specific

markers like SA-β-gal, p16, p53, and p21 [437, 438]. However, in aged mice (18-month-old), the hepatocytes express higher levels of senescence-specific markers compared to 2-month-old mice hepatocytes. Moreover, compared to 2N and 4N hepatocytes, 8N hepatocytes express much higher levels of senescence markers and have lower repopulation potential [390, 438]. These studies demonstrate that during aging, polyploidy might induce senescence-type changes.

Taken together, these observations suggest that there is an intricate relationship between polyploidy, proliferation and aging in hepatocytes.

2.5.2 Polyploidy changes gene expression in hepatocytes

A linear model would suggest that the number of transcription products will increase in proportion with the amount of DNA, for example, a 4N hepatocyte will have double the amount of total RNA transcripts as compared to a 2N cell. However, in a microarray-based study using wild-type mice, Lu et al. found only a handful of differentially expressed genes (DEGs) between 2N, 4N and 8N hepatocytes which were purified by FACS [439]. This indicates that gene expression does not increase linearly with ploidy or DNA content. Kreutz et al. used insulin binding for separating diploid mouse hepatocytes (high insulin binding) from polyploid hepatocytes (low insulin binding). Microarray analysis revealed that > 30% of genes were differentially expressed between these two populations which reiterate the fact that gene expression and DNA content are not linearly correlated in mouse hepatocytes [440]. Many genes in prokaryotes and eukaryotes are transcribed in ‘bursts’ in a stochastic manner [441]. Using single-molecule fluorescence *in situ* hybridization (smFISH) in intact mouse liver, Itzkovitz and team showed that transcriptional bursts occur in many hepatocyte genes and these bursts are lower in 4N hepatocytes compared to 2N cells [442]. This implies that liver polyploidzation leads to a relatively controlled gene

expression possibly resulting in reduced cellular heterogeneity. Taken together, these studies implicate that the transcriptional output of polyploid hepatocytes does not correlate linearly with DNA content and their gene expression is relatively stable compared to diploid cells. This indirectly supports the notion that different ploidy hepatocytes may have distinct functions.

2.5.3 Polyploidy and liver cancer

Nearly 30% of solid tumours have polyploid or near-polyploid karyotype [443, 444]. The human adult liver in normal physiology is polyploid. However, if hepatocyte polyploidy has a role in liver cancer is not clear. The most widely accepted theory is that liver polyploidy functions as a tumourigenesis gatekeeper [445]. Recently, Zhang et al. reported tumour suppressive roles of polyploid hepatocytes in the mouse liver using *Anln*, and *E2f8* knockdown (KD) mouse models [446]. KD of *Anln*, an actin-binding protein required for cytokinesis, results in increased polyploid hepatocytes, while KD of *E2f8*, which is required for liver polyploidization, leads to increment in diploid hepatocytes. The authors observed that *Anln* KD mice, when challenged with cancer-inducing agents, show a significant reduction in tumour incidence compared to *E2f8* KD mice indicating that polyploidy can aid in tumour prevention. On the same line, Wister rats treated sequentially with different carcinogens, diethylnitrosamine and 2-acetylaminofluorene, underwent hepatocarcinogenesis and their livers contain mainly diploid hepatocytes compared to controls which were mainly polyploid [447, 448]. These rodent data suggest that polyploidy plays a protective role in tumourigenesis.

However, in humans, the relationship between polyploidy and hepatocellular carcinoma (HCC) is inconclusive. One study using HCC biopsy samples showed that there is a decrease in polyploid hepatocytes and an increment in diploid cells

compared to controls. In the same experiment, mir-122, which has tumour-suppressive roles, was also found to be downregulated in the HCC samples. It is important to note that mir-122 is essential and sufficient for polyploidization in mouse liver and found to be downregulated in HCC patients [449],110-112]. Therefore, downregulation of mir-122 may be responsible for lesser polyploidization in HCC. Similarly, another study with HCC patients reported increased diploid hepatocytes and reduction in polyploid hepatocytes in carcinoma while the surrounding liver tissue ploidy remained normal [450]. However, in a recent report, Bou-Nader et al. found that the binucleate polyploid fraction (cellular ploidy) has significantly decreased (5 percent in tumoural tissues versus 15 percent in normal tissues), whereas the mononucleate polyploid fraction (nuclear ploidy) has increased (33% in tumoural tissues versus 12% in normal tissues) in surgically resected tissues from HCC patients [451].

2.5.4 Polyploidization as a mediator for genetic diversity

Polyploidy in itself can contribute to genetic diversity [452]. Moreover, as stated earlier, hepatocytes increase their DNA content by polyploidization (using cytokinesis failure) and decrease through ploidy reversal (using reductive mitosis) [432, 453, 454]. It has been shown that chromosome segregation errors occur when multipolar mitotic spindles are formed. In hepatocytes, this error leads to random whole-chromosome gains and/or losses forming aneuploid hepatocytes [432, 453]. This relationship between polyploidy, ploidy reversal and aneuploidy has been explained in the “ploidy conveyor” model proposed by the Duncan group [455]. However, the degree of aneuploidy in hepatocytes has been hotly debated. High rates of chromosome segregation defects and approximately 60 percent of aneuploidy were discovered in proliferating polyploid hepatocytes in primary mouse culture [432, 456]. On the other hand, single-cell sequencing of hepatocytes in mouse and human liver tissues showed

only a fraction (~5%) of cells exhibits aneuploidy which is comparable to aneuploidy levels in other body tissues [457].

Grompe et al. developed a multicolor reporter allele system that allows genetically marking and monitoring of mouse polyploid hepatocytes *in situ* [458]. They demonstrated that the polyploid hepatocytes repair wounded livers when undergoing ploidy reduction [459]. Ploidy-depleted progenies multiply and maintain their capacity to increase ploidy content. They also discovered that chromosome segregation during ploidy reduction is not random. Taken together, these findings suggest that hepatocytes can change their ploidy status and as a consequence help in mediating genetic diversity in the liver under normal physiological conditions.

2.5.5 Polyploidization during fatty liver disease

Polyploidy profile also changes during metabolic disorders of the liver. Using non-alcoholic fatty liver disease (NAFLD) model of ob/ob mice, and wild-type (WT) mice fed with a methionine-choline-deficient diet (MCD) or a high-fat diet (HFD), Gentric et al. discovered an increment in highly polyploid hepatocytes in the fatty liver parenchyma [460]. The same study also observed a similar pattern of polyploidy in biopsies of patients suffering from non-alcoholic steatohepatitis (NASH) [460]. In primary cultures, NAFLD hepatocytes advanced through G1 to S-phase, but their departure from the S phase was delayed, and they get arrested in the G2 phase. Moreover, the authors reported that oxidative stress stimulates the emergence of highly polyploid cells by demonstrating that NAFLD hepatocytes treated with antioxidants restored normal cell division and returned to a physiologically normal polyploidy level. These findings suggest that pathological polyploidization may play a key role in NAFLD.

2.6 Hypothesis and objectives:

One direct consequence of polyploidy is that it increases the copy number of the genes and may lead to higher gene expression. This increase in expression may be beneficial considering the high metabolic output of the hepatocytes. Moreover, as detailed in section 2.5, polyploidy have been shown to have some impact on liver. For example, polyploidy improves genetic diversity in hepatocytes, polyploid hepatocytes have fewer transcriptional bursts, polyploidy have been shown to play tumour suppressive roles in rodent livers, and polyploid hepatocytes have reduced proliferation rate, etc. It is well-established that the polyploidization of hepatocytes is maintained in the adult liver and several liver anomalies are associated with changes in ploidy profile. These observations suggest that liver polyploidy is important for normal liver functioning.

Therefore, we hypothesize that polyploid hepatocytes have functional significance with different ploidy populations serving different functions in the adult liver. These functional differences can be investigated by studying differential gene expression patterns and gene regulatory mechanisms in different ploidy hepatocytes. To explore our hypothesis, we have set the objective to investigate differential gene expression in different ploidy hepatocytes and explore the pathways upregulated in each ploidy hepatocytes. To achieve our objectives, we used the following strategy as shown in figure 2.2 below:

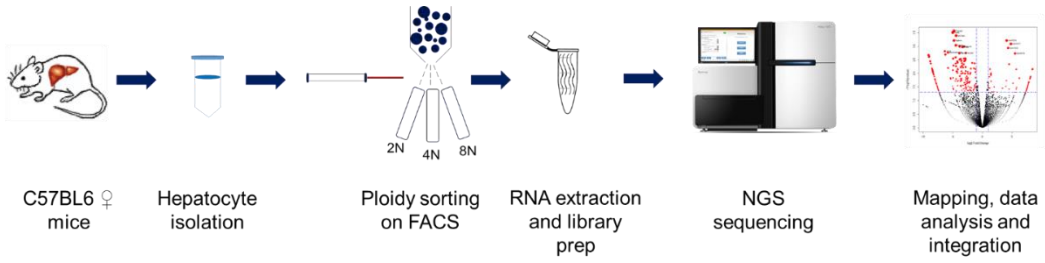

Figure 2.2: Strategy to isolate different ploidy mouse hepatocytes and study their gene expression using RNA-seq.

2.7 Materials and Methods:

2.7.1 Liver perfusion and hepatocyte isolation

Animal: C57BL/6 female mice were used for all the experiments. For RNA-seq experiments of with different ploidy hepatocytes, we used 8-week and 32-week-old mice. Mice were housed in a temperature-controlled facility with a 12/12 hour light on-and-off cycle with ad libitum feeding. All animal studies were carried out according to the IACUC (Institutional Animal Care and Use Committee) approved protocol (Protocol # 151054- Improvement of liver regeneration, Genome Institute of Singapore, Singapore, PI- Torsten Wuestefeld).

Different ploidy populations of hepatocytes were isolated from mouse liver using two-step collagenase-based perfusion following the IACUC (Institutional Animal Care and Use Committee) approved protocol (Protocol # 151054- Improvement of liver regeneration, Genome Institute of Singapore, Singapore, PI- Torsten Wuestefeld). Briefly, the mouse was anaesthetized by intraperitoneal injection of Ketamine and Xylazine (150 mg/kg body weight of Ketamine and 10mg/kg body weight of Xylazine) and the pedal reflex was monitored to assess their consciousness state. Following anaesthesia, a superficial incision was made through the skin of the lower abdomen. The cannula was inserted into intrahepatic vena cava and perfusion was performed for 10 minutes at a 2.5 mL/min flow rate with pre-warmed Liver Perfusion Medium (Thermo Fisher Scientific, cat # 17701-038). The inferior vena cava was clamped above the diaphragm and the hepatic artery was then incised to allow the blood to flow out. Next, the liver tissue was enzymatically digested by perfusing the pre-warmed Liver Digestion Medium (Thermo Fisher Scientific, cat # 17703-034) for 10 minutes at a flow rate of 2.5 mL/min. The enzymatically digested liver was aseptically transferred to a 10-cm petri dish containing 10 mL of cold Hepatocyte Wash Medium (Thermo

Fisher Scientific, cat # 17704-024). Using sterile forceps and scissors, the liver tissue was mechanically shredded into smaller chunks and filtered through a 100 µm cell strainer (BD Biosciences, cat # 352360). The cell strainer was washed twice with 10 mL Wash Medium to recover the maximum number of liver cells. The cell suspension containing viable liver cells was centrifuged at 50 x g for 5 min at 4 ºC. The supernatant was discarded and the liver cell pellet was processed for hepatocyte purification.

2.7.2 Removal of red blood cells (RBCs)

The cell pellet was resuspended in 25 mL of RBC lysis buffer (155 mM NH_4Cl, 12 mM $NaHCO_3$ and 0.1 mM EDTA and final pH adjusted to 7.3) and incubated for 10 min at room temperature (RT). The cell suspension was centrifuged at 50 x g for 5 min at 4 ºC and the cell pellet was resuspended in 30 mL of Hepatozyme–SFM (Thermo Fisher Scientific, cat # 17705-021). The number of viable hepatocytes was counted using a hemocytometer. Routinely, we recovered around 30-40 million cells from each mouse liver.

2.7.3 Hepatocyte staining for sorting based on ploidy

Cell permeable Hoechst 33342 dye (Sigma-Aldrich cat # B2261) was used to stain nuclear DNA for sorting the perfused hepatocytes based on the genome content. Additionally, reserpine (Sigma-Aldrich cat # 83580) was used to stop the efflux of Hoechst 33342 dye by viable hepatocytes. Reserpine blocks the ABCG2 drug transporters which act as the efflux pump in hepatocytes for excluding the dye from the cells. For staining, the hepatocyte suspension was first diluted to a concentration of 1 million cells/mL. Hoechst 33342 (final concentration 10 µg/mL) and reserpine (final concentration 5 mM) were added to the cell suspension and incubated at 37 ºC for 60 min in a shaking incubator at 150 rpm. After incubation, the cell suspension was

washed and resuspended in 1X Phosphate Buffered Saline (PBS) and sorted using FACS.

2.7.4 Sorting of hepatocytes

BD FACSAria Fusion cell sorter with 130 µm nozzle was used for sorting hepatocytes at the SIgN Flow Cytometry Platform at A*STAR, Singapore. Following gating strategy was used for sorting of hepatocytes of different ploidy: FSC-A vs SSC-A (voltage optimization to gate the maximum number of desired populations), FSC-W vs FSC-H (for doublet exclusion), and SSC-W vs SSC-H (for doublet exclusion), as well as histogram of count vs BV-421-A (for identification 2N, 4N and 8N peaks). Liver cells from an individual mouse were sorted to obtain different ploidy populations for a particular experiment and each ploidy population was collected in a separate 1.5 mL tube containing 200 µL of cold 1X DPBS (Dulbecco's phosphate-buffered saline). The sorted cells were centrifuged at 10,000 x g for 5 min at 4 ^{o}C, supernatants were discarded, and cell pellets were immediately placed on dry ice before transferring them to -80 ^{o}C freezer for storage.

2.7.5 RNA extraction

Total RNA was extracted from different ploidy populations of hepatocytes using ReliaPrep RNA Cell Miniprep kit (Promega, cat # Z6010) following the manufacturer's protocol. Briefly, frozen cell pellet was first thawed on ice. For cell lysis, 500 µL BL + TG buffer was added to the tube and the cell suspension was repeatedly passed through 1 mL syringe. Next, 170 µL of isopropanol was added to the tube and vortexed briefly for 5 sec. ReliaPrep minicolumn was assembled in the collection tube and the lysate was transferred to the minicolumn, centrifuged at 14,000 × g for 30 sec at RT, and the flow-through was discarded. ReliaPrep™ minicolumn was then washed with 500 µL of RNA wash solution and centrifuged at 14,000 × g for 30 sec at RT. The flow-

through was discarded and the minicolumn was transferred back to the collection tube. For removal of residual genomic DNA contamination, 30 µL of DNase I solution (prepared in yellow core buffer containing $MnCl_2$) was directly added to the membrane of the minicolumn and incubated for 20 min at RT. After the incubation, 200 µL of column wash solution was added and centrifuged at 14,000 x g for 30 sec at RT and the flow-through was discarded. Following that, 500 µL of RNA wash solution was added to the minicolumn and centrifuged at 14,000 x g for 30 sec at RT. Next, ReliaPrep minicolumn was transferred into a new collection tube and 300 µL of RNA wash solution was added and centrifuged at 18,000 × g for 2 min at RT. The minicolumn was then placed into an elution tube and 30 µL of nuclease-free water was added and incubated for 5 min at RT. The minicolumn was centrifuged at 18,000 x g for 5 min at RT and the eluate containing total RNA was collected. The concentration of total RNA was measured on a Qubit 3 Fluorometer (Invitrogen, cat # Q33216) using Qubit RNA HS assay kit (Thermo Fisher Scientific, cat # Q32852). RNAs from different samples were transferred to the -80 ^{o}C freezer for storage until further use.

2.7.6 RNA sequencing

We processed RNA samples for RNA-seq library preparation which have DV200 values of >85%. The DV200 quality metric can be defined as the percentage of RNA fragments>200 nucleotides in size. Paired-end library for RNA-seq was prepared by a third-party service provider from total RNA using TruSeq Stranded Total RNA kit (Illumina) with Ribo-Zero Mouse kit based on TruSeq stranded total RNA sample preparation guide (part #15031048 rev. E). We have also added the ERCC RNA spike-in mix (Invitrogen cat # 4456740) in the sequencing libraries. RNA-seq libraries were sequenced on Illumina Novaseq 6000 platform with 2 x 151 bp multiplex protocol for

32-week-old sorted hepatocyte samples whereas 8-week-old sorted hepatocyte samples were sequenced on Illumina HiSeq 4000 platform with 2 x 151 bp protocol.

2.7.7 RNA-seq data analysis

The data analysis can be broadly divided into three stages- alignment of sequencing reads to the mouse reference genome, counting of reads to genomic features (genes), and downstream analyses such as identification of DEGs, data clustering, etc.

Read alignment: We used STAR 2.5a (Spliced Transcripts Alignment to a Reference) package [461] to align RNA-seq fastq files to the *Mus musculus* reference genome GRCm38 (mm10). There are two stages in the STAR workflow – generation of genome index files and mapping reads to the genome.

Generation of genome index files: We downloaded reference genome sequence FASTA file and GTF files containing gene annotations for mm10 version from GENCODE (version M19). FASTA and GTF files for ERCC (RNA spike-in) were appended to the GENCODE files and used for generating genome index using default commands.

Mapping reads to the genome: The genome index generated in previous step is used for mapping RNA-seq fastq files to the mouse reference genome (mm10) using default commands.

Read assignment: The mapped reads obtained from STAR were assigned to genes using the featureCounts package [462]. In simple term, using featureCounts package, we determine the number of reads uniquely mapped to each gene. We used the same GTF file which was used to generate STAR index for read alignment. The mapped reads were annotated with mouse Ensemble gene IDs using awk command.

Read filtering for low expressed genes: Genes with very low (<10) raw reads are generally filtered out from RNA-seq analysis to exclude ‘noise’ or artefacts. For read

filtering, we created a data frame with raw read counts file. Using this data frame, we selected those genes that have ≥10 raw read counts in at least one dataset and the rest were filtered out.

Read normalization: After read filtering step, the mapped reads were normalized for sequencing depth using R package EDAseq [464] employing the “between lane normalization” function. The normalized values were used for designing matrix and measuring of dispersion by edgeR [463].

Principal component analysis (PCA): PCA is widely used for dimensionality reduction, where each data point is projected onto only the first few principal components to produce lower-dimensional data while maintaining as much variance as possible. The first principal component can be characterized as a path that maximizes the projected data's variance. The i^{th} principal component maximizes the variance of the predicted data in a direction orthogonal to the first i-1 principal components. The data was normalized and plotPCA command from R package edgeR [463] was used to plot PCA.

Differential gene expression analysis:

The edgeR [463] package from R was used to identify DEGs between samples. The default TMM (trimmed mean of M values) normalization method was used to calculate the effective library size and to avoid RNA composition bias, which is caused by highly abundant transcripts. Calling of DEGs was performed using edgeR’s generalized linear model (glm) functionality using a pair of samples.

Pathway analysis:

We performed differential pathway analysis using gene set enrichment analysis (GSEA) [465] to identify pathways differentially regulated in different samples based on edgeR normalized counts. In brief, we used the GSEA desktop application. The

expression datasets and phenotype labels were formatted based on the instructions (http://software.broadinstitute.org/cancer/software/gsea/wiki/index.php/Data_formats) . We selected Reactome MSigDB gene set for this analysis with default 1000 permutations. Mouse gene symbols were first converted to human orthologues using GSEA inbuilt mouse to human annotations. We used log2 ratio of classes as the metric for ranking genes keeping other parameters at default settings to identify differential pathways.

Transcripts per million (TPM) computation:

Transcripts Per Million (TPM) means that "for every 1,000,000 RNA molecules in the RNA-seq sample, “x” came from this gene/transcript”. TPM is a normalization method for RNA-seq and therefore the biases from different number of reads can be neglected using TPM based normalisation.

The steps to calculate TPM are as below:

1- Calculating the normalized transcript-level expression (reads per kilo bases):

   For each transcript in the gene model, the number (raw count) of reads mapped is divided by the transcript's length which is further divided by 1000, giving a normalized transcript-level expression.

2- Calculating the scaling factor (per million scaling factor):

   The sum of ALL normalized transcript expression values is divided by 1,000,000, to create a scaling factor.

3- Calculating TPM:

   Each transcript's normalized expression is divided by the scaling factor, which results in the TPM value. Gene-level TPM's are calculated by summing up the transcript-level TPM for each gene. In this scaling, the sum of all TPMs (transcript-level or gene-level) should always equal 1,000,000. For cells that have

approximately the same number of transcripts-per-cell, the TPM expression values can be compared between these cells to estimate relative abundance.

We used TPM normalization describing average gene expression using the following script in R language:

```
getTPM <- function(readCounts,geneLength)
{       reads_per_kilo_bases<-readCounts/(geneLength/1000)
        per_million_scaling_factor<-as.numeric(sum(reads_per_kilo_bases)/1000000)
        transcript_per_million<-reads_per_kilo_bases/per_million_scaling_factor
        return(transcript_per_million)
}
```

where, readCounts is the raw read counts of the gene and geneLength is length of the corresponding gene in bp. **Average gene expression**

After TPM is calculated, we determined the average TPM for replicate 1 and replicate 2 of each sample and calculated log2 for each average TPM value.

For example, 8W_2N = log2(average(TPM_8W_2N_R1 and TPM_8W_2N_R2))

where, 8W_2N is the average gene expression of both replicates of 2N hepatocytes from 8-weeks old mouse, TPM_8W_2N_R1 is the TPM value of replicate 1 of 2N samples from 8-weeks old mouse and TPM_8W_2N_R2 is the TPM value of replicate 2 of 2N samples from 8-weeks old mouse.

We then used R package beanplot to plot the gene expression distribution of each sample. The lines going through middle of beans represents the average gene expression for samples.

2.7.8 Ploidy profile analysis of diet-induced NASH mice

To investigate alteration of ploidy profile during the progression of NAFLD, we established a diet-induced NASH mouse model by feeding the mice with CDHFD

(Choline deficient L-amino acid defined high fat diet with 0.1% methionine (ResearchDiets, cat# A06071302i). In brief, 6-week- old C57/BL6 female mice were fed with CDHF diet for 3 months for NASH development and the age-matched control animal was fed with normal chow for the same interval. We isolated the hepatocytes from mice using two-step collagenase-based perfusion as detailed in section 2.7.1. We removed the RBCs using RBC lysis buffer as detailed in section 2.7.2 and stained the hepatocytes with Hoechst 33342 for 60 minutes before estimating the ploidy profile on flow cytometer (as described in section 2.7.3).

2.7.9 Ploidy specific gene expression analysis of NAFLD associated genes

We manually curated 200 genes involved in NAFLD from human patient studies published earlier [169-171]. The curated gene list was provided in appendix 2. We used g:Profiler's orthology search option (g:Orth) to find the mouse orthologous genes to these NAFLD associated human genes [466]. Next, from the orthologous gene list, we filtered out genes whose expression is low in our datasets with following criteria: Only those genes with raw reads counts are greater than or equal to 10 in at least one of the ploidy samples will be considered for analysis. After this filtering step, we analysed the expression of 141 genes in our ploidy-specific RNA-seq data.

Hierarchical clustering of NAFLD associated gene in different ploidy hepatocytes

We used IDEP 0.91 to perform hierarchical clustering with heatmap [48]. The transformed data is used by IDEP to rank all genes by standard deviation across all samples. Hierarchical clustering is performed on genes using the heatmap.2 function in R. The samples can be re-odered in the heatmap based on the distance matrix 1-r where r is the Pearson's correlation coefficient calculated using R function cor().

2.8 Results

2.8.1 Hepatocyte ploidy profile changes with age

We performed two-step collagenase-based perfusion to isolate hepatocytes. We stained the hepatocyte with 0.4% tryphan blue and visualized them under the bright-field microscope. As expected, we found that the perfused hepatocytes have different cell sizes. The cell sizes are also positively correlate with nuclear sizes (nuclear ploidy). Moreover, these hepatocytes also exhibit cellular ploidy with one (mono-nucleated) or two nuclei (bi-nucleated) per cell **(Figure 2.3A)**. Next, we estimated the age-dependent changes in ploidy profiles using Hoechst 33342 stained mouse hepatocytes from different age groups (4 to 63-week-old). The ploidy profiles showed an age-dependent increment in higher ploidy populations (**Figure 2.3B and Table 2.1**). For example, 4-week-old mouse has 30.58% of 2N, 62.14% of 4N and 7.28% 8N hepatocytes. Gradually, the number of higher ploidy hepatocytes increases with age and by 63 weeks, mouse liver has 11.39% of 2N, 23.22% of 4N, 58.15% of 8N, 6.69% of 16N and 0.55% of 32N hepatocytes (**Figure 2.4**). All these percentages are computed based on manual gate selection in Flow-Jo software. The percentages were calculated in such a way that sum of percentages of all ploidy populations in a particular profile adds up to 100%.

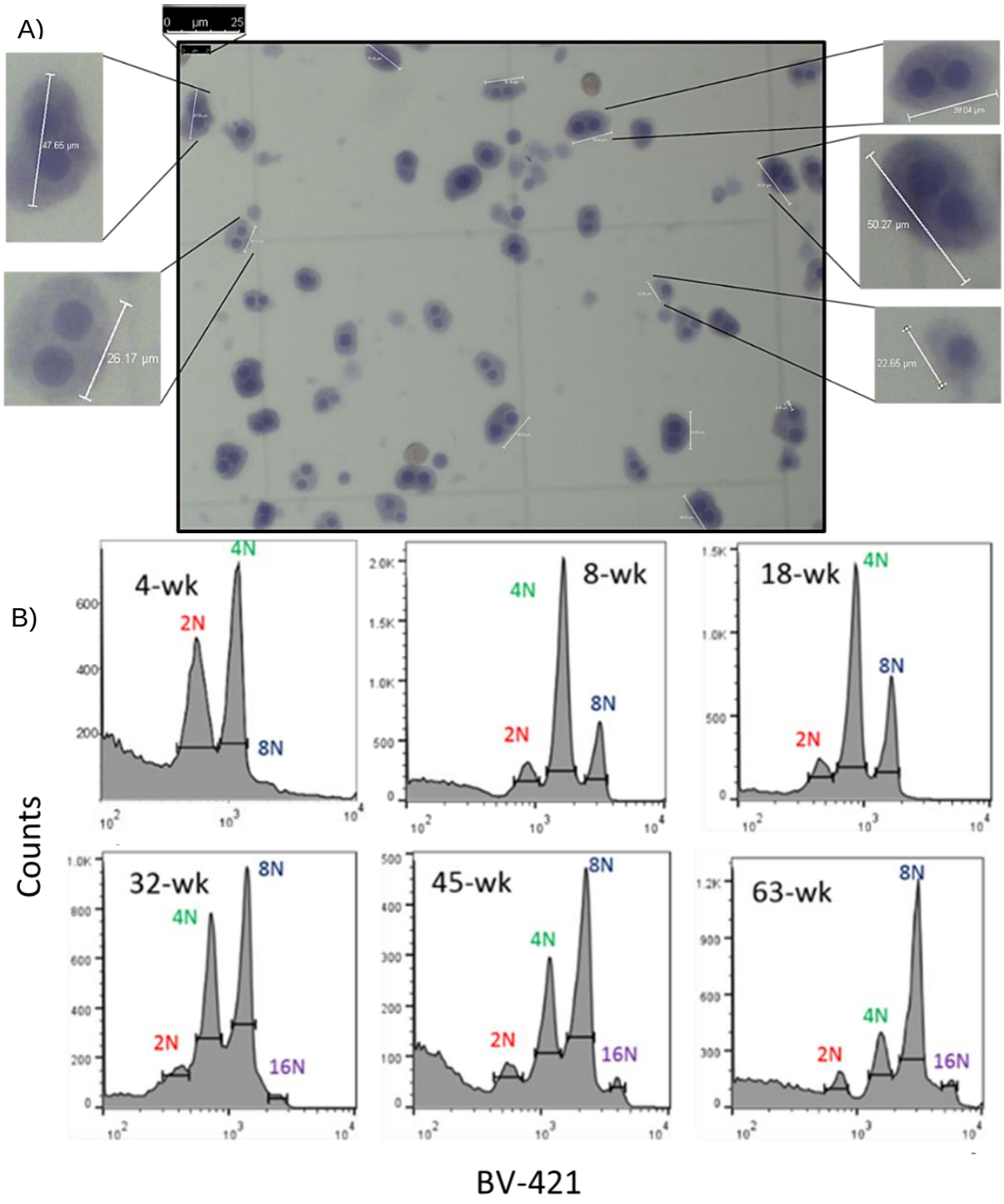

Figure 2.3 Hepatocytes ploidy changes with age A) 8-weeks-old mouse perfused liver hepatocytes stained with 0.4% tryphan blue. All images 20X magnification. Inset shows the hepatocytes of different cellular and nuclear ploidy. Scale bar 25 µm. B) FACS based ploidy profiles of mouse hepatocytes at different ages. X-axis sjows the DNA content (represented by BV-421 excitation based on Hoechst 33342 signals) and Y-axis represents counts. Diploid (2N), tetraploid (4N), octaploid (8N) and decahexploid (16N) populations are marked in different age hepatocytes.

Table 2.1: Age-dependent changes in ploidy profiles of mouse hepatocytes. Table shows mean percentage of different ploidy populations (based on multiple replicates) in different age groups of mice

Age	2N	4N	8N	16N	32N
4-wk	30.58252	62.13592	7.281553	0	0
8-wk	8.297384	69.04771	22.65491	0	0
18-wk	12.67725	55.16922	28.46587	3.687666	0
32-wk	9.526995	41.3524	43.46124	5.65936	0
45-wk	10.79137	30.57554	48.92086	9.71223	0
63-wk	11.39148	23.2218	58.14591	6.692265	0.548546

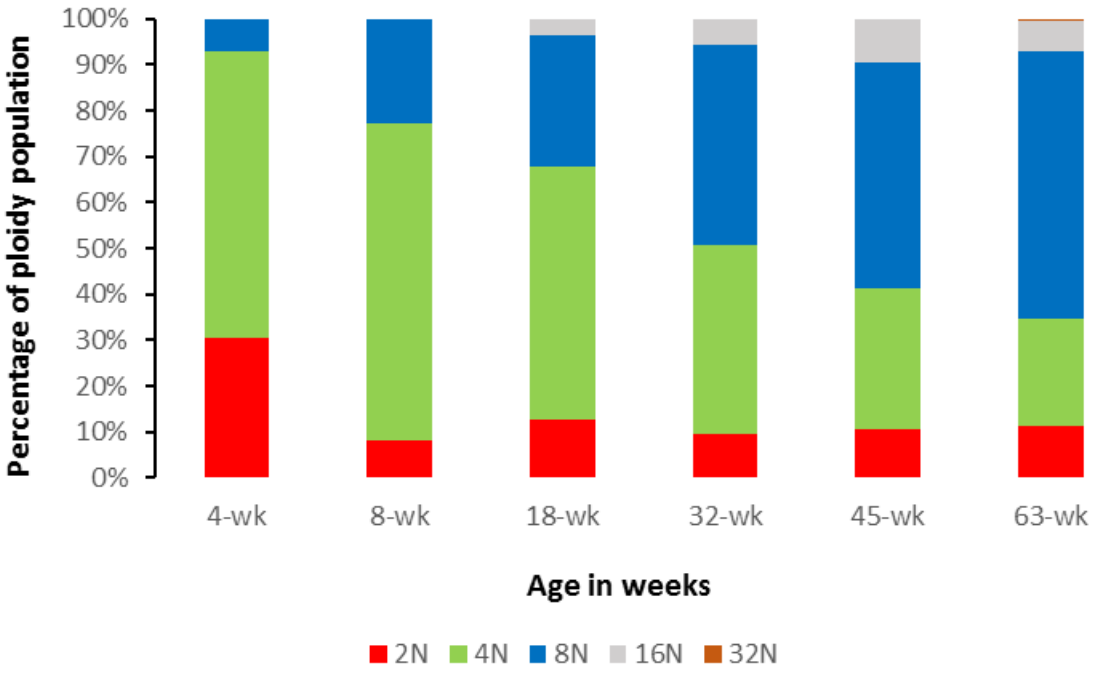

Figure 2.4: Histogram showing ploidy dynamics at different age mouse hepatocytes (based on Table 2.1). X-axis represents different age groups and Y-axis represents the percentage of ploidy in a certain age hepatocyte population. Different ploidy populations are colour coded in this figure.

2.8.2 Hepatocytes with different ploidy have different gene signatures

To understand ploidy-specific gene expression profiles, we performed RNA-seq analysis of FACS-sorted 2N, 4N, and 8N populations isolated from 8-week and 32-week mouse livers (**Figure 2.5**). We have used two biological replicates (n=2) for each age group and compared 2N, 4N and 8N hepatocyte populations isolated from same animal to avoid bias introduced by inter-animal variability. Ploidy profiles of 8-week and 32-week hepatocytes exhibit drastic changes. While majority of 8-week hepatocytes is 4N, 32-week hepatocytes have 8N population as the most abundant cells (**Figure 2.5 and Table 2.1**). It is worthy to mention here that female mice reach complete sexual maturity by 8 weeks to reproduce and by 8 months most females of inbred strains show decline in reproductive ability [467]. Therefore, our data can capture the comparative changes in female mouse liver in these two age groups. The read statistics of RNA-seq of different ploidy populations, including number of sequenced reads, alignment percentage, feature count statistics, etc., are provided in **Table 2.2**. We normalised the data to take care of the variability among samples. We performed PCA which simplifies data by geometrically projecting data onto smaller dimensions known as principal components (PCs), to obtain the best summary of the data with the fewest possible PCs [468]. The first principal component (PC1) explains the maximum variance in data, followed by second principal component (PC2) with second-highest variance which is uncorrelated to previous PCs, and so on, till the sum of all variances explained by PCs becomes 100% [469]. PCA between different ploidy populations of the same age (either 8-week or 32-week-old) revealed that variance in gene expression between diploid (2N) and polyploid hepatocytes (4N and 8N) is larger compared to variance between 4N and 8N hepatocytes along the PC1 axis **(Figure 2.6)**. Next, on comparing the polyploid hepatocytes (4N and 8N) of same age (either

8-week or 32-week-old), we observed the variance in gene expression between 4N and 8N hepatocytes in the PC2 axis **(Figure 2.6)**. Thus, each ploidy appears to have variation in gene expression when compared with other.

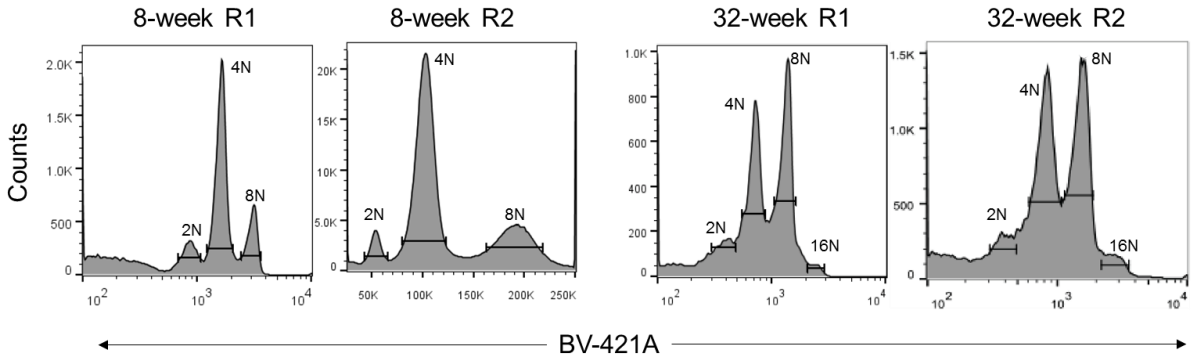

Figure 2.5: FACS profiles of two biological replicates (R1 and R2) of 8-week (left) and 32-week-old (right) mouse hepatocytes used in this study. BV-421 excitation shows DNA content based on Hoechst 33342 signals. 8-week R1 was acquired in linear scale while rest samples were acquired in log scale and analysed in FlowJo software.

Table 2.2: Read statistics of RNA-seq samples. Number of reads in each sample, the percentage of uniquely mapped reads to mouse reference genome (mm10) and number of counts assigned to genes in each sample were denoted.

Samples	#Reads (PE)	STAR uniquely mapped reads (%)	featureCounts assigned reads
2N_8-weekR1	48566976	72.58	24151050
4N_8-weekR1	49457118	65.92	19999571
8N_8-weekR1	49242538	70.71	24485543
2N_8-weekR2	41949080	64.29	15942133
4N_8-weekR2	44447705	66.07	19180538
8N_8-weekR2	40871933	64.15	17443551
2N_32-weekR1	51195121	72.39	25144956
4N_32-weekR1	51967417	82.14	28496994
8N_32-weekR1	50122960	83.33	27193150
2N_32-weekR2	44527448	68.3	24943820
4N_32-weekR2	48688120	90.19	37228507
8N_32-weekR2	50332110	89.15	37748358

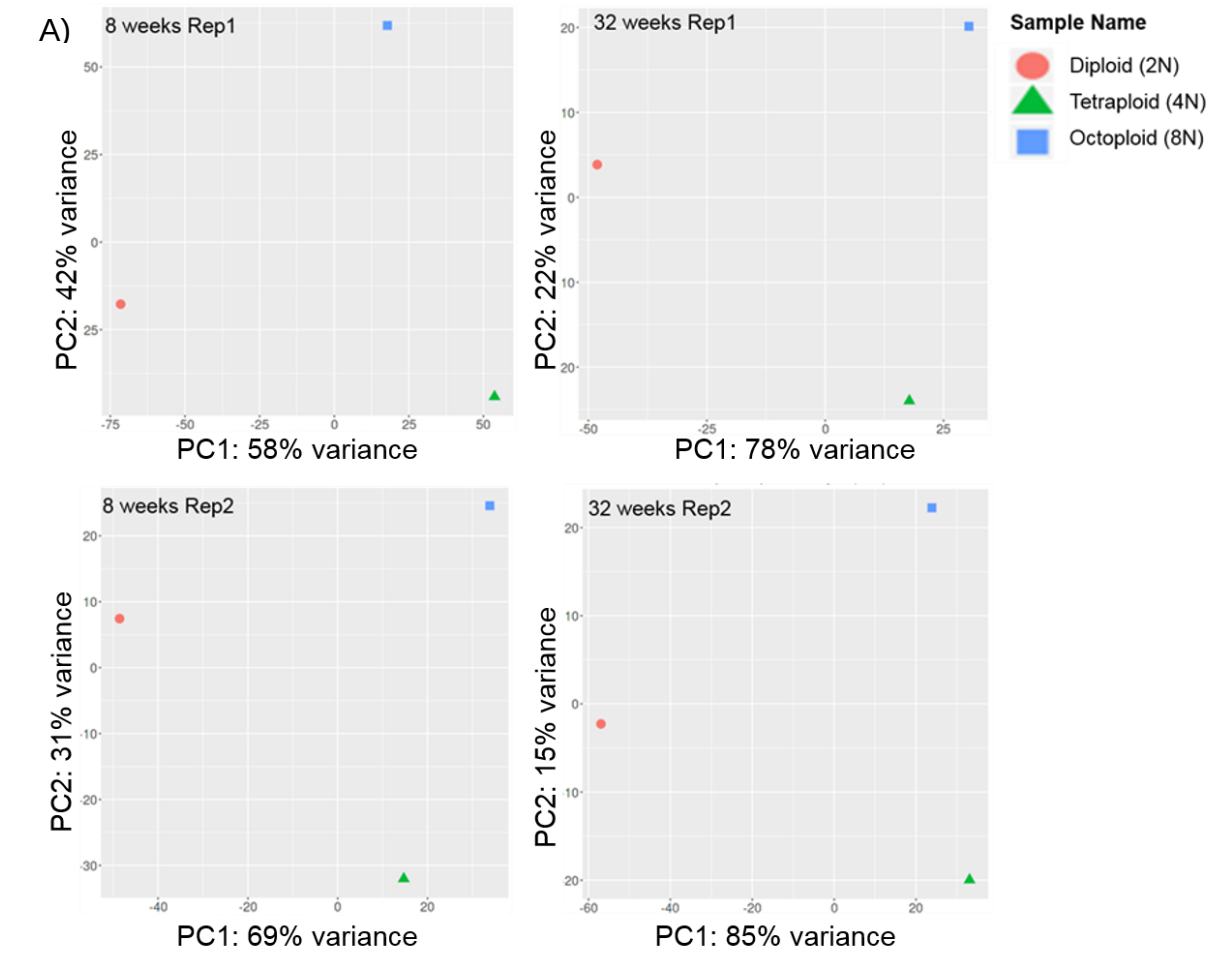

B)

Low

High

	2N_8W	4N_8W	8N_8W
2N_8W	1	0.959	0.957
4N_8W	0.959	1	0.981
8N_8W	0.957	0.981	1

	2N_32W	4N_32W	8N_32W
2N_32W	1	0.984	0.982
4N_32W	0.984	1	0.995
8N_32W	0.982	0.995	1

Figure 2.6: Gene expression profiles between different ploidy hepatocytes are different: a) PCA reveals that 2N, 4N and 8N hepatocytes are different from each other in both 8-weeks (left) and 32-weeks (right) hepatocytes b) Pearson correlations between different ploidy hepatocytes of 8-week (left) and 32-week-old (right) mouse livers.

Next, we computed the average normalized counts from two replicates of each ploidy population of the same age group and performed a Pearson correlation analysis. We found that for 8-week hepatocytes, the correlation coefficient between 4N and 8N is higher (0.981) compared to that of 2N and 4N (0.959) or 2N and 8N (0.957). Similarly, for 32-week hepatocytes, the correlation coefficient between 4N and 8N is higher (0.995) compared to that of 2N and 4N (0.984) or 2N and 8N (0.982) **(Figure 2.6B).** Thus, based on PCA and Pearson correlation analysis, we found that overall gene expression patterns between diploid and polyploid hepatocytes are different. Moreover, we also noted differences between gene expression of 4N and 8N hepatocytes. In conclusion, our RNA-seq datasets reveal that hepatocyte populations have differential gene expression signatures based on their ploidy.

2.8.3 Average gene expression between different ploidy hepatocytes

We estimated the average gene expression (in TPM) for each ploidy population. The bean plots of gene expressions in different ploidy populations showed an increment in average gene expression level in polyploid hepatocytes (4N and 8N) compared to 2N in 32-week mouse liver (Wilcoxon rank sum test; 2N vs. 4N p-value $<2.2 \times 10^{-16}$, and 2N vs. 8N p-value $< 2.2 \times 10^{-16}$). However, the variation in gene expression is negligible between diploid and polyploid hepatocytes in 8-week mouse liver (Wilcoxon rank sum test; 2N vs. 8N p-value = 0.092, and 2N vs. 4N p-value = 0.02) **(Figure 2.7)**.

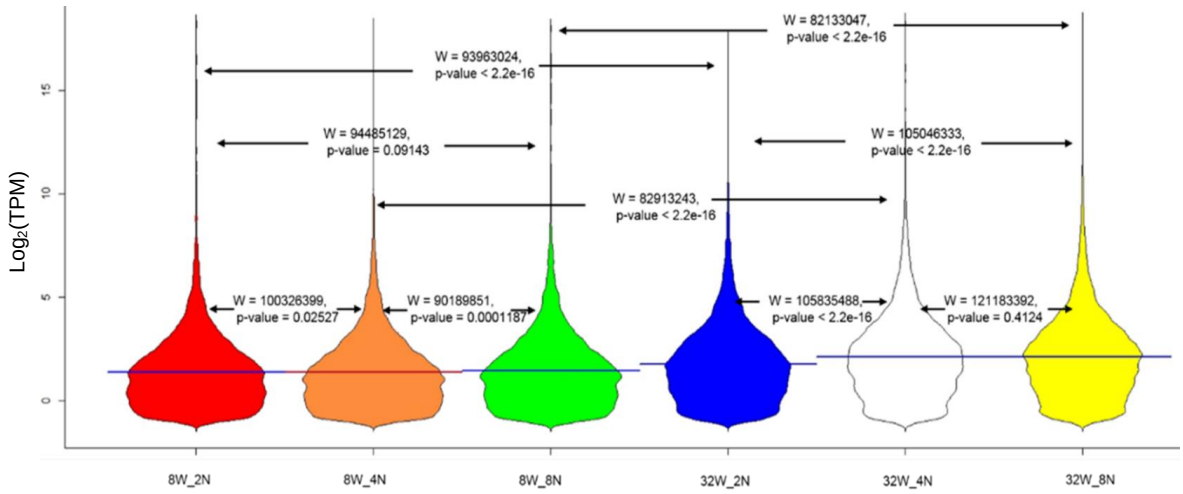

Figure 2.7: Bean plots of gene expression values (in log2 average TPM) of different ploidy hepatocytes in 8-week (left) and 32-week (right) mouse hepatocytes. Wilcoxon rank-sum test p-values are mentioned and W denotes sum of the ranks of the first sample. The lines going through middle of beans represents the average gene expression for samples.

2.8.4 Hepatocytes of different ploidy are enriched in different signalling/molecular pathways

We performed gene set enrichment analysis (GSEA) by combining the RNA-seq datasets of each ploidy population from 8-week and 32-week-old mouse livers to investigate the ploidy-specific differential pathways. We have chosen canonical pathway: Reactome gene set from the Molecular Signature Database for this analysis. We found several ploidy specific pathways. The list of pathways enriched in each ploidy population is provided in appendix 1. We have analysed our results from the perspective of differences between diploid (2N) and polyploid hepatocytes as well as differences between tetraploid (4N) and octaploid (8N). For the first analysis, we combined 2N hepatocytes from 8-weeks and 32-weeks together as one sample and polyploid hepatocytes (4N and 8N) from 8-weeks and 32-weeks together as second sample. For comparing 4N and 8N hepatocytes, we grouped 4N hepatocytes from 8-

weeks and 32-weeks together as one sample while 8N hepatocytes from 8-weeks and 32-weeks together as second sample.

The major findings from the comparative analysis between diploid and polyploid hepatocytes are discussed below.

Pathways enriched in polyploid cells compared to diploid hepatocytes

GSEA produces 419 pathways and after a p-value cutoff of ≤ 0.05, we obtained 208 pathways. Many of these pathways were related or part of a larger group. Therefore, we manually categorized related pathways based on their similarity in biological or molecular function. For example, pathways like FCERI mediated NF-κB activation, Dectin 1 mediated non-canonical NF-κB signalling, and Tnfr2 non-canonical NF-κB pathway is grouped under the NF-κB signalling. Following this manual categorization, we grouped important pathways into 19 classes that are enriched in polyploid hepatocytes compared to diploid cells (**Figure 2.8)**.

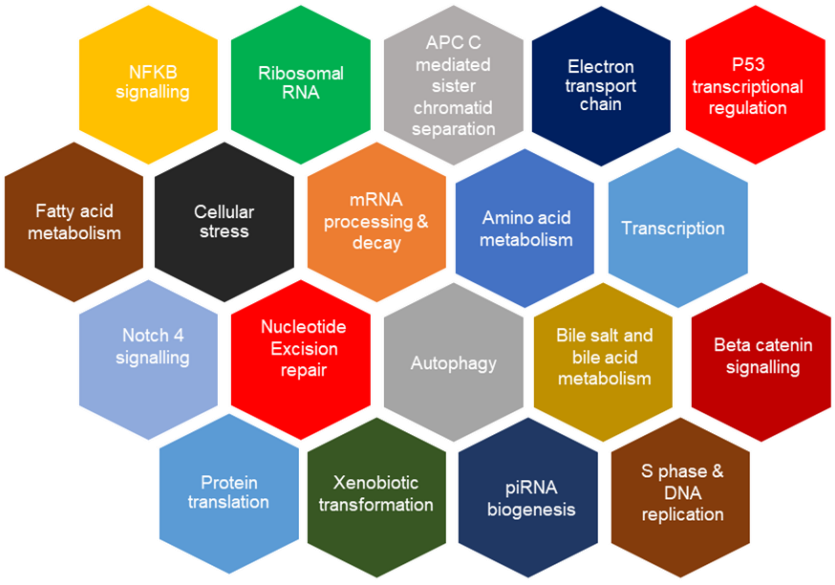

Figure 2.8: Reactome pathways enriched in polyploid hepatocytes compared to diploid hepatocytes.

<u>DNA replication, transcription, translational related:</u>

We observed that pathways related to DNA replication, transcription and mRNA processing are enriched in polyploid hepatocytes. Moreover, pathways related to amino acid metabolism are also observed in polyploid populations which were previously documented by Olga et al [423]. Additionally, we observed enrichment of many ribosomal RNA genes and protein translational pathways in polyploid cells. Taken together, these findings hint that DNA replication, gene transcription and protein translation may be heightened in polyploid hepatocytes. Our average gene expression analysis of different ploidy populations (except 2N vs. 8N in 8-week-old mouse livers which is not statistically significant) (**Figure 2.8**) also supports the findings of this pathway enrichment data. This suggests polyploid cells have relatively higher gene expression levels and possibly higher levels of mRNA processing than their diploid counterparts. The enrichment of DNA replication pathway in polyploid cells can be attributed to increment in genome content.

Detoxification, metabolism, beta-oxidation and electron transport chain:

One of the major roles of the liver is detoxification of xenobiotic compounds and bile metabolism. Polyploid hepatocytes are enriched in pathways related to detoxification and bile metabolism which supports the hypothesis that polyploidy aids or supports the high metabolic function of hepatocytes [359, 390, 470, 471]. We also found that pathways related to fatty acid metabolism, their beta-oxidation and mitochondrial electron transport chain are enriched in polyploid hepatocytes.

DNA repair, stress pathways, p53, NF-κB and Hedgehog signalling:

Strikingly, we found enrichment of DNA-repair pathways, especially NER (nucleotide excision repair) pathway. This increment could be due to increased DNA damage in polyploid hepatocytes which could be a result of enhanced levels of various kinds of

stresses in polyploid hepatocytes. In fact, we found enrichment of several cellular stress pathways in polyploid hepatocytes, such as hypoxia stress, chemical stress, stress due to starvation, replication stress, etc. The cellular stress can lead to stimulation of p53 transcription factor [472]. Consequentially, we observed pathways related to p53 based regulation of transcription and DNA repair to be activated in polyploid hepatocytes. Additionally, as discussed in section 2.4, the PIDDosome-p53 axis has been shown to regulate hepatocyte ploidy during postnatal liver growth [417]. Another transcription factor pathway, NF-κB (nuclear factor kappa-light-chain-enhancer of activated B cells) was found to be activated in polyploid hepatocytes. NF-κB has been associated with both hepatocyte proliferation and apoptosis and mice lacking the p65 subunit of NF-κB, die during gestation from hepatocyte apoptosis [473]. TNF-induced proliferation was blocked in hepatocyte cell lines when NF-κB was inhibited, and these cells were more susceptible to apoptosis [474, 475]. This highlights that though polyploidy hepatocytes are continuously challenged by cellular and DNA damages, they are protected from DNA-damage mediated apoptosis possibly through NF-κB mediated signalling. Another signalling pathway that was found to be enriched in polyploid hepatocytes is Hedgehog signalling. The Hedgehog pathway appears to be a vital regulator of adult liver repair during liver injury such as liver fibrosis and during regeneration [476-479]. Moreover, the Hedgehog signalling controls many elements of DNA repair [480, 481]. Taken together, the pathway analysis shows the likely presence of an active DNA repair machinery in polyploid hepatocytes.

Autophagy:

We found that pathways related to autophagy are upregulated in polyploid hepatocytes. Autophagy plays important roles in the liver, including the degradation of

cellular materials such as organelles and proteins, which helps in cellular homeostasis [482]. Change in autophagic potential of hepatocytes can result in many liver diseases [483, 484]. Autophagy might be up in polyploid hepatocytes as a helping mechanism against stress, as well as to remove degraded molecules and organelles [485].

Wnt/β-catenin and Notch signalling:

The wnt/β-catenin pathway is involved in many important functions including proliferative and pro-survival signalling [486]. Similarly, Notch signalling controls cell differentiation, cell fate determination, proliferation, and apoptosis in a variety of tissues during postnatal growth [487]. Downregulation of Wnt/β-catenin and Notch pathways in polyploid hepatocytes indicates that they have less proliferative potential compared to diploid hepatocytes, which is in line with the observation of Wilkinson et al. that polyploidy limits hepatocyte proliferation [404].

APC/C and piRNAs:

Another important factor enriched in polyploid hepatocytes is the anaphase-promoting complex/cyclosome (APC/C). APC/C is a multifunctional ubiquitin ligase that regulates many cellular processes including cell division, differentiation, genome stabilization, energy metabolism, cell death, autophagy, and carcinogenesis by ubiquitylating various substrates [488]. Cdc20 and Cdh1, two WD-40 domain proteins, are primarily responsible for APC/C activity. The activity of Cdh1 is known to regulate polyploidization [489, 490] which is a possible explanation for this observation. We also noticed that pathway related to the PIWI (P-element-induced wimpy testis) interacting RNAs (piRNAs) is also enriched in polyploid hepatocytes. The piRNAs play a role in genome stabilization by suppressing transposon activity, telomere protection complex assembly, RNA silencing, and epigenetic regulation of gene expression via

the creation of a repressive chromatin state [131, 491, 492]. Thus, piRNAs may play a role in maintaining genome integrity and stability in polyploid hepatocytes.

Pathways enriched in diploid cells compared to polyploid hepatocytes

GSEA produces 507 pathways and after a p-value cutoff of ≤ 0.05, we obtained 180 pathways. Many of these pathways were related or part of a larger group. Therefore, we manually categorized related pathways based on their similarity in biological or molecular function. Following the manual categorization, we grouped important pathways into 16 pathways that are enriched in diploid hepatocytes compared to polyploid hepatocytes.

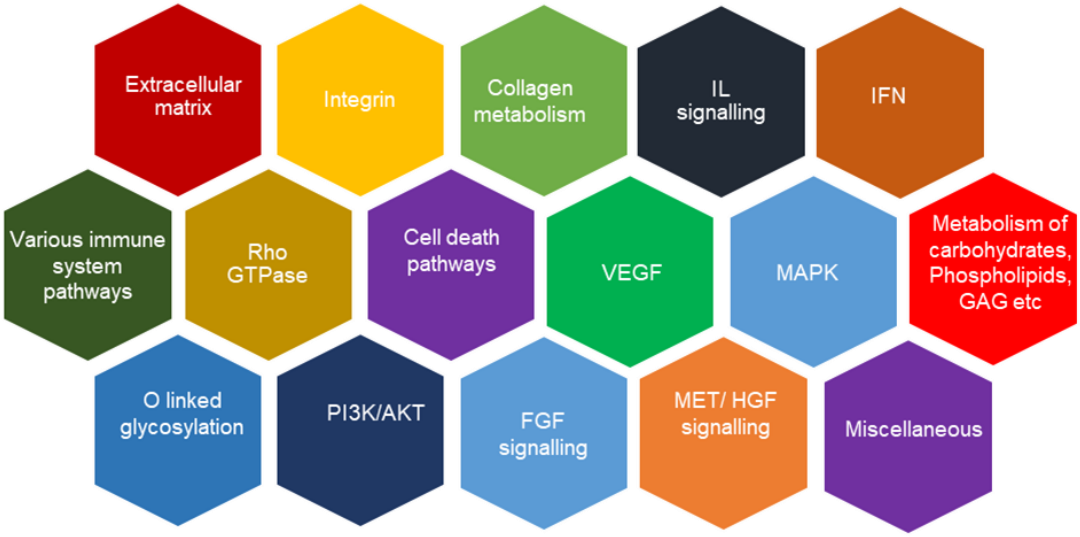

Figure 2.9: Pathways upregulated in diploid hepatocytes compared to polyploid hepatocytes.

<u>MET, PI3K/Akt, MAPK, VEGF and FGF signalling:</u>

Pathways related to hepatocyte growth factor receptor (HGFR) or c-MET were found to be enriched in 2N hepatocytes. Proliferation, motility, cell survival, morphogenesis, and angiogenesis are biological responses induced by MET activation [493]. HGFR/c-MET signalling stimulates several other pathways, including PI3K/Akt, MAPK, and

others [494-496]. We also found enrichment of pathways related to PI3K/Akt and MAPK in diploid hepatocytes as shown in figure 2.9. As mentioned in section 2.4, the PI3K-AKT pathway controls cytokinesis by regulating actin cytoskeleton reorganization at the cleavage plane [393]. On the other hand, MAPK regulates fundamental cellular processes such as proliferation, differentiation, motility, stress response, apoptosis, and survival by transmitting signals from cell surface receptors to the genome [497] and was found to be enriched in diploid hepatocytes in a 2017 study [440]. PI3K/Akt and MAPK pathways are involved in the regulation of vascular endothelial growth factor (VEGF) expression. Consequently, pathways related to VEGF were found to be enriched in diploid hepatocytes. Moreover, 2N hepatocytes were also enriched in fibroblast growth factor (FGF) signaling which governs liver specification and regulates lipid, cholesterol, and bile acid metabolism in mammals. FGF signaling also stimulates hepatocyte proliferation and aids in the detoxification of hepatotoxin during liver regeneration following partial hepatectomy [498, 499]. It has been described earlier that diploid hepatocytes have higher proliferation rate compared to the polyploid cells. Therefore, upregulation of proliferation pathways like MET, MAPK, and VEGF may play a role in higher proliferative potential of diploid hepatocytes.

Rho-GTPases:

We also observed enrichment of pathways related to Rho-GTPases in 2N hepatocytes. Rho-GTPases are important players in ensuring efficient cytokinesis by controlling the actin cytoskeleton organization and myosin II function at the cleavage plane [500-502].

Extracellular matrix components:

Pathways related to metabolism of extracellular matrix components, such as collagen, proteoglycans, laminin, etc., were found to be highly enriched in diploid hepatocytes. Diploid hepatocytes were also enriched in pathways related to metabolism of carbohydrates, phospholipids and glycosaminoglycan. We also observed different kinds of immune system-related pathways to be higher in diploid cells.

Overall, we observed that diploid and polyploid hepatocytes show differential enrichment of several Reactome pathways. This data corroborates with the PCA analysis which demonstrated variation in gene expression signatures between diploid and polyploid hepatocytes.

After investigating diploid versus polyploid hepatocytes, we performed GSEA analysis to identify differential pathways between 4N and 8N hepatocytes of 8-week and 32-week-old mouse livers.

Pathways enriched in 4N hepatocytes compared to 8N hepatocytes

GSEA produces 453 pathways and after a p-value cutoff of ≤ 0.05, we obtained 22 pathways. The following 12 important pathways were manually categorized which showed enrichment in 4N hepatocytes compared to 8N hepatocytes.

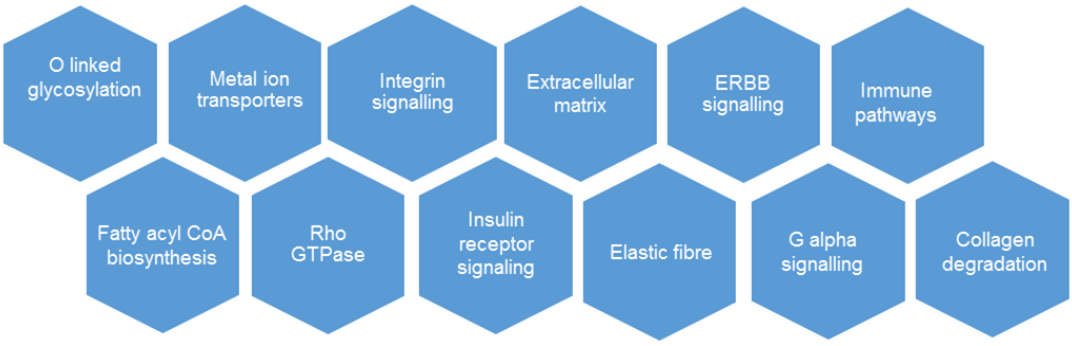

Figure 2.10: Pathways enriched in 4N compared to 8N hepatocytes

EGFR:

We observed that 4N hepatocytes are enriched in pathways related to epidermal growth factor receptor (EGFR), which is also called as erythroblastic oncogene B (ERBB) pathway. This signalling pathway has been described as a central player in the liver's response to injury from early inflammation and hepatocellular proliferation to fibrogenesis and neoplastic transformation [503]. EGFR activation is normally correlated with four major downstream pathways: Phospholipase C-gamma 1 (PLC1), Ras/MAPK, PI3K/Akt, and JAK-Stats (Janus kinase-signal transducer and activator of transcription) pathways [504] which are involved in various cellular processes. EGFR controls a variety of signalling processes like cell proliferation, cell motility, anti-apoptotic decrease, to epithelial-mesenchymal transition, upregulation of matrix metalloproteinases, and has even been proposed to be involved in stem-cell maintenance [505]. Notably, ERBB4 functions as a suppressor of HCC [506]. Moreover, ERBB3 and EGFR are necessary for CCl_4-induced liver fibrosis [507]. As discussed earlier, polyploid cells are known to play a tumour suppressive role in mouse hepatocytes and are found to be enriched during NASH. Whether 4N hepatocytes are drivers of these pathways needs further investigation.

Rho-GTPase and extracellular matrix:

Next, pathways related to Rho-GTPase and extracellular matrix protein including collagen and integrin are enriched in 4N hepatocytes. However, the functional consequences of enrichment of these pathways are currently not known.

Pathways enriched in 8N compared to 4N hepatocytes

GSEA produces 473 pathways and after a p-value cutoff of ≤ 0.05, we obtained 19 pathways. Many of these pathways were related or part of a larger group. Manual

categorization of important pathways yielded 17 pathways that were found to be enriched in 8N hepatocytes compared to 4N hepatocytes.

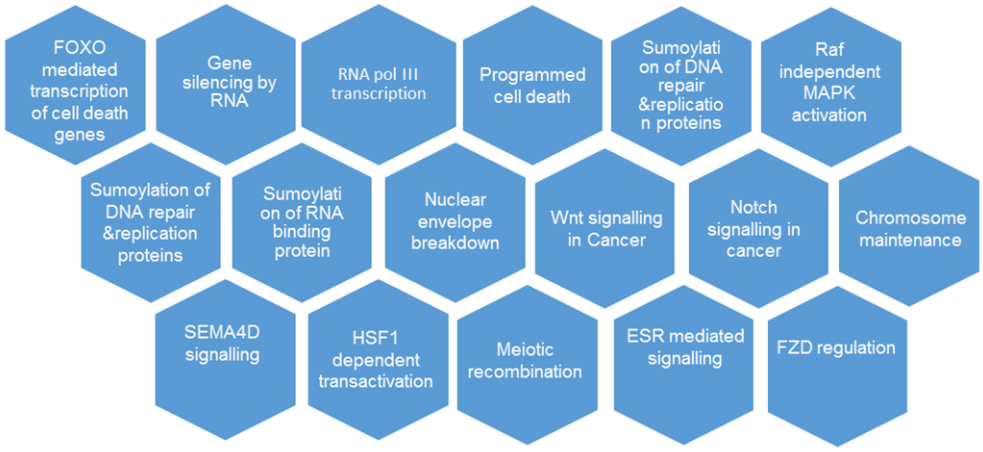

Figure 2.11: Pathways enriched in 8N compared to 4N hepatocytes

FOXO and Wnt signalling:

We noticed that 8N hepatocytes are enriched in Forkhead box O (FOXO)-mediated transcription of cell death gene pathway. FOXO transcription factors are downstream targets of the serine/threonine-protein kinase B (PKB)/Akt. FOXOs facilitate cell growth inhibition, cell cycle arrest and/or apoptosis [508]. Interestingly, FOXO can be activated by different stress pathways. We observed increment in stress response pathways, such as HSF1 (heat shock factor 1), DNA repair, chromosome maintenance, etc., in 8N hepatocytes indicating higher stress signalling in 8N hepatocytes compared to 4N possibly owing to its higher genomic content. We observed that 8N hepatocytes are enriched in Wnt (and Frizzled), Notch and estrogen receptor signalling pathways which indicates that 8N hepatocytes may have better proliferation potential compared to 4N hepatocytes. However, there is no experimental evidence to support this notion.

Overall, we observed that specific molecular and biological pathways are enriched in each ploidy population.

2.8.4 Differential gene expression analysis between different ploidy hepatocytes

We identified several hundred DEGs ($Log_2FC \geq 1$ & p-value ≤ 0.05) between hepatocytes of different ploidy populations isolated from 8-week and 32-week-old mouse livers using edgeR. Intriguingly, we found that there are far more DEGs between diploid and polyploid hepatocytes compared to between two polyploid populations (4N and 8N) (**Figure 2.12)**. For 8-week data, the number of DEGs between 2N and 8N is 1391 and between 2N and 4N is 1360 whereas the number of DEGs between two polyploid populations (4N and 8N) is 621. Similarly, for 32-week data, the number of DEGs between 2N and 8N is 722 and between 2N and 4N is 731 whereas the number of DEGs between 4N and 8N is 103 (**Figure 2.12)**. It is worthy to mention here that we observed a higher Pearson correlation in gene expression between polyploid hepatocytes (4N and 8N) compared to between diploids and polyploid cells in both age groups (**Figure 2.6)**. Therefore, our results revealed that gene expression patterns of polyploid hepatocytes (4N and 8N) are more similar when compared to their individual relatedness to diploid (2N) hepatocytes. Strikingly, we also observed that number of ploidy-specific DEGs decreases with age (8-week: 2N=989, 4N=268 and 8N=208 vs. 32-week: 2N=640, 4N=56 and 8N=29) (**Figure 2.12**). This observation may be interpreted in multiple ways. We know that polyploidy increases with age and transcriptional output of polyploidy hepatocytes are less noisy/stochastic compared to diploid hepatocytes and may express in a relatively steady-state manner [442], which may explain the reduction in DEGs with age. Another interpretation could be that 3D chromatin organization and epigenetic processes may be responsible for the age-dependent reduction in DEGs.

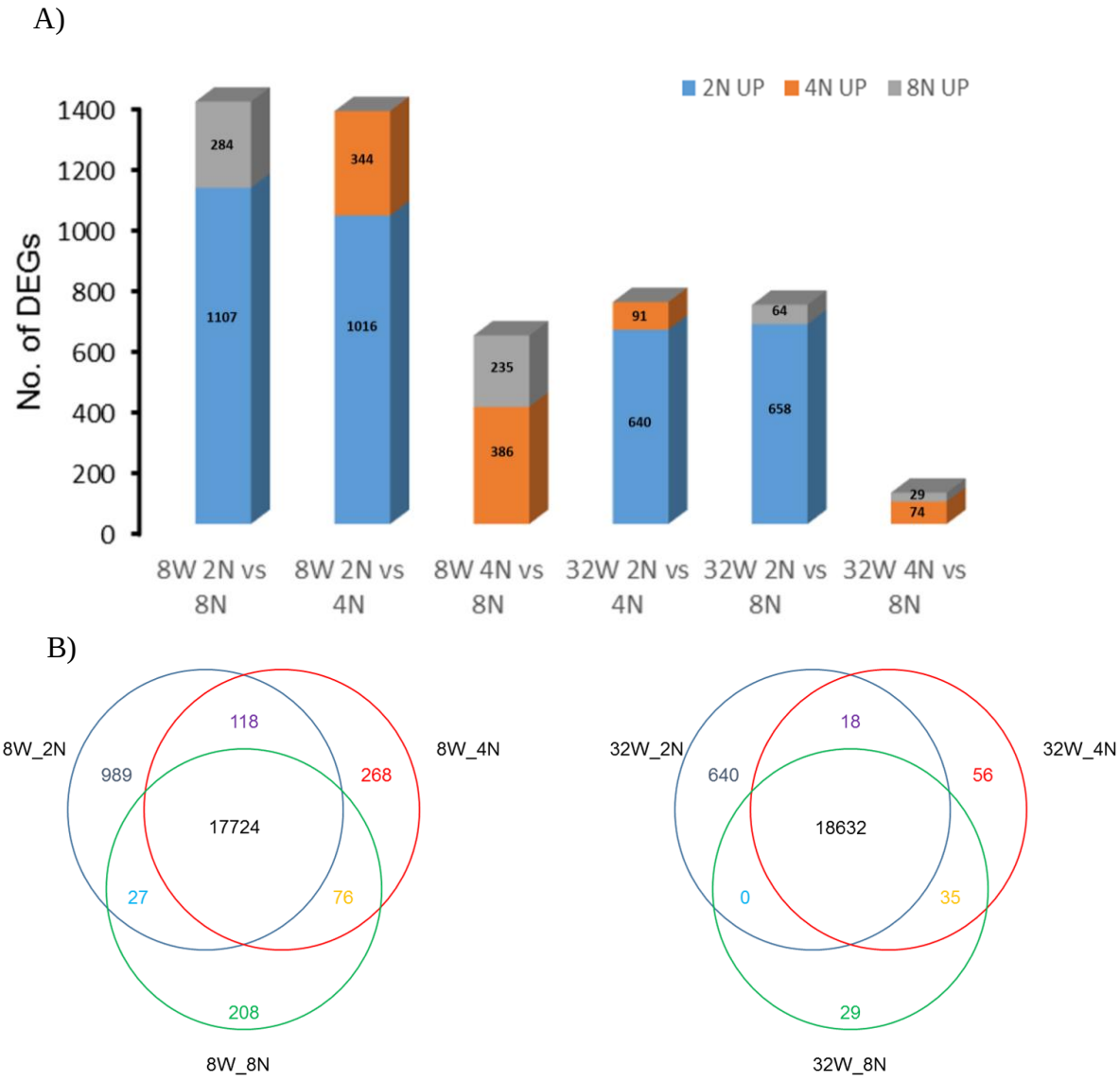

Figure 2.12: DEGs between different ploidy populations across 8-week-old and 32-week-old mice: A) Bar chart showing number of DEGs for each age-wise combination. B) 3-way Venn diagram showing DEGs for each age group (left: 8-week; right: 32-week).

2.8.5 Age is a major driver of gene expression

As shown in figure 2.6, gene expression signatures of polyploid and diploid hepatocytes are different in 8-week and 32-week-old mouse livers. However, when we combined 8-week and 32-week RNA-seq datasets and performed the PCA, we observed that age-related gene expression variation surmounted the ploidy-based gene expression variation (**Figure 2.13**). This is evident from figure 2.15, where PC1 accounts for 57% variation in the data. This variation can be explained by the difference in age of mouse livers in these datasets. Moreover, we found that along PC2 axis, the variation between 2N and polyploid cells is more as compared to between polyploid populations (4N and 8N) which reiterates our previous observation that gene expression between diploid and polyploid show higher variability than between polyploid populations. Additionally, we also observed that different ploidy populations from 32-week hepatocytes are relatively closer to each other (along PC2 axis) compared to 8-week hepatocytes of different ploidy. This corroborates with our observation that a higher number of DEGs was observed between 8-week hepatocytes compared to 32-week hepatocytes. Overall, this suggests that age imparts a stronger effect on hepatocytes gene expression pattern compared to ploidy-specific differences.

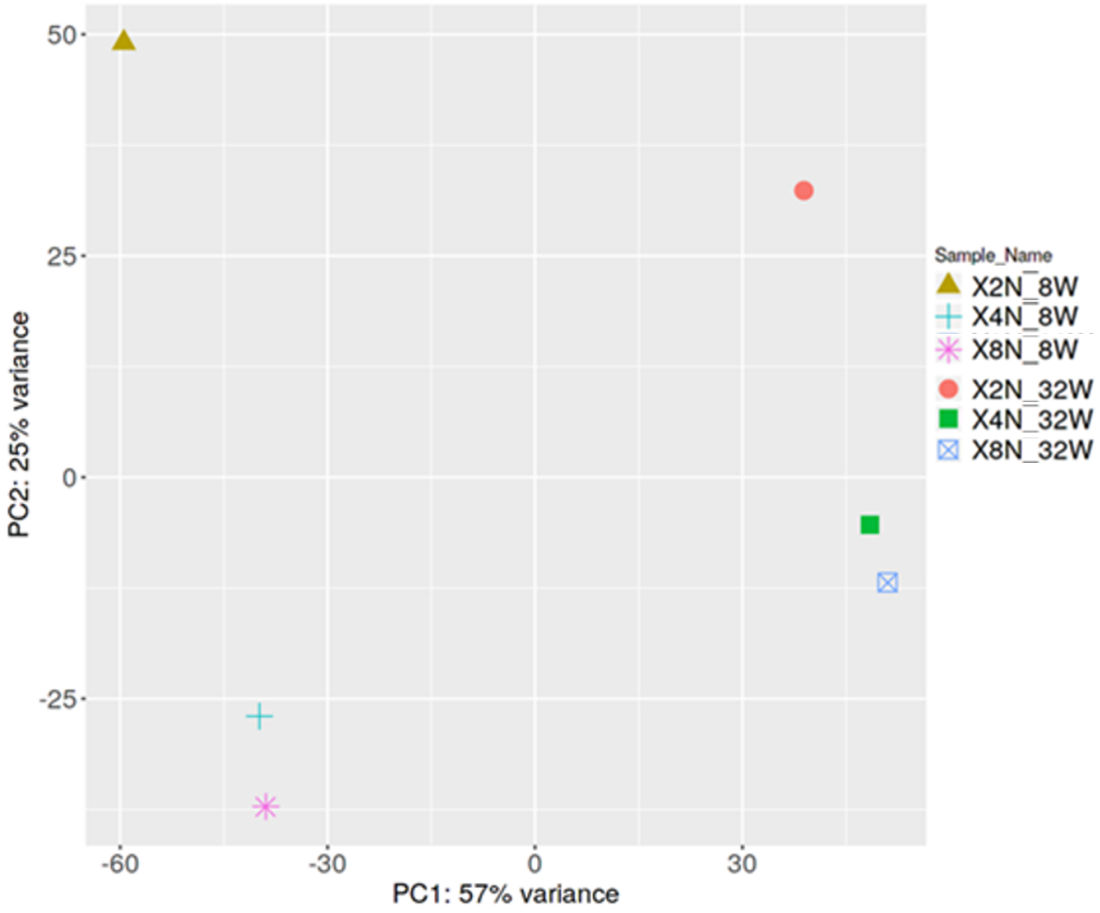

Figure 2.13: PCA of different ploidy samples from 8-week-old and 32-week-old hepatocytes analysed together taking average of replicates for each age group.

2.8.6 Liver polyploidy and fatty liver disease

As mentioned in section 2.7.8, we developed a diet-induced NASH mouse model. We perfused these mouse livers to obtain total hepatocytes and determined their ploidy profiles. We found enrichment of higher ploidy (≥ 8N) hepatocytes in NASH mice compared to age-matched control. For example, CDHFD mice have 41% 8N and 11% 16N populations whereas aged-matched control mouse has 31.6% 8N and 0.8% 16N populations **(Figure 2.14).** Our result corroborates well with previous studies using diet-induced NAFLD mouse models [460].

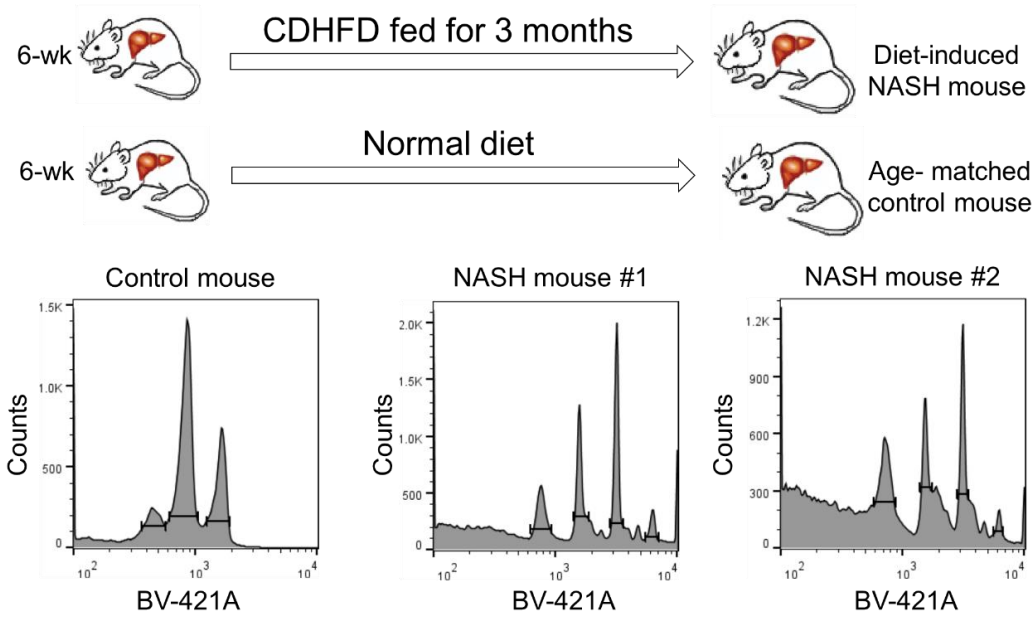

Figure 2.14: NASH model development and ploidy profiles- Top: The NASH mouse model was developed by feeding mice with CDHF diet. Bottom: The FACS profiles of normal chow-fed age-matched control (left) and NASH mice (right).

Using NAFLD associated gene as detailed in section 2.7.9, we performed unsupervised hierarchical clustering. We observed that the fatty liver associated genes express differentially in different ploidy hepatocytes at both 8-week and 32-week age groups (**Figure 2.15**). During the hierarchical clustering, the algorithm tries to put more similar samples together and hence re-arrange the order of samples in figure 2.15. However, we noticed in both age groups, 4N and 8N are closer to each other compared to their distance from 2N.

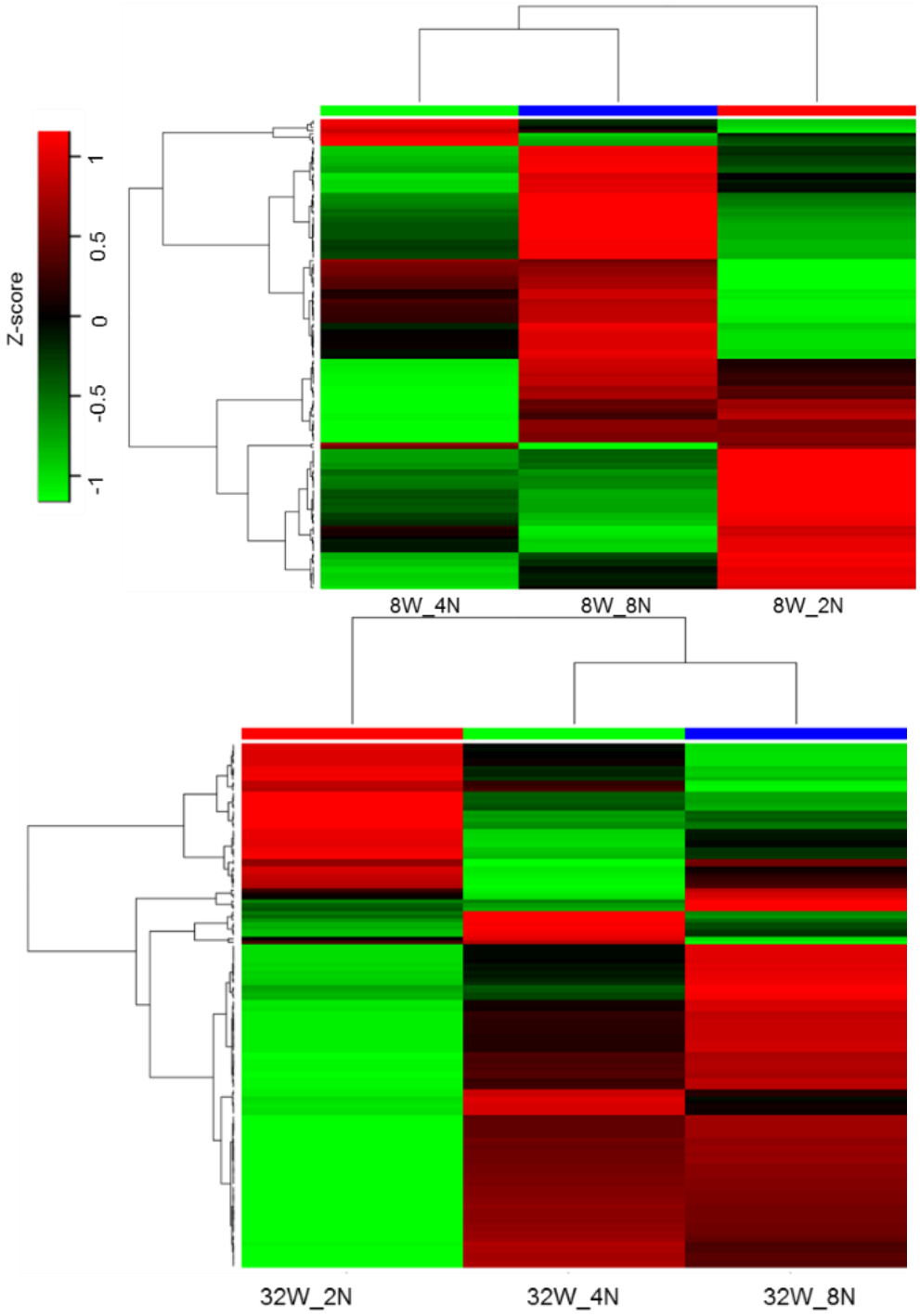

Figure 2.15: Gene expression of NAFLD associated genes- Hierarchical clustering of orthologs of NAFLD-associated genes in 2N, 4N and 8N hepatocyte RNA-seq samples generated in this study from 8-week (top) and 32-week (bottom) wild-type (normal) hepatocytes.

2.9 Discussion

Hepatocyte polyploidization is well documented for over 100 years, however, their significance is yet to be determined. Over the years, some studies have linked hepatocyte polyploidization with a protective mechanism against HCC a way to improve genetic diversity, etc. One obvious hypothesis for the existence of polyploid hepatocytes is that polyploidy can assist in increased transcriptional output which in turn can lead to increase in metabolic output and thus overall function of liver. This increase in expression may be beneficial considering the high metabolic output of the hepatocytes. However, this may bring negative effects in scenarios where the genes are required to express in a correct dosage for the proper functioning of cells. In such a scenario, we envisage that polyploid hepatocytes have gene regulatory mechanisms to compensate for dosage increment (dosage compensation) such as in the cases of imprinted genes and genes located on X chromosomes.

In this study, we attempted to investigate if different ploidy populations of hepatocytes have distinct gene signatures and if they play different roles in liver function. We successfully optimized the isolation procedure of different ploidy hepatocytes using FACS and performed RNA-seq analysis to study their gene expressions.

We observed that percentage of polyploid hepatocytes increases with developmental age in mouse liver, which is in line with previous studies **(Figure 2.3)** [61, 90, 96, 126]. Using RNA-seq data, we found a general trend that average gene expressions in polyploid populations are higher than diploid population of same age mice **(Figure 2.9)**. Moreover, PCA and Pearson correlation analysis revealed that diploid hepatocytes vary in their gene expression patterns compared to polyploid hepatocytes in both age groups **(Figure 2.6)**. Subsequently, we used GSEA to identify differential

pathways between polyploid and diploid hepatocytes combining the RNA-seq data of 8-weeks-old and 32-weeks-old age groups. The polyploid hepatocytes are enriched in pathways related to replication, transcriptional and translational processes as well as signalling pathways related to liver functions such as detoxification and metabolism. We also found gene signatures that polyploid hepatocytes have less proliferative potential while possessing more energy-producing pathways compared to their diploid counterparts. We also noticed the activation of different stress pathways as well as DNA repair machinery in polyploid hepatocytes.

Strikingly, we found a larger share of DEGs between diploid and polyploid hepatocytes compared to between two polyploid populations (**Figure 2.12**). Moreover, number of ploidy specific genes decreases with age (**Figure 2.12**). As mentioned before, the hepatocytes polyploidy increases with age and polyploid hepatocytes have more steady-state gene expression compared to diploid. This could explain why fewer ploidy specific genes are expressed in 32-week hepatocytes compared to 8-week.

However, there can be other reasons for this observation such as a possible change in 3D chromatin organization or epigenome of hepatocytes with age which may lead to lesser number of DEGs. Interestingly, when we performed PCA taking 8-week and 32-week-old hepatocytes together, we observed that variation in gene expression between these two age groups is larger compared to variation between different ploidy populations within a specific age group **(Figure 2.13)**. This suggests that aging could be the major driver of transcriptional programs in mouse hepatocytes.

The change in polyploidy profile has been also documented during liver diseases like hepatocellular carcinoma and metabolic disorders of the liver. This manifestation of different pathological conditions with changes in polyploidy profile hints towards the involvement of polyploidy in the maintenance of liver homeostasis. Using CDHF diet-

induced NASH mice **(Figure 2.14)**, we demonstrated the increment in hepatocyte polyploidization with the development of NASH which has been previously documented [460]. We then mined NAFLD-related genes from published literature and curated a gene list associated with this disease. We checked the expression of these selected genes in different ploidy samples of our data and our analysis showed that NAFLD-associated genes are differentially expressed in different ploidy hepatocytes of same age (either 8-weeks-old or 32-weeks-old).

Thus, our major findings from the study of 8-week and 32-week female hepatocytes are:

1- The gene expression signatures of different ploidy hepatocytes are divergent.

2- Each ploidy population of hepatocytes exhibits upregulation of specific molecular or biological pathways.

3- The manually curated NAFLD-associated genes are differentially expressed in different ploidy hepatocytes in normal liver in both age groups.

4- Aging appears to be the main driver of gene expression in hepatocytes.

Therefore, we need to understand how hepatocytes gene expression is regulated with age. In the next chapter, we have addressed these age-dependent gene expression and gene regulation changes in mouse hepatocytes in 8-week and 32-week age groups using RNA-seq, ChIP-seq and 3C-seq experiments.

2.10 Work contribution

Agnes Ong and I carried out two-step collagenase-based mouse liver perfusion. I purified the mouse hepatocytes based on ploidy using FACS, extracted total RNA from these cells and performed all the analyses of the RNA-seq data presented in this chapter. The experiments and data analysis were performed under the guidance of my supervisor, Dr. Amartya Sanyal and our collaborator, Dr. Torsten Wuestefeld.

Chapter 3: Age-dependent transcriptional and epigenetic changes in mouse hepatocytes

3.1 Introduction

Aging deteriorates an organism's capacity to maintain homeostasis and makes the organism more vulnerable to damages due to external stress [17]. A variety of physiological and biochemical activities performed by the liver are profoundly affected by aging and multiple studies have shown that aging increases the risk of a variety of liver diseases [305, 306, 509, 510]. Many hepatic metabolic and detoxifying processes are thought to be significantly impaired as a result of aging-dependent changes in liver structure and functioning [511]. As discussed in Chapter 1, aging-related alterations in the liver include a decline in liver volume, increased polyploidy in hepatocytes, accumulation of lipofuscin in hepatocytes, a reduced area of smooth endoplasmic reticulum in hepatocytes, pseudocapillarization in liver endothelial sinusoidal cells, a decreasing quantity and functioning of mitochondria in hepatocytes, etc. [307]. In the following sections, age-dependent molecular changes during liver development and disease will be briefly described.

3.1.1 Age-dependent transcriptional changes in the liver

Several studies have identified different genes and molecular pathways that are altered with aging. Using RNA-seq analysis, White et al. identified variations in gene expression between 4-month and 28-month old mice [512]. The study identified extensive changes in protein-coding genes associated with cell activation, RNA modification, immune response, and metabolic processes between the two age groups. Moreover, multiple lncRNAs (*Meg3*, *Rian*, *Mirg*, etc.) were also upregulated in aged 28-month-old mouse liver. Network analysis between these age-altered protein-coding and non-coding RNAs revealed inflammation, cellular proliferation, and

metabolism as the dominant aging phenotypes in mouse liver [512]. A recent single-cell RNA-seq study also found inflammatory markers to be highly upregulated in aged mouse liver [289]. Similarly, a microarray-based gene expression comparison between 7-month and 27-month-old mouse livers revealed that aging promotes inflammation, cellular stress, and fibrosis, while suppresses apoptosis, xenobiotic metabolism, normal cell-cycling, and DNA replication [513]. Another microarray study with liver of 8-month and 32-month-old mice showed that aging is accompanied by down-regulation of genes associated with insulin growth factor-1/growth hormone pathways, xenobiotic metabolism, peroxisomal biogenesis, carbohydrate metabolism, and ATP biosynthesis [514].

3.1.2 DNA repair in aging liver

Various studies in rodent models have found that the presence of senescent hepatocytes correlates strongly with the presence of DNA lesions (such as oxidized bases or persistent breaks) which increases with age [515]. Activation of carcinogens and reduced capacity to repair DNA can impact the level of DNA damage and/or mutation [515]. For example, there is a two to four-fold increase in point mutation frequency between livers of 10 and 30-month-old mice [516]. Strikingly, DNA repair-deficient mouse models show important changes in the expression of liver genes involved in stress response, cell proliferation, apoptosis, glucose and/or lipid metabolism, and inflammatory response, in addition to reduced health and/or life span and the early appearance of age-related phenotypes [515]. Studies found that genes associated with base excision repair (*Neil1*, *Wrn*), nucleotide excision repair (*Csb*, *Ercc1*, *Xpa*, *Xpd*), and non-homologous end-joining (DNA-PKcs/Ku complex genes) are also involved (directly or indirectly) in the transcription of a subset of genes (or pathways) crucial for aging phenotypes in the mouse liver [515].

3.1.3 Age-dependent alteration in liver chromatin

The chromatin structure was found to be altered in multiple liver aging studies. For example, Bochkis et al. performed MNase-seq in 3-month and 21-month-old mice and found regions of age-dependent increase and decrease in nucleosome occupancy mostly at distal elements (50-500 kb from the transcription start site (TSS)) [517]. A recent report of ChIP-sequencing of histone H3 in 3, 12, and 29-month-old male mouse livers revealed that the remodelling of the H3 nucleosome landscape is confined to few loci during aging [518]. This study found negligible genome-wide changes in H3 occupancy but a limited number of genomic loci exhibited altered (both increased and decreased) occupancy which were mainly concentrated in the distal regulatory region of the genome (5-500 kb from TSS) [518]. Using quantitative mass spectrometry, Tvardovskiy et al. showed age-dependent accumulation of histone variant H3.3 in many mouse tissues including the liver [519]. This replacement of canonical H3.1/2 isoforms with histone variant H3.3 reached saturation levels (≈99% of the total H3 pool) by the age of 18 months in the mouse liver. Moreover, the study reported profound changes, both increase (example- H3K36me2, H3K4me1, and H3K23me1) and decrease (example- H3R17me2, H3K27me3, and H3K9me2), in global levels of H3 methylation modifications along with the age-dependent accumulation of H3.3 in the mouse liver [519].

DNA methylation is a critical epigenetic regulatory mechanism that has been linked to gene silencing in the course of development, maturity, and aging [520]. DNA methylation patterns were found to be remodelled in liver samples obtained from 45 healthy liver donors ranging in age from 13 to 90 years old [521]. As predicted by Horvath's epigenetic clock, these age-related alterations in DNA methylation patterns

tend to level out at the age of 60. Interestingly, by combining DNA methylation and gene expression data, this study reported Wnt-signaling pathways genes role in aging of human liver (*ZIC1*, *NEFM*, *FOXD3*, *MIR155HG*, *CELS3*, *and HEYL*)[521].

As mentioned in section 1.3.3.1, the 3D genome organisation is altered with aging in many tissues. Interestingly, a recent study highlighted the existence of chromatin architecture associated with organ-specific gene regulation [522]. This study focused on two polyploid and metabolically active organs, the heart and the liver, and found that their 3D genome organisations are different [522]. For example, 66.7% of heart-specific genes were found in active (A) chromatin compartments while 66.1% of liver-specific genes were found in inactive (B) compartments, which hints that the genome organisation of each organ manifests in different ways. There are published reports of 3D genome organisation of the mammalian liver (mouse, rabbit, macaque, dog, and human) but how this organisation changes with age remains unexplored [523, 524].

3.1.4 Liver regeneration and aging

The ability of the liver to regenerate its mass after partial hepatectomy is a unique trait. According to reports, aging reduces the liver's regeneration capability, both in terms of the rate and extent to which the organ's original volume is restored [525]. In aged rats, a decrease in hepatic sensitivity to growth factors, such as epidermal growth factor (EGF), appears to decrease regeneration rate [525]. This study has demonstrated (a) a 60 percent decline in EGF binding to hepatocyte plasma membranes, (b) reduced expression of the hepatic high-affinity EGF receptor, and (c) a block between G1 and S-phases of the cell cycle in old rats following EGF stimulation [525]. Other studies have shown that with age, there is a decrease in the expression of a forkhead box transcription factor, FoxM1B, which is important for growth hormone-stimulated liver regeneration in hepatectomized mice. Therefore, aging appears to

impede liver regeneration by impacting numerous pathways, the effect of which is a reduction in the pace of regeneration [525].

3.1.5 Aging and liver diseases

Aging increases the risk of liver disease-associated mortalities. A brief discussion about how aging influences a variety of prevalent liver diseases is provided in the following sections.

3.1.5.1 Aging and non-alcoholic fatty liver disease (NAFLD)

The aging markers in liver cells are positively correlated with the progression of NAFLD [526]. In a study between elderly groups (aged more than 65 years) and 18-64-year old humans, the older participants had a greater NASH prevalence rate than the younger participants as well as a greater incidence of liver fibrosis [527]. Increased ROS formation, telomere shortening, activation of p300-C/EBP-dependent neutral fat synthesis, DNA damage, expanded nuclear areas, activation of nuclear factor-kappa B pathways, increased p21 expression, and M1 macrophage inflammatory responses and decreased autophagy are the molecular mechanisms responsible for the accumulation of excessive fat in the liver that damage hepatic cells which positively correlates with aging [306, 526, 528-530].

3.1.5.2 Aging and alcoholic liver disease

Alcohol expedites the advancement of chronic hepatitis caused by the hepatitis B and C viruses, as well as other liver disorders such as NAFLD and hemochromatosis [531]. Although the clinical signs of alcoholic liver disease in the elderly are comparable to those in younger people, the elderly have a greater rate of complications [532]. Around 79 percent of patients with alcoholic liver disease over the age of 60 years develop complications such as liver cirrhosis, and 40 percent of patients with alcoholic cirrhosis

develop alcoholic hepatitis with a 15–25 percent death rate [533-536]. Alcoholic hepatitis has a poor prognosis when people get older. Furthermore, aging raises the likelihood of comorbidities, and hence, older persons are frequently prescribed various medications. Since ethanol and most medications are metabolized in the liver, older individuals with alcoholic liver disease are at a higher risk of hepatotoxicity due to drug interactions [482].

3.1.5.3 Aging and chronic viral hepatitis C

The patient's age at the time of diagnosis of hepatitis C virus (HCV) infection was found to be positively correlated with the development of liver fibrosis, cirrhosis, and hepatocellular cancer [537-539]. Patients over 40 years old at the onset of HCV infection had a quicker development of liver fibrosis than those under 40 years of age, and those over 65 years old had an even higher relative risk of severe liver fibrosis (Metavir stage F2 or higher) than those under 65 years [539].

3.1.6 Hypothesis and objectives

As discussed in previous sections, aging leads to transcriptomic and chromatin-level changes in the liver. Moreover, aging causes a decline in DNA repair and liver regeneration machinery. Additionally, the risk of liver diseases has been found to positively correlate with aging in various models and patient studies. We know that aging does not follow a universal pattern of alterations in different tissues. Therefore, a cell type-specific study is essential to learn about age-associated changes in a particular organ. Hepatocytes are the most abundant cells in the liver and perform the majority of its functions. In chapter 2, we identified aging as an important driver of changes in gene expression of mouse hepatocytes. Surprisingly, molecular signatures of hepatocyte aging have not been explored well. Moreover, age-dependent epigenetic and chromatin-level alterations are still unexplored in hepatocytes.

Therefore, we hypothesised that hepatocyte aging is driven by changes in gene expression and this age-associated transcriptional reprogramming is controlled by epigenetic mechanisms which include specific histone post-translational modifications (PTMs) and spatial genome organisation. To test our hypothesis, we set the following objectives:

- To investigate gene expression signatures of mouse hepatocytes isolated from different age groups
- To study age-dependent changes in active and inactive histone PTMs and 3D genome organisation in hepatocytes of different ages and decipher their roles in gene regulatory mechanisms of age-dependent hepatocyte gene expression

To achieve our objectives, we isolated hepatocytes from mouse livers of different age groups and generated RNA-seq, ChIP-seq of different histone PTMs and 3C-seq datasets as shown in figure 3.1

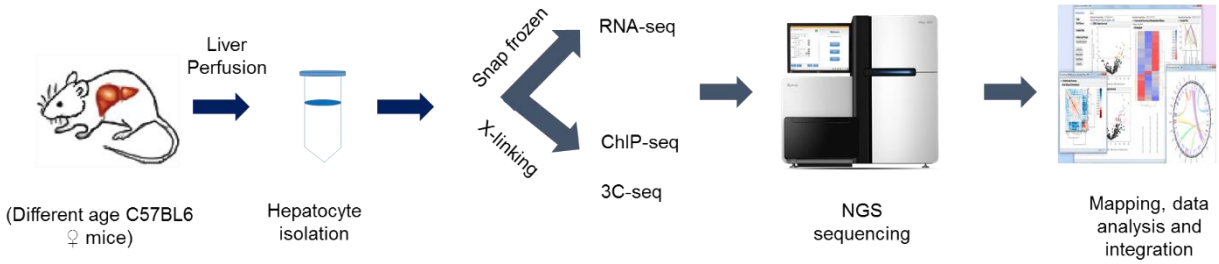

Figure 3.1: Strategy to isolate hepatocytes and study their gene expression and epigenetic regulation in different ages. Hepatocytes were isolated using two-step collagenase-based perfusion, followed by gene expression analysis using RNA-seq and gene regulation investigation using ChIP-seq of different histone PTMs and 3C-seq. Each study will have its unique data analysis and integration pipeline.

3.2 Materials and Methods

Animal: C57BL/6 female mice were used for all the experiments. For RNA-seq experiments of the total hepatocytes, we used 8-week, 32-week, and 94-week-old mice while ChIP-seq and 3C-seq were performed with total hepatocytes isolated from 8-week and 32-week mouse livers only. Mice were housed in a temperature-controlled facility with a 12/12 hour light on-and-off cycle with ad libitum feeding. All animal studies were carried out according to the IACUC (Institutional Animal Care and Use Committee) approved protocol (Protocol # 151054- Improvement of liver regeneration, Genome Institute of Singapore, Singapore, PI- Torsten Wuestefeld).

3.2.1 Liver perfusion and hepatocyte isolation

Hepatocytes were isolated from C57BL/6 female mouse livers of different ages using two-step collagenase-based perfusion as explained in sections 2.7.1 and 2.7.2. The RBCs were then removed, hepatocytes were counted and processed for RNA-seq, ChIP-seq, and 3C-seq experiments according to the respective protocol which is described in the following sections.

3.2.2 RNA extraction

Total RNA was extracted from total hepatocytes isolated by perfusion from mouse livers of different ages as described in section 2.7.5. Briefly, total RNA was extracted from different age hepatocytes using the ReliaPrep RNA Cell Miniprep kit (Promega, cat # Z6010). The concentration of total RNA was measured on a Qubit 3 Fluorometer (Invitrogen, cat # Q33216) using Qubit RNA HS assay kit (Thermo Fisher Scientific, cat # Q32852).

3.2.3 RNA sequencing

We processed RNA samples for RNA-seq library preparation which have DV200 values of >85%. Paired-end library for RNA-seq was prepared by the third-party service provider from total RNA using TruSeq Stranded Total RNA kit (Illumina) with Ribo-Zero Mouse kit based on TruSeq stranded total RNA sample preparation guide (part #15031048 rev. E). We have also added ERCC RNA spike-in mix (Invitrogen cat # 4456740) in the sequencing libraries. RNA-seq libraries were sequenced on Illumina Novaseq 6000 platform with 2 x 151 bp multiplex protocol for 32-week and 94-week hepatocytes whereas 8-week hepatocyte samples were sequenced on Illumina HiSeq 4000 platform with 2 x 151 bp protocol.

3.2.4 RNA-seq data analysis

We performed the RNA-seq data analysis as detailed in section 2.7.7. Briefly, we used STAR 2.5a for sequencing read alignment and featureCounts for sequencing read assignment to particular gene. We used edgeR for identifying differentially expressed genes (DEGs). PCA, read normalisation, read filtering, TPM calculation and beanplot analysis was performed as mentioned in section 2.7.7.

3.2.4.1 The k-means clustering

The k-means clustering is an unsupervised method for clustering genes into groups based on their expression pattern across all samples. We used IDEP 0.91 to perform k-means clustering [48]. Based on the elbow plot, we heuristically choose k (number of clusters) = 3 for this analysis. We performed the KEGG pathway analysis on the 3 clusters obtained from clustering analysis using the option in IDEP 0.91.

3.2.4.2 Pathway analysis

We identified differential pathways using gene set enrichment analysis (GSEA) and ConsensusPathDB (CPDB) [540]. Using these two approaches we identified the important pathways enriched in hepatocytes of different ages.

GSEA (gene set enrichment analysis)

We used the GSEA java desktop application for our analysis. For this analysis, we considered all expressed genes (which have raw count greater than or equal to 10 in at least one sample) with their normalized counts. The expression datasets and phenotype labels were formatted based on the instructions (http://software.broadinstitute.org/cancer/software/gsea/wiki/index.php/Data_formats) . We selected the Reactome MSigDB gene set for this analysis with default 1000 permutations. Mouse gene symbols were first converted to human orthologues using GSEA inbuilt mouse to human annotations. We used the log2 ratio of classes as the metric for ranking genes keeping other parameters at default settings to identify differential pathways. The pathways were shortlisted based on a normalized p-value cutoff of ≤ 0.05 and then similar pathways were grouped under a broad heading manually.

CPDB-mouse (ConsensusPathDB-mouse)

We used the CPDB-mouse web browser for this analysis. Briefly, we uploaded the list of genes highly-expressed in 8-week (1267), 32-week (1029), and 94-week (1121) to the CPDB-mouse gene over-representation portal along with the background list which consists of all genes used for DEG estimation. We used default settings to get a list of pathways and downloaded them from the web portal. Next, pathways were

shortlisted based on the normalized p-value cutoff of ≤ 0.05 and we grouped the similar pathways manually under a broad heading.

3.2.5 Formaldehyde fixation for chromatin immunoprecipitation sequencing (ChIP-seq)

Around 2 x 10^6 hepatocytes were used for each ChIP-seq experiment. The ChIP experiments were conducted in parallel for four histone modification marks (H3K27me3, H3K27ac, H3K4me3, and H3K9me3). For the crosslinking, the isolated hepatocytes were counted using a hemocytometer, and aliquoted in multiple 1.5 mL microcentrifuge tubes with each containing 3 x 10^6 cells in hepatozyme SFM medium (Thermo Fisher Scientific, cat # 17705-021). The tubes containing total hepatocytes were centrifuged at 200 x g for 5 min at 4 ^oC. The supernatants were discarded and the cell pellets were resuspended in 1 mL of phosphate-buffered saline (PBS) and the hepatocytes in each tube were chemically cross-linked with formaldehyde (1% (v/v) final concentration) for exactly 10 min at room temperature (RT). The crosslinking reaction was quenched by adding glycine (125 mM final concentration) and the tubes were incubated for 10 min at RT followed by on ice for another 15 min. The tubes were then centrifuged at 10,000 x g for 5 min at 4 ^oC. The supernatants were discarded and the cross-linked cell pellets were stored at -80 ^oC freezer until further use.

3.2.6 Chromatin Immunoprecipitation sequencing (ChIP-seq)

We used hepatocytes isolated from 8-week and 32-week mouse livers for performing ChIP-seq experiments of histone PTMs. The major steps for ChIP-seq are detailed in subsequent sections below. These steps are- lysis of cross-linked cells, chromatin fragmentation, chromatin immunoprecipitation, DNA purification, NGS library preparation, and NGS sequencing.

3.2.6.1 Lysis of crosslinked cells

Frozen cross-linked cell pellets were thawed on ice and about 1 x 10^7 cross-linked cells were resuspended in 1 mL of ice-cold hypotonic cell lysis buffer [20 mM Tris-Cl pH 8.0, 85 mM KCl, 0.5% NP-40, freshly added 10 µL protease inhibitor cocktail (Sigma-Aldrich, cat # P8340)] and incubated for 10 min on ice. Cells were centrifuged at 1000 x g for 5 min at 4 ^oC and the supernatant was discarded. The cell pellet was then resuspended in 300 µL of nuclei lysis buffer [50 mM Tris-Cl pH 8.0, 10 mM EDTA pH 8.0, 1% SDS (sodium dodecyl sulfate), freshly added 20 µL protease inhibitor cocktail (Sigma-Aldrich)].

3.2.6.2 Chromatin fragmentation by sonication

Exactly 130 µL of the above nuclear extract was loaded onto an AFA Fiber Pre-Slit Snap microTUBE (Covaris, cat # 520045) and sonicated on a focused ultrasonicator (Covaris M220) using optimized parameters (peak incident power = 75, duty factor = 2%, cycles per burst = 200 and time = 5 min). The sonicated chromatin was then added to a tube containing 2340 µL of ChIP dilution buffer [50 mM Tris-HCl pH 8, 0.167 M NaCl, 1.1% Triton X-100, 0.11% sodium deoxycholate, 26 µL of protease inhibitor cocktail (Sigma-Aldrich)]. We repeat the sonication step using another aliquot of 130 µL of the nuclear extract and collect the sonicated samples in the same ChIP dilution buffer. We set aside 4 µL (1% of the 400 µL of diluted chromatin sample used for each ChIP reaction) of this diluted sonicated chromatin to be used as ChIP input control. For 8-week and 32-week-old hepatocyte samples, we collected ChIP input controls separately.

3.2.6.3 Dynabead protein G and antibody binding

In parallel to cell lysis and sonication steps, specific antibodies were conjugated with magnetic beads for each histone PTM ChIP experiment. Briefly, Dynabeads Protein

G (Invitrogen, #10017D) were mixed well and 50 µL of beads were aliquoted in each of the four 1.5 mL Eppendorf DNA LoBind tubes (Eppendorf, cat # 0030108051). Four tubes correspond to ChIP experiments for different histone PTMs for each age group. The beads were first washed with 500 µL of ice-cold RIPA-150 buffer (50 mM Tris-HCl pH 8, 0.15 M NaCl, 1 mM EDTA pH 8, 0.1% SDS, 1% Triton X-100, 0.1% sodium deoxycholate) by gentle vortexing. The tubes were then placed in a magnetic separation rack and beads were allowed to aggregate under the magnetic field for ~1 min. The RIPA-150 buffer was pipetted out from each tube and this washing step is repeated once more. Next, the beads were resuspended in 300 µL of ChIP dilution buffer. Four microliter (4 µg- each antibody has concentration of 1 mg/mL) of antibody against specific histone PTM (H3K27me3- Abcam, cat # ab222481, H3K9me3- Abcam, cat # ab8898, H3K27ac- Abcam, cat # ab4729 and H3K4me3- Abcam, cat # ab8580) was added to corresponding tube, vortexed and incubated for 3 hours at 4 ^{0}C on a HulaMixer (Thermo Fisher Scientific, # 15920D) (settings: orbital-8; reciprocal-50^{o}; Vibro/pause-50; time-3 hours) for magnetic bead-antibody conjugation.

3.2.6.4 Chromatin Immunoprecipitation

After 3-hour incubation, each tube containing antibody-conjugated Dynabeads Protein G (section 3.2.6) was placed on a magnetic separation rack for 2 min. The supernatant was removed and 400 µL of RIPA-150 buffer was added to each tube and mixed well. The tube was again placed on a magnetic rack and the supernatant was removed. This washing step with RIPA-150 buffer was repeated two more times. Then, 400 µL of the diluted sonicated chromatin sample (section 3.2.7) was added to each tube containing specific antibodies conjugated to magnetic beads and vortexed gently. The tubes were incubated overnight on a HulaMixer inside a cold room for antibody-chromatin binding.

3.2.6.5 Washing

After overnight incubation, the tubes were briefly centrifuged and placed in the magnetic rack for 2 min and the supernatants were discarded. Beads were washed once with 400 µL of RIPA-150 buffer, the tubes were incubated on ice for 5 minutes, transferred to a magnetic stand for 2 minutes and the supernatants were removed. Beads were then washed twice with 400 µL of RIPA-500 buffer (50 mM Tris-HCl pH 8, 0.5 M NaCl, 1 mM EDTA pH 8, 0.1% SDS, 1% Triton X-100, 0.1% sodium deoxycholate) using the magnetic rack. Beads were subsequently washed with 400 µL of RIPA-LiCl buffer (50 mM Tris-HCl pH 8, 1 mM EDTA pH 8, 1% Nonidet P-40, 0.7% sodium deoxycholate, 0.5 M LiCl) two times followed by washing twice with 400 µL of 1X TE buffer (10 mM Tris·Cl, pH 8.0 and 1 mM EDTA, pH 8.0). At the end, 200 µL of elution buffer (10 mM Tris-HCl pH 8, 0.3 M NaCl, 5 mM EDTA pH 8.0, 0.5% SDS) and 5 µL of 10 mg/mL Proteinase K (Invitrogen, cat # 25530-031) were added to each tube, mixed well and incubated overnight at 65 ^{o}C for DNA elution. Parallelly, 200 µL of ChIP dilution buffer and 5 µL of Proteinase K (10 mg/ml Invitrogen, cat # 25530-031) were added to input controls and incubated at 65 ^{o}C overnight.

3.2.6.6 Desalting

After overnight incubation, all the tubes were briefly centrifuged and placed on the magnetic rack for 2 min and the supernatants containing DNA were transferred to a fresh Eppendorf DNA LoBind tube (cat # 0030108051). Exactly 300 µL of TE buffer (pH 8.0) was added to each tube to make the total volume of 500 µL and the solution was transferred to Amicon Ultra-0.5 mL centrifugal filters (Merck, cat # C82301) for DNA purification and concentration, and centrifuged at 18000 x g for 5 min at RT. The flow-through was discarded. The Amicon filter was washed three times with 450 µL of TE buffer (pH 8.0) (18000 x g for 5 min at RT). The Amicon filter was inverted, placed

on a new collection tube, and centrifuged at 1000 X g for 2 min at RT for DNA recovery. To the eluate, TE buffer (pH 8.0) was added to make the final volume to 100 µL. For removal of the contaminating RNA, 0.5 µL (20 mg/ml) of RNase A (Life Technologies, cat # 12091021) was added to each tube and incubated at 37 ^{o}C for 20 min.

3.2.6.7 Purification using AMPure beads

The Agencourt AMPure XP (Beckman Coulter, cat # A63881) beads at RT were vortexed briefly and added to each immunoprecipitated (i.p.)/ input DNA in the ratio of 1:1.8 (180 µL of AMPure beads added to 100 µL of the i.p. DNA sample), mixed well by pipetting and incubated for 5 min at RT. The tubes were then placed on a magnetic rack for 2 min. The supernatant was removed and 200 µL of 70% ethanol was added and incubated for 30 sec. The tubes were transferred to a magnetic rack and beads in each tube were allowed to aggregate due to the magnetic field for 2 min. The ethanol was aspirated out and this ethanol washing step was repeated once more. About 15 µL of 1X TE buffer (pH 8.0) was added to the AMPure beads, mixed well by pipetting, and incubated for 2 min at RT. The tube was centrifuged at 15000 x g for 3 min and then placed on a magnetic rack for 2 min and the ChIP/input DNA was eluted. The DNA was quantified in Qubit 3.0 using Qubit DNA BR assay kit (ThermoFisher Scientific, #Q32850) and stored at -20^{0} C until further use.

3.2.6.8 NGS paired-end library preparation for Illumina sequencing

The NGS library was prepared using SMARTer ThruPLEX DNA-seq 12S Kit (Takara Bio, cat # R400428). The main steps are described below:

Template Preparation Step: Exactly 3 µL of template preparation master mix, prepared by mixing 1µL of template preparation enzyme in 2 µL of template preparation buffer, was added to 10 µL of individual ChIP/ input DNA sample in a 500-µL PCR tube. The

reaction mixture was mixed thoroughly, centrifuged briefly, and transferred to a PCR machine. The incubation steps were carried out with the following protocol: 22 ^{o}C for 25 min, 55 ^{o}C for 20 min, and 4 ^{o}C for 5 min. After the incubation, the samples were centrifuged briefly.

Library Synthesis Step: To the above sample, 2 µL of the Library Synthesis Master Mix, prepared by mixing 1 µL of Library Synthesis Enzyme (Yellow cap) and 1 µL of Library Synthesis Buffer (Yellow cap), was added, mixed, centrifuged briefly and incubated at 22 ^{o}C for 40 min in a PCR machine. After the incubation, the sample was centrifuged briefly.

Library Amplification Step: The Library Amplification Master Mix for each reaction was prepared by mixing 1 µL of Library Amplification Enzyme, 25 µL of Library Amplification Buffer, and 4 µL nuclease-free water. Exactly 30 µL of this Library Amplification Master Mix was added to the 15 µL of ChIP/ input DNA sample from *Library Synthesis Step.* Then 5 µL of specific indexing reagent (containing indexed PCR primers for multiplex NGS run) was added and PCR was carried out with the following programme to generate the ChIP-seq or input-DNA library:

	Stage	Temperature	Time	# cycles
Extension & Cleavage	1 2	72 ^{o}C 85 ^{o}C	3 min 2 min	1 1
Denaturation	3	98 ^{o}C	2 min	1
Addition of indexes	4	98 ^{o}C 67 ^{o}C 72 ^{o}C	20 sec 20 sec 40 sec	4
Library amplification	5	98 ^{o}C 72 ^{o}C	20 sec 50 sec	10 (8 cycles for input samples)
	6	4 ^{o}C	5 min	1

Library Quantification and pooling: All the libraries were quantified using KAPA library quantification kit (Roche, kit # KK4824) for Illumina platforms using the manufacturer's

protocol. Briefly, the kit consists of 6 standards of different concentrations (0.0002 pM to 20 pM). Each ChIP-seq library and input control samples were diluted to 1:10K and 1:100K. Duplicates of 6 standards and 'no template controls' were used for the two-step cycling qPCR reaction. The qPCR reaction was performed on a BioRad Real-Time PCR machine with the following settings: Initial Denaturation- 95 ^{o}C for 5 min, Denaturation- 95 ^{o}C for 30 sec, Extension/ Amplification- 60 ^{o}C for 45 sec, and followed by melt curve analysis from 65 ^{o}C - 95 ^{o}C. After the qPCR reaction was over, 6µL of PCR products were run on a 1.5% Agarose-TBE gel to check the ChIP-seq library size (data not shown). The concentration of each ChIP-seq library was calculated based on the standards. For the multiplex sequencing run, we pooled 10 samples containing 4 histone modification ChIP-seq libraries and one input control each for 8-week and 32-week mouse hepatocyte samples. About 20 ng of each indexed NGS library was pooled together and the volume was made up to 150 µL using TE buffer (pH 8.0).

Size-selection of pooled NGS library: Pooled ChIP-seq library was size-selected using AMPure beads to obtain DNA fragments with 250-400 bp length. To the 150 µL of the pooled library, 90µL of AMPure beads was added and incubated on a magnetic rack for 2 min. The supernatant was transferred to a new 1.5 mL microcentrifuge tube and 45 µL of AMPure beads were again added and incubated on a magnetic rack for 2 min. The supernatant was discarded and the beads were washed with 200 µL of 70% ethanol twice. Following ethanol wash, 30 µL of TE buffer (pH 8.0) was added to the AMPure beads, mixed well by pipetting, and incubated for 2 min at RT. The tube was centrifuged at 15000 x g for 3 min. The tube was then placed on the magnetic rack for 2 min and the supernatant containing the size-selected pooled ChIP-seq library DNA was eluted and stored at -20 ^{o}C.

Pooled library quantification: The size-selected pooled ChIP-seq library was again quantified using KAPA library quantification kit (Roche, kit # KK4824) for Illumina platforms as described above (step *Library Quantification and pooling*) using three dilutions 10K, 100K, and 1000K in duplicates. The pooled and size-selected ChIP-seq library (concentration: 3.28 ng/µL and volume: 30 µL) was submitted to theird party vendor for sequencing on an Illumina HiSeq X platform with 2 x 150 bp read length.

3.2.7 ChIP-seq data analysis

(i) Read mapping and peak calling: Fastq files containing paired-end reads were mapped to the mouse reference genome (mm10) using bowtie2 [541] with default parameters. After read filtering (reads with MAPQ>1 were accepted, reads from chromosome Y and M were removed, PCR duplicates and non-unique reads were removed), the resultant BAM files (for ChIP and the corresponding input DNA) were processed using MACS2 [542, 543] to identify the H3K27ac, and H3K4me3 ChIP-seq peaks with --broad option.

(ii) Computation of ChIP-seq signal: The BAM files generated from the above analysis were sorted and indexed by SAMtools. To generate the input subtracted signal, the bamCompare utility in deepTools [544] package was used with options --scaleFactorsMethod None, --operation subtract, and --normalizeUsing RPKM, where BAM files for ChIP and input DNA were used as treatment and control data respectively. The signals were generated at different bin sizes and normalized to reads per kilobase per million (RPKM).

(iii) Peak annotation using hypergeometric optimization of motif enrichment (HOMER)

The bed files obtained from MACS2 were used for peak annotation by HOMER [545]. The HOMER inbuilt program, annotatePeaks.pl, was utilised for peak annotation using

default scripts. The annotated peaks were segregated as exon, intron, intergenic, promoter-TSS (transcription start site), and TTS (transcription termination site) and represented as a pie-chart in the result section.

(iv) Read coverage representation using deepTools

We used deepTools tools, namely plotHeatmap and plotProfile, with default parameters for plotting average scaled enrichment (ASE) plot of ChIP signal of a group of genes across TSS and the entire length of the gene or for plotting read coverages across genic regions of a group of genes [109].

3.2.8 Chromosome conformation capture (3C)-sequencing of mouse hepatocytes isolated from different age groups

The 3C libraries of 8-week and 32-week hepatocytes were prepared based on the previously described method [546]. The detailed steps of 3C library preparation were described below.

Formaldehyde crosslinking: About 3 million hepatocytes were used for the 3C-seq experiments. Crosslinking was performed as described in section 3.2.5 with the following changes. We used formaldehyde at a final concentration of 2% (v/v) and the crosslinking reaction was quenched by adding glycine to a final concentration of 250 mM. Crosslinked cells were centrifuged, the supernatant was discarded and the cell pellet was stored at -80 ^{o}C until further use.

Cell lysis and chromatin solubilization: The crosslinked cell pellet was thawed on ice and then 1 mL of ice-cold Lysis buffer [10 mM Tris-HCl pH 8.0, 10 mM sodium chloride, and 0.2% (v/v) Igepal CA 630 (Sigma-Aldrich, cat# I8896-100 ML), freshly added 50 µL of protease inhibitor cocktail (Sigma-Aldrich, cat # P8340)] was added and incubated on ice for 15 min. Using a Dounce homogenizer, the crosslinked cells were

lysed by applying 10 strokes with the pestle (Pestle A, loose-fitting), incubated on ice for 2 min, and then an additional 10 strokes were applied. The lysed cell suspension was transferred to a 1.5 mL microcentrifuge tube and the tube was centrifuged at 2000 x g for 5 min at RT. The supernatant was discarded and the pellet was washed with 1 mL of 1X NEBuffer 3.1 (NEB, cat # B7203S). The tube was centrifuged at 2000 x g for 5 min at RT and supernatant was discarded. The lysed pellet was resuspended in 100 µL of 1.25X NEBuffer 3.1 and aliquoted equally in two 1.5 mL microcentrifuge tubes containing 312 µL of 1.25X NEBuffer 3.1. About 38 µL of 1% SDS solution (in water) was added to each tube to solubilize the chromatin. The suspension was mixed well and incubated at 65 ^{0}C for exactly 10 min. After incubation, the tubes were immediately transferred on ice, and SDS was quenched by adding 44 µL of 10% Triton X-100 to each tube.

Restriction enzyme digestion: One thousand units of DpnII (NEB cat# R0543M) was added to each tube, mixed well, and incubated for restriction digestion at 37 ^{0}C overnight on an Eppendorf ThermoMixer C. Next day, DpnII enzyme was heat-inactivated by incubating the tubes at 65 ^{0}C for 20 min and then the tubes were transferred to ice.

Sticky-end ligation: During the heat-inactivation step, the ligation master mix [10X ligation buffer (500 mM Tris-HCl pH 7.5, 100 mM magnesium chloride, and 100 mM Dithiothreitol) - 745 µL , 10 mg/mL BSA - 80 µL, 100mM ATP - 80 µL, and autoclaved water - 6705 µL] was prepared in a 15-mL centrifuge tube on ice. Digested chromatin sample from each tube from the above step was transferred to the 15-mL tube containing ligation master mix. Then, 50 U of T4 DNA ligase (Life technologies, cat # 15224090; 1 U/µL) was added to each 15-mL tube, and ligation was carried out at 16

^{0}C for 6 hours. This ligation reaction will result in 3C library which needs to be reverse crosslinked and purified.

Reverse crosslinking: After the ligation step, reverse crosslinking was carried out on the 3C library by adding 100 µL of 10 mg/mL Proteinase K (Invitrogen, cat # 25530-031) in each ligation tube, mixed by inverting the tube and incubated in 65 ^{0}C water bath overnight.

DNA purification and desalting: The reverse crosslinked 3C library DNA of the same age group was pooled together in one 50 mL centrifuge tube, and an equal volume of Tris-saturated phenol pH 8-chloroform 1:1 (v/v) was added to the pooled sample. The aqueous phase was carefully transferred to a clean 50 mL tube and the phenol-chloroform extraction step was carried out once more. The aqueous phase was then divided equally into two Oak Ridge tubes. Next, DNA was concentrated by standard ethanol precipitation in presence of 0.3 M sodium acetate pH 5.2 (final concentration) and the tubes were incubated for 3 hours at -80 ^{o}C. The 3C DNA was pelleted down by centrifugation at 12,000 x g for 20 min at 4 ^{o}C. The supernatant was discarded and the DNA pellet was dissolved in 500 µL of 1X TE buffer (pH 8.0). The 3C DNA solution was aliquoted into a new 1.5 mL microcentrifuge tube and the second round of phenol-chloroform extraction was carried out followed by ethanol precipitation. DNA pellet was obtained by centrifuging the tubes at 18,000 x g for 20 min at 4 ^{o}C and the supernatant was discarded. The entire 3C DNA from each sample was finally resuspended in 500 µL of 1X TE buffer (pH 8.0) and transferred into an Amicon Ultra 0.5mL (30 KDa molecular weight cutoff) centrifugal filter (Merck, cat # C82301) and centrifuged at 18,000 x g for 5 min. The supernatant was discarded and the column was washed four times by adding 450 µL of 1X TE Buffer (pH 8.0) to remove any traces of salt and impurities. The 3C DNA was collected by inverting the column and placing it inside a

new collection tube followed by centrifugation at 1,000 x g for 2 min. The eluted DNA volume was made up to 95 µL with 1X TE Buffer (pH 8.0). For RNA removal, 1 µL of RNase A (20 mg/mL Invitrogen, cat #12091021) per sample was added and incubated at 37^0 C for 30 min. The 3C libraries were quantified using Qubit 3.0 using dsDNA HS Assay kit (Thermo fisher scientific, cat # Q32851) and stored at -20 ^{0}C till further use.

Sonication: About 12 µg of each library were topped up to 130 µL with 1X IDTE buffer, transferred to AFA Fiber Pre-Slit Snap microTUBE (Covaris, cat # 520045) and sonicated on a focused ultrasonicator (Covaris M220) using optimized parameters (Intensity: 3, Cycles per burst: 1000, Duty factor: 10%, Time: 50s).

Library size selection: Sonicated libraries were size-selected for fragments equivalent to the size of two ligated DpnII restriction fragments, ~500 bp. 65 µL cold Ampure XP beads were mixed with the libraries by pipetting at least 10 times. The reaction is incubated at room temperature for 5 minutes. Tubes were placed on a magnetic stand for beads to separate. Cleared supernatant was transferred to a clean microfuge tube and a further 26 µL of cold beads were mixed. After 5 minutes of incubation at room temperature, tubes were placed back onto the magnetic stand and the supernatant was discarded. To wash bound DNA, 200 µL of freshly-prepared 70% ethanol was dispensed onto the beads, and carefully removed by pipetting. The wash step was carried out once more. Beads were air-dried and 50 µL 1X IDTE buffer pH 8.0 was added when it is still glossy and dark brown. After mixing, the reaction mix was incubated for 2 minutes at room temperature. Tubes were transferred back to the magnetic stand and supernatant was pipetted into a new microfuge tube.

NGS library preparation: The 3C-seq NGS libraries of 8-week and 32-week hepatocytes were generated using the NEBNext Ultra II DNA library prep kit for

Illumina (NEB cat # E7645S) according to the manufacturer's protocol. The NGS libraries were then quantified using KAPA library quantification kit (Roche, kit # KK4824) for Illumina platforms library quantification and purified with AMPure XP beads to remove PCR primers and adapters. Each 3C-seq NGS library was eluted in 50 µL of 1X TE buffer (pH 8) and transferred to a DNA LoBind tube (Eppendorf, cat # 0030108051) and stored at -20 °C.

NGS paired-end sequencing: Sequencing of the 3C-seq libraries was carried out on Illumina HiSeq X platform with 2 X 150 bp multiplex protocol by third-party service provider.

3.2.9 3C-seq data analysis

The 3C-seq data was analyzed by the Python-based hiclib package [548]. Following steps were performed based on this package which includes iterative mapping, fragment assignment, fragment filtering, binning, bin filtering, iterative bias correction, and compartment analysis. A brief discussion about each step is given below:

(i) Iterative mapping. The side 1 and side 2 of paired-end sequencing reads were separately aligned to the mouse reference genome mm10, to acquire the genomic information of restriction fragments from both sides of the ligation junction. The genome assembly file was downloaded from the UCSC genome browser (https://www.genome.ucsc.edu). The unlocalized sequences starting with "chrUn" or terminating with "random" or "hap" were excluded from the analysis. The indexes were created on the remaining sequences using the build-in command of bowtie2 package [541, 549]. Iterative mapping was performed to align the side 1 and side 2 of the reads separately [548] using bowtie2 with *--very-sensitive* option. , increasing truncation length reads were aligned until they either mapped uniquely with mapping quality

scores (MAPQ) ≥ 1 or the iteration reached the end of a read. A sequence alignment/map (SAM) file with alignment results [550] was created for every iteration. The SAM files need more space and processing time, hence, they were converted to binary format BAM using SAMtools [550].

(ii) Fragment assignment and fragment filter. The reads, which were aligned uniquely and have mapping quality score (MAPQ) ≥ 1 were further parsed to fragment assignment and fragment filtering steps. Reads which were aligned to chromosome Y and mitochondrial chromosome were filtered out from the downstream analysis. Based on the sequence IDs in the BAM files, the alignment results from both sides were paired, keeping those reads which had at least one side aligned. Based on the aligned positions, the reads were assigned to restriction fragments. All the required information like restriction sites, chromosome IDs, positions, fragment IDs, and strand information of one side or both sides of the reads were saved in an HDF5 dictionary file. The fragment filter function then removed reads which had: 1) aligned to only 1 side; 2) both sides aligned to the same restriction fragment (including self-circles, dangling ends, and error pairs) and; 3) two sides extremely close to each other (could be an outcome of incomplete digestion or re-ligation of neighbouring restriction fragments). Duplicate reads (reads with the same chromosome IDs and same positions on both sides) were also filtered out from remaining valid pairs.

(iii) Binning and bin filter. After fragment assignment and filtering step, the unique valid pairs were binned into equal-sized non-overlapping genomic intervals. This binning created a symmetrical genome-wide interaction matrix. The bin filtering step then sequentially removed bins where more than half of the bases were uncertain in the reference genome (such as near centromeres and telomeres). Similarly,

interaction counts in each bin were summed up and bins with the lowest 1% sums (excluding zero-summed bins) were discarded.

(iv) Iterative bias correction. Systematic biases can be introduced in the chromatin interaction data due to experimental protocol such as differences in ligation efficiencies of restriction fragments of different lengths, amplification bias, etc, as well as due to different GC-content, and differential mappability of sequences, just to name a few [548]. These systematic biases adversely affect the interaction values of genomic bins. With an assumption that each bin should theoretically have equal visibility in the experiment, ICE (Iterative Correction and Eigenvector decomposition) implicitly corrects the interaction matrix from these biases by a matrix-balancing method [548]. This bias correction was iteratively performed to obtain a corrected genome-wide interaction matrix as described previously [548] and this matrix was used for downstream analysis.

(v) Heatmap generation. To compare datasets with different read coverage, the corrected interaction matrix was first normalized to a contact probability matrix where the sum of each row/column approximates to 1. Heatmap in log2 color scale was used to visualize the data, and the Python-based software matplotlib [551] was used for this purpose. The heatmap's resolution was determined by the matrix's bin size. Nearby *cis* interactions have a higher frequency than far-away interactions which is represented by a distinct and strong diagonal signal in the chromosome-wide heatmap.

(vi) A/B compartment analysis The A and B chromatin compartments were identified using the corrected interaction matrix. An observed/expected ratio matrix was initially produced for each chromosome-wide matrix, with the expected matrix

consisting of the mean interaction frequencies at certain distances. The correlation coefficients of interaction patterns between genomic bins were then calculated using Pearson correlation on the observed/expected ratio matrix, resulting in a Pearson correlation matrix. Then, using the premise that the interaction matrix can be divided into independent principal components (eigenvectors) that represent each bin's interaction preferences, principal component analysis (PCA) was performed [49]. The most important interaction preference is the leading eigenvector/principal component (PC1) with the highest magnitude of eigenvalues, which is generally linked with numerous genomic features. The sign of PC1 in each chromosome was oriented and a positive Spearman's correlation was obtained between sign of PC1 and GC-content. '**A**' and '**B**' compartments were then assigned to bins with positive and negative eigenvalues respectively.

3.3 Results

3.3.1 Hepatocyte transcriptome changes with age

To investigate age-dependent gene expression changes in mouse hepatocytes, we performed RNA sequencing of total hepatocytes in three age groups, *viz.* 8-week, 32-week and 94-week-old female mice. These age groups represent different stages of reproductive aging in female mice. For example, at 8-week age, the mice are considered sexually mature young adults, by 32-week the reproductive capabilities of female mice start to decline (especially the litter size), and by 94-week age, the mice are reproductively sterile [467]. We isolated hepatocytes by perfusion from female mouse livers of different age groups, extracted total RNA and performed the RNA sequencing on these samples. The NGS read statistics of each RNA-seq sample, including number of sequenced reads, alignment percentage, featureCounts assigned reads, etc., are provided in the **Table 3.1**. After performing the PCA to check variance in our RNA-seq datasets, we observed that biological replicates are clustered together which indicates minimal inter-animal variation in each age group (**Figure 3.2**). Moreover, we observed striking variance in gene expression of different age hepatocytes along the PC1 axis. About 42% of the variance in RNA-seq data (along PC1 axis) can be explained based on age variability between samples (**Figure 3.2**). This is consistent with our findings in chapter 2 where we observed age as a dominant factor for change in gene expression in different ploidy hepatocytes (**Figure 2.1**).

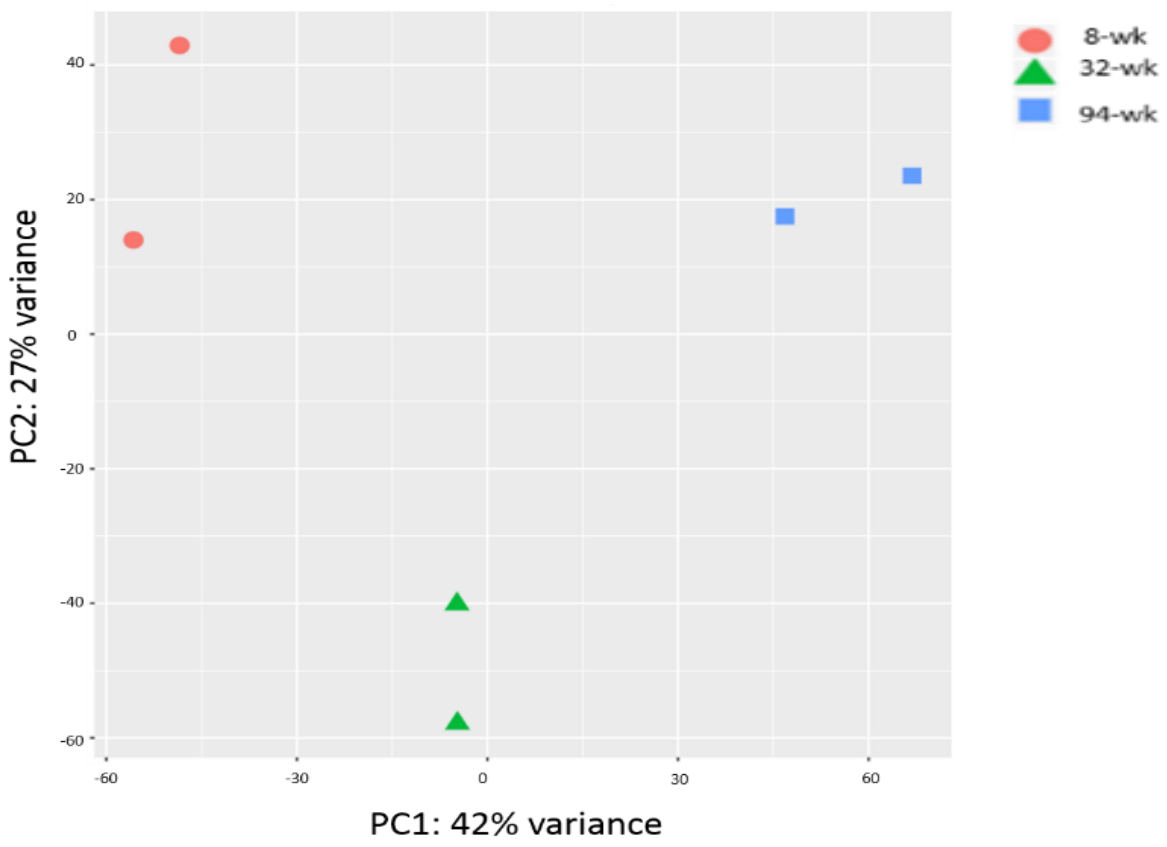

Figure 3.2: PCA of RNA-seq data of total mouse hepatocytes isolated from three different age groups, *viz.* 8-week (red circle), 32-week (green triangle) and 94-week (blue square).

Table 3.1: Read statistics of RNA-seq samples of total hepatocytes isolated from different age groups. R1- replicate 1 and R2- replicate 2.

Samples	# Reads (PE)	STAR uniquely mapped reads (%)	featureCounts assigned reads
8-week-R1	48,180,545	73.3	23,702,863
8-week-R2	41,282,399	76.91	20,374,312
32-week-R1	49,029,017	89.31	27,429,478
32-week-R2	42,472,504	90.86	26,652,836
94-weeks-R1	45,157,467	84.65	30,748,918
94-weeks-R2	41,764,995	78.6	27,166,139

3.3.2 Average gene expression changes with age in mouse hepatocytes

We next investigated if the average gene expression output of mouse hepatocytes varies with age. For that, we estimated transcripts per million (TPM) values of genes and used beanplot analysis to compare the datasets. (**Figure 3.3**).

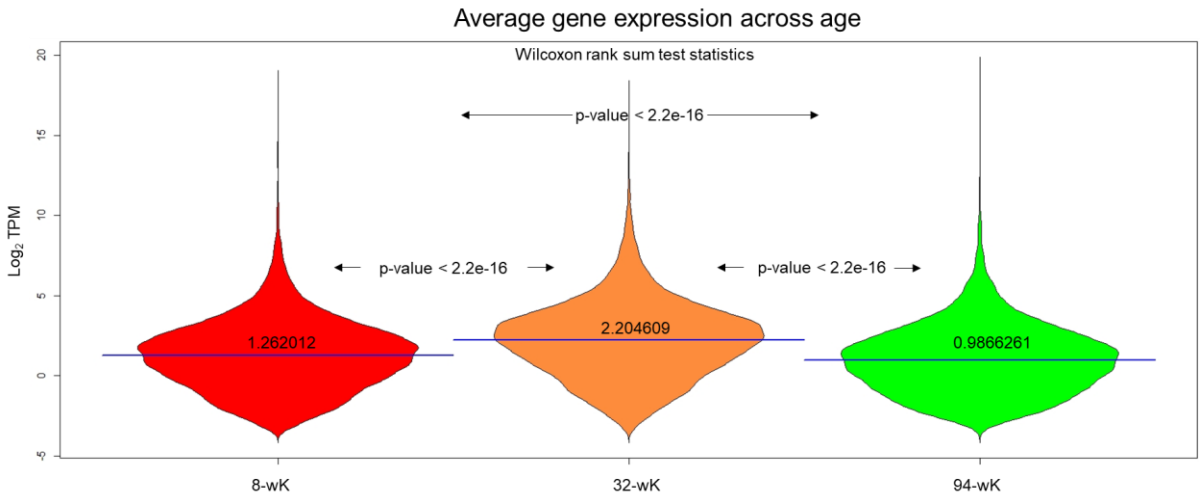

Figure 3.3 Beanplot showing the gene expression values (log2 TPM) of mouse hepatocytes at 8-week (red; left), 32-week (orange; middle) and 94-week (green; right) age. The average gene expression in each sample is represented by blue horizontal line going through the middle of each bean with the mean log2 TPM value indicated above each line. The p-values are indicated which are calculated based on Wilcoxon rank-sum test.

Bean plots revealed an increase in mean gene expression of 32-week hepatocytes compared to 8-week and 94-week hepatocytes (for both comparison, Wilcoxon rank-sum test; p-values < 2.2×10^{-16}). Additionally, mean gene expression of aged 94-week hepatocytes is lower than hepatocytes of sexually mature 8-week-old young adults (p-value< 2.2×10^{-16}) (**Figure 3.3)**. At around 32-week, the hepatocytes are at the peak of their function [467] and this fact may explain the higher level of average gene expression at 32-week compared to 8-week or 94-week-old age groups. Moreover, using assay of template-engaged RNA polymerase II (responsible for hnRNA

transcription) in the cerebral hemisphere of 18-20 week-old and 90-97 week-old rats, Chaturvedi et. al reported a decreased transcriptional activity in an old-age brain compared to the young age [552]. In our hepatocyte data, we also observed similar situation that at 94-week, the average transcriptional output of hepatocytes is lowest compared to younger (8-week or 32-week) age groups. Thus, the average gene expression changes significantly over these time points in mouse hepatocytes. Therefore, it is imperative to perform differential gene expression analysis in mouse hepatocytes between these three age groups to understand age-dependent transcriptional related changes.

3.3.3 Differential gene expression analysis identified age-related gene expression differences in hepatocytes

As described in section 3.2.4, we estimated differential gene expression between datasets using edgeR. We used a p-value cut-off of ≤ 0.05, and $\log_2$ fold-change ≥ 1 to identify differentially expressed genes (DEGs) in female mouse hepatocytes at different age groups. We identified 3034 DEGs between 8-week and 94-week-old hepatocytes, 2832 DEGs between 8-week-old and 32-week-old, and 2738 DEGs between 32-week and 94-week-old hepatocytes **(Figure 3.4)**. Moreover, the age-exclusive DEGs were lowest in 32-week hepatocytes (1029) compared to 8-week (1267) and 94-weeks (1121) (**Figure 3.4**).

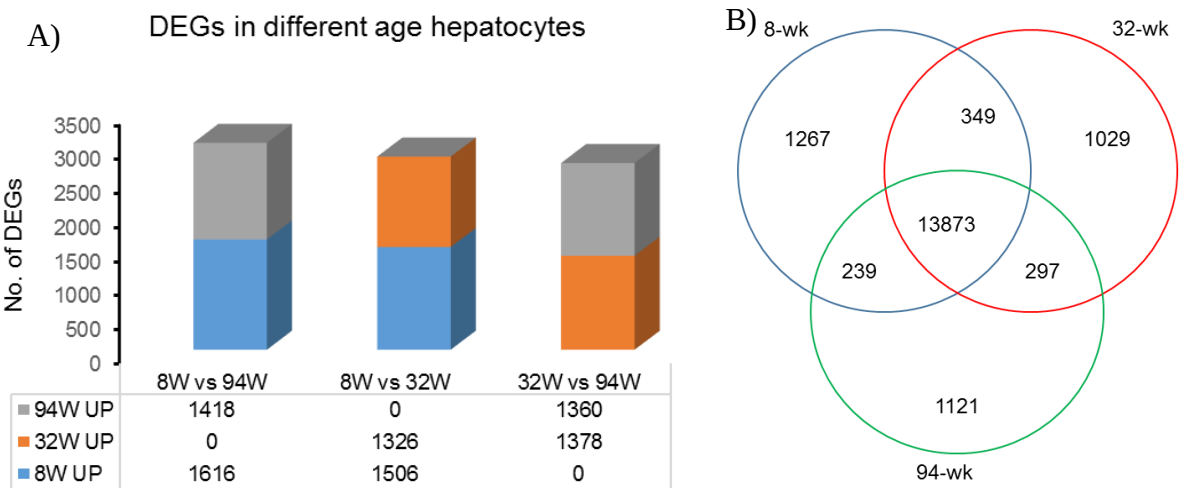

Figure 3.4: Differentially expressed genes between different age groups hepatocytes- A) Bar chart showing number of DEGs for each age-wise combination. B) 3-way Venn diagram showing DEGs for each age group.

3.3.4 Hepatocytes have differential molecular pathways enriched in each age group

From section 3.3.1 - 3.3.3, it is established that in mouse hepatocytes the gene expression changes with age. We next attempted various approaches, *viz.* k-means clustering, gene set enrichment analysis and gene overrepresentation analysis, to study gene expression datasets of hepatocytes from different ages. The results of these approaches are discussed in subsequent sections.

3.3.4.1 The k-means clustering of RNA-seq datasets revealed age-dependent gene signatures

The k-means clustering of RNA-seq data revealed that there are age-dependent distinct gene clusters in mouse hepatocytes **(Figure 3.5)**. For example, genes of cluster **A** was expressed at higher level in 94-week hepatocytes, cluster **B** in 8-week hepatocytes, and cluster **C** was enriched in 32-week hepatocytes. KEGG pathway analysis on these clusters of genes revealed that they are enriched in distinct molecular or biological pathways **(Figure 3.5)**.

Genes in cluster A, which are expressed at high levels in aged 94-week hepatocytes, are enriched in pathways such as PI3K-Akt, Ras signalling, Rap1 signalling, MAPK signalling, cancer-related pathways, TNF alpha, relaxin signalling, etc. These pathways are well-documented in aging studies of vertebrates. Role of P13K-Akt and TNF-alpha pathways during aging have already been elaborated in section 1.3.7. Ras signalling is known to promote aging [553, 554]. Similarly, aged mice express elevated levels of MAPK components (MKK 3/4/7) [555, 556]. In mice, relaxin plays an important role in protecting organs from age-dependent excess accumulation of extracellular matrix and relaxin-null mice develop widespread fibrosis with aging [557-559]. Rap1 (repressor activator protein 1) is a part of shelterin complex and mice lacking Rap1 (Rap1-/-) exhibit early onset of aging pathologies and higher incidences of diethylnitrosamine (DEN)-induced hepatocellular carcinoma [560, 561]. Moreover, cancer and aging share many common characteristics such as increased genomic instability, and aging escalates the chances of cancer development and progression [562-566]. Thus, genes in the cluster **A**, which are highly expressed in aged 94-week mice, are enriched in aging-related pathways **(Figure 3.5)**.

Genes in cluster **B** is expressed at an elevated level in 8-week young adult mice. Pathways such as oxidative metabolism, RNA splicing and metabolism, and chromatin binding were found to be enriched in cluster **B**. As mentioned in section 1.3.5, mitochondrial dysfunction is one of the hallmarks of aging characterized by the impairment of oxidative phosphorylation [567-569]. Moreover, mice at 8-week age are growing adults and they continue to gain body weight and grow in size [570]. Therefore, mice may increase their metabolism during this developmental phase which is supported by increased oxidative phosphorylation. Previous studies using human blood have demonstrated that pathways related to RNA splicing and

metabolism are negatively correlated with age [571-574] which may explain enrichment of pathways related to RNA processing and splicing in cluster **B**. Thus, in a nutshell, cluster **B** is enriched in pathways that are generally associated with youth, vigour and vitality.

The genes in cluster **C** is upregulated in hepatocytes of 32-week-old female mice. At this age, the mouse hepatocyte function is at their peak. In this cluster, we observed that pathways related to typical liver functions, such as metabolism of compounds, xenobiotic transformations and cholesterol biosynthesis, are highly enriched. Around this “middle age” period, the hepatocytes are at the peak of their maturity, linear increase in body weight and food intake and thus require highest levels of metabolic and transformation functions (amongst the most crucial liver functions) are required which begin to decline with aging [570, 575-577].

Thus, taken together, k-means clustering revealed the presence of age-specific gene signatures in hepatocytes of female C57BL6 mice.

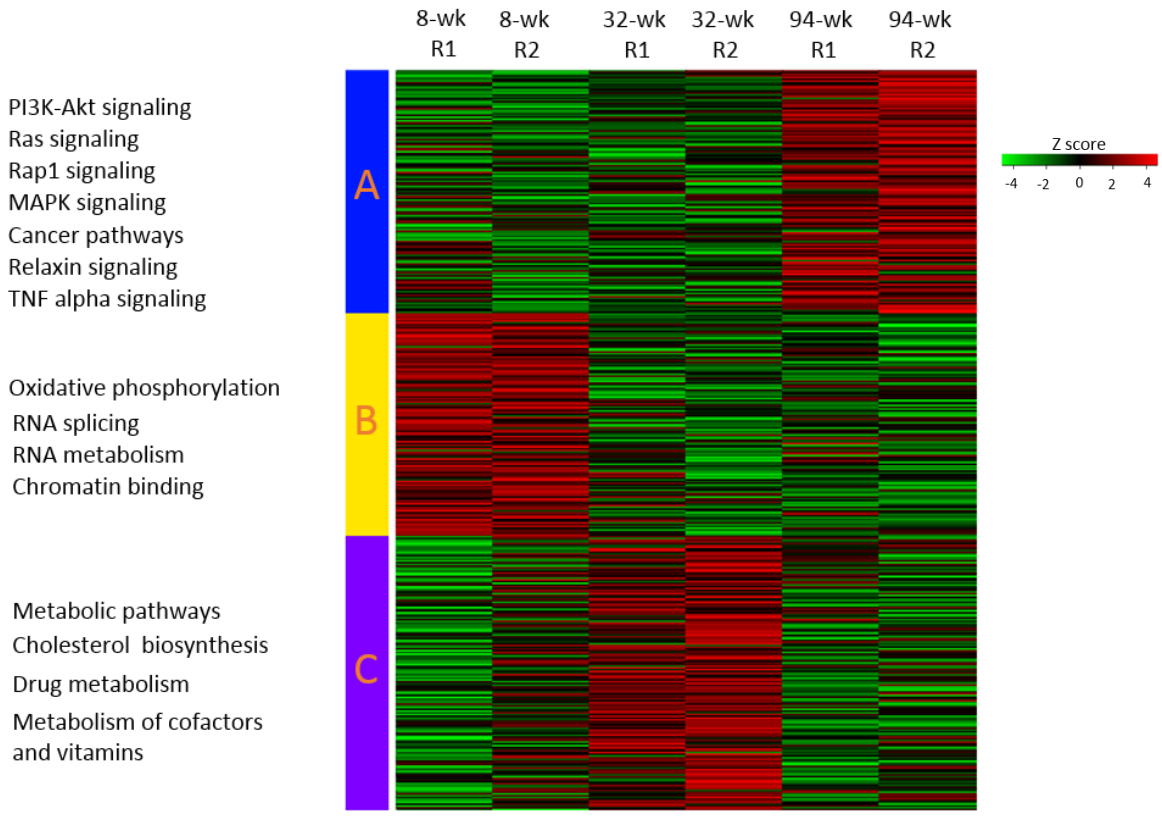

Figure 3.5: A k-means clustering of RNA-seq samples of different ages – genes in cluster A (blue) is enriched in 94-week hepatocytes, cluster B (yellow) in 8-week and cluster C (violet) is enriched in 32-week hepatocytes. The KEGG pathways enriched in each cluster are shown on the left sides of respective clusters (only selected pathways are shown).

3.3.4.2 Pathway analysis revealed comprehensive molecular pathways signature for each age group

To obtain a comprehensive list of pathways enriched in each age group, we performed gene set enrichment analysis (GSEA) using GSEA-desktop application and gene over-representation analysis (ORA) using ConsensusPathDB (CPDB) web server. In GSEA, after p-value cutoff of ≤ 0.05 and based on our manual grouping (as detailed in section 3.2.4.2), we obtained 8 classes in 8-week, 14 classes in 32-week and 16 classes in 94-week hepatocytes (**Figure 3.6**). In case of CPDB, using a p-value cutoff of ≤ 0.05 and manual grouping (as detailed in section 3.2.4.2), we obtained 9 classes

in 8-week, 14 classes in 32-week and 15 classes in 94-week hepatocytes. The complete list of pathways from GSEA and CPDB are shown in Appendix 3.

We compared the results of both GSEA and gene over-representation analysis (CPDB) and selected important ones to get a consensus list of age-specific enriched biological and molecular pathways in mouse hepatocytes as shown in Table 3.2.

Table 3.2: Important pathways identified using GSEA and CPDB in 8-week, 32-week, and 94-week hepatocytes.

8-week	32-week	94-week
Regulation by E2f	Metabolism	Collagen synthesis
mRNA processing	Detoxification	Rho GTPase
G2M	Biological oxidation	Insulin signaling
Glycolysis	Bile synthesis	Death signalling
Cell cycle	Fatty acid synthesis	GPCR signalling
FGF down regulation	DNA repair	Met signalling
	Transcriptional regulation by small RNA	PI3K
	Estrogen signalling	mTOR
	Transporters	MAPK
	Protein localization	Ras
	LDL clearance	
	Epigenetic regulation of DNA, histone and rRNA	

In the following sections, the enriched pathways will be discussed for each age group separately.

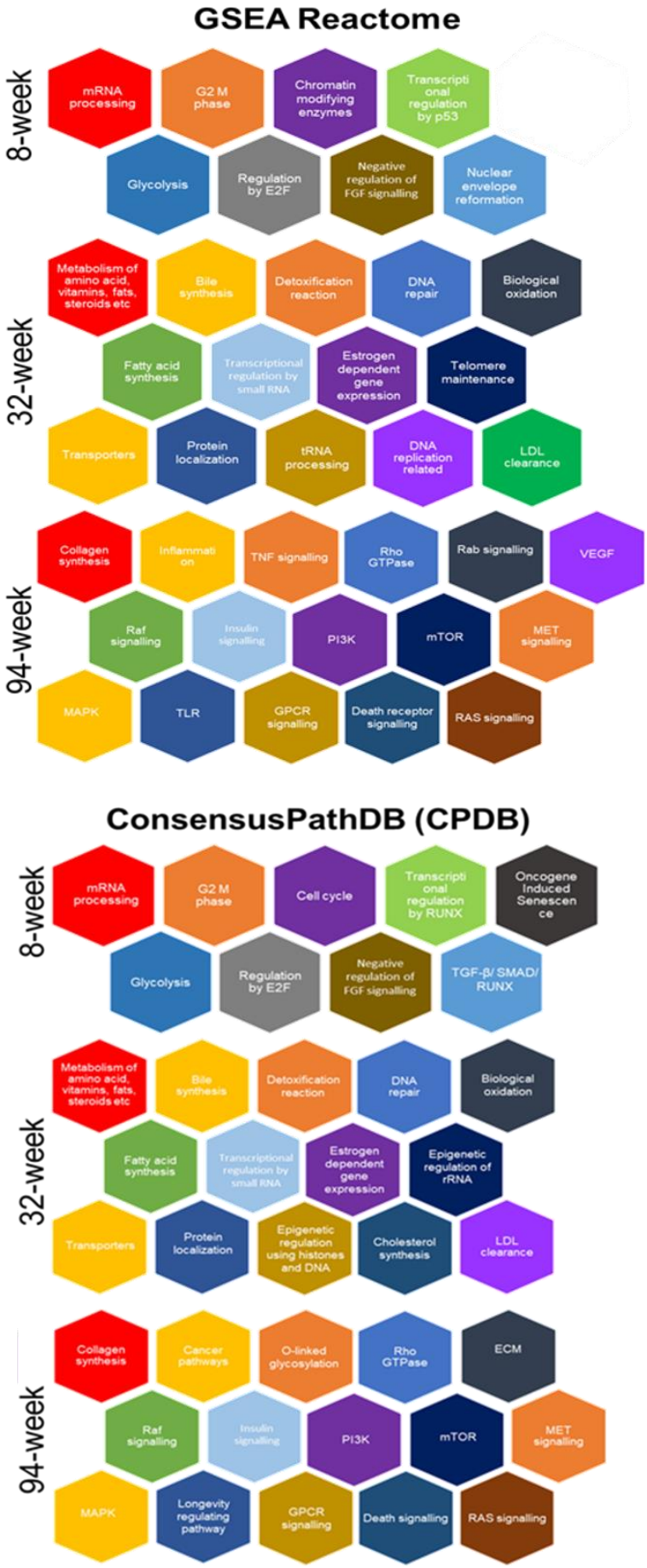

Figure 3.6: Pathways upregulated specifically in 8-week (top), 32-week (middle) and 94-week (bottom) hepatocytes as identified by GSEA (top) and CPDB (bottom).

8-week enriched molecular pathways:

Regulation by E2f

E2F transcription factors are important cell cycle regulators [578]. It has been shown that aging reduces the proliferation rate of hepatocytes by the repression of E2f transcription factors [579]. Consequently, hepatocyte gene expression of 8-week-old mice, the youngest age group in our study, may be under the influence of E2f transcription factor-mediated regulation.

The mRNA processing

Dysregulation in mRNA processing is one of the gene expression hallmarks of cellular aging [580]. Moreover, the percentage of polyadenylated cytosolic RNAs in livers of aged rats was shown to be three times lower than in younger rats [571]. Microarray-based gene expression analysis of human peripheral blood leucocytes in 698 individuals revealed that mRNA splicing, polyadenylation and related post-transcriptional pathways negatively correlates with aging [581]. This may likely explain the observation that mRNA processing and related pathways are enriched in this youngest age group animals of our study.

Cell cycle, Fgf signalling, glycolysis and related pathways

It is well-established that the cell division rate decreases with increasing age [582]. Moreover, fibroblast growth factor (FGF) signalling also stimulates hepatocyte proliferation while also regulating lipid, cholesterol, and bile acid metabolism [498]. Additionally, we know that younger mice have more proportion of diploid hepatocytes than older mice. We also observed higher cell cycle and fgf signalling in diploid hepatocytes compared to polyploid hepatocytes in chapter 2. Thus, 8-week hepatocytes have higher proliferation rate which could be contributed by higher diploid

hepatocyte proportion compared to older mice. Moreover, glycolysis has been found to decline during normal aging and stimulation of glycolysis promotes metabolic health and longevity in *Drosophila* [123].

Taken together, 8-week hepatocytes are enriched in growth and proliferation relation pathways.

32-week enriched pathways:

Metabolism, detoxification, biological oxidation, bile synthesis, fatty acid synthesis, protein localization and LDL clearance

These pathways related to important liver functions are highly enriched in 32-week hepatocytes. As mentioned before, mice reach their pinnacle of sexual maturity, linear increase in body weight and food intake around 32-week and thus they also require maximum levels of metabolic and transformation functions [570, 575-577]. Therefore, the fatty acid synthesis, protein localization, and transporters could be upregulated to meet metabolism related demand in 32-week age mice.

DNA repair

Hepatocytes are subjected to various kinds of metabolic and toxic stress as a result of the production of a range of metabolites by liver and during performing xenobiotic reactions. A large number of free radicals are produced during metabolism, which can form ROS and cause DNA damage in hepatocytes [419]. As a result, an active DNA repair machinery is required for maintaining the genomic integrity. Consequently, DNA repair pathways may have been enriched in 32-week-old hepatocytes.

Estrogen signalling

By 32-week, the reproductive capabilities of female mice begin to decline (especially the litter size) [467]. After 8-months, the female mice have elevated levels of estrogen

and hypothalamic desensitization to estradiol [583]. This could be a possible reason for enrichment of estrogen signalling in 32-week-old hepatocytes.

Epigenetic regulation of DNA, histone and rRNA

It is well established that epigenetic mechanisms play crucial roles in DNA compaction, histone modification and rRNA regulation. Moreover, epigenetic alterations are one of the hallmarks of aging [17].

94-week enriched pathways:

Insulin signalling

The insulin and IGF-1 signalling (IIS) pathways are the most evolutionarily conserved age-regulating pathways, with numerous downstream targets including the mTOR complexes and the FOXO transcription factor family that are highly conserved and implicated in aging phenotypes [232, 584, 585]. In worms, downregulation of IIS pathway genes resulted in a significant increase in longevity, whereas increase in IIS resulted in a decrease in longevity [586, 587]. Thus, the IIS pathway is usually upregulated in aging and may be the reason why it is enriched in aged 94-week hepatocytes.

MET, PI3K-mTOR, Ras-MAPK

Inflammation is the most widely accepted hallmark of aging and has been documented in aged hepatocytes [567]. MET has been demonstrated to have a hepatoprotective effect by reducing chronic inflammation and fibrosis progression [588]. Thus, MET could be involved in hepatoprotective roles in 94-week hepatocytes. Moreover, phosphorylation of MET can activate many downstream signalling pathways including PI3K-mTOR and Ras-MAPK [589-592]. The PI3K-mTOR is categorized as pro-aging pathways and has been discussed in section 1.3.7. For example, Harrison et al.

observed extended longevity in mice treated with rapamycin [593]. Therefore, it may be expected that 94-week hepatocytes will have enriched PI3K-mTOR pathways. Similarly, the role of Ras-MAPK signalling as pro-aging has been well documented [553, 554, 594, 595].

Collagen synthesis

As discussed in section 1.5, with age, collagen is deposited in the liver. Collagen synthesis was found to be increased in old rat livers [596, 597]. Hence, this pathway is expected to be enriched in aged hepatocytes.

RhoGTPase

RhoGTPase (such as Cdc42) are elevated in several aging tissues of mouse including liver [598]. Recently, Cdc42 has been proposed as a blood biomarker of both chronological aging and aging-associated diseases like cardiovascular disease and myocardial infarction [599].

Death signalling

As explained earlier, liver is constantly under different kinds of stress leading to deleterious effects which pile up with age. Hepatocyte death via apoptosis could have impact on aging liver [600]. Therefore, activation of apoptotic machinery may be an obvious manifestation of aging in 94-week hepatocytes.

3.3.5 Age-dependent changes in histone PTMs

It is well established that epigenetic regulation is at the epicentre of transcriptional reprogramming [601]. Moreover, the role of epigenetics in aging is well-established using several model systems including humans [602]. Additionally, the roles of specific histone PTMs in aging have been emphasized as described in detail in the introduction chapter (**section 1.3.3.3**). Strikingly, we also observed that pathways related to epigenetic regulation of histone and DNA are enriched in 32-week hepatocytes

(section 3.3.4.2). Therefore, we hypothesized that epigenetic regulation may be a crucial mechanism in age-dependent gene expression changes. Therefore, we investigated the genome-wide changes in histone PTMs in 8-week and 32-week hepatocytes. For this analysis, we studied two active histone marks, H3K27ac and H3K4me3, and two inactive/repressed histone marks, H3K9me3 and H3K27me3.

The read statistics of each ChIP-seq experiment, including number of sequenced reads, alignment percentage, etc., are provided in Table 3.3. Briefly, we obtained 24-64 million paired-end reads and 92% to 96% overall alignment for each sample.

Table 3.3: Read statistics of ChIP-seq experiments showing the total number of paired-end reads obtained and read alignment for each ChIP experiment and corresponding input sample.

Age (wks)	Histone mark	Total reads	Overall alignment (%)
8-week	Input	64,428,782	93.79
8-week	H3K4me3	25,506,759	96.20
8-week	H3K9me3	31,146,161	95.10
8-week	H3K27ac	30,436,029	95.55
8-week	H3K27me3	36,323,345	94.07
32-week	Input	24,768,479	92.76
32-week	H3K4me3	40,776,712	95.42
32-week	H3K9me3	43,814,174	94.08
32-week	H3K27ac	32,208,383	95.98
32-week	H3K27me3	33,793,966	92.95

Based on the property of histone PTMs that we investigated, we divided the analysis in two parts, one covering the impact of aging on active histone marks (H3K27ac and H3K4me3) and other detailing its influence on repressed histone marks (H3K9me3 and H3K27me3).

3.3.5.1 Age-dependent changes in active chromatin marks

H3K27ac

As mentioned in section 1.3.3.3, histone H3K27ac signal is present at both active promoters and distal enhancers and is strongly associated with transcription factor binding and gene expression [603]. Interestingly, H3K27ac ChIP-seq data of 8-week and 32-week hepatocytes revealed some compelling findings. First, based on visual inspection in UCSC genome browser**,** we noticed at the genome-wide (all chromosomes) level, the signal distribution of H3K27ac exhibits marginal changes but the signal intensity reduces in 32-week hepatocytes compared to 8-week cells. Figure 3.7 represents the UCSC genome browser snapshots showing H3K27ac signals across selected chromosomes (Chr# 1, 2 and 4) in 8-week and 32-week hepatocytes.

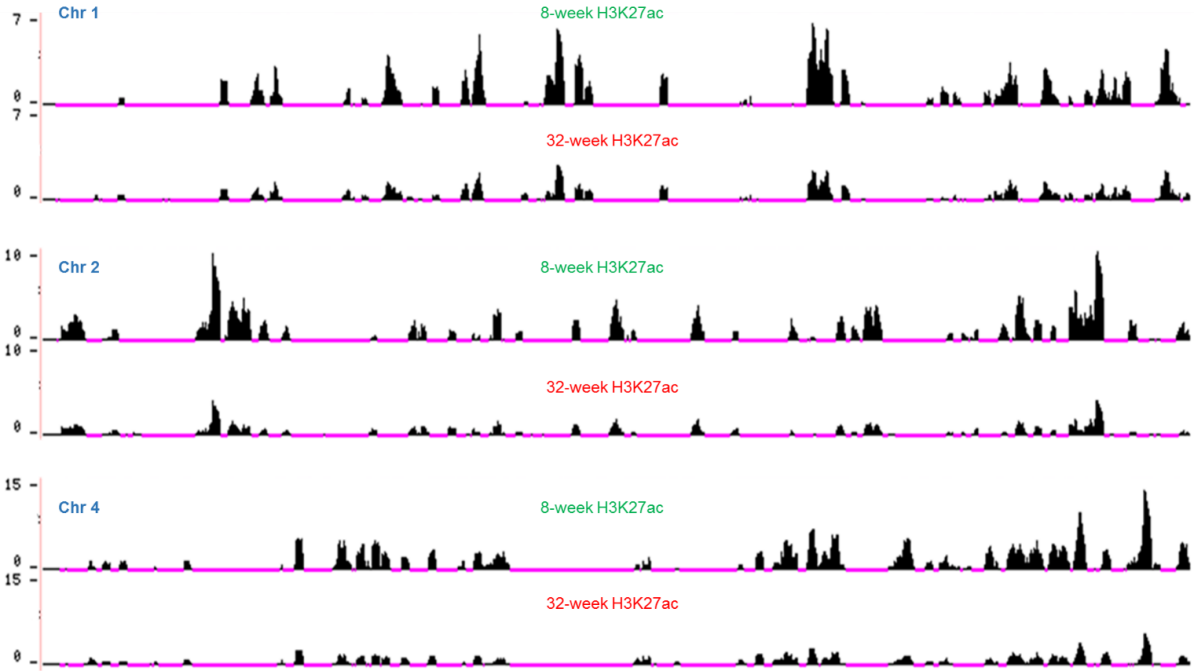

Figure 3.7: UCSC genome browser snapshot for H3K27ac signals across Chr 1 (top), chr2 (middle) and chr4 (bottom) in 8-week and 32-week hepatocytes. Overall, H3K27ac signal distribution remains largely unchanged but signal intensity reduces in 32-week hepatocytes compared to 8-week hepatocytes.

Furthermore, we identified H3K27ac peaks in 8-week and 32-week hepatocytes using MACS2 peak calling algorithm [542]. Using this approach, we found that total number of H3K27ac peaks is comparable between 8-week (36028) and 32-week (35752) hepatocytes (**Figure 3.8A**). Additionally, we used HOMER's in built annotatePeaks program to group these MACS2 peaks into 5 categories, *viz.* exonic, intronic, intergenic, promoter-TSS (transcription start site), and TTS (transcription termination site) [545]. We observed that peak distribution of H3K27ac remains unchanged between 8-week and 32-week hepatocytes where 48% of peaks are intronic, 22% are intergenic, 20% promoter-TSS, 6% exonic while only 4% in TTS regions (**Figure 3.8C**). Furthermore, read coverage analysis using deepTools revealed that at the genic regions, the average signal intensity of H3K27ac is reduced in 32-week hepatocytes compared to 8-week hepatocytes (**Figure 3.8B and 3.8D**). This reduction

in H3K27ac signal intensity at genic regions is consistent with genome-wide reduction in H3K27ac ChIP signal as visually observed using UCSC genome browser in 32-week hepatocytes (**Figure 3.7, 3.8B and 3.8D)**. In our gene expression data, we observed an interesting trend of increased expression of many HDACs in 32-week hepatocytes compared to 8-week cells (**Figure 3.9)**. These HDACs are involved in histone deacetylation which may partly explain the reduction in H3K27ac signal in 32-week hepatocytes.

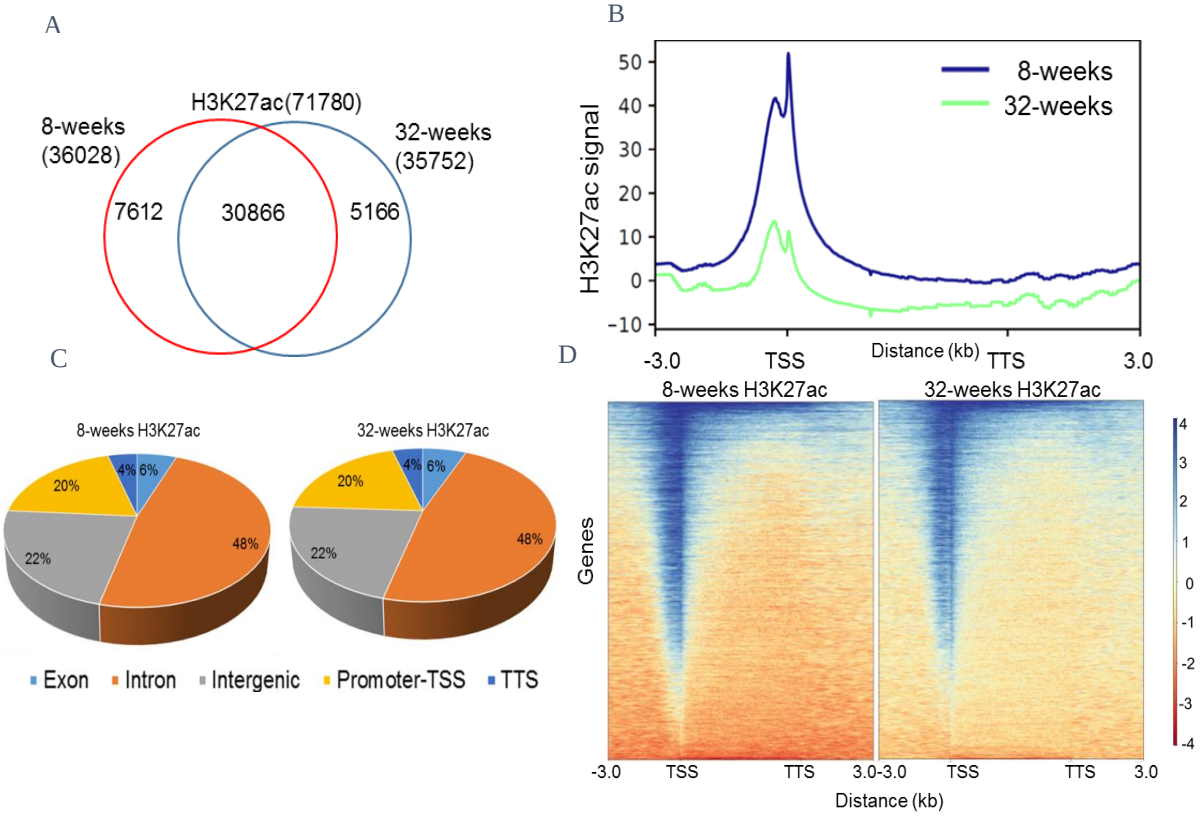

Figure 3.8: H3K27ac signals in 8-week and 32-week hepatocytes- A) Number of H3K27ac MACS2 peaks called in 8-week (red) and 32-week (blue) hepatocytes. B) Average scaled enrichment (ASE) plot of H3K27ac ChIP signal in genic regions comprising TSS, gene body, 3kb upstream of TSS, and 3kb downstream from TTS in 8-week (blue) and 32-week hepatocytes (green). C) H3K27ac peaks annotated based on HOMER peakannotation in 8-week (left) and 32-week (right) hepatocytes. D) H3K27ac read coverage in genic regions of 8-week (left) and 32-week hepatocytes (right), where color scale denotes heatmap intensity.

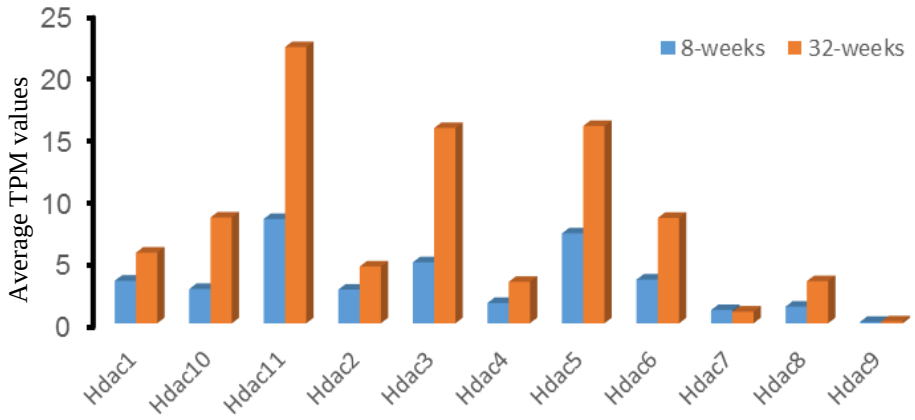

Figure 3.9: Gene expression levels of different Hdacs in 8-week (blue) and 32-week (orange) hepatocytes. The average TPM values based on two replicates are plotted on the y-axis.

H3K4me3

Histone H3K4me3 signal is generally present near transcription start sites of active promoters and positively regulate transcription by bringing histone acetylases and nucleosome remodelling enzymes (NURF) [603]. Strikingly, H3K4me3 ChIP-seq in 8-week and 32-week hepatocytes revealed some drastic changes between two age groups. First, based on visual inspection in UCSC genome browser, we observed that at genome-wide (all chromosomes) level, H3K4me3 signal increases in intensity and distribution in 32-week hepatocytes compared to 8-week hepatocytes. Figure 3.10 represents the UCSC genome browser snapshots showing H3K4me3 signals across selected chromosomes (Chr# 12, 9 and 13) in 8-week and 32-week hepatocytes.

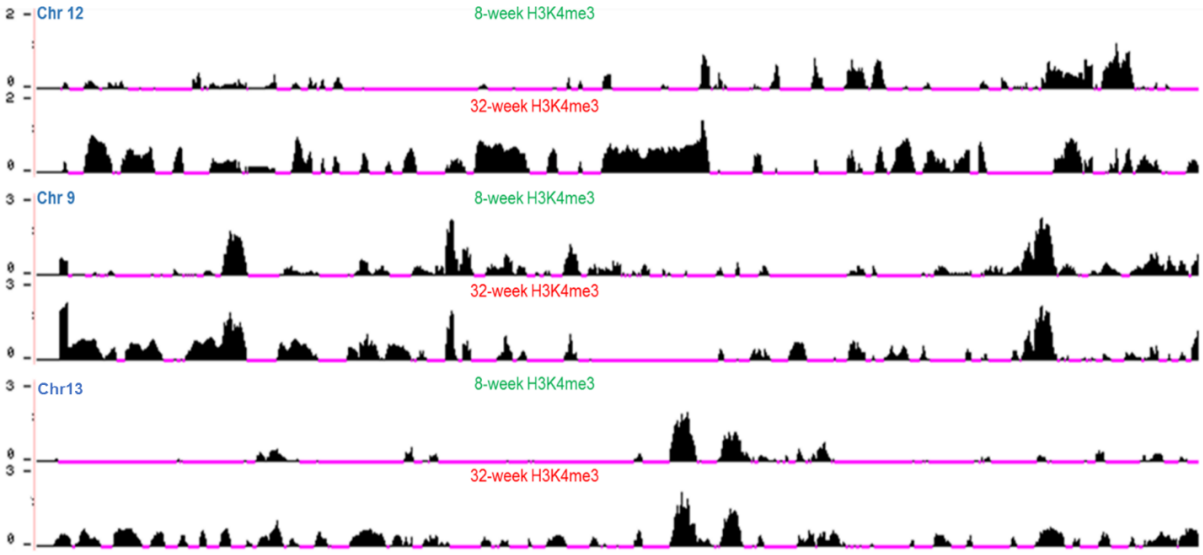

Figure 3.10: UCSC genome browser snapshots of H3K4me3 ChIP signals across chr12 (top), chr9 (middle) and chr13 (bottom) in 8-week and 32-week hepatocytes. The signal distribution of H3K4me3 increases in 32-week hepatocytes compared to 8-week cells.

Furthermore, we identified H3K4me3 peaks in our ChIP-seq datasets using MACS2 and found that the total number of H3K4me3 peaks increase in 32-week (16041) compared to 8-week (12610) (**Figure 3.11A**). Therefore, we next checked the peak locations using HOMER based peak annotation which revealed slight differences in peak distribution between 8-week and 32-week hepatocytes. As expected Promoter-TSS peaks amount to the highest percentage in both age groups (**Figure 3.11C**). This could be important as increase in active promoters could increase gene expression. There were small variations amongst other peak categories like intergenic peaks increases from 6% to 11%, intronic peaks from 29% to 30%, and TTS peaks from 3% to 4% in 8 weeks to 32-week while exonic peaks decrease from 14% to 13% from 8-week to 32-week hepatocytes (**Figure 3.11C**). Strikingly, the average signal intensity of H3K4me3 in genic regions was not as drastically different between two age groups as observed in genome-wide UCSC genome browser (**Figure 3.10, 3.11B and D**).

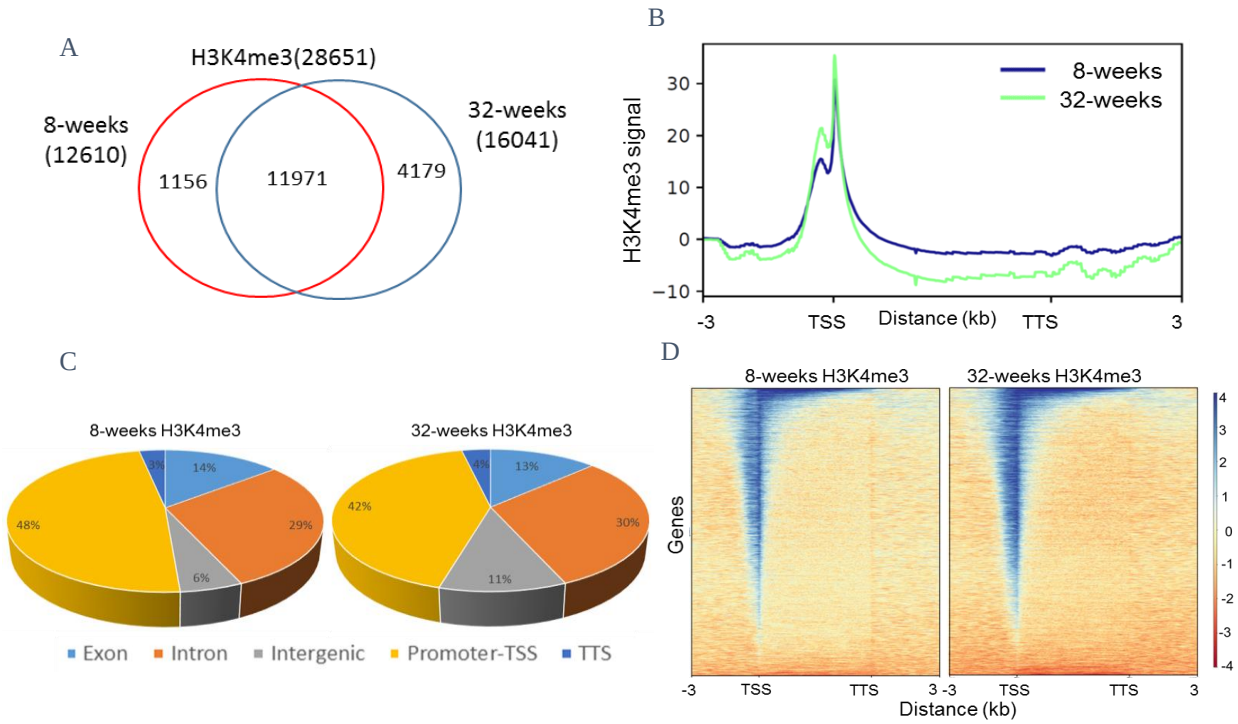

Figure 3.11: H3K4me3 signals in 8-week and 32-week hepatocytes- A) Number of H3K4me3 MACS2 peaks called in 8-week (red) and 32-week (blue) hepatocytes. B) Average scaled enrichment (ASE) plot of H3K4me3 ChIP signals in genic regions comprising TSS, gene body, 3kb upstream of TSS, and 3kb downstream from TTS in 8-week (blue) and 32-week hepatocytes (green). C) H3K4me3 peaks annotated based on HOMER peak annotation in 8-week (left) and 32-week (right) hepatocytes. D) H3K4me3 read coverage in genic region of 8-week (left) and 32-week hepatocytes (right), where color scale denotes heatmap intensity.

3.3.5.2 Age-dependent changes in closed chromatin marks

H3K9me3

H3K9me3 is prevalent in constitutive heterochromatic regions such as repetitive elements and pericentromeric regions, where it plays an important role in chromatin compaction [104]. Interestingly, H3K9me3 ChIP-seq in 8-week and 32-week hepatocytes showed negligible changes. Based on visual inspection of H3K9me3 ChIP signal in UCSC genome browser, we observed that H3K9me3 signal intensity and signal distribution remains largely unchanged between 8-week and 32-week hepatocytes in a genome-wide manner. Figure 3.12 represents the UCSC genome browser snapshots showing H3K9me3 signals across selected chromosomes (Chr# 1, 2 and 9) in 8-week and 32-week hepatocytes.

When we quantified the signal intensity at the genic regions, we noticed that the signal intensity of H3K9me3 is reduced in 32-week hepatocytes. This reduction in signal intensity is most drastic around the TSS region in 32-week hepatocytes **(Figure 3.13A and B**).

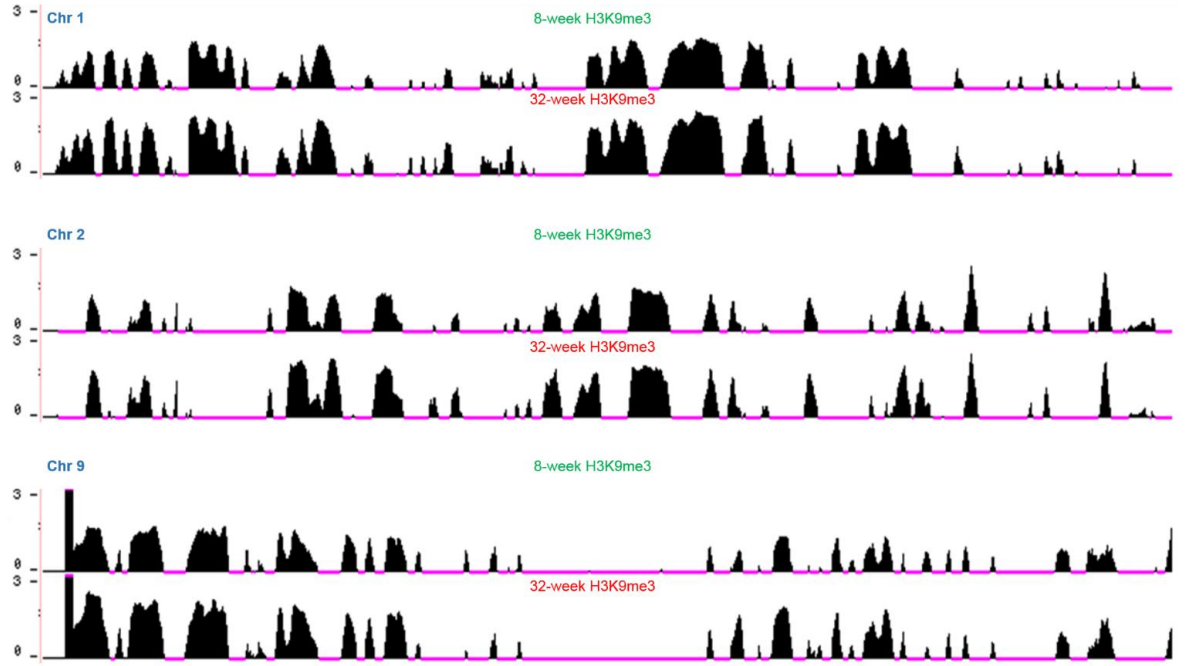

Figure 3.12: UCSC genome browser snapshots of H3K9me3 ChIP signals across chr1 (top), chr2 (middle) and chr9 (bottom) in 8-week and 32-week hepatocytes. Overall, the signal intensity and distribution remains largely invariant between 8-week and 32-week hepatocytes.

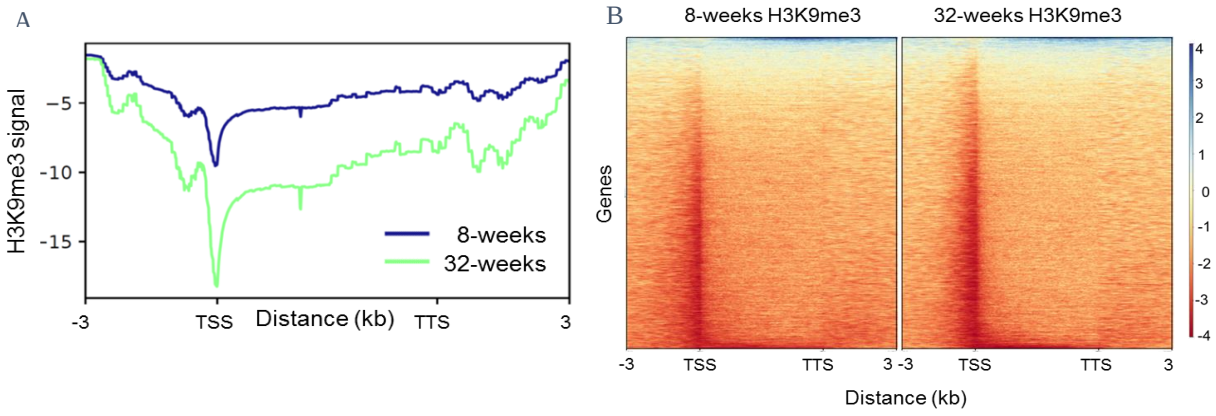

Figure 3.13: H3K9me3 signals in 8-week and 32-week hepatocytes- A) Average scaled enrichment (ASE) plot of H3K4me3 ChIP signals in genic regions comprising TSS, gene body, 3kb upstream of TSS, and 3kb downstream from TTS in 8-week (blue) and 32-week hepatocytes (green). B) H3K9me3 read coverage in genic regions of 8-week (left) and 32-week (right) hepatocytes, where color scale denotes heatmap intensity.

H3K27me3

The H3K27me3 accumulates over cell-type-specific repressed genes (facultative heterochromatin) and inactivated X chromosome [105-107]. The trimethylation of histone H3 at Lysine 27 residue is mediated by methyltransferase enhancer of Zeste homolog 2 (EZH2), a part of Polycomb repressive complex 2 (PRC2) [603]. Whereas, demethylation of H3K27 is mediated by KDM6A/UTX and KDM6B/JMJD3 [604].

Strikingly, H3K27me3 ChIP-seq exhibited the most drastic changes between 8-week and 32-week hepatocytes. First, based on visual inspection in UCSC genome browser, we observed that genome-wide H3K27me3 signal intensity and distribution increases drastically in 32-week hepatocytes compared to 8-week cells. Figure 3.14 represents the UCSC genome browser snapshots showing H3K27me3 signals across selected chromosomes in 8-week and 32-week hepatocytes. Interestingly, when we compared 32-week H3K27me3 and H3K9me3 signals, we found that they overlap in several genomic loci (**Figure 3.15**).

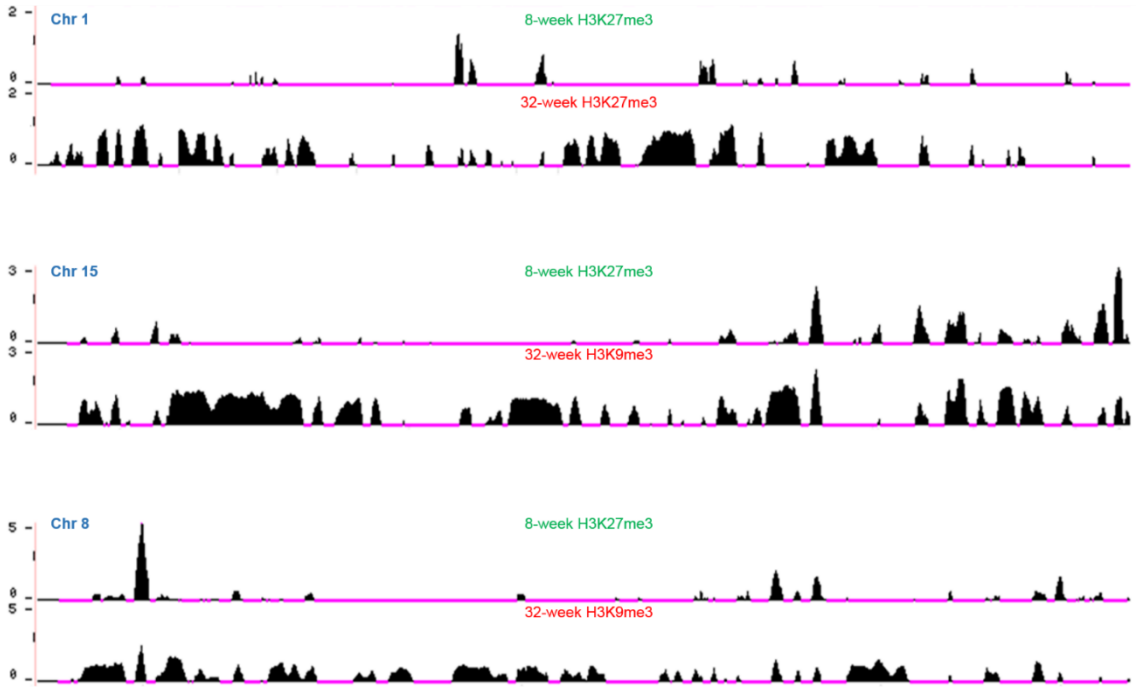

Figure 3.14: UCSC genome browser snapshots of H3K27me3 ChIP signals across chr1 (top), chr15 (middle) and chr8 (bottom) of 8-week and 32-week hepatocytes. H3K27me3 signal distribution increases genome-wide in 32-week hepatocytes compared to 8-week hepatocytes.

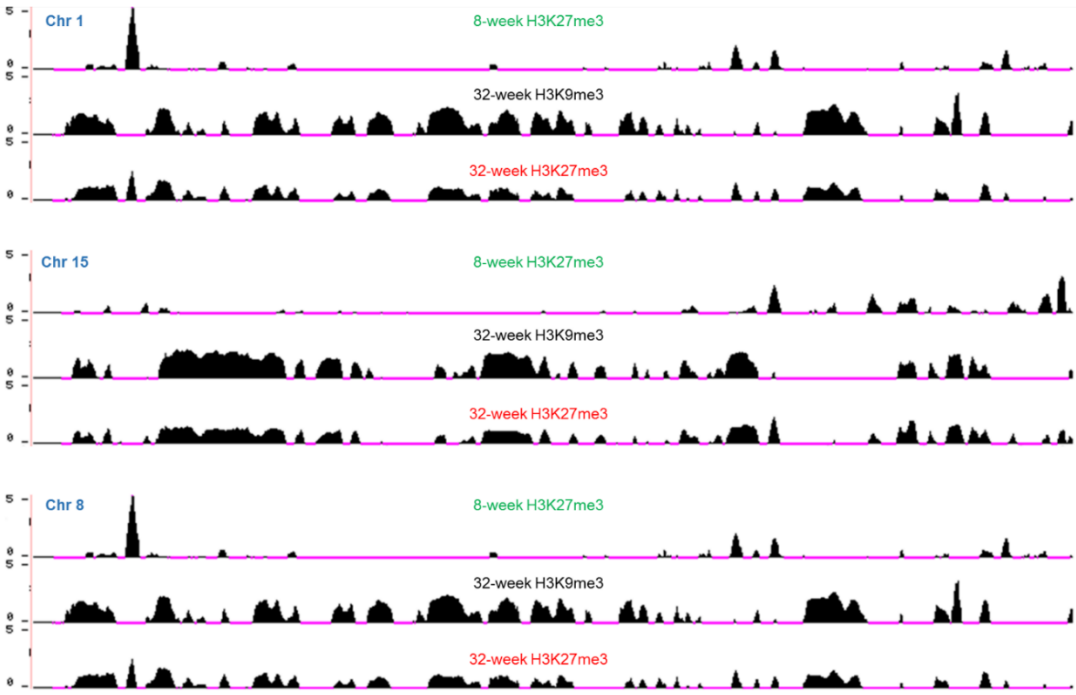

Figure 3.15: UCSC genome browser snapshots of 8-week H3K27me3 signal, 32-week H3K9me3 signal and 32-week H3K27me3 signal across chr1 (top), chr15 (middle) and chr8 (bottom).

When we quantified the signal intensity at the genic regions, we noticed that the signal intensity of H3K27me3 has reduced in 32-week hepatocytes compared to 8-week hepatocytes. This reduction in signal intensity is most drastic around the TSS region in 32-week hepatocytes (**Figure 3.16A and B**). This is in contrast to genome-wide increase in the H3K27me3 signals and distribution in 32-week hepatocytes (**Figure 3.14**). This conflicting observation of H3K27me3 signal at the genic and genome-wide levels in 32-week hepatocytes hints towards an intricate epigenetic regulatory mechanism that differentially modulates chromatin structure at the genic regions to allow gene expression while repressing non-coding genome in 32-week hepatocytes.

To understand the genome-wide increment in H3K27me3 signal in 32-week hepatocytes, we examined the expressions of PRC2 complex genes (responsible for methylating H3K27) from our RNA seq data. We noticed increase in expression of *Ezh1/2, Eed and Aebp2* genes in 32-week hepatocytes compared to 8-week (**Figure 3.17A**). Increase in the expression of these PRC2 complex associated genes can partly explain the increment in histone H3K27me3 mark in 32-week hepatocytes.

As shown in section 3.3.2, we observed that the average gene expression level is higher in 32-week hepatocytes compared to 8-week hepatocytes (**Figure 3.3**). Reduction in H3K27me3 in the genic region and most importantly in TSS region might help in opening up chromatin for gene transcription and hence their higher expression. To investigate further in this direction, we scanned the H3K27me3 signal at the DEGs upregulated in 32-week hepatocytes compared to 8-week. Overall, we noticed a general pattern of decline in H3K27me3 signal of DEGs in 32-week hepatocytes compared to 8-week cells (**Figure 3.17B**). Next, we focussed on 5 selected DEGs, previously implicated in aging or senescence, which showed higher expression in 32-week hepatocytes and studied the H3K27me3 signal alterations on these loci. These

genes are- *Atf3, Efna1*, *Fos*, *Fosb* and *Btg2*. The importance of these cherry-picked genes are discussed below:

Activating transcription factor 3 (ATF3) is a AP-1 transcription factor which is induced by stress signals and plays important role in modulating metabolism, oncogenesis and immunity [605]. ATF3 have been shown to alter chromatin accessibility and promote cellular senescence [606].

EFNA1 is a prototypic ligand for EphA2 receptor tyrosine kinase and is bound to the cell membrane by a glycosyl-phosphatidylinositol (GPI) linkage which regulates cell growth and migration [607]. EFNA1 signalling was found to be associated with age-dependent senescence and reduced migration of human cardiac progenitor cells [608].

In humans, Fos gene family consists of 4 members: *FOS*, *FOSB*, *FOSL1*, and *FOSL2*. FOS is a part of AP-1 transcriptional complex and plays important role in development, cell proliferation, and differentiation [609]. FOS is associated with age-related changes and with the attenuated cellular response in older cells [610]. The *c-Fos* was found to be a biomarker for liver cancer [611, 612]. Similarly, *Fosb* was demonstrated to be elevated in senescent cells [613].

BTG Anti-Proliferation Factor 2 (*Btg2*) is a member of BTG/Tob family of anti-proliferative genes and have been found to play important roles in cell cycle progression, differentiation, apoptosis and promoting p53-dependent replicative senescence [614, 615]. Btg2 is induced by different cellular stresses through p53-dependent and p53-independent processes [616].

Interestingly, we noticed that the H3K27me3 signals in these 5 gene loci have a common theme in 32-week hepatocytes - reduction in H3K27me3 signal and

increased gene expression (**Figure 3.18**). From figure 3.16A, we observed that in 32-week hepatocytes, H3K27me3 signal is reduced at TSS of genes and in figure 3.18 we provided evidence of reduction in repressive H3K27me3 signal in selected genes highly expressed in 32-week hepatocytes which could be attributed to their higher gene expression. This means that in 32-week hepatocytes if all chromosomes have reduced H3K27me3 signal at TSS then possibly genes from each chromosome should have higher average expression compared to 8-week hepatocytes. Therefore, we next investigated the average gene expression levels in each chromosome in 8-week and 32-week hepatocytes. We found that the average gene expression of genes from every chromosome is higher in 32-week hepatocytes compared to 8-week cells (**Figure 3.19)** which supports our speculation.

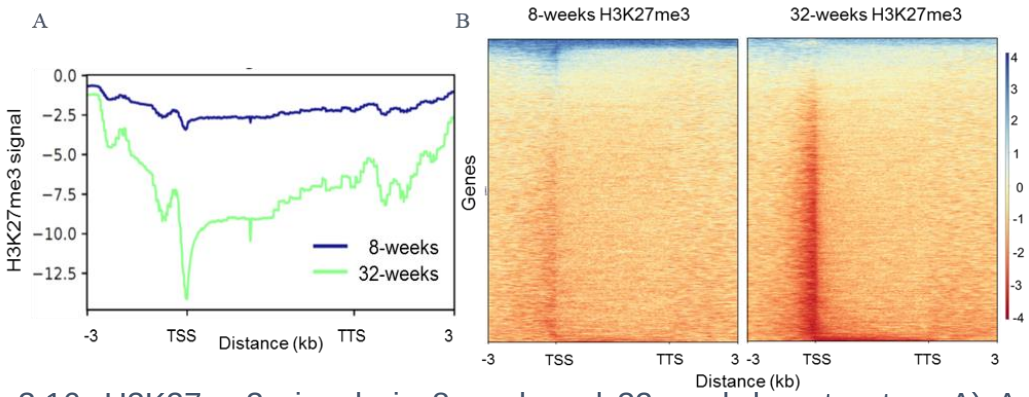

Figure 3.16: H3K27me3 signals in 8-week and 32-week hepatocytes- A) Average scaled enrichment (ASE) plot of H3K27me3 ChIP signals in genic regions comprising TSS, gene body, 3kb upstream of TSS, and 3kb downstream from TTS in 8-week (blue) and 32-week hepatocytes (green). B) H3K27me3 read coverage in genic regions of 8-week (left) and 32-week (right) hepatocytes, where color scale denotes heatmap intensity.

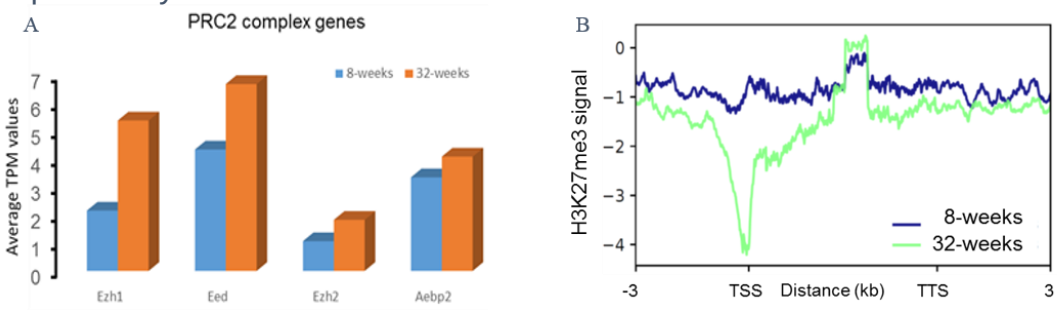

Figure 3.17: Can PRC2 complex genes explain H3K27me3 signals in 8-week and 32-week hepatocytes?- A) Gene expression of PRC2 complex genes (average TPM values of two replicates) in 8-week (blue) and 32-week (orange) hepatocytes.B) ASE

plot of H3K27me3 ChIP signals in genic regions (as in A) of 32-week upregulated DEGs and shown for both 8-week (blue) and 32-week (green) data

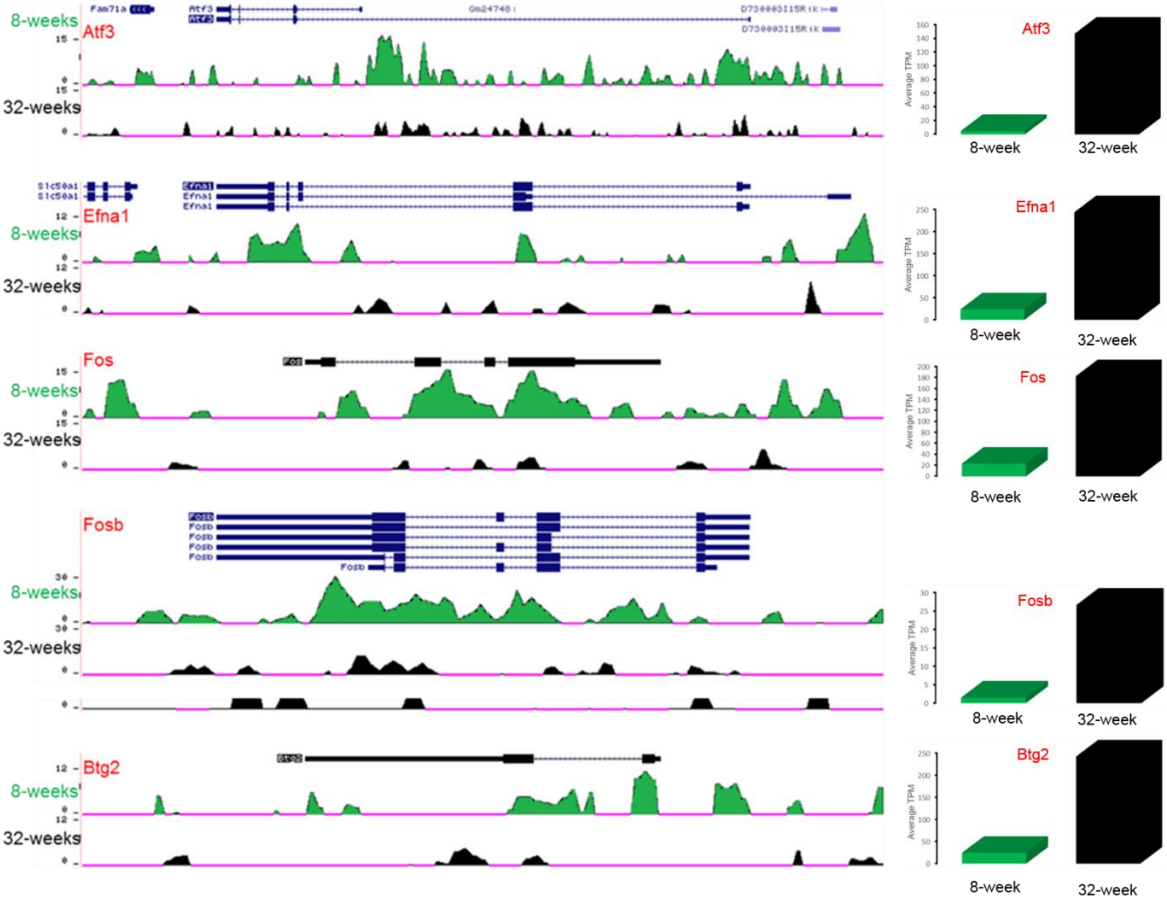

Figure 3.18: H3K27me3 signals are reduced at genic region of 32-week upregulated genes- Left: UCSC genome browser snapshots of H3K27me3 ChIP signals at selected 32-week upregulated genes in 8-week and 32-week hepatocytes. Right: The corresponding gene expression data of those selected genes in 8-week (green) and 32-week (black) hepatocytes are shown. The gene expression are calculated as average TPM values from 2 replicates in 8-week and 32-week hepatocytes RNA-seq.

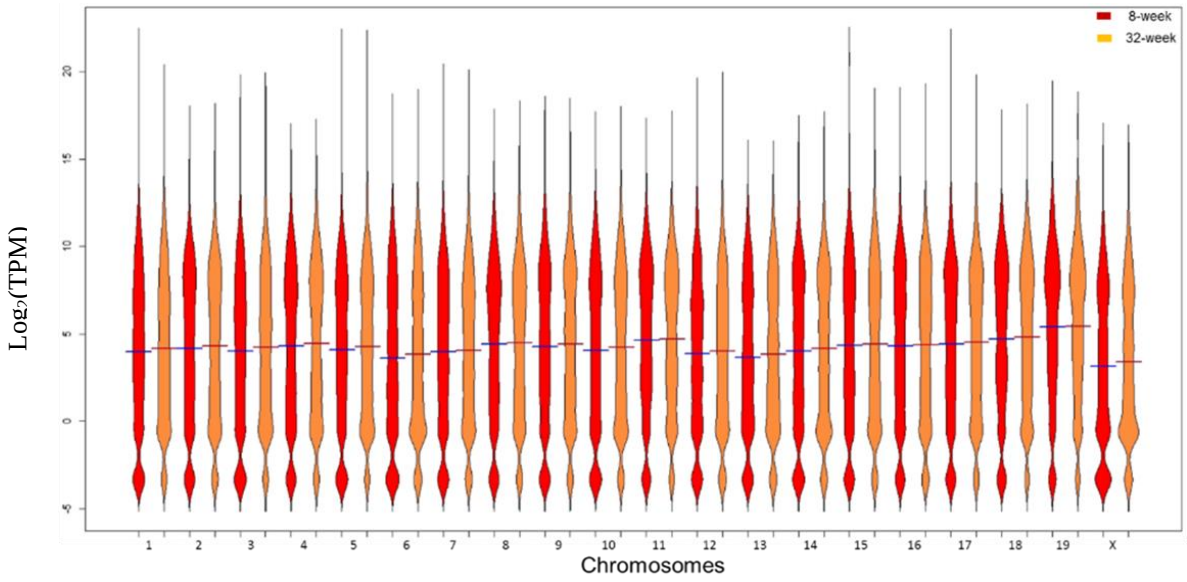

Figure 3.19 Beanplot showing the gene expression levels (log2 TPM) in hepatocytes at 8-week (red) and 32-week (orange) age. The average gene expression in each sample is represented by blue line (in 8-week) and red line (in 32-week) passing through the middle of each bean.

Overall, we observed alterations in histone PTMs between 8-week and 32-week

female mouse hepatocytes which are summarized in Table 3.4.

Table 3.4: Summary of genome-wide and genic region impact in active and inactive histone PTMs alterations in 32-week hepatocytes compared to 8-week hepatocytes.

Histone PTM	Type	Genome-wide impact in 32-week compared to 8-week	Genic region impact in 32-week compared to 8-week
H3K27ac	Active	signal distribution exhibit marginal changes but the signal intensity reduces	average signal intensity reduces
H3K4me3	Active	signal intensity and distribution increases	average signal intensity comparable
H3K9me3	Inactive	signal intensity and distribution remains largely unchanged	average signal intensity reduces
H3K27me3	Inactive	signal intensity and distribution drastically increases	average signal intensity reduces

3.3.6 Three-dimensional chromatin organization of 8-week and 32-week mouse hepatocytes

It is well known that changes in genome architecture contribute to changes in gene expression. Accordingly, changes in 3D genome organization have been implicated in senescence, aging as well as in accelerated aging models as described in the Introduction. Therefore, we aim to study if there are alterations in spatial chromatin conformations between 8-week and 32-week mouse hepatocytes using 3C sequencing (3C-seq). The read statistics obtained from hiclib output of 3C-seq experiments are provided in Table 3.5

Table 3.5: 3C-seq read statistics obtained from hiclib output: 8-week (left) and 32-week (right).

Statistics	**8-week reads**	**32-week reads**
MappedSide1	123385983	73562364
MappedSide2	121807086	72503568
TotalReads	130042420	77529605
totalDSReads	115150649	68536327
DS+SS	130042420	77529605
SSReadsRemoved	14891771	8993278
Self-Circles	14867	7721
DandlingEnds	96352187	55013325
extraDandlingEndsRemoved	8881084	7041785
ValidPairs	9899883	6472577
duplicatesRemoved	748250	410121

First, using hiclib package, we constructed the genome-wide chromatin contact heatmaps of 8-week and 32-week mouse hepatocytes from corresponding contact probability matrices (**Figure 3.20**). As expected, visual inspection of the heatmaps notably showed a strong intra-chromosomal interaction (*cis*) compared to inter-chromosomal (*trans*) interactions. This can be attributed to the nuclear topological

arrangement of chromosomes into chromosome territories (CTs) which is a characteristic feature of the mammalian interphase nuclei [49].

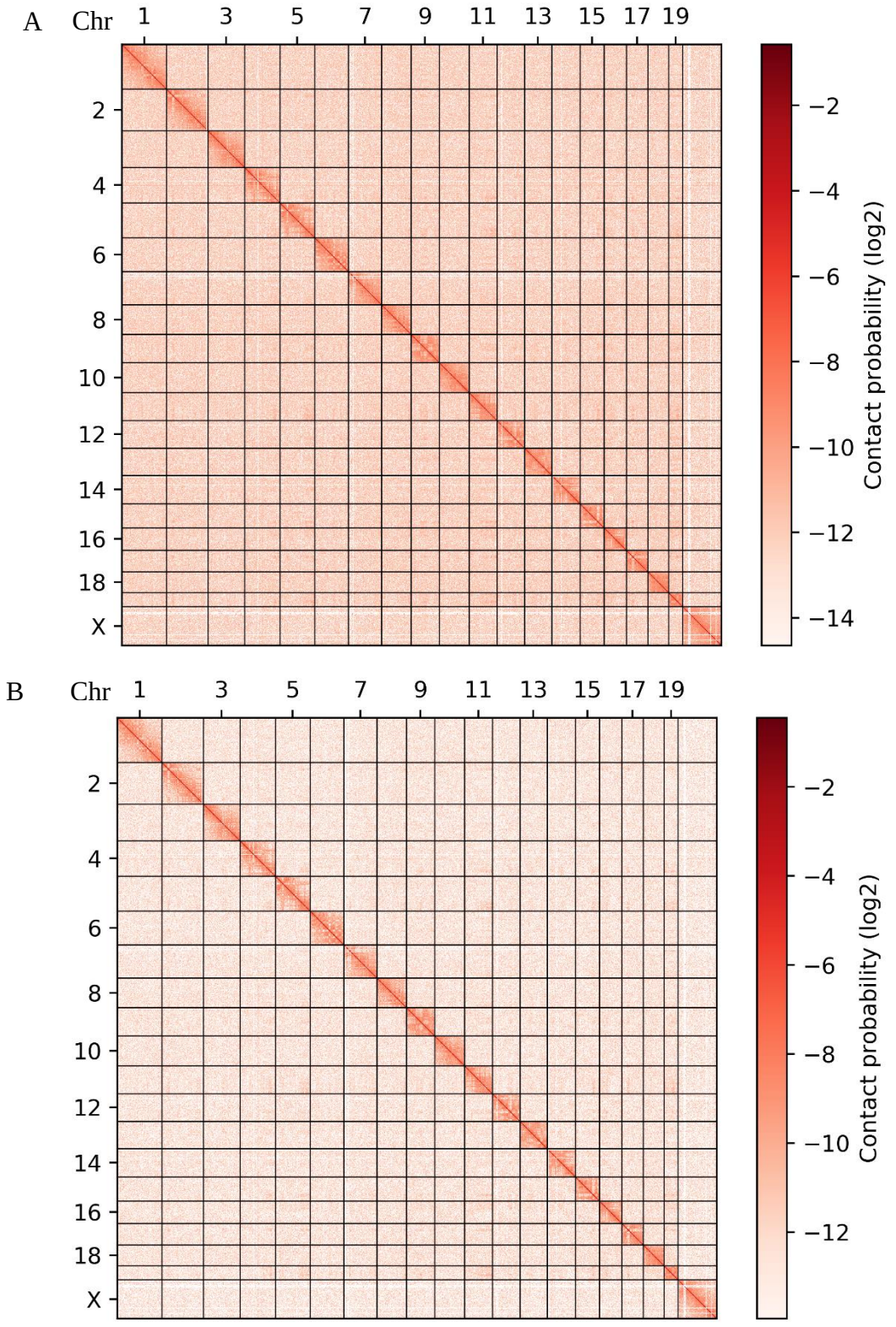

Figure 3.20 Genome-wide chromatin contact heatmaps (bin size = 1 Mb) of 8-week (A) and 32-week (B) hepatocytes. Chromosomes are labelled on the axes of the heatmaps. Color bar denotes the log2 contact probability.

3.3.6.1 Compartment analysis between 8-week and 32-week hepatocytes

Chromatin are organized in higher-order structures of different length scales. Based on the genome-wide chromatin interaction data, one can predict the A (active) and B (inactive/repressed) chromatin compartments. Therefore, to investigate if there are changes in A/B compartments between two age groups, we performed PCA analysis on the Pearson correlation heatmaps. The PC1 value was determined as described in **section 3.2.16,** for each chromosome-wide matrix with bin size of 1 Mb. The sign of the eigenvector was oriented to positively correlate with GC-content of the genome. The genome was then segmented into A and B compartments with positive and negative eigen values respectively. As compartment A is associated with active chromatin while compartment B is linked with inactive chromatin, the PC1 eigen values should positively correlate with active histone PTMs and negatively with inactive histone PTMs [49, 133]. Moreover, the average gene expression should be higher in compartment A compared to compartment B, as genes located in the open/active chromatin region are generally considered to be transcriptionally active [49, 133]. Therefore, we next compared PC1 eigen values to our histone PTMs datasets to determine the relationship between A (active) and B (inactive) compartments with the active and inactive histone PTMs. Spearman correlation analysis showed that for both age groups, PC1 eigenvectors were found to positively correlate with active histone marks, such as H3K27ac (8-week: Spearman rho = 6.84×10^{-1} and 32-week: Spearman rho = 5.34×10^{-1}) and H3K4me3 (8-week: Spearman rho = 4.18×10^{-1} and 32-week: Spearman rho = 3.3×10^{-1}). We also observed that PC1 eigenvectors were negatively correlated with inactive marks, H3K9me3 (8-week: Spearman rho = -7.48×10^{-1} and 32-week: Spearman rho = -8.2×10^{-1}) and H3K27me3 (8-week: Spearman rho = -2.2×10^{-1} and 32-week: Spearman rho = -6.7×10^{-1}) **(Figure 3.21A).** When we

checked the average gene expression levels in A and B compartments, we discovered that genes residing in A compartments are expressed at a significantly higher level (Wilcoxon rank-sum test, p-value < 2.2×10^{-16}) compared to genes located in B compartments in both 8-week and 32-week hepatocytes **(Figure 3.21B)**.

However, when we compared the A/B compartments between 8-week and 32-week hepatocytes**,** we noticed that there are almost invariant across chromosomes (**Figure 3.22B).** This indicates that even though the gene expression and histone modifications can change drastically, the higher-order chromatin organization at the A/B compartment level remains stable at least till the 32-week age suggesting the robustness of these compartments (**Figure 3.22).**

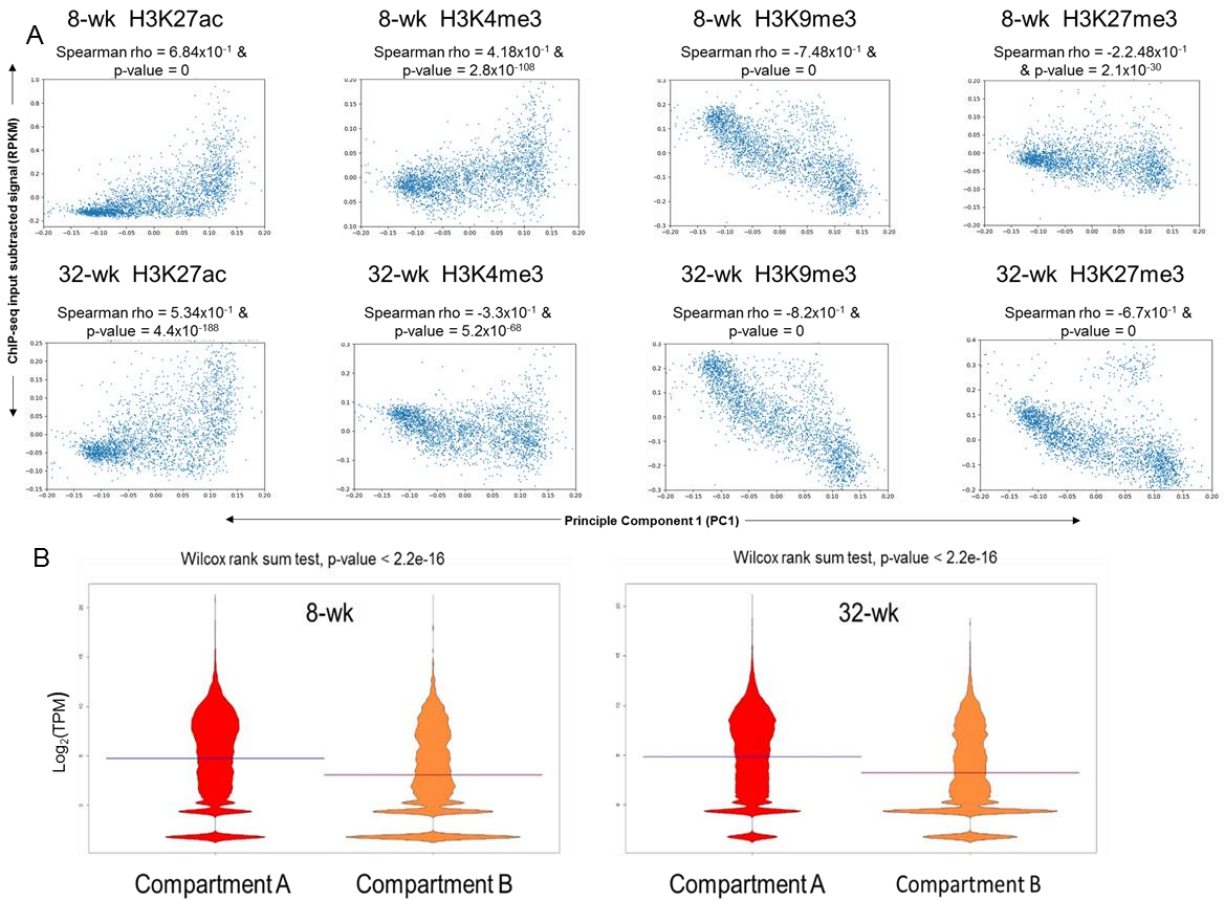

Figure 3.21 (A) Correlation between PC1 eigenvectors and histone ChIP-seq signals (bin size = 1Mb; left panel) in 8-week (top) and 32-week (bottom) hepatocytes. Spearman's correlation coefficients (rho) and p-values were shown on top of each panel. (B) Bean plot of log_2(TPM) values of genes residing in A and B compartments generated for 8-week (left) and 32-week (right) hepatocytes. The statistics and p-values from Wilcoxon rank-sum tests were shown on top of each panel.

A

Sample	8-weeks	32-weeks
No. of bins in compartment **A**	1192	1191
No. of bins in compartment **B**	1352	1352

B

8-weeks	32-weeks
Compartment **A** (1192)	Compartment **A** (1104)
	Compartment **B** (88)
Compartment **B** (1352)	Compartment **A** (1264)
	Compartment **B** (87)

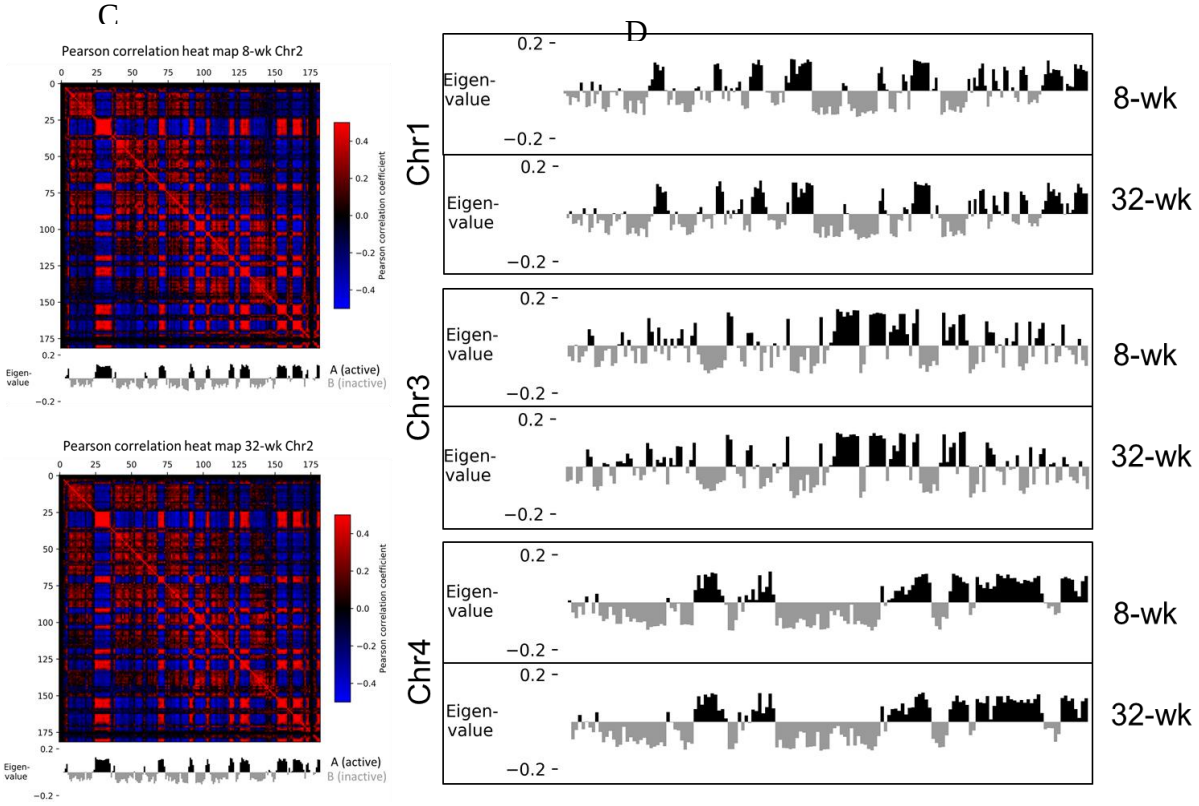

Figure 3.22: The A/B compartment analysis between 8-week and 32-week hepatocytes- A) Number of bins (1 Mb bin size) in A and B compartments in 8-week and 32-week hepatocytes. B) Number of compartments that switched/ remain invariant between 8-week and 32-week hepatocytes. C) Chromosome-wide Pearson correlation heatmaps of chromosome 2 in 8-week (top) and 32-week (bottom) hepatocytes. D) Chromosome wide eigen value profiles in 8-week (top panel) and 32-week (bottom panel) hepatocytes across chromosome 1, 3 and 4.

3.4 Discussion

Age acts as one of the most prominent risk factors for various diseases, however, transcriptomic and epigenetic manifestations of aging are not universal for every tissue or organ of our body. The liver is a metabolically active and essential organ that performs many crucial functions to sustain body homeostasis. The majority of these

liver functions are performed by hepatocytes. Despite undergoing various kinds of stresses, rodent hepatocytes are amongst the longest living cells with an average lifespan of 200-400 days. Thus, hepatocytes serve as a unique model for studying aging. Because of its short lifetime and similar genome and physiology to humans, the mouse has quickly become the mammalian model organism of choice in aging research. In this chapter, we have generated molecular blueprints of developmental age-specific changes in mouse hepatocytes at transcriptomic, epigenetic, and 3D genome organisation levels.

RNA-sequencing of 8-week, 32-week and 94-week-old mouse hepatocytes revealed differential upregulation of various biological/molecular pathways in these cells isolated from different age groups. For example, pathways upregulated in 8-week hepatocytes indicate that they are more proliferative, they have better mRNA processing compared to other age groups. Similarly, 32-week hepatocytes that are at the peak of metabolic maturation are enriched in liver-specific functions like metabolism, detoxification, bile synthesis, etc. DNA repair pathways are also enriched at this stage probably to safeguard from ROS or xenobiotic-mediated DNA damage owing to their high metabolic and detoxification function at this age. The aged 94-week hepatocytes showed enrichment in pathways considered as hallmarks of aging such as PI3K-mTOR-Ras-MAPK, etc. In short, we found developmental age-associated molecular pathways in our data.

The average gene expression level of 32-week hepatocytes was found to be significantly higher compared to 8-week and 94-week hepatocytes. Interestingly, aged 94-week hepatocytes exhibit the lowest average gene expression compared to the other two younger ages. It is well established that mice are at their peak of maturity at around 32-week of age as around this age, the mice reach the plateau of their food

intake and pinnacle of linear increase in body weight in most strains [570]. The age-associated progressive decline in cellular function begins after this age.

Histone PTMs are known regulators of gene expression. Therefore, we performed ChIP-seq with active and inactive histone marks in 8-week and 32-week hepatocytes to study age-dependent alterations and their effect on gene expression, if any, in these two age groups. We observed striking genome-wide changes in 32-week hepatocytes compared to 8-week cells. For example, based on visual observation of ChIP-seq signals at UCSC genome browser, distributions of H3K27me3 and H3K4me3 signals increase, H3K27ac signal decreases and H3K9me3 appears to be largely unchanged at genome-wide scale in 32-week hepatocytes compared to 8-week cells. However, at the genic level, we observed reduction in H3K27me3, H3K9me3 and H3K27ac signals while no change at TSS regions of H3K4me3 in 32-week hepatocytes compared to 8-week. Moreover, many genes related to members of the PRC2 complex showed elevated expressions in 32-week hepatocytes. We used examples of genes upregulated in 32-week (*Atf3*, *Efna1*, *Fos*, *Fosb* and *Btg2*) compared to 8-week in our RNA-seq data and provided evidence that reduction in H3K27me3 signals at genic regions possibly result in increased gene expression in 32-week hepatocytes. Reduction in H3K27me3 in genic regions hints that those regions have comparatively open chromatin and thus are more accessible to transcriptional complexes, leading to higher gene expression.

However, the reason for the increased H3K27me3 at the genome-wide level is not clear. The drastic change in genome-wide H3K27me3 level could be attributed to many factors. One reason for increased H3K27me3 could be hepatocyte polyploidy. With age, the ploidy proportion of hepatocytes increase but based on our study we know that gene expression does not increase linearly with ploidy (DNA content).

Therefore, there are chances that with age, as the ploidy increases, hepatocytes need to adapt to the 'excess' burden of genome content and also maintain the genome integrity as polyploidization is linked to cancer in mammalian cells. We speculate that possibly polyploid hepatocytes (which increases with age) repress most of the genomic regions by chromatin compaction which manifests in an increase in the H3K27me3 signal. This is also important for genomic integrity and stability by keeping the transposable elements silent. However, it is still not clear why there is an increased overlap of the H3K27me3 signal with the H3K9me3 signal in 32-week hepatocytes though H3K9me3 signal remains largely invariant between 8-week and 32-week hepatocytes. In the future, this can be addressed by performing H3K27me3 and H3K9me3 ChIP-seq experiments in different ploidy hepatocytes. However, in the present study, we are limited by the small number of sorted 2N, 4N, and 8N hepatocytes isolated from a single animal. Hence, we could not perform these experiments. Moreover, senescence and aging are intricately connected in mouse liver and other organs. Accordingly, in our RNA-seq data, we observed upregulation of senescence-associated genes in 32-week hepatocytes (for example, average TPM of *Glb1:* 8-week = 3.44 and 32-week = 12.16*, Atf3:* 8-week = 5.11 and 32-week = 146.81). There is a possibility that alteration in H3K27me3 is a senescence-associated phenotype in 32-week hepatocytes [617]. However, this drastic change in histone H3K27me3 did not influence spatial genome organisation at least at Mb-scale. The 3C-seq data established that A and B compartments remain largely invariant between 8-week and 32-week female mouse hepatocytes. This observation suggests that the A/B compartments are highly stable chromatin structure at least till 32 weeks in mouse hepatocytes. However, this does not rule out the possibility of alterations in chromatin structure at the level of TADs or long-range looping interactions. In the future, our 3C-

seq data needs to be analyzed to investigate TAD boundary changes and alterations in looping interactions and correlate them with gene expression changes.

3.5 Work contributions

Agnes Ong and I carried out two-step collagenase-based mouse liver perfusion. I purified the mouse hepatocytes and processed them for RNA-seq, histone PTM ChIP-seq, and 3C-seq experiments. I prepared the ChIP-seq libraries with Dr. Aravinda Chavalmane (postdoc from Sanyal lab), and 3C libraries with Dr. Amartya Sanyal. I optimised the data analysis pipelines and performed all the data analysis of the RNA-seq, ChIP-seq and 3C seq experiments. A/B compartments using 3C-seq data were called by Dr. Yao Chen (PhD student from Sanyal lab). The experiments and data analysis were conducted under the guidance of my supervisor, Dr. Amartya Sanyal and our collaborator, Dr. Torsten Wuestefeld.

Chapter 4: Conclusion and future work

There is an increase in global human life expectancy over the last 100 years due to improvements in environment, food availability, and medicine. As the global population ages, the prevalence of chronic age-related illnesses will rise, placing a significant strain on healthcare resources. Long considered to be an inevitable path to disease and decline, aging is surprisingly changeable. Plasticity like this might be used to take a fresh look at age-related biological changes. Genetic and epigenetic mechanisms are considered to play roles in most of the variability in health-span and lifespan in humans. Therefore, understanding the genetic and epigenetic mechanisms of aging is a primary objective in aging research. A large body of evidence has firmly established the laboratory mouse as an excellent model of human aging [585, 618]. Mice allow maximum lifespan studies due to their relatively short lifespan, and the environmental factors affecting aging can be precisely controlled to study genetic factors. Additionally, the mouse aging phenotypes not only closely resemble humans, but they also share genetic loci controlling lifespan and health-span [618, 619].

In this thesis, we have presented the work on aging-associated alterations in mouse hepatocytes. We hypothesised that hepatocyte aging is driven by alterations in gene expression and this age-associated transcriptional reprogramming is regulated by epigenetic mechanisms including specific histone PTMs and spatial genome organisation. The majority of the published aging research using various mouse organs or tissues was generally focussed on two end points that include young (1-3 months) and old (20-30 months) animals. As discussed in chapter 1, the liver is an excellent aging model where despite different kinds of stresses, hepatocytes can live astonishingly longer lives. The liver consists of several different cell types and each might have its progression of age-dependent changes. Moreover, to the best of our

knowledge, there is no availability of any systematic data for age-dependent changes in genome, epigenome, and spatial chromatin organisation levels in mouse hepatocytes. We bridge these gaps by investigating gene expression profiles of hepatocytes from young (8-week), middle-age (32-week), and old-age (94-week) female mice and also studied epigenome and chromatin interactome of hepatocytes isolated from 8 and 32-week mouse livers. Overall, we performed an integrated analysis of age-dependent changes in female mouse hepatocytes at DNA (ploidy), RNA (gene expression), epigenome (histone PTMs), and spatial 3D chromosome organisation (A/B compartment) levels.

One of the most noticeable age-associated changes in hepatocytes is an increment in polyploidy. Hepatocyte polyploidy is known for many decades but whether it is a consequence of stresses (genotoxic, metabolic, oxidative stress, etc.), or a buffering against ROS induced DNA damage/ mutations or driver of age-dependent changes which can lead to an increase in metabolic output in the liver, is still not clear. Our RNA-seq analysis using hepatocytes of different ploidy levels revealed that polyploid hepatocytes exhibit a trend of relatively higher average gene expression compared to their diploid counterparts of the same age. This observation partly supports the hypothesis that polyploidy helps in increasing transcriptional output which in turn increases metabolic output and liver function. This increment in average gene expression owing to an increase in DNA ploidy may be helpful for elevated metabolic output but also bring unique sets of challenges. For example, an increase in DNA ploidy will result in the expansion of non-coding regions of the genome which include repetitive elements, transposable elements (TE), etc., and if left unchecked they can lead to genetic and structural aberrations in the genome [620, 621]. Similarly, an increase in gene copy (by polyploidization) may result in inadequate dosage

compensation of imprinted genes and genes residing in X chromosome in polyploids, which could have deleterious effects in mammals [622]. However, silencing of TE and dosage compensation are epigenetically regulated in mammals and thus chances are intricate epigenetic regulation is assisting mouse hepatocytes to ameliorate the consequences of polyploidization. Thus, studying epigenetic mechanisms such as histone PTMs could reveal the transcriptional regulatory code of polyploid hepatocytes.

Our data also showed that each ploidy population has a unique gene expression signature and distinct upregulation of molecular pathways and thus hinting towards a ploidy-specific functional role in the liver. This could further explain why the liver maintains a fixed proportion of polyploidy and might hold the clue for aberrations in hepatocyte ploidy profiles and their associations with several liver diseases. The differential gene expression in different ploidy hepatocytes could be a result of multiple phenomena. First, it is widely known that an increase in ploidy leads to an increment in cell size and subsequently their volume. However, the cell surface can only increase 1.59 times for every two times increase in cell volume, which results in a reduced surface-to-volume ratio in polyploid hepatocytes [623]. This lower ratio may influence gene expression [624]. Changes in epigenome could be one of the drivers of altered gene expression in polyploid cells [625, 626]. For example, in the giant polyploid trophoblast cells (TGCs) of the placenta in mice, some X-linked genes escape X chromosome inactivation (XCI) which is associated with accumulation of active (H3K4me3) and inactive (H3K27me3) histone PTMs [625]. The presence of “bivalent chromatin” (both H3K4me3 and H3K27me3) is believed to be a reason to maintain key genes in a poised state and allow their expression in response to external stimulus in TGCs [626, 627]. In the present study, we could not perform any epigenetic

investigation on sorted 2N, 4N, and 8N hepatocytes isolated from a single animal due to their low numbers. Nevertheless, it would be interesting to study the epigenetic regulation in different ploidy populations in the future by adapting ChIP-seq and 3C-seq protocols for low-input samples.

On a different note, the relationship between ploidy and liver zonation is still debatable. According to one study, hepatocytes are generally diploid in the pericentral regions and polyploid in the periportal regions [628] while another claims that multinucleated hepatocytes are seen around the pericentral areas [629]. Contrary to the above studies, Tanami et al. suggested that 4N and 8N polyploid hepatocytes are located in the mid-lobule zone rather than periportal and pericentral areas [630]. It is important to note that we have perfused the whole liver for isolating hepatocytes of different ploidy. Therefore, our current data cannot be used to study if there are liver zone-specific roles of diploid and polyploid hepatocytes or to understand the complex relationship between ploidy and metabolic zonation. Additionally, we addressed the relationship between ploidy and NAFLD and demonstrated that NAFLD-associated genes are differentially expressed in different ploidy hepatocytes. NAFLD is the manifestation of metabolic stress due to excess fat accumulation in the liver. As ploidy is increased in diet-induced NAFLD mice, one can argue that this pathological polyploidization is a consequence of stress.

We learned that aging is a major contributor to changes in gene expression based on RNA-seq data of 8-week and 32-week hepatocytes. We identified different molecular signatures and pathways in 8-week, 32-week, and 94-week hepatocytes using RNA-seq. We also found that average gene expression is higher in 32-week hepatocytes compared to 8-week and 94-week hepatocytes. As histone modifications are widely associated with transcriptional reprogramming, we studied the locations of histone

H3K27me3, H3K27ac, H3K4me3, and H3K9me3 signals in 8-week and 32-week hepatocytes. ChIP-seq analysis with different histone PTMs revealed differential chromatin compaction (as evidenced by H3K27me3 and H3K9me3 signals) at genic and genome-wide levels in 32-week hepatocytes compared to 8-weeks. Moreover, we argued that reduction in H3K27me3 at gene body and TSS regions could be the reason for a higher level of gene expression in 32-week hepatocytes compared to 8-week. Moreover, expressions of senescence-associated genes are increased in 32-week hepatocytes (for example average TPM of Glb1: 8-week = 3.44 and 32-week = 12.16, Atf3: 8-week = 5.11 and 32-week = 146.81). Strikingly, cellular senescence is widely believed to be the result of changes in epigenetic regulators such as increased facultative heterochromatinisation by the formation of senescence-associated heterochromatic foci (SAHF) [631]. These SAHF foci have compacted chromatin and are enriched in inactive histone PTMs like H3K27me3 and H3K9me3, which results in transcriptional downregulation of proliferation-related genes [632, 633]. Moreover, SAHF has been shown to reduce DNA repair, which could protect senescent cells from apoptosis [632, 634]. Interestingly, there is a reduction in lamin B1 levels in senescent cells [635] that results in loss of heterochromatin from nuclear periphery and redistribution of heterochromatin to be incorporated in SAHF [632, 636, 637]. Moreover, the lamin B1 preferentially binds H3K27me3-enriched sites that are associated with transcriptional repression and the SAHF during cellular senescence [637]. Lamin B1 depletion could cause a redistribution of histone marks, including enrichment in H3K27me3 and H3K4me marks within lamin B1-associated domains and depletion in H3K27me3 marks in enhancers and genes. Moreover, genes lacking H3K27me3 marks that were upregulated were found to be senescence-related genes, including SASP genes [636]. Taken together, all these observations hint that 32-week

hepatocytes have age or senescence-associated changes at transcriptomic and epigenetic levels. However, an increase in H3K27me3 level as observed in our data resulted in the formation of SAHF, a typical marker of senescence, in 32-week hepatocytes requires experimental validation using imaging studies.

Strikingly, the 3D genome organisation exhibits negligible changes between 8-week and 32-week hepatocytes at Mb-scale A and B compartments. However, we are yet to analyse our 3C-seq data for long-range interaction and TAD level changes which may reveal some interesting results.

One important thought-provoking question that can stimulate interesting discussion is whether animals kept under controlled conditions throughout their lifespan will represent the true aging characteristics. Laboratory inbred mouse strains have a lifespan of about 2-3 years under a controlled environment and older mice exhibit typical aging phenotypes [570]. However, in the wild, 90% of mice die mostly from infection, predation, and starvation before they reach 32-week age [638]. Therefore, most mice in a wild environment do not survive to experience senescence and aging phenotypes. Similarly, human life expectancy at birth (LEB) was 22-33 years in the Paleolithic era, which increased to 31-32 years by 1900 (world average LEB) [639, 640]. However, within the next 120 years, the average LEB has increased to 72.6-73.2 [641]. This stark improvement in LEB means most people will experience old age and thus will experience age-related diseases. Therefore, whether or not aging is the aftermath of a longer lifespan is open to interpretation.

Aging has been long thought to be an inexorable path of decline in cellular function. Changes in DNA methylation, histone post-translational modification, and chromatin structure and remodelling impact health-span and longevity according to recent animal

research [520]. As epigenetic changes are reversible, researchers are searching for ways to reverse the aging process [642]. For example, Fahy et al. found that a cocktail of three common drugs - human growth hormone (hGH), dehydroepiandrosterone (DHEA), and metformin - reduced ~2.5 years of biological age of healthy volunteers between 51-65 years of age as revealed by their DNA methylation patterns [643]. Similarly, metabolic manipulations in association with epigenetics have been shown to influence aging [644]. Dietary restriction, such as daily or intermittent calorie restriction (CR), is a simple and non-invasive metabolic modification technique that can help people to live longer and increase their health-span [645]. DNA methylation and histone modification are two examples of how CR affects epigenetic processes. CR, for example, stimulates DNA methyltransferases (DNMTs), which hypermethylate the promoter regions of aging-promoting genes (such as those producing p16 and RAS, whose activation causes cellular senescence), thereby shutting down their production. CR also alters the global DNA methylation landscape by modulating ten–eleven translocations (TETs). CR has been shown to activate Sir2 or the seven mammalian homologues of SIR2 (SIRT1–SIRT7) at the histone level. CR, on the other hand, enhances adult neurogenesis by causing SIRT1 redistribution on chromatin, enrichment of Lys9-acetylated histone H3 (H3K9ac) at the promoters of Hes1 (a basic helix–loop–helix transcriptional regulator), and redistribution of SIRT1 on chromatin. Other histone deacetylases (HDACs) may be blocked by CR, resulting in increased levels of H3K9ac at the Foxo3 promoter and triggering antioxidant responses. The preservation of global chromatin condensation, reversal of aberrant gene expression, and eventual extension of health-span and lifespan are all outcomes of CR-induced epigenetic alterations [642]. In total, CR reduces the levels of systemic biomarkers of aging using epigenetic alterations. As mentioned before, hepatocyte polyploidization

profile is altered with age and during liver diseases. Strikingly, Enseco et al. studied Swiss albino mice and found that age-associated liver polyploidization is reduced in a restricted diet (4% protein) compared to a normal diet (26% protein) [646]. As polyploidization profile is decreasing with CR diet, this observation suggest polyploidization could serve as an indicator liver age. Therefore, further research with CR mice could help investigate the link between aging, polyploidy, and gene expression in hepatocytes.

The age dynamics of human mortality are described by the Gompertz–Makeham law of mortality. According to this law, the human death rate is the sum of age-dependent and age-independent components [647, 648]. The age-dependent component increases exponentially with age in mammals, for example, in humans, it doubles every 8 years beyond the age of 30 [649]. This effect, which occurs once an animal reaches adulthood, applies to all mammals — except the naked mole-rat! A recent study in naked mole-rat revealed that they can survive even beyond 30 years of age, much higher compared to their predicted age by Gompertz–Makeham law [650]. Highly active DNA repair machinery and a large amount of chaperons are suspected to be responsible for this extended age in naked mole rats [650]. It will be interesting to estimate the ploidy profile of hepatocytes isolated from naked mole rats with age and study the chromatin basis of their gene expression.

The main shortcomings of our present study include: a) lack of epigenetic data on different ploidy hepatocytes, b) use of only female mice and therefore the findings may not be directly applicable to male mice given the gender-specific nature of genetic and epigenetic regulations, and c) inability to correlate ploidy or aging biomarkers with metabolic zonation studies. Nevertheless, some of these studies are either currently underway or planned for the future. For future work, ChIP-seq with H3K27me3 and

H3K9me3 can be performed in different ploidy hepatocytes, which could give us a clear picture of epigenetic changes in different ploidy hepatocytes. As we now know that H3K27me3 is drastically changed with age, we need to adapt ChIP protocols for low-input samples. Moreover, experiments to study age-associated changes in various histone PTMs and chromatin organisation of old mouse hepatocytes (94-week) are already in the pipeline. We observed negligible changes at A/B compartment level between 8-week and 32-week hepatocytes. How the 3D genome organisation changes with aging will be interesting to investigate. The observed low-level average gene expression in 94-week hepatocytes compared to the younger mice can be attributed to an increment in repressed histone marks and chromatin condensation. Therefore, experiments targeted towards histone PTMs and 3D genome organization could reveal important regulatory information about age-dependent gene expression in mouse hepatocytes.

Appendix 1: Reactome pathways identified by GSEA

Pathways upregulated in diploid compared to polyploid hepatocytes

NAME	NES	NOM p-val
EXTRACELLULAR MATRIX ORGANIZATION	-2.50484	0
INTEGRIN CELL SURFACE INTERACTIONS	-2.44435	0
COLLAGEN FORMATION	-2.40234	0
IMMUNOREGULATORY INTERACTIONS BETWEEN A LYMPHOID AND A NON LYMPHOID CELL	-2.3997	0
COLLAGEN BIOSYNTHESIS AND MODIFYING ENZYMES	-2.3058	0
NON INTEGRIN MEMBRANE ECM INTERACTIONS	-2.30542	0
ASSEMBLY OF COLLAGEN FIBRILS AND OTHER MULTIMERIC STRUCTURES	-2.2973	0
INTERLEUKIN 10 SIGNALING	-2.29398	0
ECM PROTEOGLYCANS	-2.2823	0
INTERFERON GAMMA SIGNALING	-2.26711	0
CELL SURFACE INTERACTIONS AT THE VASCULAR WALL	-2.2441	0
FCGAMMA RECEPTOR FCGR DEPENDENT PHAGOCYTOSIS	-2.24374	0
O GLYCOSYLATION OF TSR DOMAIN CONTAINING PROTEINS	-2.24256	0
ELASTIC FIBRE FORMATION	-2.2022	0
SIGNALING BY GPCR	-2.18603	0
DEGRADATION OF THE EXTRACELLULAR MATRIX	-2.17788	0
FCGR3A MEDIATED IL10 SYNTHESIS	-2.17186	0
SENSORY PROCESSING OF SOUND BY OUTER HAIR CELLS OF THE COCHLEA	-2.17	0
COLLAGEN DEGRADATION	-2.16224	0
SIGNALING BY PDGF	-2.15325	0
COLLAGEN CHAIN TRIMERIZATION	-2.13653	0
O LINKED GLYCOSYLATION	-2.13623	0
CONSTITUTIVE SIGNALING BY ABERRANT PI3K IN CANCER	-2.13425	0
PARASITE INFECTION	-2.13052	0
INTERLEUKIN RECEPTOR SHC SIGNALING	-2.126	0
NCAM1 INTERACTIONS	-2.09656	0
GPVI MEDIATED ACTIVATION CASCADE	-2.094	0
LEISHMANIA INFECTION	-2.09059	0
MET ACTIVATES PTK2 SIGNALING	-2.07964	0
NCAM SIGNALING FOR NEURITE OUT GROWTH	-2.0769	0
MOLECULES ASSOCIATED WITH ELASTIC FIBRES	-2.07504	0
GENERATION OF SECOND MESSENGER MOLECULES	-2.07471	0
CHEMOKINE RECEPTORS BIND CHEMOKINES	-2.07271	0
PLATELET ACTIVATION SIGNALING AND AGGREGATION	-2.07235	0
LAMININ INTERACTIONS	-2.06714	0
INTERLEUKIN 3 INTERLEUKIN 5 AND GM CSF SIGNALING	-2.06368	0
HEMOSTASIS	-2.06147	0
ANTIGEN ACTIVATES B CELL RECEPTOR BCR LEADING TO GENERATION OF SECOND MESSENGERS	-2.05226	0
RET SIGNALING	-2.05018	0
DISEASES ASSOCIATED WITH O GLYCOSYLATION OF PROTEINS	-2.02866	0

SEMAPHORIN INTERACTIONS	-2.02855	0
SENSORY PROCESSING OF SOUND	-2.01718	0
CDC42 GTPASE CYCLE	-2.00616	0
INTERLEUKIN 2 FAMILY SIGNALING	-1.99875	0
RHO GTPASES ACTIVATE NADPH OXIDASES	-1.99452	0
G ALPHA I SIGNALING EVENTS	-1.97948	0
CLASS A 1 RHODOPSIN LIKE RECEPTORS	-1.97897	0
RAC1 GTPASE CYCLE	-1.96572	0
DOWNSTREAM SIGNAL TRANSDUCTION	-1.95736	0
MET PROMOTES CELL MOTILITY	-1.95464	0
REGULATION OF INSULIN LIKE GROWTH FACTOR IGF TRANSPORT AND UPTAKE BY INSULIN LIKE GROWTH FACTOR BINDING PROTEINS IGFBPS	-1.94285	0
ANTI INFLAMMATORY RESPONSE FAVOURING LEISHMANIA PARASITE INFECTION	-1.94225	0
SYNDECAN INTERACTIONS	-1.93685	0
OTHER SEMAPHORIN INTERACTIONS	-1.93369	0
NEGATIVE REGULATION OF THE PI3K AKT NETWORK	-1.93116	0
CHONDROITIN SULFATE DERMATAN SULFATE METABOLISM	-1.93055	0
RHOA GTPASE CYCLE	-1.92741	0
GPCR LIGAND BINDING	-1.92092	0
INITIAL TRIGGERING OF COMPLEMENT	-1.91612	0
LISTERIA MONOCYTOGENES ENTRY INTO HOST CELLS	-1.90815	0.001653
RAC2 GTPASE CYCLE	-1.89919	0
INFLAMMASOMES	-1.89495	0
MATURATION OF SARS COV 2 SPIKE PROTEIN	-1.89214	0.001513
ROLE OF PHOSPHOLIPIDS IN PHAGOCYTOSIS	-1.88506	0.001513
SIGNALING BY SCF KIT	-1.88371	0
G ALPHA Q SIGNALING EVENTS	-1.88347	0
PEPTIDE LIGAND BINDING RECEPTORS	-1.88335	0
RHO GTPASE CYCLE	-1.88295	0
EFFECTS OF PIP2 HYDROLYSIS	-1.88241	0
GLYCOSAMINOGLYCAN METABOLISM	-1.88097	0
COSTIMULATION BY THE CD28 FAMILY	-1.87936	0
NEUTROPHIL DEGRANULATION	-1.85945	0
INTERLEUKIN 4 AND INTERLEUKIN 13 SIGNALING	-1.85709	0
PI3K AKT SIGNALING IN CANCER	-1.85244	0
DISEASES OF GLYCOSYLATION	-1.85133	0
G ALPHA 12 13 SIGNALING EVENTS	-1.84593	0
NRAGE SIGNALS DEATH THROUGH JNK	-1.84174	0
PLATELET AGGREGATION PLUG FORMATION	-1.83878	0
INTEGRIN SIGNALING	-1.83162	0.001563
CELL DEATH SIGNALING VIA NRAGE NRIF AND NADE	-1.82608	0
NEPHRIN FAMILY INTERACTIONS	-1.82458	0.00316
G ALPHA S SIGNALING EVENTS	-1.81794	0.003958
VEGFR2 MEDIATED CELL PROLIFERATION	-1.81722	0.00159
SIGNALING BY VEGF	-1.8144	0
SIGNALING BY MODERATE KINASE ACTIVITY BRAF MUTANTS	-1.81272	0.001493

RHOB GTPASE CYCLE	-1.81268	0.001385
NUCLEAR SIGNALING BY ERBB4	-1.81161	0
RAC3 GTPASE CYCLE	-1.81139	0
HEPARAN SULFATE HEPARIN HS GAG METABOLISM	-1.80314	0.001453
NUCLEOTIDE BINDING DOMAIN LEUCINE RICH REPEAT CONTAINING RECEPTOR NLR SIGNALING PATHWAYS	-1.79023	0.001439
THE NLRP3 INFLAMMASOME	-1.78249	0.001597
PLATELET HOMEOSTASIS	-1.78203	0
PURINERGIC SIGNALING IN LEISHMANIASIS INFECTION	-1.76728	0.003077
SIGNALING BY MET	-1.75961	0.00135
CELL CELL COMMUNICATION	-1.75877	0
N GLYCAN ANTENNAE ELONGATION IN THE MEDIAL TRANS GOLGI	-1.75673	0.009554
SIGNALING BY RECEPTOR TYROSINE KINASES	-1.73404	0
BINDING AND UPTAKE OF LIGANDS BY SCAVENGER RECEPTORS	-1.73375	0
P75 NTR RECEPTOR MEDIATED SIGNALING	-1.73037	0
HS GAG DEGRADATION	-1.72683	0.009631
SYNTHESIS OF PIPS AT THE PLASMA MEMBRANE	-1.72492	0.002841
SEMA3A PAK DEPENDENT AXON REPULSION	-1.72319	0.006452
TOLL LIKE RECEPTOR CASCADES	-1.72163	0.001211
REGULATION OF KIT SIGNALING	-1.71988	0.0096
REGULATION OF SIGNALING BY CBL	-1.71977	0.009077
DISEASES ASSOCIATED WITH GLYCOSAMINOGLYCAN METABOLISM	-1.7164	0.008746
RESPONSE TO ELEVATED PLATELET CYTOSOLIC CA2	-1.71502	0
O LINKED GLYCOSYLATION OF MUCINS	-1.70415	0.002954
FCERI MEDIATED CA 2 MOBILIZATION	-1.69934	0.005944
EPHRIN SIGNALING	-1.69804	0.008039
CA DEPENDENT EVENTS	-1.69528	0.015129
SHC1 EVENTS IN ERBB2 SIGNALING	-1.68929	0.014019
CTLA4 INHIBITORY SIGNALING	-1.66754	0.012638
BASIGIN INTERACTIONS	-1.6617	0.009202
GLYCOSPHINGOLIPID METABOLISM	-1.6548	0.018072
PLATELET CALCIUM HOMEOSTASIS	-1.65307	0.014196
INTERFERON SIGNALING	-1.65242	0
RND3 GTPASE CYCLE	-1.64344	0.008772
ION HOMEOSTASIS	-1.63428	0.018841
RHOC GTPASE CYCLE	-1.63181	0.004065
G PROTEIN MEDIATED EVENTS	-1.62816	0.011852
SEMA4D INDUCED CELL MIGRATION AND GROWTH CONE COLLAPSE	-1.62754	0.015129
DEATH RECEPTOR SIGNALING	-1.6178	0.001227
NITRIC OXIDE STIMULATES GUANYLATE CYCLASE	-1.61755	0.014286
KERATAN SULFATE KERATIN METABOLISM	-1.6154	0.01875
CARDIAC CONDUCTION	-1.61222	0.006935
A TETRASACCHARIDE LINKER SEQUENCE IS REQUIRED FOR GAG SYNTHESIS	-1.61118	0.020408
CELL EXTRACELLULAR MATRIX INTERACTIONS	-1.60804	0.020093
FCERI MEDIATED MAPK ACTIVATION	-1.60726	0.013889
RHOQ GTPASE CYCLE	-1.60111	0.011127

DAG AND IP3 SIGNALING	-1.59941	0.019697
SURFACTANT METABOLISM	-1.59673	0.027244
CD28 CO STIMULATION	-1.59186	0.021773
EPH EPHRIN MEDIATED REPULSION OF CELLS	-1.5887	0.015896
EPHA MEDIATED GROWTH CONE COLLAPSE	-1.58755	0.026074
TRANSLATION OF SARS COV 2 STRUCTURAL PROTEINS	-1.58755	0.007396
INTERLEUKIN 37 SIGNALING	-1.58715	0.027687
DISEASES OF METABOLISM	-1.58252	0.001185
SIGNAL TRANSDUCTION BY L1	-1.58063	0.029366
SEMA4D IN SEMAPHORIN SIGNALING	-1.5801	0.022258
POTASSIUM CHANNELS	-1.57835	0.02008
NEGATIVE REGULATION OF FGFR1 SIGNALING	-1.57584	0.026984
ANTIMICROBIAL PEPTIDES	-1.56541	0.025118
SIGNALING BY ERBB2	-1.55778	0.016129
MAP2K AND MAPK ACTIVATION	-1.55182	0.026277
G ALPHA Z SIGNALING EVENTS	-1.55164	0.031437
LONG TERM POTENTIATION	-1.55162	0.035831
INTERFERON ALPHA BETA SIGNALING	-1.54814	0.01462
SIGNALING BY FGFR1	-1.54263	0.024217
OTHER INTERLEUKIN SIGNALING	-1.53941	0.029549
P130CAS LINKAGE TO MAPK SIGNALING FOR INTEGRINS	-1.53914	0.027732
GASTRIN CREB SIGNALING PATHWAY VIA PKC AND MAPK	-1.53914	0.040064
SIGNALING TO RAS	-1.53882	0.033816
SIGNALING BY INTERLEUKINS	-1.53711	0
HS GAG BIOSYNTHESIS	-1.53133	0.033981
SLC MEDIATED TRANSMEMBRANE TRANSPORT	-1.5281	0.002398
APOPTOTIC CLEAVAGE OF CELLULAR PROTEINS	-1.52345	0.033141
GRB2 SOS PROVIDES LINKAGE TO MAPK SIGNALING FOR INTEGRINS	-1.51696	0.029221
ONCOGENIC MAPK SIGNALING	-1.51539	0.018568
SYNTHESIS OF IP3 AND IP4 IN THE CYTOSOL	-1.50544	0.041335
DAP12 INTERACTIONS	-1.49854	0.039063
INOSITOL PHOSPHATE METABOLISM	-1.49236	0.039474
SARS COV 2 INFECTION	-1.49151	0.022942
TRANSPORT OF INORGANIC CATIONS ANIONS AND AMINO ACIDS OLIGOPEPTIDES	-1.49121	0.02228
DOWNREGULATION OF ERBB2 SIGNALING	-1.48894	0.03876
RHOU GTPASE CYCLE	-1.48858	0.046512
EPH EPHRIN SIGNALING	-1.48778	0.013021
NETRIN 1 SIGNALING	-1.48434	0.044604
SIGNALING BY EGFR	-1.484	0.036466
NEURONAL SYSTEM	-1.47466	0.004561
ION TRANSPORT BY P TYPE ATPASES	-1.47207	0.042641
RHOJ GTPASE CYCLE	-1.46106	0.037396
PLATELET SENSITIZATION BY LDL	-1.44666	0.049505
METABOLISM OF CARBOHYDRATES	-1.42779	0.008
MUSCLE CONTRACTION	-1.42644	0.021411

SIGNALING BY ERBB4	-1.41928	0.047009
L1CAM INTERACTIONS	-1.38426	0.043307
PHOSPHOLIPID METABOLISM	-1.36118	0.023725
TRANSMISSION ACROSS CHEMICAL SYNAPSES	-1.33749	0.030197
MAPK FAMILY SIGNALING CASCADES	-1.32213	0.022297

Pathways upregulated in polyploid compared to diploid hepatocytes

NAME	NES	NOM p-val
EUKARYOTIC TRANSLATION ELONGATION	3.205036	0
SELENOAMINO ACID METABOLISM	3.147448	0
SRP DEPENDENT COTRANSLATIONAL PROTEIN TARGETING TO MEMBRANE	3.140022	0
REGULATION OF EXPRESSION OF SLITS AND ROBOS	3.106138	0
TRANSLATION	3.074225	0
EUKARYOTIC TRANSLATION INITIATION	3.073731	0
RESPONSE OF EIF2AK4 GCN2 TO AMINO ACID DEFICIENCY	3.060512	0
NONSENSE MEDIATED DECAY NMD	2.91068	0
RRNA PROCESSING	2.894669	0
RESPIRATORY ELECTRON TRANSPORT	2.878059	0
INFLUENZA INFECTION	2.863384	0
MITOCHONDRIAL TRANSLATION	2.805024	0
CELLULAR RESPONSE TO STARVATION	2.800618	0
RESPIRATORY ELECTRON TRANSPORT ATP SYNTHESIS BY CHEMIOSMOTIC COUPLING AND HEAT PRODUCTION BY UNCOUPLING PROTEINS	2.786106	0
METABOLISM OF AMINO ACIDS AND DERIVATIVES	2.752811	0
THE CITRIC ACID TCA CYCLE AND RESPIRATORY ELECTRON TRANSPORT	2.720843	0
SCF SKP2 MEDIATED DEGRADATION OF P27 P21	2.691788	0
COMPLEX I BIOGENESIS	2.65013	0
ACTIVATION OF THE MRNA UPON BINDING OF THE CAP BINDING COMPLEX AND EIFS AND SUBSEQUENT BINDING TO 43S	2.558406	0
DEGRADATION OF AXIN	2.479312	0
SYNTHESIS OF BILE ACIDS AND BILE SALTS VIA 7ALPHA HYDROXYCHOLESTEROL	2.468743	0
DEGRADATION OF GLI1 BY THE PROTEASOME	2.466932	0
SIGNALING BY ROBO RECEPTORS	2.458666	0
NEGATIVE REGULATION OF NOTCH4 SIGNALING	2.450805	0
AUF1 HNRNP D0 BINDS AND DESTABILIZES MRNA	2.424052	0
MITOCHONDRIAL FATTY ACID BETA OXIDATION	2.408055	0
METABOLISM OF POLYAMINES	2.405204	0
DEGRADATION OF DVL	2.3423	0
ORC1 REMOVAL FROM CHROMATIN	2.298424	0
PROTEIN LOCALIZATION	2.290303	0
DEFECTIVE CFTR CAUSES CYSTIC FIBROSIS	2.282048	0
CELLULAR RESPONSE TO HYPOXIA	2.281498	0
COOPERATION OF PREFOLDIN AND TRIC CCT IN ACTIN AND TUBULIN FOLDING	2.277333	0
STABILIZATION OF P53	2.273133	0
THE ROLE OF GTSE1 IN G2 M PROGRESSION AFTER G2 CHECKPOINT	2.268546	0

CYCLIN A CDK2 ASSOCIATED EVENTS AT S PHASE ENTRY	2.25359	0
HEDGEHOG LIGAND BIOGENESIS	2.237665	0
NUCLEOTIDE EXCISION REPAIR	2.212708	0
FORMATION OF TC NER PRE INCISION COMPLEX	2.197218	0
G1 S DNA DAMAGE CHECKPOINTS	2.196281	0
REGULATION OF HMOX1 EXPRESSION AND ACTIVITY	2.191049	0
DNA REPLICATION PRE INITIATION	2.185716	0
ABC TRANSPORTER DISORDERS	2.183807	0
REGULATION OF PTEN STABILITY AND ACTIVITY	2.165907	0
TRANSCRIPTION COUPLED NUCLEOTIDE EXCISION REPAIR TC NER	2.160053	0
CYTOPROTECTION BY HMOX1	2.15992	0
ASSEMBLY OF THE PRE REPLICATIVE COMPLEX	2.154144	0
MRNA SPLICING	2.146036	0
DUAL INCISION IN TC NER	2.139764	0
CROSS PRESENTATION OF SOLUBLE EXOGENOUS ANTIGENS ENDOSOMES	2.117739	0
DECTIN 1 MEDIATED NONCANONICAL NF KB SIGNALING	2.089084	0
BIOLOGICAL OXIDATIONS	2.082274	0
APC C MEDIATED DEGRADATION OF CELL CYCLE PROTEINS	2.081975	0
SEPARATION OF SISTER CHROMATIDS	2.081363	0
MITOCHONDRIAL PROTEIN IMPORT	2.078118	0
ASYMMETRIC LOCALIZATION OF PCP PROTEINS	2.075655	0
REGULATION OF RUNX2 EXPRESSION AND ACTIVITY	2.067318	0
PEROXISOMAL LIPID METABOLISM	2.066887	0
CELLULAR RESPONSE TO CHEMICAL STRESS	2.065892	0
SIGNALING BY NOTCH4	2.06388	0
PROCESSING OF CAPPED INTRON CONTAINING PRE MRNA	2.063709	0
PEROXISOMAL PROTEIN IMPORT	2.058948	0
UCH PROTEINASES	2.054058	0
SYNTHESIS OF BILE ACIDS AND BILE SALTS	2.052646	0.00277
SWITCHING OF ORIGINS TO A POST REPLICATIVE STATE	2.04322	0
REGULATION OF MRNA STABILITY BY PROTEINS THAT BIND AU RICH ELEMENTS	2.043006	0
APC C CDH1 MEDIATED DEGRADATION OF CDC20 AND OTHER APC C CDH1 TARGETED PROTEINS IN LATE MITOSIS EARLY G1	2.039963	0
GLOBAL GENOME NUCLEOTIDE EXCISION REPAIR GG NER	2.029038	0
FORMATION OF ATP BY CHEMIOSMOTIC COUPLING	2.028274	0
HEDGEHOG OFF STATE	2.010599	0
FORMATION OF TUBULIN FOLDING INTERMEDIATES BY CCT TRIC	2.007417	0
MITOTIC METAPHASE AND ANAPHASE	2.007311	0
MRNA CAPPING	2.00204	0.002747
DOWNSTREAM SIGNALING EVENTS OF B CELL RECEPTOR BCR	1.998126	0
S PHASE	1.992337	0
BRANCHED CHAIN AMINO ACID CATABOLISM	1.984905	0.002809
CRISTAE FORMATION	1.981346	0
DNA REPLICATION	1.980925	0
BILE ACID AND BILE SALT METABOLISM	1.976785	0
TRANSLESION SYNTHESIS BY POLH	1.973094	0

REGULATION OF RUNX3 EXPRESSION AND ACTIVITY	1.968803	0
G2 M CHECKPOINTS	1.954748	0
CLASS I PEROXISOMAL MEMBRANE PROTEIN IMPORT	1.951605	0
PHASE II CONJUGATION OF COMPOUNDS	1.944346	0
DEGRADATION OF BETA CATENIN BY THE DESTRUCTION COMPLEX	1.940332	0
PHASE I FUNCTIONALIZATION OF COMPOUNDS	1.938545	0
MITOTIC G2 G2 M PHASES	1.925655	0
DNA DAMAGE RECOGNITION IN GG NER	1.896004	0
HIV TRANSCRIPTION INITIATION	1.891838	0
RNA POLYMERASE II TRANSCRIBES SNRNA GENES	1.890827	0
FORMATION OF INCISION COMPLEX IN GG NER	1.871442	0
HEDGEHOG ON STATE	1.859139	0
REGULATION OF RAS BY GAPS	1.856408	0
NEDDYLATION	1.855697	0
HOST INTERACTIONS OF HIV FACTORS	1.839351	0
PTEN REGULATION	1.82707	0
RNA POLYMERASE II TRANSCRIPTION TERMINATION	1.814199	0
HSP90 CHAPERONE CYCLE FOR STEROID HORMONE RECEPTORS SHR	1.811443	0.006079
HIV INFECTION	1.802976	0
FCERI MEDIATED NF KB ACTIVATION	1.792972	0
TRANSCRIPTION OF THE HIV GENOME	1.791531	0
MITOTIC G1 PHASE AND G1 S TRANSITION	1.777928	0
ACTIVATION OF ATR IN RESPONSE TO REPLICATION STRESS	1.777872	0
CHOLESTEROL BIOSYNTHESIS	1.777676	0
PINK1 PRKN MEDIATED MITOPHAGY	1.776218	0.012594
LAGGING STRAND SYNTHESIS	1.769573	0.005263
VITAMIN B5 PANTOTHENATE METABOLISM	1.764011	0.007958
PYRUVATE METABOLISM	1.759439	0.005831
TRANSLESION SYNTHESIS BY Y FAMILY DNA POLYMERASES BYPASSES LESIONS ON DNA TEMPLATE	1.755593	0.006452
RUNX1 REGULATES TRANSCRIPTION OF GENES INVOLVED IN DIFFERENTIATION OF HSCS	1.753758	0
DNA DAMAGE BYPASS	1.752843	0
FORMATION OF RNA POL II ELONGATION COMPLEX	1.742908	0.00361
GAP JUNCTION ASSEMBLY	1.735014	0.008571
CELL CYCLE CHECKPOINTS	1.732312	0
HIV TRANSCRIPTION ELONGATION	1.730435	0.003436
PYRUVATE METABOLISM AND CITRIC ACID TCA CYCLE	1.728133	0.003584
FATTY ACID METABOLISM	1.723512	0
MRNA SPLICING MINOR PATHWAY	1.722451	0.003497
SULFUR AMINO ACID METABOLISM	1.719743	0.005848
RNA POLYMERASE I TRANSCRIPTION INITIATION	1.714288	0.003378
HDR THROUGH SINGLE STRAND ANNEALING SSA	1.71397	0.011594
ABC FAMILY PROTEINS MEDIATED TRANSPORT	1.713701	0
RESOLUTION OF SISTER CHROMATID COHESION	1.712741	0
TRANSLESION SYNTHESIS BY POLK	1.70343	0.013966
MAPK6 MAPK4 SIGNALING	1.694952	0

AGGREPHAGY	1.69114	0
PROCESSING OF CAPPED INTRONLESS PRE MRNA	1.674613	0.017241
SIGNALING BY HEDGEHOG	1.669778	0
SNRNP ASSEMBLY	1.664511	0
DUAL INCISION IN GG NER	1.65994	0.009464
DEADENYLATION OF MRNA	1.657651	0.016575
RRNA MODIFICATION IN THE NUCLEUS AND CYTOSOL	1.649998	0.003597
ENDOGENOUS STEROLS	1.644817	0.031088
RNA POLYMERASE I TRANSCRIPTION TERMINATION	1.637535	0.008596
INTERCONVERSION OF NUCLEOTIDE DI AND TRIPHOSPHATES	1.635521	0.020958
TRNA PROCESSING	1.626563	0.010309
M PHASE	1.621011	0
PCP CE PATHWAY	1.615267	0
PIWI INTERACTING RNA PIRNA BIOGENESIS	1.611634	0.028871
METABOLISM OF COFACTORS	1.605935	0.036723
UB SPECIFIC PROCESSING PROTEASES	1.605561	0
NUCLEAR RECEPTOR TRANSCRIPTION PATHWAY	1.598389	0.010949
METABOLISM OF STEROIDS	1.598143	0
INTERLEUKIN 1 SIGNALING	1.594367	0
PROCESSIVE SYNTHESIS ON THE LAGGING STRAND	1.592453	0.039578
CYTOSOLIC TRNA AMINOACYLATION	1.590043	0.027322
PROCESSIVE SYNTHESIS ON THE C STRAND OF THE TELOMERE	1.578516	0.03183
REGULATION OF PYRUVATE DEHYDROGENASE PDH COMPLEX	1.573485	0.02551
RNA POLYMERASE III TRANSCRIPTION	1.573436	0.017606
TERMINATION OF TRANSLESION DNA SYNTHESIS	1.566263	0.033435
PROTEIN FOLDING	1.566168	0
MEIOSIS	1.564915	0.010601
TRNA AMINOACYLATION	1.56237	0.01227
TRANSPORT OF MATURE TRANSCRIPT TO CYTOPLASM	1.559473	0.0125
TP53 REGULATES TRANSCRIPTION OF DNA REPAIR GENES	1.554176	0.007246
TP53 REGULATES METABOLIC GENES	1.55045	0.007905
FORMATION OF THE EARLY ELONGATION COMPLEX	1.527735	0.027108
PROCESSING OF SMDT1	1.527637	0.042667
VIRAL MESSENGER RNA SYNTHESIS	1.525521	0.019868
CYTOCHROME P450 ARRANGED BY SUBSTRATE TYPE	1.52486	0.015873
RNA POLYMERASE I PROMOTER ESCAPE	1.523226	0.017301
GLYOXYLATE METABOLISM AND GLYCINE DEGRADATION	1.514813	0.026786
MITOTIC PROMETAPHASE	1.514165	0
E3 UBIQUITIN LIGASES UBIQUITINATE TARGET PROTEINS	1.513073	0.019355
COOPERATION OF PDCL PHLP1 AND TRIC CCT IN G PROTEIN BETA FOLDING	1.509345	0.037037
HIV LIFE CYCLE	1.509307	0.005348
TELOMERE C STRAND LAGGING STRAND SYNTHESIS	1.50811	0.02029
POSTMITOTIC NUCLEAR PORE COMPLEX NPC REFORMATION	1.503901	0.031339
CHROMOSOME MAINTENANCE	1.502242	0.004444
RNA POLYMERASE III TRANSCRIPTION INITIATION FROM TYPE 3 PROMOTER	1.500332	0.027933

HOMOLOGOUS DNA PAIRING AND STRAND EXCHANGE	1.500125	0.036697
NEGATIVE EPIGENETIC REGULATION OF RRNA EXPRESSION	1.499916	0.003484
PCNA DEPENDENT LONG PATCH BASE EXCISION REPAIR	1.492255	0.045845
OLFACTORY SIGNALING PATHWAY	1.481309	0.025271
ANTIGEN PROCESSING UBIQUITINATION PROTEASOME DEGRADATION	1.478532	0
REGULATION OF TP53 ACTIVITY THROUGH PHOSPHORYLATION	1.47646	0.021097
REPRODUCTION	1.476214	0.01145
HIV ELONGATION ARREST AND RECOVERY	1.472467	0.033445
TRNA PROCESSING IN THE NUCLEUS	1.463763	0.040404
NUCLEAR ENVELOPE NE REASSEMBLY	1.463516	0.026217
AUTOPHAGY	1.460157	0.005348
PROTEIN UBIQUITINATION	1.458313	0.026316
CELL CYCLE MITOTIC	1.450913	0
RECOGNITION OF DNA DAMAGE BY PCNA CONTAINING REPLICATION COMPLEX	1.447733	0.046647
SELECTIVE AUTOPHAGY	1.440458	0.025532
TRANSCRIPTIONAL REGULATION BY TP53	1.439994	0
BIOSYNTHESIS OF SPECIALIZED PRORESOLVING MEDIATORS SPMS	1.432262	0.0475
DETOXIFICATION OF REACTIVE OXYGEN SPECIES	1.419318	0.04902
METABOLISM OF NUCLEOTIDES	1.414176	0.016194
GENE SILENCING BY RNA	1.409758	0.034188
DISORDERS OF TRANSMEMBRANE TRANSPORTERS	1.404206	0.005181
DEADENYLATION DEPENDENT MRNA DECAY	1.404053	0.025974
MITOCHONDRIAL BIOGENESIS	1.403475	0.025751
REGULATION OF LIPID METABOLISM BY PPARALPHA	1.403443	0
TRANSCRIPTIONAL REGULATION BY RUNX2	1.377592	0.016461
RNA POLYMERASE I TRANSCRIPTION	1.372233	0.048507
TNFR2 NON CANONICAL NF KB PATHWAY	1.370959	0.02439
SUMOYLATION OF DNA DAMAGE RESPONSE AND REPAIR PROTEINS	1.367844	0.037037
RECRUITMENT OF NUMA TO MITOTIC CENTROSOMES	1.363858	0.015625
TCF DEPENDENT SIGNALING IN RESPONSE TO WNT	1.355624	0.006329
DEUBIQUITINATION	1.353489	0
HDR THROUGH HOMOLOGOUS RECOMBINATION HRR	1.35247	0.043478
METABOLISM OF VITAMINS AND COFACTORS	1.340628	0.006452
ORGANELLE BIOGENESIS AND MAINTENANCE	1.338556	0.017699
DNA REPAIR	1.335954	0.00813
INTERLEUKIN 1 FAMILY SIGNALING	1.334515	0.021164
PROCESSING OF DNA DOUBLE STRAND BREAK ENDS	1.323209	0.05
CLASS I MHC MEDIATED ANTIGEN PROCESSING PRESENTATION	1.194094	0.025316

Pathways upregulated in 4N compared to 8N hepatocytes

NAME	NES	NOM p-val
METAL ION SLC TRANSPORTERS	1.757673	0
DISEASES OF IMMUNE SYSTEM	1.732271	0
DEGRADATION OF THE EXTRACELLULAR MATRIX	1.685703	0.013304
EXTRACELLULAR MATRIX ORGANIZATION	1.680632	0.037445
REGULATION OF TLR BY ENDOGENOUS LIGAND	1.650411	0
P130CAS LINKAGE TO MAPK SIGNALING FOR INTEGRINS	1.64001	0
INTEGRIN CELL SURFACE INTERACTIONS	1.628135	0.037281
DOWNREGULATION OF ERBB2 SIGNALING	1.6263	0
ELASTIC FIBRE FORMATION	1.574169	0.012931
MOLECULES ASSOCIATED WITH ELASTIC FIBRES	1.573032	0.012931
COLLAGEN DEGRADATION	1.561198	0.035417
IRAK4 DEFICIENCY TLR2 4	1.547493	0
G ALPHA I SIGNALING EVENTS	1.532709	0
NUCLEAR SIGNALING BY ERBB4	1.51758	0.020704
SIGNALING BY ERBB4	1.508257	0
GRB2 SOS PROVIDES LINKAGE TO MAPK SIGNALING FOR INTEGRINS	1.489028	0.041322
ZINC TRANSPORTERS	1.485048	0
RHO GTPASES ACTIVATE IQGAPS	1.480962	0.016461
SIGNALING BY INSULIN RECEPTOR	1.447039	0
O LINKED GLYCOSYLATION OF MUCINS	1.432136	0.037611
INTEGRIN SIGNALING	1.410619	0.034836
FATTY ACYL COA BIOSYNTHESIS	1.354477	0.043299

Pathways upregulated in 8N compared to 2N hepatocytes

NAME	NES	NOM p-val
SIGNALING BY NOTCH1 HD DOMAIN MUTANTS IN CANCER	-1.77411	0
FOXO MEDIATED TRANSCRIPTION OF CELL DEATH GENES	-1.69882	0
REGULATION OF FZD BY UBIQUITINATION	-1.62878	0.039215688
SUMOYLATION OF DNA DAMAGE RESPONSE AND REPAIR PROTEINS	-1.61002	0
SUMOYLATION OF DNA REPLICATION PROTEINS	-1.60068	0.041152265
RNA POLYMERASE III TRANSCRIPTION	-1.58779	0
RAF INDEPENDENT MAPK1 3 ACTIVATION	-1.53215	0
SUMOYLATION OF RNA BINDING PROTEINS	-1.50853	0.012448133
GENE SILENCING BY RNA	-1.4914	0.032258064
NUCLEAR ENVELOPE BREAKDOWN	-1.46927	0.03984064
SIGNALING BY WNT IN CANCER	-1.40096	0.036511157
SEMA4D INDUCED CELL MIGRATION AND GROWTH CONE COLLAPSE	-1.39369	0
SEMA4D IN SEMAPHORIN SIGNALING	-1.39273	0
CHROMOSOME MAINTENANCE	-1.37989	0.019607844
DISEASES OF PROGRAMMED CELL DEATH	-1.36861	0.016

FOXO MEDIATED TRANSCRIPTION	-1.35414	0.040935673
HSF1 DEPENDENT TRANSACTIVATION	-1.34882	0.04225352
MEIOTIC RECOMBINATION	-1.31375	0.049309663
ESR MEDIATED SIGNALING	-1.28428	0.044

Appendix 2: NAFLD associated genes passing filter cutoff and their Log_2RPKM values in ploidy samples.

Ensemble_Gene_ID	2N 8-weeks-old	4N 8-weeks-old	8N 8-weeks-old	2N 32-weeks-old	4N 32-weeks-old	8N 32-weeks-old
ENSMUSG00000053647.4	0.27	0.26	0.19	1.12	0.65	0.91
ENSMUSG00000034192.5	0.30	0.15	0.12	0.43	0.28	0.25
ENSMUSG00000023919.7	0.44	0.50	0.61	0.58	1.45	1.66
ENSMUSG00000022370.13	0.44	0.42	0.51	1.61	2.02	2.17
ENSMUSG00000061758.13	0.52	0.15	0.12	0.46	0.33	0.19
ENSMUSG00000062515.3	0.53	0.25	0.35	0.40	0.22	0.24
ENSMUSG00000038541.8	0.69	0.50	0.74	1.66	1.70	1.89
ENSMUSG00000049892.7	0.71	0.62	1.14	0.74	0.32	0.93
ENSMUSG00000038545.13	0.76	0.86	1.16	2.83	2.95	3.32
ENSMUSG00000030752.8	0.80	0.59	0.50	2.29	1.94	2.05
ENSMUSG00000004837.2	0.85	0.52	0.80	1.65	0.93	1.14
ENSMUSG00000027082.15	0.88	0.49	1.09	1.13	0.57	0.93
ENSMUSG00000059824.12	1.01	0.53	0.53	5.38	2.31	2.65
ENSMUSG00000020828.13	1.04	0.92	1.00	2.94	2.70	3.12
ENSMUSG00000031683.16	1.07	1.41	1.58	2.50	2.91	3.57
ENSMUSG00000041688.16	1.11	1.00	0.92	1.54	1.36	1.26
ENSMUSG00000029053.16	1.18	1.30	1.32	4.74	5.11	6.29
ENSMUSG00000015702.13	1.20	1.25	1.26	1.40	2.07	1.55
ENSMUSG00000045932.12	1.23	0.21	0.50	1.16	0.62	0.53
ENSMUSG00000037296.7	1.40	1.44	0.93	2.52	2.73	2.90
ENSMUSG00000054932.6	1.43	1.55	1.40	4.38	4.78	4.70
ENSMUSG00000040740.7	1.52	1.12	0.87	5.40	4.65	4.96
ENSMUSG00000032596.14	1.56	0.81	1.12	6.35	5.53	6.26
ENSMUSG00000021457.14	1.58	0.15	0.11	0.72	0.22	0.10
ENSMUSG00000037348.15	1.68	1.53	1.75	5.00	5.98	5.94
ENSMUSG00000020105.9	1.68	1.69	1.74	3.98	4.22	4.32
ENSMUSG00000022400.9	1.69	2.22	2.53	3.04	3.84	4.14
ENSMUSG00000032860.5	1.74	0.98	0.79	3.53	3.36	3.03
ENSMUSG00000051316.8	1.75	1.85	2.24	2.67	3.28	4.00
ENSMUSG00000067199.4	1.77	1.38	1.44	2.83	2.52	2.73
ENSMUSG00000016308.12	1.86	2.37	2.98	2.65	2.20	2.44
ENSMUSG00000034259.8	1.92	2.23	1.80	4.54	5.29	4.88
ENSMUSG00000026288.14	1.95	0.22	0.39	0.82	0.41	0.26
ENSMUSG00000031821.11	1.99	1.41	1.31	3.27	3.19	3.73
ENSMUSG00000050965.14	2.01	1.45	1.25	5.43	4.93	4.95

ENSMUSG00000037674.15	2.01	1.96	2.08	2.81	2.93	3.17
ENSMUSG00000034177.15	2.02	3.74	4.83	8.29	10.32	13.58
ENSMUSG00000061559.15	2.11	2.27	2.71	4.73	6.46	6.84
ENSMUSG00000019763.11	2.14	1.99	2.37	5.85	6.59	5.92
ENSMUSG00000052997.15	2.16	1.79	2.35	4.44	5.64	4.81
ENSMUSG00000029524.16	2.22	1.85	2.62	3.07	4.12	4.22
ENSMUSG00000028271.9	2.24	1.67	1.53	4.72	5.30	5.41
ENSMUSG00000018604.18	2.35	4.85	7.68	1.79	2.78	3.89
ENSMUSG00000043964.14	2.42	1.63	2.38	5.88	6.74	6.06
ENSMUSG00000074781.5	2.49	1.82	2.28	3.59	4.24	4.14
ENSMUSG00000031585.13	2.52	1.96	1.83	3.37	3.77	3.98
ENSMUSG00000024048.15	2.54	1.88	2.58	6.07	7.05	8.40
ENSMUSG00000045038.14	2.55	2.16	2.21	7.52	6.39	6.86
ENSMUSG00000035596.14	2.57	2.73	2.63	7.82	6.03	6.53
ENSMUSG00000015568.16	2.57	0.31	0.23	0.83	0.22	0.10
ENSMUSG00000036295.5	2.59	3.12	2.44	7.80	9.86	11.17
ENSMUSG00000031601.16	2.71	3.20	2.95	4.68	5.11	5.64
ENSMUSG00000033355.6	2.73	2.15	2.20	3.77	4.67	4.59
ENSMUSG00000033543.17	2.82	2.96	3.15	3.63	4.78	5.18
ENSMUSG00000037709.13	2.86	2.85	3.08	5.92	6.48	6.63
ENSMUSG00000031537.15	2.92	2.61	2.92	5.94	6.40	6.77
ENSMUSG00000053964.17	2.96	3.30	3.92	8.90	9.64	10.96
ENSMUSG00000024231.14	2.99	3.20	4.31	4.98	7.22	7.81
ENSMUSG00000022781.8	3.00	2.79	3.04	4.50	4.79	4.65
ENSMUSG00000020027.18	3.11	4.57	5.42	5.62	7.06	8.14
ENSMUSG00000021948.17	3.13	1.08	1.44	4.34	3.26	3.92
ENSMUSG00000024018.17	3.16	2.71	2.89	9.49	10.49	11.13
ENSMUSG00000029649.10	3.68	3.72	5.03	6.28	7.97	9.06
ENSMUSG00000014402.15	3.74	3.50	3.89	6.46	7.30	7.25
ENSMUSG00000021737.4	4.02	4.89	5.41	11.05	13.37	14.55
ENSMUSG00000041653.5	4.06	2.91	1.74	16.42	14.98	13.81
ENSMUSG00000020357.3	4.08	2.37	5.19	3.64	2.20	2.29
ENSMUSG00000014956.15	4.16	3.82	3.97	3.13	5.09	4.96
ENSMUSG00000079435.9	4.42	6.30	7.05	12.87	21.76	21.76
ENSMUSG00000062929.8	4.91	5.27	4.65	5.87	7.04	6.91
ENSMUSG00000090862.3	5.29	5.27	7.08	10.89	14.79	13.25
ENSMUSG00000016933.17	5.29	4.97	6.15	13.51	15.26	17.40
ENSMUSG00000034902.17	5.44	3.45	3.90	10.36	8.39	9.27
ENSMUSG00000018401.17	5.66	5.16	5.21	14.53	17.37	19.13
ENSMUSG00000057342.15	5.75	5.17	5.25	18.78	17.18	20.38
ENSMUSG00000009621.18	5.82	4.90	4.79	17.10	16.68	18.81
ENSMUSG00000062960.10	6.01	4.74	10.39	9.01	5.43	5.96
ENSMUSG00000058600.13	6.03	6.35	7.75	7.83	14.20	15.12
ENSMUSG00000046364.14	6.14	7.18	7.94	21.50	29.91	31.03
ENSMUSG00000017776.15	6.23	5.66	6.26	7.70	9.27	9.58

ENSMUSG00000021594.11	6.29	3.90	3.45	11.58	10.53	7.96
ENSMUSG00000021832.8	6.62	8.15	8.83	10.64	15.73	15.31
ENSMUSG00000090733.6	6.87	7.90	10.87	33.18	47.35	49.40
ENSMUSG00000030751.18	6.88	8.17	10.09	9.90	16.00	15.78
ENSMUSG00000029859.6	7.22	6.23	6.02	27.60	26.45	25.76
ENSMUSG00000028936.15	7.30	7.18	9.41	12.39	17.25	17.84
ENSMUSG00000029304.14	7.41	1.98	1.01	6.97	3.75	2.04
ENSMUSG00000009927.9	7.58	8.36	11.73	16.35	26.81	23.93
ENSMUSG00000066319.6	7.77	6.67	7.66	5.35	7.80	6.77
ENSMUSG00000022181.16	8.07	1.13	0.95	4.25	2.74	1.65
ENSMUSG00000020720.13	8.09	7.38	9.46	8.62	14.33	12.82
ENSMUSG00000036151.15	8.31	7.00	7.49	31.80	30.49	30.24
ENSMUSG00000028240.2	8.35	23.83	29.74	17.50	30.66	40.30
ENSMUSG00000012405.16	8.38	7.55	8.99	18.13	23.08	23.77
ENSMUSG00000067144.7	9.06	6.17	3.28	26.55	18.06	12.12
ENSMUSG00000047215.14	9.14	10.05	12.61	31.24	35.58	38.60
ENSMUSG00000008475.13	9.19	8.43	7.26	10.77	12.35	12.40
ENSMUSG00000005534.10	9.86	8.99	9.34	34.36	33.36	32.79
ENSMUSG00000022228.14	10.17	10.41	11.76	21.16	23.61	26.54
ENSMUSG00000048217.11	10.83	9.80	11.60	24.22	29.27	31.00
ENSMUSG00000026781.17	10.91	13.84	14.06	13.58	18.36	19.86
ENSMUSG00000052681.8	11.15	6.56	7.82	7.78	8.43	7.18
ENSMUSG00000024254.15	11.57	14.62	14.67	38.69	50.83	55.57
ENSMUSG00000030909.6	11.75	12.37	11.95	18.60	19.93	20.68
ENSMUSG00000032301.13	11.75	15.53	18.37	14.74	21.94	20.51
ENSMUSG00000043013.10	12.42	12.67	12.74	11.89	11.89	14.14
ENSMUSG00000021024.14	12.42	9.80	15.56	12.03	23.68	20.71
ENSMUSG00000020390.12	13.10	15.24	14.45	22.27	27.29	29.64
ENSMUSG00000061477.4	13.22	12.50	14.71	14.51	22.87	23.02
ENSMUSG00000022383.13	13.83	18.25	19.62	37.66	46.62	58.76
ENSMUSG00000006699.17	15.02	12.01	14.36	18.85	22.68	22.45
ENSMUSG00000040181.14	18.44	20.72	22.98	26.95	41.62	44.73
ENSMUSG00000032418.15	19.24	17.08	19.39	22.21	27.13	24.85
ENSMUSG00000045128.9	21.01	20.75	23.84	25.36	38.41	39.15
ENSMUSG00000047675.15	22.38	23.91	28.06	53.26	80.27	82.09
ENSMUSG00000025794.9	22.56	18.61	21.96	34.01	46.06	46.39
ENSMUSG00000036781.13	22.89	29.92	38.01	28.97	47.91	47.28
ENSMUSG00000074063.10	24.95	28.76	29.07	36.32	42.62	53.16
ENSMUSG00000024978.10	25.22	23.84	25.63	120.57	148.43	149.84
ENSMUSG00000031844.8	26.27	29.04	31.61	92.47	118.59	111.52
ENSMUSG00000029656.13	27.37	24.87	28.12	61.16	79.13	66.68
ENSMUSG00000038274.12	29.62	28.05	31.70	73.56	107.35	103.73
ENSMUSG00000028979.17	30.12	29.88	30.59	103.25	107.53	107.47
ENSMUSG00000023942.15	32.15	33.03	36.60	122.49	125.57	138.20
ENSMUSG00000041798.15	35.22	36.18	44.18	79.39	113.40	140.12

ENSMUSG00000030834.7	36.35	37.34	38.50	216.23	186.44	208.78
ENSMUSG00000062328.7	37.76	40.64	53.84	49.64	121.40	108.32
ENSMUSG00000020122.16	38.84	37.44	36.44	46.35	48.73	47.64
ENSMUSG00000035780.2	50.57	49.53	55.90	145.91	170.50	144.93
ENSMUSG00000022149.17	51.72	45.98	42.09	77.02	81.23	65.68
ENSMUSG00000041237.12	53.08	44.28	39.83	53.49	47.43	41.10
ENSMUSG00000023951.17	63.11	66.24	65.94	161.77	135.98	160.01
ENSMUSG00000010663.4	63.49	58.47	63.82	149.38	166.64	158.59
ENSMUSG00000034957.10	68.83	64.84	68.75	109.51	89.73	98.57
ENSMUSG00000020017.14	79.67	51.14	33.37	254.79	229.04	179.51
ENSMUSG00000026385.16	88.06	112.55	142.14	169.12	242.81	249.55
ENSMUSG00000028179.12	88.82	79.33	84.45	282.15	350.59	345.99
ENSMUSG00000047822.8	91.32	102.69	114.50	184.63	210.71	228.55
ENSMUSG00000024665.7	98.69	95.69	102.12	250.58	237.80	242.85
ENSMUSG00000026715.12	123.19	111.68	129.90	397.35	430.14	392.73
ENSMUSG00000033860.13	790.47	829.16	952.86	2620.85	3031.21	2948.61

Appendix 3: GSEA and CPDB pathways upregulated in 8-week, 32-week and 94-week hepatocytes

CPDB pathway enriched in 8-week hepatocytes	**p-value**
mRNA processing	1.42853E-07
Processing of Capped Intron-Containing Pre-mRNA	3.47573E-07
The role of GTSE1 in G2/M progression after G2 checkpoint	4.13211E-07
G2/M Transition	5.11088E-07
Cell Cycle, Mitotic	5.40742E-07
Mitotic G2-G2/M phases	6.41774E-07
mRNA Splicing	1.02433E-06
Cell Cycle	4.24237E-06
Spliceosome - Mus musculus (mouse)	5.13414E-06
Metabolism of RNA	9.39704E-06
Separation of Sister Chromatids	1.53164E-05
Mitotic Anaphase	2.02179E-05
Cell Cycle Checkpoints	2.10895E-05
Mitotic Metaphase and Anaphase	2.21354E-05
mRNA Splicing - Major Pathway	2.84778E-05
mRNA surveillance pathway - Mus musculus (mouse)	5.30774E-05
Mitotic Spindle Checkpoint	6.91474E-05
M Phase	0.000116294
mRNA Splicing - Minor Pathway	0.000144696
E3 ubiquitin ligases ubiquitinate target proteins	0.000241406
Amplification of signal from unattached kinetochores via a MAD2 inhibitory signal	0.00026044
Amplification of signal from the kinetochores	0.00026044

RHO GTPases Activate Formins	0.00045024
Autodegradation of the E3 ubiquitin ligase COP1	0.000602342
Mitotic Prometaphase	0.000741988
Resolution of Sister Chromatid Cohesion	0.0007712
Protein ubiquitination	0.000842023
Degradation of beta-catenin by the destruction complex	0.000884645
Transcriptional regulation by RUNX3	0.001188194
APC/C:Cdh1 mediated degradation of Cdc20 and other APC/C:Cdh1 targeted proteins in late mitosis/early G1	0.00122594
Cilium Assembly	0.001390167
Signaling pathways regulating pluripotency of stem cells - Mus musculus (mouse)	0.001461193
Cyclin A/B1/B2 associated events during G2/M transition	0.00146561
Oncogene Induced Senescence	0.001754555
Cellular responses to stress	0.002143243
Activated NOTCH1 Transmits Signal to the Nucleus	0.002354642
Downregulation of SMAD2/3:SMAD4 transcriptional activity	0.002716603
Negative regulation of FGFR1 signaling	0.002777999
Activation of APC/C and APC/C:Cdc20 mediated degradation of mitotic proteins	0.002777999
Anchoring of the basal body to the plasma membrane	0.003071419
Stabilization of p53	0.003284518
Regulation of RUNX2 expression and activity	0.003284518
Prostate cancer - Mus musculus (mouse)	0.003796283
Transcriptional regulation by RUNX2	0.003988493
Autodegradation of Cdh1 by Cdh1:APC/C	0.003988493
G1/S Transition	0.00417509
Glycolysis	0.00417509
Synthesis of active ubiquitin: roles of E1 and E2 enzymes	0.004206795
Regulation of RUNX3 expression and activity	0.004409976
Josephin domain DUBs	0.004409976
APC/C:Cdc20 mediated degradation of Securin	0.00475367
RHO GTPase Effectors	0.004854536
Organelle biogenesis and maintenance	0.004978929
APC/C:Cdc20 mediated degradation of Cyclin B	0.005611591
Inhibition of replication initiation of damaged DNA by RB1/E2F1	0.00574188
E2F mediated regulation of DNA replication	0.00574188
Degradation of DVL	0.00574188
Thyroid cancer - Mus musculus (mouse)	0.006095021
Regulation of APC/C activators between G1/S and early anaphase	0.006095021
Regulation of HSF1-mediated heat shock response	0.006331762
Cellular responses to external stimuli	0.006640406
Signaling by TGF-beta family members	0.007014482

RNA transport - Mus musculus (mouse)	0.007351802
Signaling by Rho GTPases	0.007405464
APC-Cdc20 mediated degradation of Nek2A	0.007624158
Negative regulation of MAPK pathway	0.008511316
Gene expression (Transcription)	0.008511872
Huntington disease - Mus musculus (mouse)	0.008737715
glycolysis III	0.00878747
Polo-like kinase mediated events	0.009548935
Aflatoxin B1 metabolism	0.009548935

CPDB pathway enriched in 32-week hepatocytes	p-value
Metabolism	6.37115E-21
Oxidative phosphorylation - Mus musculus (mouse)	5.67792E-11
Biological oxidations	6.75728E-11
Drug metabolism - other enzymes - Mus musculus (mouse)	9.61696E-11
Complement and coagulation cascades - Mus musculus (mouse)	1.20014E-10
Cytoplasmic Ribosomal Proteins	1.22973E-10
Cholesterol metabolism - Mus musculus (mouse)	2.78833E-10
Ribosome - Mus musculus (mouse)	5.78502E-10
aerobic respiration -- electron donor II	8.94304E-10
Thermogenesis - Mus musculus (mouse)	1.33984E-09
Electron Transport Chain	7.21875E-09
Complement and Coagulation Cascades	8.09966E-09
Non-alcoholic fatty liver disease (NAFLD) - Mus musculus (mouse)	1.99309E-08
Respiratory electron transport, ATP synthesis by chemiosmotic coupling, and heat production by uncoupling proteins.	2.82971E-08
Chemical carcinogenesis - Mus musculus (mouse)	1.1211E-07
Phase I - Functionalization of compounds	1.16647E-07
Chromosome Maintenance	1.89707E-07
Oxidative phosphorylation	2.1141E-07
Complement cascade	3.84547E-07
Huntington disease - Mus musculus (mouse)	4.53696E-07
Regulation of Complement cascade	4.93074E-07
NADH to cytochrome bo oxidase electron transfer	6.774E-07
NADH to cytochrome bd oxidase electron transfer	6.774E-07
Cholesterol metabolism (includes both Bloch and Kandutsch-Russell pathways)	9.73514E-07
Estrogen-dependent gene expression	1.01097E-06
Metabolism of xenobiotics by cytochrome P450 - Mus musculus (mouse)	1.28025E-06
cholesterol biosynthesis III (via desmosterol)	1.34054E-06
The citric acid (TCA) cycle and respiratory electron transport	1.67242E-06
Deposition of new CENPA-containing nucleosomes at the centromere	1.71565E-06
Nucleosome assembly	1.71565E-06

Metabolism of lipids	1.75307E-06
Drug metabolism - cytochrome P450 - Mus musculus (mouse)	1.8286E-06
ESR-mediated signaling	2.45991E-06
cholesterol biosynthesis I	2.59273E-06
Translation	2.77958E-06
Signaling by Nuclear Receptors	3.16492E-06
Parkinson disease - Mus musculus (mouse)	3.19794E-06
Plasma lipoprotein assembly, remodeling, and clearance	3.98332E-06
Steroid biosynthesis - Mus musculus (mouse)	4.42675E-06
cholesterol biosynthesis II (via 24,25-dihydrolanosterol)	4.508E-06
Respiratory electron transport	4.74893E-06
Post-translational protein phosphorylation	4.97679E-06
glutathione-mediated detoxification	5.8603E-06
Regulation of Insulin-like Growth Factor (IGF) transport and uptake by Insulin-like Growth Factor Binding Proteins (IGFBPs)	8.37191E-06
Gene Silencing by RNA	8.5781E-06
B-WICH complex positively regulates rRNA expression	1.06943E-05
Positive epigenetic regulation of rRNA expression	1.06943E-05
Complex I biogenesis	1.23529E-05
nicotine degradation III	1.28692E-05
Transcriptional regulation by small RNAs	1.31485E-05
Metabolism of steroids	1.77592E-05
Glucuronidation	1.8797E-05
Innate Immune System	1.94761E-05
NoRC negatively regulates rRNA expression	2.04054E-05
Mitochondrial translation elongation	2.06276E-05
Oxidative Stress Induced Senescence	2.07847E-05
Lysosome - Mus musculus (mouse)	2.52401E-05
Mitochondrial translation termination	2.67184E-05
RNA Polymerase I Promoter Opening	2.80087E-05
SIRT1 negatively regulates rRNA expression	2.80087E-05
Mitochondrial translation	3.03147E-05

Formation of the beta-catenin:TCF transactivating complex	3.03147E-05
Negative epigenetic regulation of rRNA expression	3.2651E-05
superpathway of cholesterol biosynthesis	3.44359E-05
Activated PKN1 stimulates transcription of AR (androgen receptor) regulated genes KLK2 and KLK3	3.7942E-05
Metabolism of amino acids and derivatives	4.17502E-05
Cholesterol biosynthesis	4.55502E-05
Retinol metabolism - Mus musculus (mouse)	4.92718E-05
nicotine degradation II	5.29421E-05
Metabolism of proteins	5.29852E-05
Alzheimer disease - Mus musculus (mouse)	5.32829E-05
Alanine and aspartate metabolism	5.59606E-05
Nonhomologous End-Joining (NHEJ)	6.20001E-05
RNA Polymerase I Promoter Clearance	6.87889E-05
RUNX1 regulates genes involved in megakaryocyte differentiation and platelet function	7.52107E-05
RNA Polymerase I Transcription	7.62671E-05
Formation of Fibrin Clot (Clotting Cascade)	0.000107479
Common Pathway of Fibrin Clot Formation	0.000112739
Epigenetic regulation of gene expression	0.000113717
Condensation of Prophase Chromosomes	0.000113845
PRC2 methylates histones and DNA	0.000129107
HDMs demethylate histones	0.000137624
Fatty Acid Biosynthesis	0.000149942
SUMOylation of chromatin organization proteins	0.000170315
Plasma lipoprotein clearance	0.000190204
Cholesterol Biosynthesis	0.000192475
Staphylococcus aureus infection - Mus musculus (mouse)	0.00025046
Recruitment and ATM-mediated phosphorylation of repair and signaling proteins at DNA double strand breaks	0.00025046
Vitamin digestion and absorption - Mus musculus (mouse)	0.000253088
DNA Double Strand Break Response	0.000288283
Phase II - Conjugation of compounds	0.000317359

Plasma lipoprotein remodeling	0.000322136
RHO GTPases activate PKNs	0.000403988
Antigen Presentation: Folding, assembly and peptide loading of class I MHC	0.000412113
Systemic lupus erythematosus - Mus musculus (mouse)	0.000430857
LDL clearance	0.00049829
fatty acid β-oxidation II (core pathway)	0.00049829
fatty acid β-oxidation I	0.000503875
Chylomicron clearance	0.000557129
Transport of small molecules	0.000561827
Steroid hormone biosynthesis - Mus musculus (mouse)	0.000605184
Neutrophil degranulation	0.000614374
Viral carcinogenesis - Mus musculus (mouse)	0.000617616
Glycolysis and Gluconeogenesis	0.000643739
Statin Pathway	0.000654732
Arginine biosynthesis - Mus musculus (mouse)	0.000654732
Fat digestion and absorption - Mus musculus (mouse)	0.000804354
Blood Clotting Cascade	0.000845225
Unfolded Protein Response (UPR)	0.000845225
Synthesis of PE	0.000883461
Porphyrin and chlorophyll metabolism - Mus musculus (mouse)	0.000937868
Fatty acid metabolism	0.000956551
arginine biosynthesis IV	0.001081959
Cytochrome P450 - arranged by substrate type	0.001260936
G2/M DNA damage checkpoint	0.001412841
Mitotic Prophase	0.001469018
urate degradation to allantoin	0.001520191
PKMTs methylate histone lysines	0.001527719
Phagosome - Mus musculus (mouse)	0.001539779
HATs acetylate histones	0.001549172
Intrinsic Pathway of Fibrin Clot Formation	0.001665311

Kennedy pathway	0.001678763
Senescence-Associated Secretory Phenotype (SASP)	0.001761444
Fatty Acid Beta Oxidation	0.001816537
Pentose and glucuronate interconversions - Mus musculus (mouse)	0.001816537
Glycolysis	0.002121329
Cellular Senescence	0.002142015
Formation of the ternary complex, and subsequently, the 43S complex	0.00214504
Regulation of TLR by endogenous ligand	0.002219232
Aflatoxin activation and detoxification	0.002465652
N-Glycan biosynthesis - Mus musculus (mouse)	0.002740067
phosphatidylethanolamine biosynthesis II	0.002856903
Primary bile acid biosynthesis - Mus musculus (mouse)	0.002868633
Mitochondrial biogenesis	0.002956256
G2/M Checkpoints	0.003020449
Xenobiotics	0.00308133
bupropion degradation	0.003269001
Glutathione metabolism - Mus musculus (mouse)	0.003297452
Ascorbate and aldarate metabolism - Mus musculus (mouse)	0.003513615
Biosynthesis of DHA-derived SPMs	0.003738581
Translation initiation complex formation	0.003860353
Ribosomal scanning and start codon recognition	0.003860353
Fluid shear stress and atherosclerosis - Mus musculus (mouse)	0.003919547
Biosynthesis of maresin-like SPMs	0.004142575
Oxidative Stress	0.004142575
Protein export - Mus musculus (mouse)	0.004142575
Biosynthesis of specialized proresolving mediators (SPMs)	0.004256385
SUMO E3 ligases SUMOylate target proteins	0.004300299
Activation of the mRNA upon binding of the cap-binding complex and eIFs, and subsequent binding to 43S	0.0043018
Glycerophospholipid metabolism - Mus musculus (mouse)	0.00450405
Formation of ATP by chemiosmotic coupling	0.004533665
Cristae formation	0.004533665

Other glycan degradation - Mus musculus (mouse)	0.004533665
L13a-mediated translational silencing of Ceruloplasmin expression	0.004780368
Synthesis of bile acids and bile salts via 7alpha-hydroxycholesterol	0.00484795
RMTs methylate histone arginines	0.005260248
Biosynthesis of maresins	0.0056345
Irinotecan Pathway	0.005774561
Iron uptake and transport	0.005856466
Formation of a pool of free 40S subunits	0.006127773
Platelet degranulation	0.006163982
Bile secretion - Mus musculus (mouse)	0.006256332
SUMOylation	0.006368816
TCF dependent signaling in response to WNT	0.006437564
Amino acid synthesis and interconversion (transamination)	0.006506913
Transferrin endocytosis and recycling	0.006506913
Synthesis of epoxy (EET) and dihydroxyeicosatrienoic acids (DHET)	0.006748753
Hypertrophy Model	0.006748753
Urea cycle and metabolism of amino groups	0.006748753
Cap-dependent Translation Initiation	0.007103956
Chylomicron remodeling	0.007712161
Chylomicron assembly	0.007712161
Ubiquinone and other terpenoid-quinone biosynthesis - Mus musculus (mouse)	0.007712161
Gamma-carboxylation of protein precursors	0.007712161
Metabolism of Angiotensinogen to Angiotensins	0.00808396
Response to elevated platelet cytosolic Ca2+	0.008191817
Eukaryotic Translation Initiation	0.008538229
DNA Double-Strand Break Repair	0.008653719
Cholesterol biosynthesis via desmosterol	0.008655234
Cholesterol biosynthesis via lathosterol	0.008655234
Reuptake of GABA	0.008655234
Mitochondrial ABC transporters	0.008655234
Scavenging by Class A Receptors	0.008655234

Metapathway biotransformation	0.009135705
Transcriptional regulation by RUNX1	0.009420466
ABC transporters - Mus musculus (mouse)	0.009471414
Endosomal/Vacuolar pathway	0.009581296
Prion diseases - Mus musculus (mouse)	0.009684652
Phenylalanine and tyrosine catabolism	0.009988394

CPDB pathway enriched in 32-week hepatocytes	**p-value**
XPodNet - protein-protein interactions in the podocyte expanded by STRING	3.28E-10
Focal Adhesion	3.68E-08
PI3K-Akt signaling pathway - Mus musculus (mouse)	5.44E-08
Extracellular matrix organization	0.000000112
Focal Adhesion-PI3K-Akt-mTOR-signaling pathway	0.000000618
ECM-receptor interaction - Mus musculus (mouse)	0.00000154
Hemostasis	0.00000473
Focal adhesion - Mus musculus (mouse)	0.00000886
Proteoglycans in cancer - Mus musculus (mouse)	0.0000137
O-glycosylation of TSR domain-containing proteins	0.0000449
Cytoplasmic Ribosomal Proteins	0.0000839
Osteoclast	0.000111564
DARPP-32 events	0.000130076
Collagen chain trimerization	0.000157719
Collagen biosynthesis and modifying enzymes	0.000259812
Intracellular signaling by second messengers	0.00029423
Integration of energy metabolism	0.000300113
Rho GTPase cycle	0.000300811
Platelet activation, signaling and aggregation	0.000327271
O-linked glycosylation	0.000367262
Pathways in cancer - Mus musculus (mouse)	0.00044705
Integrin cell surface interactions	0.000643187
Myometrial Relaxation and Contraction Pathways	0.000796387
Platelet activation - Mus musculus (mouse)	0.000811244
Osteoblast	0.00085364
Collagen formation	0.000904766
PIP3 activates AKT signaling	0.001033355
Protein digestion and absorption - Mus musculus (mouse)	0.001125694
Elastic fibre formation	0.001132555
Dysregulated miRNA Targeting in Insulin-PI3K-AKT Signaling	0.001164305
Keratan sulfate biosynthesis	0.001164305
Negative regulation of the PI3K/AKT network	0.001195637
Small cell lung cancer - Mus musculus (mouse)	0.00136779
Regulation of insulin secretion	0.001576156
Ras signaling pathway - Mus musculus (mouse)	0.001753474
Platelet degranulation	0.001795266
MAPK signaling pathway - Mus musculus (mouse)	0.001808912
Translocation of ZAP-70 to Immunological synapse	0.001864038
PTK6 promotes HIF1A stabilization	0.001936241

PI5P, PP2A and IER3 Regulate PI3K/AKT Signaling	0.001981654
Hypertrophic cardiomyopathy (HCM) - Mus musculus (mouse)	0.002071573
Long-term depression - Mus musculus (mouse)	0.002261477
NFG and proNGF binds to p75NTR	0.002270071
PodNet- protein-protein interactions in the podocyte	0.002333633
Rap1 signaling pathway - Mus musculus (mouse)	0.002379028
mTOR signalling	0.002554902
Response to elevated platelet cytosolic Ca2+	0.002577368
cGMP effects	0.002591765
Keratan sulfate/keratin metabolism	0.003040879
Molecules associated with elastic fibres	0.003040879
Vascular smooth muscle contraction - Mus musculus (mouse)	0.003352916
Phosphorylation of CD3 and TCR zeta chains	0.003492952
Glycosaminoglycan metabolism	0.003500222
Phospholipase D signaling pathway - Mus musculus (mouse)	0.004127273
Renal cell carcinoma - Mus musculus (mouse)	0.004786613
Hematopoietic cell lineage - Mus musculus (mouse)	0.005021657
Human papillomavirus infection - Mus musculus (mouse)	0.005305866
PD-1 signaling	0.00588648
Nitric oxide stimulates guanylate cyclase	0.00588648
cGMP-PKG signaling pathway - Mus musculus (mouse)	0.006499977
Insulin signaling pathway - Mus musculus (mouse)	0.00694708
Renin secretion - Mus musculus (mouse)	0.006990263
Regulation of actin cytoskeleton - Mus musculus (mouse)	0.007129638
AKT phosphorylates targets in the nucleus	0.00730225
Formyl peptide receptors bind formyl peptides and many other ligands	0.00730225
Acetylcholine regulates insulin secretion	0.00730225
p75NTR recruits signalling complexes	0.00730225
Cell death signalling via NRAGE, NRIF and NADE	0.007646291
Integrin-mediated Cell Adhesion	0.007978383
Glycosphingolipid biosynthesis - lacto and neolacto series - Mus musculus (mouse)	0.008175908
Endochondral Ossification	0.00889408
Longevity regulating pathway - multiple species - Mus musculus (mouse)	0.00889408
Signaling by PTK6	0.009086117
Signaling by Non-Receptor Tyrosine Kinases	0.009086117
Calcium Regulation in the Cardiac Cell	0.00937011

GSEA pathways enriched in 8-week hepatocytes	**NES**	**NOM p-val**
RESPONSE OF MTB TO PHAGOCYTOSIS	1.6452805	0
DEADENYLATION OF MRNA	1.5755353	0
INITIATION OF NUCLEAR ENVELOPE NE REFORMATION	1.5245562	0
CHROMATIN MODIFYING ENZYMES	1.4984912	0
GLYCOLYSIS	1.4581758	0
TRANSCRIPTIONAL ACTIVATION OF MITOCHONDRIAL BIOGENESIS	1.4512202	0
INTRAFLAGELLAR TRANSPORT	1.4405229	0
CONSTITUTIVE SIGNALING BY LIGAND RESPONSIVE EGFR CANCER VARIANTS	1.4285127	0
RECRUITMENT OF MITOTIC CENTROSOME PROTEINS AND COMPLEXES	1.4025347	0
REGULATION OF PLK1 ACTIVITY AT G2 M TRANSITION	1.3967361	0
CILIUM ASSEMBLY	1.3900093	0

ZINC TRANSPORTERS	1.3828933	0
SUMOYLATION OF TRANSCRIPTION COFACTORS	1.3801373	0
RECRUITMENT OF NUMA TO MITOTIC CENTROSOMES	1.3741059	0
RAF INDEPENDENT MAPK1 3 ACTIVATION	1.3723485	0
TRANSCRIPTIONAL REGULATION BY E2F6	1.3510301	0
SIGNAL TRANSDUCTION BY L1	1.3462267	0
ANCHORING OF THE BASAL BODY TO THE PLASMA MEMBRANE	1.3310444	0
SUMOYLATION	1.3223641	0
LISTERIA MONOCYTOGENES ENTRY INTO HOST CELLS	1.3131877	0
INFECTION WITH MYCOBACTERIUM TUBERCULOSIS	1.3078566	0
PROCESSING OF CAPPED INTRONLESS PRE MRNA	1.3061873	0
FORMATION OF SENESCENCE ASSOCIATED HETEROCHROMATIN FOCI SAHF	1.3053981	0
NEGATIVE REGULATION OF FGFR2 SIGNALING	1.2973365	0
ORGANELLE BIOGENESIS AND MAINTENANCE	1.2936	0
NEGATIVE REGULATION OF FGFR1 SIGNALING	1.2737887	0
TP53 REGULATES TRANSCRIPTION OF ADDITIONAL CELL CYCLE GENES WHOSE EXACT ROLE IN THE P53 PATHWAY REMAIN UNCERTAIN	1.2711058	0
MITOTIC G2 G2 M PHASES	1.2692283	0
TRANSCRIPTIONAL REGULATION BY TP53	1.2673401	0
SUMOYLATION OF TRANSCRIPTION FACTORS	1.2229629	0
SUMOYLATION OF DNA REPLICATION PROTEINS	1.2156872	0
EPIGENETIC REGULATION OF GENE EXPRESSION	1.1732619	0
DEUBIQUITINATION	1.164578	0
GOLGI ASSOCIATED VESICLE BIOGENESIS	1.1572089	0
SIGNALING BY FGFR	1.0925132	0

GSEA pathways enriched in 32-week hepatocytes	**NES**	**NOM p-val**
MITOCHONDRIAL TRNA AMINOACYLATION	1.608259	0
METABOLISM OF STEROID HORMONES	1.605499	0
ABC TRANSPORTERS IN LIPID HOMEOSTASIS	1.580175	0
DEFECTS IN VITAMIN AND COFACTOR METABOLISM	1.560766	0
METABOLISM OF PORPHYRINS	1.548682	0
LDL CLEARANCE	1.538069	0
PCNA DEPENDENT LONG PATCH BASE EXCISION REPAIR	1.529107	0
HDR THROUGH SINGLE STRAND ANNEALING SSA	1.528728	0
PHASE II CONJUGATION OF COMPOUNDS	1.526216	0
BILE ACID AND BILE SALT METABOLISM	1.519155	0
GAMMA CARBOXYLATION HYPUSINE FORMATION AND ARYLSULFATASE ACTIVATION	1.50049	0
METABOLISM OF VITAMINS AND COFACTORS	1.497678	0
RESOLUTION OF AP SITES VIA THE MULTIPLE NUCLEOTIDE PATCH REPLACEMENT PATHWAY	1.494919	0
DUAL INCISION IN GG NER	1.475104	0
METABOLISM OF STEROIDS	1.463844	0
METABOLISM OF AMINO ACIDS AND DERIVATIVES	1.45669	0
MITOCHONDRIAL FATTY ACID BETA OXIDATION	1.438117	0
TRANSLESION SYNTHESIS BY POLK	1.434669	0

ANTIGEN PRESENTATION FOLDING ASSEMBLY AND PEPTIDE LOADING OF CLASS I MHC	1.433655	0
TELOMERE MAINTENANCE	1.426364	0
DISEASES OF CARBOHYDRATE METABOLISM	1.425704	0
MITOCHONDRIAL PROTEIN IMPORT	1.425342	0
LAGGING STRAND SYNTHESIS	1.42481	0
METABOLISM OF WATER SOLUBLE VITAMINS AND COFACTORS	1.422695	0
FATTY ACID METABOLISM	1.421045	0
GLUCONEOGENESIS	1.413902	0
PROTEIN LOCALIZATION	1.411241	0
ABC FAMILY PROTEINS MEDIATED TRANSPORT	1.401564	0
MITOCHONDRIAL TRANSLATION	1.398193	0
SYNTHESIS OF BILE ACIDS AND BILE SALTS	1.38506	0
PINK1 PRKN MEDIATED MITOPHAGY	1.376487	0
SLC TRANSPORTER DISORDERS	1.361069	0
GLYOXYLATE METABOLISM AND GLYCINE DEGRADATION	1.360947	0
INHIBITION OF DNA RECOMBINATION AT TELOMERE	1.358522	0
DISEASES ASSOCIATED WITH N GLYCOSYLATION OF PROTEINS	1.348651	0
MICRORNA MIRNA BIOGENESIS	1.33231	0
DISORDERS OF TRANSMEMBRANE TRANSPORTERS	1.329792	0
SYNTHESIS OF BILE ACIDS AND BILE SALTS VIA 7ALPHA HYDROXYCHOLESTEROL	1.319277	0
BIOLOGICAL OXIDATIONS	1.31319	0
NOTCH2 ACTIVATION AND TRANSMISSION OF SIGNAL TO THE NUCLEUS	1.311199	0
VITAMIN B5 PANTOTHENATE METABOLISM	1.305664	0
RESOLUTION OF ABASIC SITES AP SITES	1.301473	0
INTRINSIC PATHWAY OF FIBRIN CLOT FORMATION	1.29698	0
GLUTATHIONE CONJUGATION	1.293684	0
TRANSCRIPTIONAL REGULATION BY SMALL RNAS	1.279231	0
CLASS I PEROXISOMAL MEMBRANE PROTEIN IMPORT	1.275971	0
HOMOLOGOUS DNA PAIRING AND STRAND EXCHANGE	1.274243	0
CYTOCHROME P450 ARRANGED BY SUBSTRATE TYPE	1.267629	0
TRNA PROCESSING	1.260237	0
MITOPHAGY	1.258247	0
PROCESSIVE SYNTHESIS ON THE LAGGING STRAND	1.257505	0
CELLULAR RESPONSE TO STARVATION	1.255226	0
GLYCOGEN STORAGE DISEASES	1.233508	0
BRANCHED CHAIN AMINO ACID CATABOLISM	1.233279	0
METABOLISM OF FAT SOLUBLE VITAMINS	1.22575	0
METABOLISM OF NUCLEOTIDES	1.206437	0
RNA POLYMERASE III TRANSCRIPTION INITIATION FROM TYPE 3 PROMOTER	1.184459	0
GLYCOSPHINGOLIPID METABOLISM	1.17552	0
METABOLIC DISORDERS OF BIOLOGICAL OXIDATION ENZYMES	1.169944	0
PHASE I FUNCTIONALIZATION OF COMPOUNDS	1.162867	0
THE CANONICAL RETINOID CYCLE IN RODS TWILIGHT VISION	1.155279	0
COMPLEMENT CASCADE	1.138655	0

VISUAL PHOTOTRANSDUCTION	1.120983	0
ARACHIDONIC ACID METABOLISM	1.105301	0
ESTROGEN DEPENDENT GENE EXPRESSION	1.094353	0
ASSOCIATION OF TRIC CCT WITH TARGET PROTEINS DURING BIOSYNTHESIS	1.093634	0
FORMATION OF FIBRIN CLOT CLOTTING CASCADE	1.073878	0
INFLUENZA INFECTION	1.072062	0

GSEA pathways enriched in 94-week hepatocytes	**NES**	**NOM p-val**
NOD1 2 SIGNALING PATHWAY	1.6077578	0
G ALPHA Z SIGNALLING EVENTS	1.5625931	0
CD209 DC SIGN SIGNALING	1.5574236	0
SIGNALING BY ERYTHROPOIETIN	1.5425098	0
SIGNALING BY PDGF	1.5384134	0
RAB GEFS EXCHANGE GTP FOR GDP ON RABS	1.5300416	0
N GLYCAN ANTENNAE ELONGATION IN THE MEDIAL TRANS GOLGI	1.5216314	0
OPIOID SIGNALLING	1.5127105	0
RAB GERANYLGERANYLATION	1.5110319	0
INTRA GOLGI TRAFFIC	1.5100564	0
VEGFR2 MEDIATED CELL PROLIFERATION	1.5087711	0
INTERLEUKIN 4 AND INTERLEUKIN 13 SIGNALING	1.4958652	0
INTEGRATION OF ENERGY METABOLISM	1.4900635	0
REGULATION OF INSULIN SECRETION	1.4808043	0
TRAF6 MEDIATED IRF7 ACTIVATION	1.4718275	0
G BETA GAMMA SIGNALLING THROUGH PI3KGAMMA	1.468809	0
G PROTEIN BETA GAMMA SIGNALLING	1.4644351	0
RECYCLING PATHWAY OF L1	1.4631886	0
SYNTHESIS OF PIPS AT THE PLASMA MEMBRANE	1.4569467	0
SIGNALING BY FLT3 ITD AND TKD MUTANTS	1.4528807	0
SIGNAL AMPLIFICATION	1.4522191	0
DARPP 32 EVENTS	1.4510815	0
PI METABOLISM	1.44232	0
COLLAGEN CHAIN TRIMERIZATION	1.4362363	0
GLUCAGON SIGNALING IN METABOLIC REGULATION	1.4358028	0
CONSTITUTIVE SIGNALING BY AKT1 E17K IN CANCER	1.4349896	0
INTERLEUKIN 37 SIGNALING	1.434603	0
ACTIVATED TAK1 MEDIATES P38 MAPK ACTIVATION	1.4317573	0
VASOPRESSIN REGULATES RENAL WATER HOMEOSTASIS VIA AQUAPORINS	1.4314203	0
RAF ACTIVATION	1.4295962	0
FCGR3A MEDIATED IL10 SYNTHESIS	1.4283286	0
RAB REGULATION OF TRAFFICKING	1.4279563	0
INOSITOL PHOSPHATE METABOLISM	1.4226668	0
INTERLEUKIN 17 SIGNALING	1.4211493	0
MTOR SIGNALLING	1.4200115	0
TNF SIGNALING	1.4134823	0
RHO GTPASES ACTIVATE NADPH OXIDASES	1.4040337	0
MET ACTIVATES PTK2 SIGNALING	1.4004703	0
ONCOGENIC MAPK SIGNALING	1.3934227	0
EPHB MEDIATED FORWARD SIGNALING	1.3918084	0
SIGNALING BY NTRK2 TRKB	1.3866115	0

SIGNALLING TO ERKS	1.3858507	0
EXTRACELLULAR MATRIX ORGANIZATION	1.3854305	0
NEUROTRANSMITTER RECEPTORS AND POSTSYNAPTIC SIGNAL TRANSMISSION	1.3761714	0
ADP SIGNALLING THROUGH P2Y PURINOCEPTOR 1	1.3743356	0
NCAM1 INTERACTIONS	1.3596874	0
EXTRA NUCLEAR ESTROGEN SIGNALING	1.3595853	0
DISEASES ASSOCIATED WITH GLYCOSAMINOGLYCAN METABOLISM	1.3558915	0
COLLAGEN DEGRADATION	1.354978	0
AQUAPORIN MEDIATED TRANSPORT	1.3525456	0
GABA RECEPTOR ACTIVATION	1.3496618	0
RHOV GTPASE CYCLE	1.3424925	0
GLUCAGON LIKE PEPTIDE 1 GLP1 REGULATES INSULIN SECRETION	1.3408862	0
TNFR1 INDUCED NFKAPPAB SIGNALING PATHWAY	1.3397255	0
THROMBOXANE SIGNALLING THROUGH TP RECEPTOR	1.3343923	0
FCERI MEDIATED MAPK ACTIVATION	1.3341808	0
COLLAGEN BIOSYNTHESIS AND MODIFYING ENZYMES	1.3316327	0
DEATH RECEPTOR SIGNALLING	1.3305933	0
ACTIVATION OF KAINATE RECEPTORS UPON GLUTAMATE BINDING	1.3287716	0
THROMBIN SIGNALLING THROUGH PROTEINASE ACTIVATED RECEPTORS PARS	1.3230951	0
TOLL LIKE RECEPTOR TLR1 TLR2 CASCADE	1.3205757	0
CTLA4 INHIBITORY SIGNALING	1.311757	0
SIGNALING BY INTERLEUKINS	1.3108524	0
G ALPHA I SIGNALLING EVENTS	1.3089911	0
ANTI INFLAMMATORY RESPONSE FAVOURING LEISHMANIA PARASITE INFECTION	1.3067816	0
INTEGRIN CELL SURFACE INTERACTIONS	1.3061613	0
ZBP1 DAI MEDIATED INDUCTION OF TYPE I IFNS	1.305033	0
TOLL LIKE RECEPTOR 9 TLR9 CASCADE	1.3042221	0
RHOU GTPASE CYCLE	1.3028259	0
SIGNALLING TO RAS	1.3010715	0
ECM PROTEOGLYCANS	1.2989162	0
ADORA2B MEDIATED ANTI INFLAMMATORY CYTOKINES PRODUCTION	1.2987556	0
A TETRASACCHARIDE LINKER SEQUENCE IS REQUIRED FOR GAG SYNTHESIS	1.2940379	0
NEGATIVE REGULATION OF THE PI3K AKT NETWORK	1.2897776	0
INTRACELLULAR SIGNALING BY SECOND MESSENGERS	1.2880368	0
TRANSMISSION ACROSS CHEMICAL SYNAPSES	1.2844381	0
MYD88 INDEPENDENT TLR4 CASCADE	1.2834346	0
MOLECULES ASSOCIATED WITH ELASTIC FIBRES	1.2802172	0
DEGRADATION OF THE EXTRACELLULAR MATRIX	1.2749484	0
HEPARAN SULFATE HEPARIN HS GAG METABOLISM	1.2741709	0
G PROTEIN MEDIATED EVENTS	1.2735593	0
ELASTIC FIBRE FORMATION	1.2727143	0
COLLAGEN FORMATION	1.2699991	0
CELL SURFACE INTERACTIONS AT THE VASCULAR WALL	1.265383	0
SIGNALING BY BRAF AND RAF FUSIONS	1.2636648	0
TRANSLOCATION OF SLC2A4 GLUT4 TO THE PLASMA MEMBRANE	1.2598984	0
DAG AND IP3 SIGNALING	1.2592251	0
MET PROMOTES CELL MOTILITY	1.2576308	0
SIGNALING BY RECEPTOR TYROSINE KINASES	1.2567215	0

NUCLEOTIDE BINDING DOMAIN LEUCINE RICH REPEAT CONTAINING RECEPTOR NLR SIGNALING PATHWAYS	1.2566732	0
COSTIMULATION BY THE CD28 FAMILY	1.2547785	0
CA DEPENDENT EVENTS	1.2518777	0
CROSSLINKING OF COLLAGEN FIBRILS	1.2511716	0
RAP1 SIGNALLING	1.2472577	0
GABA B RECEPTOR ACTIVATION	1.246345	0
ACTIVATION OF NMDA RECEPTORS AND POSTSYNAPTIC EVENTS	1.2456644	0
SIGNALING BY GPCR	1.2430232	0
ASSEMBLY OF COLLAGEN FIBRILS AND OTHER MULTIMERIC STRUCTURES	1.2401876	0
SIALIC ACID METABOLISM	1.2333709	0
SIGNALING BY CSF3 G CSF	1.2248048	0
O GLYCOSYLATION OF TSR DOMAIN CONTAINING PROTEINS	1.2188822	0
LEISHMANIA INFECTION	1.2111439	0
RAS PROCESSING	1.2011904	0
RHO GTPASES ACTIVATE PAKS	1.1931616	0
PI3K AKT SIGNALING IN CANCER	1.1919584	0
WNT5A DEPENDENT INTERNALIZATION OF FZD4	1.1911501	0
DISEASES OF GLYCOSYLATION	1.1849152	0
METABOLISM OF NITRIC OXIDE NOS3 ACTIVATION AND REGULATION	1.1775755	0
NON INTEGRIN MEMBRANE ECM INTERACTIONS	1.17006	0
C TYPE LECTIN RECEPTORS CLRS	1.149861	0
MUSCLE CONTRACTION	1.1447977	0
MAPK FAMILY SIGNALING CASCADES	1.1289003	0
G ALPHA Q SIGNALLING EVENTS	1.124955	0

References

1. SF, G., *Aging: The Biology of Senescence.* Developmental Biology. 6th edition. , 2000.
2. L. Robert, *Longevity and aging, genetic and post-genetic mechanisms. Which target to choose for postponing and treating age-related diseases.* European Geriatric Medicine, 2012. **3**(1): p. 61-66.
3. Kirkwood, T.B., *Understanding ageing from an evolutionary perspective.* J Intern Med, 2008. **263**(2): p. 117-27.
4. Kirkwood, T.B. and S. Melov, *On the programmed/non-programmed nature of ageing within the life history.* Curr Biol, 2011. **21**(18): p. R701-7.
5. Zimniak, P., *What is the Proximal Cause of Aging?* Front Genet, 2012. **3**: p. 189.
6. Skulachev, V.P., *Aging as a particular case of phenoptosis, the programmed death of an organism (a response to Kirkwood and Melov "On the programmed/non-programmed nature of ageing within the life history").* Aging (Albany NY), 2011. **3**(11): p. 1120-3.
7. Bjorksten, J., *The crosslinkage theory of aging.* J Am Geriatr Soc, 1968. **16**(4): p. 408-27.
8. Harman, D., *Aging: a theory based on free radical and radiation chemistry.* J Gerontol, 1956. **11**(3): p. 298-300.
9. Gerschman, R., et al., *Oxygen poisoning and x-irradiation: a mechanism in common.* Science, 1954. **119**(3097): p. 623-6.
10. Jin, K., *Modern Biological Theories of Aging.* Aging Dis, 2010. **1**(2): p. 72-74.
11. Davidovic, M., et al., *Old age as a privilege of the "selfish ones".* Aging Dis, 2010. **1**(2): p. 139-46.
12. Cornelius, E., *Increased incidence of lymphomas in thymectomized mice--evidence for an immunological theory of aging.* Experientia, 1972. **28**(4): p. 459.
13. Schibler, U., *The daily rhythms of genes, cells and organs. Biological clocks and circadian timing in cells.* EMBO Rep, 2005. **6 Spec No**: p. S9-13.
14. van Heemst, D., *Insulin, IGF-1 and longevity.* Aging Dis, 2010. **1**(2): p. 147-57.
15. Prinzinger, R., *Programmed ageing: the theory of maximal metabolic scope. How does the biological clock tick?* EMBO Rep, 2005. **6 Spec No**: p. S14-9.
16. Campisi, J., *Cancer, aging and cellular senescence.* In Vivo, 2000. **14**(1): p. 183-8.
17. Lopez-Otin, C., et al., *The hallmarks of aging.* Cell, 2013. **153**(6): p. 1194-217.
18. Shen, Z., *Genomic instability and cancer: an introduction.* J Mol Cell Biol, 2011. **3**(1): p. 1-3.
19. Aguilera, A. and B. Gomez-Gonzalez, *Genome instability: a mechanistic view of its causes and consequences.* Nat Rev Genet, 2008. **9**(3): p. 204-17.
20. F. Faggioli, T.W., J. Vijg, C. Montagna, *Chromosome-specific accumulation of aneuploidy in the aging mouse brain.* Hum. Mol. Genet, 2012: p. 5246-5253.
21. L.A. Forsberg, C.R., H.R. Razzaghian, G. Pakalapati, L. Waite, K.S. Thilbeault, A. Ronowicz, N.E. Wineinger, H.K. Tiwari, D. Boomsma, et al., *Age-related somatic structural changes in the nuclear genome of human blood cells.* Am. J. Hum. Genet., 2012: p. 17-228.
22. C.B. Park, N.G.L., *Mitochondrial DNA mutations in disease and aging.* J. Cell Biol., 2011: p. 809-818.

23. A. Trifunovic, A.W., M. Falkenberg, J.N. Spelbrink, A.T. Rovio, C.E. Bruder, M. Bohlooly-Y, S. Gidlöf, A. Oldfors, R. Wibom, et al., *Premature ageing in mice expressing defective mitochondrial DNA polymerase.* Nature, 2004: p. 417-423.
24. M. Vermulst, J.W., G.C. Kujoth, J.H. Bielas, P.S. Rabinovitch, T.A. Prolla, L.A. Loeb, *DNA deletions and clonal mutations drive premature aging in mitochondrial mutator mice* Nat. Genet., 2008: p. 392-394.
25. R. Cabanillas, J.C., J.A. Villameytide, M. Pérez, J. Longo, J.M. Richard, R. Alvarez, N.S. Durán, R. Illán, D.J. González, C. López-Otín, *Néstor-Guillermo progeria syndrome: a novel premature aging condition with early onset and chronic development caused by BANF1 mutations.* Am. J. Med. Genet. A., 2011: p. 2617-2625.
26. M. Eriksson, W.T.B., L.B. Gordon, M.W. Glynn, J. Singer, L. Scott, M.R. Erdos, C.M. Robbins, T.Y. Moses, P. Berglund, et al., *Recurrent de novo point mutations in lamin A cause Hutchinson-Gilford progeria syndrome.* Nature Reviews Cancer, 2003: p. 293-298.
27. A.A. Moskalev, M.V.S., E.N. Plyusnina, A. Zhavoronkov, A. Budovsky, H. Yanai, V.E. Fraifeld, *The role of DNA damage and repair in aging through the prism of Koch-like criteria.* Ageing Res. Rev. , 2012.
28. C.R. Burtner, B.K.K., *Progeria syndromes and ageing: what is the connection?* Nat. Rev. Mol. Cell Biol., 2010: p. 567-578.
29. D.J. Baker, M.M.D., T. Wijshake, K.B. Jeganathan, L. Malureanu, J.H. van Ree, R. Crespo-Diaz, S. Reyes, L. Seaburg, V. Shapiro, et al., *Increased expression of BubR1 protects against aneuploidy and cancer and extends healthy lifespan.* Nat. Cell Biol., 2013: p. 96-102, .
30. F.G. Osorio, C.L.N., J. Cadinanos, I.C. Lopez-Mejia, P.M. Quiros, C. Bartoli, J. Rivera, J. Tazi, G. Guzman, I. Varela, et al., *Splicing-directed therapy in a new mouse model of human accelerated aging.* Sci. Transl. Med., 2011.
31. I. Varela, S.P., A.P. Ugalde, C.L. Navarro, M.F. Suárez, P. Cau, J. Cadiñanos, F.G. Osorio, N. Foray, J. Cobo, et al., *Combined treatment with statins and aminobisphosphonates extends longevity in a mouse model of human premature aging.* Nat. Med, 2008: p. 767-772.
32. S.H. Yang, M.M., X. Qiao, D. Frost, J. Bauch, C. Coffinier, S. Majumdar, M.O. Bergo, S.G. Young, L.G. Fong, *A farnesyltransferase inhibitor improves disease phenotypes in mice with a Hutchinson-Gilford progeria syndrome mutation.* J. Clin. Invest., 2006: p. 2115-2121.
33. Blasco, M.A., *Telomere length, stem cells and aging.* Nat Chem Biol, 2007. **3**(10): p. 640-9.
34. Olovnikov, A.M., *Telomeres, telomerase, and aging: origin of the theory.* Exp Gerontol, 1996. **31**(4): p. 443-8.
35. de Lange, T., *How shelterin solves the telomere end-protection problem.* Cold Spring Harb Symp Quant Biol, 2010. **75**: p. 167-77.
36. Fumagalli, M., et al., *Telomeric DNA damage is irreparable and causes persistent DNA-damage-response activation.* Nat Cell Biol, 2012. **14**(4): p. 355-65.
37. Hewitt, G., et al., *Telomeres are favoured targets of a persistent DNA damage response in ageing and stress-induced senescence.* Nat Commun, 2012. **3**: p. 708.
38. E.H. Blackburn, C.W.G., J.W. Szostak, *Telomeres and telomerase: the path from maize, Tetrahymena and yeast to human cancer and aging.* Nat. Med., 2006: p. 1133-1138.

39. Blasco, M.A., *Telomere length, stem cells and aging.* Nat. Chem. Biol., 2007: p. 640-649.
40. P. Martínez, M.A.B., *Role of shelterin in cancer and aging.* Aging Cell,, 2010: p. 653-666.
41. M. Armanios, J.K.A., E.M. Parry, B. Karim, M.A. Strong, C.W. Greider, *Short telomeres are sufficient to cause the degenerative defects associated with aging.* Am. J. Hum. Genet., 2009: p. 823-832.
42. M.A. Blasco, H.W.L., M.P. Hande, E. Samper, P.M. Lansdorp, R.A. DePinho, C.W. Greider, *Telomere shortening and tumor formation by mouse cells lacking telomerase RNA.* Cell, 1997: p. 25-34.
43. Close and I.F. A. Tomás-Loba, P.J. Fernández-Marcos, M.L. Cayuela, A. Maraver, A. Tejera, C. Borrás, A. Matheu, P. Klatt, J.M. Flores, et al., *Telomerase reverse transcriptase delays aging in cancer-resistant mice.* Cell Biophys., 2008: p. 609-622.
44. M. Jaskelioff, F.L.M., J.H. Paik, E. Thomas, S. Jiang, A.C. Adams, E. Sahin, M. Kost-Alimova, A. Protopopov, J. Cadiñanos, et al., *Telomerase reactivation reverses tissue degeneration in aged telomerase-deficient mice.* Nature Reviews Cancer, 2011: p. 102-106.
45. B. Bernardes de Jesus, E.V., K. Schneeberger, A.M. Tejera, E. Ayuso, F. Bosch, M.A. Blasco, *Telomerase gene therapy in adult and old mice delays aging and increases longevity without increasing cancer.* EMBO Mol Med,, 2012: p. 691-704.
46. Hachmo, Y., et al., *Hyperbaric oxygen therapy increases telomere length and decreases immunosenescence in isolated blood cells : a prospective trial.* Aging, 2020. **12**.
47. Dogan, E.S. and C. Liu, *Three-dimensional chromatin packing and positioning of plant genomes.* Nat Plants, 2018. **4**(8): p. 521-529.
48. Meaburn, K.J. and T. Misteli, *Cell biology: chromosome territories.* Nature, 2007. **445**(7126): p. 379-781.
49. Lieberman-Aiden, E., et al., *Comprehensive mapping of long-range interactions reveals folding principles of the human genome.* Science, 2009. **326**(5950): p. 289-93.
50. Dixon, J.R., et al., *Topological domains in mammalian genomes identified by analysis of chromatin interactions.* Nature, 2012. **485**(7398): p. 376-80.
51. Dixon, J.R., et al., *Chromatin architecture reorganization during stem cell differentiation.* Nature, 2015. **518**(7539): p. 331-6.
52. Chandra, T., et al., *Global reorganization of the nuclear landscape in senescent cells.* Cell Rep, 2015. **10**(4): p. 471-83.
53. Zhan, Y., et al., *Reciprocal insulation analysis of Hi-C data shows that TADs represent a functionally but not structurally privileged scale in the hierarchical folding of chromosomes.* Genome Res, 2017. **27**(3): p. 479-490.
54. Nora, E.P., et al., *Spatial partitioning of the regulatory landscape of the X-inactivation centre.* Nature, 2012. **485**(7398): p. 381-5.
55. Phillips-Cremins, J.E. and V.G. Corces, *Chromatin insulators: linking genome organization to cellular function.* Mol Cell, 2013. **50**(4): p. 461-74.
56. Rao, S.S., et al., *A 3D map of the human genome at kilobase resolution reveals principles of chromatin looping.* Cell, 2014. **159**(7): p. 1665-80.
57. Bonev, B., et al., *Multiscale 3D Genome Rewiring during Mouse Neural Development.* Cell, 2017. **171**(3): p. 557-572 e24.

58. De Cecco, M., et al., *Genomes of replicatively senescent cells undergo global epigenetic changes leading to gene silencing and activation of transposable elements.* Aging Cell, 2013. **12**(2): p. 247-56.
59. Criscione, S.W., Y.V. Teo, and N. Neretti, *The Chromatin Landscape of Cellular Senescence.* Trends Genet, 2016. **32**(11): p. 751-761.
60. McCord, R.P., et al., *Correlated alterations in genome organization, histone methylation, and DNA-lamin A/C interactions in Hutchinson-Gilford progeria syndrome.* Genome Res, 2013. **23**(2): p. 260-9.
61. Scaffidi, P. and T. Misteli, *Lamin A-dependent nuclear defects in human aging.* Science, 2006. **312**(5776): p. 1059-63.
62. Criscione, S.W., et al., *Reorganization of chromosome architecture in replicative cellular senescence.* Sci Adv, 2016. **2**(2): p. e1500882.
63. Wang, G.G., C.D. Allis, and P. Chi, *Chromatin remodeling and cancer, Part II: ATP-dependent chromatin remodeling.* Trends Mol Med, 2007. **13**(9): p. 373-80.
64. Teif, V.B. and K. Rippe, *Predicting nucleosome positions on the DNA: combining intrinsic sequence preferences and remodeler activities.* Nucleic Acids Res, 2009. **37**(17): p. 5641-55.
65. Vaquero, A., A. Loyola, and D. Reinberg, *The constantly changing face of chromatin.* Sci Aging Knowledge Environ, 2003. **2003**(14): p. RE4.
66. Clapier, C.R. and B.R. Cairns, *The biology of chromatin remodeling complexes.* Annu Rev Biochem, 2009. **78**: p. 273-304.
67. Dang, W., et al., *Inactivation of yeast Isw2 chromatin remodeling enzyme mimics longevity effect of calorie restriction via induction of genotoxic stress response.* Cell Metab, 2014. **19**(6): p. 952-66.
68. Matilainen, O., et al., *The chromatin remodeling factor ISW-1 integrates organismal responses against nuclear and mitochondrial stress.* Nat Commun, 2017. **8**(1): p. 1818.
69. Riedel, C.G., et al., *DAF-16 employs the chromatin remodeller SWI/SNF to promote stress resistance and longevity.* Nat Cell Biol, 2013. **15**(5): p. 491-501.
70. Wu, S., et al., *BRG1, the ATPase subunit of SWI/SNF chromatin remodeling complex, interacts with HDAC2 to modulate telomerase expression in human cancer cells.* Cell Cycle, 2014. **13**(18): p. 2869-78.
71. Wu, S., et al., *BRM-SWI/SNF chromatin remodeling complex enables functional telomeres by promoting co-expression of TRF2 and TRF1.* PLoS Genet, 2020. **16**(6): p. e1008799.
72. Oudet, P., M. Gross-Bellard, and P. Chambon, *Electron microscopic and biochemical evidence that chromatin structure is a repeating unit.* Cell, 1975. **4**(4): p. 281-300.
73. Bentley, G.A., et al., *Crystal structure of the nucleosome core particle at 16 A resolution.* J Mol Biol, 1984. **176**(1): p. 55-75.
74. Kornberg, R.D. and J.O. Thomas, *Chromatin structure; oligomers of the histones.* Science, 1974. **184**(4139): p. 865-8.
75. Allan, J., et al., *The structure of histone H1 and its location in chromatin.* Nature, 1980. **288**(5792): p. 675-9.
76. Luger, K., et al., *Crystal structure of the nucleosome core particle at 2.8 A resolution.* Nature, 1997. **389**(6648): p. 251-60.
77. Alfageme, C.R., et al., *Histones of Drosophila embryos. Electrophoretic isolation and structural studies.* J Biol Chem, 1974. **249**(12): p. 3729-36.

78. Hong, L., et al., *Studies of the DNA binding properties of histone H4 amino terminus. Thermal denaturation studies reveal that acetylation markedly reduces the binding constant of the H4 "tail" to DNA.* J Biol Chem, 1993. **268**(1): p. 305-14.
79. Allfrey, V.G., R. Faulkner, and A.E. Mirsky, *Acetylation and Methylation of Histones and Their Possible Role in the Regulation of Rna Synthesis.* Proc Natl Acad Sci U S A, 1964. **51**: p. 786-94.
80. Sealy, L. and R. Chalkley, *DNA associated with hyperacetylated histone is preferentially digested by DNase I.* Nucleic Acids Res, 1978. **5**(6): p. 1863-76.
81. Vidali, G., et al., *Butyrate suppression of histone deacetylation leads to accumulation of multiacetylated forms of histones H3 and H4 and increased DNase I sensitivity of the associated DNA sequences.* Proc Natl Acad Sci U S A, 1978. **75**(5): p. 2239-43.
82. Shogren-Knaak, M., et al., *Histone H4-K16 acetylation controls chromatin structure and protein interactions.* Science, 2006. **311**(5762): p. 844-7.
83. Akhtar, A. and P.B. Becker, *Activation of transcription through histone H4 acetylation by MOF, an acetyltransferase essential for dosage compensation in Drosophila.* Mol Cell, 2000. **5**(2): p. 367-75.
84. Utley, R.T., et al., *Transcriptional activators direct histone acetyltransferase complexes to nucleosomes.* Nature, 1998. **394**(6692): p. 498-502.
85. Dawson, M.A. and T. Kouzarides, *Cancer epigenetics: from mechanism to therapy.* Cell, 2012. **150**(1): p. 12-27.
86. Graff, J. and L.H. Tsai, *Histone acetylation: molecular mnemonics on the chromatin.* Nat Rev Neurosci, 2013. **14**(2): p. 97-111.
87. Benayoun, B.A., E.A. Pollina, and A. Brunet, *Epigenetic regulation of ageing: linking environmental inputs to genomic stability.* Nat Rev Mol Cell Biol, 2015. **16**(10): p. 593-610.
88. Creyghton, M.P., et al., *Histone H3K27ac separates active from poised enhancers and predicts developmental state.* Proc Natl Acad Sci U S A, 2010. **107**(50): p. 21931-6.
89. Ernst, J., et al., *Mapping and analysis of chromatin state dynamics in nine human cell types.* Nature, 2011. **473**(7345): p. 43-9.
90. Adelman, E.R., et al., *Aging Human Hematopoietic Stem Cells Manifest Profound Epigenetic Reprogramming of Enhancers That May Predispose to Leukemia.* Cancer Discov, 2019. **9**(8): p. 1080-1101.
91. Cheng, Y., et al., *Targeting epigenetic regulators for cancer therapy: mechanisms and advances in clinical trials.* Signal Transduct Target Ther, 2019. **4**: p. 62.
92. Bannister, A.J., et al., *Spatial distribution of di- and tri-methyl lysine 36 of histone H3 at active genes.* J Biol Chem, 2005. **280**(18): p. 17732-6.
93. Wang, Z., et al., *Combinatorial patterns of histone acetylations and methylations in the human genome.* Nat Genet, 2008. **40**(7): p. 897-903.
94. Heintzman, N.D., et al., *Distinct and predictive chromatin signatures of transcriptional promoters and enhancers in the human genome.* Nat Genet, 2007. **39**(3): p. 311-8.
95. Barski, A., et al., *High-resolution profiling of histone methylations in the human genome.* Cell, 2007. **129**(4): p. 823-37.
96. Bernstein, B.E., et al., *Methylation of histone H3 Lys 4 in coding regions of active genes.* Proc Natl Acad Sci U S A, 2002. **99**(13): p. 8695-700.
97. Bernstein, B.E., et al., *Genomic maps and comparative analysis of histone modifications in human and mouse.* Cell, 2005. **120**(2): p. 169-81.

98. Peters, A.H., et al., *Partitioning and plasticity of repressive histone methylation states in mammalian chromatin.* Mol Cell, 2003. **12**(6): p. 1577-89.
99. Rice, J.C., et al., *Histone methyltransferases direct different degrees of methylation to define distinct chromatin domains.* Mol Cell, 2003. **12**(6): p. 1591-8.
100. Rea, S., et al., *Regulation of chromatin structure by site-specific histone H3 methyltransferases.* Nature, 2000. **406**(6796): p. 593-9.
101. Trojer, P. and D. Reinberg, *Facultative heterochromatin: is there a distinctive molecular signature?* Mol Cell, 2007. **28**(1): p. 1-13.
102. Strahl, B.D. and C.D. Allis, *The language of covalent histone modifications.* Nature, 2000. **403**(6765): p. 41-5.
103. Greer, E.L. and Y. Shi, *Histone methylation: a dynamic mark in health, disease and inheritance.* Nat Rev Genet, 2012. **13**(5): p. 343-57.
104. Cao, R., et al., *Role of histone H3 lysine 27 methylation in Polycomb-group silencing.* Science, 2002. **298**(5595): p. 1039-43.
105. Muller, J., et al., *Histone methyltransferase activity of a Drosophila Polycomb group repressor complex.* Cell, 2002. **111**(2): p. 197-208.
106. Czermin, B., et al., *Drosophila enhancer of Zeste/ESC complexes have a histone H3 methyltransferase activity that marks chromosomal Polycomb sites.* Cell, 2002. **111**(2): p. 185-96.
107. Margueron, R., et al., *Ezh1 and Ezh2 maintain repressive chromatin through different mechanisms.* Mol Cell, 2008. **32**(4): p. 503-18.
108. Lee, C.H., et al., *Distinct Stimulatory Mechanisms Regulate the Catalytic Activity of Polycomb Repressive Complex 2.* Mol Cell, 2018. **70**(3): p. 435-448 e5.
109. Wu, H., et al., *Structure of the catalytic domain of EZH2 reveals conformational plasticity in cofactor and substrate binding sites and explains oncogenic mutations.* PLoS One, 2013. **8**(12): p. e83737.
110. Antonysamy, S., et al., *Structural context of disease-associated mutations and putative mechanism of autoinhibition revealed by X-ray crystallographic analysis of the EZH2-SET domain.* PLoS One, 2013. **8**(12): p. e84147.
111. Jiao, L. and X. Liu, *Structural basis of histone H3K27 trimethylation by an active polycomb repressive complex 2.* Science, 2015. **350**(6258): p. aac4383.
112. Poepsel, S., V. Kasinath, and E. Nogales, *Cryo-EM structures of PRC2 simultaneously engaged with two functionally distinct nucleosomes.* Nat Struct Mol Biol, 2018. **25**(2): p. 154-162.
113. Oksuz, O., et al., *Capturing the Onset of PRC2-Mediated Repressive Domain Formation.* Mol Cell, 2018. **70**(6): p. 1149-1162 e5.
114. Margueron, R., et al., *Role of the polycomb protein EED in the propagation of repressive histone marks.* Nature, 2009. **461**(7265): p. 762-7.
115. Hojfeldt, J.W., et al., *Accurate H3K27 methylation can be established de novo by SUZ12-directed PRC2.* Nat Struct Mol Biol, 2018. **25**(3): p. 225-232.
116. Nekrasov, M., B. Wild, and J. Muller, *Nucleosome binding and histone methyltransferase activity of Drosophila PRC2.* EMBO Rep, 2005. **6**(4): p. 348-53.
117. Cao, R. and Y. Zhang, *SUZ12 is required for both the histone methyltransferase activity and the silencing function of the EED-EZH2 complex.* Mol Cell, 2004. **15**(1): p. 57-67.
118. Blackledge, N.P., et al., *PRC1 Catalytic Activity Is Central to Polycomb System Function.* Mol Cell, 2020. **77**(4): p. 857-874 e9.

119. Blackledge, N.P., et al., *Variant PRC1 complex-dependent H2A ubiquitylation drives PRC2 recruitment and polycomb domain formation.* Cell, 2014. **157**(6): p. 1445-1459.
120. Fursova, N.A., et al., *Synergy between Variant PRC1 Complexes Defines Polycomb-Mediated Gene Repression.* Mol Cell, 2019. **74**(5): p. 1020-1036 e8.
121. Rose, N.R., et al., *RYBP stimulates PRC1 to shape chromatin-based communication between Polycomb repressive complexes.* Elife, 2016. **5**.
122. Geng, Z. and Z. Gao, *Mammalian PRC1 Complexes: Compositional Complexity and Diverse Molecular Mechanisms.* Int J Mol Sci, 2020. **21**(22).
123. Ma, Z., et al., *Epigenetic drift of H3K27me3 in aging links glycolysis to healthy longevity in Drosophila.* Elife, 2018. **7**.
124. Baumgart, M., et al., *RNA-seq of the aging brain in the short-lived fish N. furzeri - conserved pathways and novel genes associated with neurogenesis.* Aging Cell, 2014. **13**(6): p. 965-74.
125. Liu, L., et al., *Chromatin modifications as determinants of muscle stem cell quiescence and chronological aging.* Cell Rep, 2013. **4**(1): p. 189-204.
126. Jin, C., et al., *Histone demethylase UTX-1 regulates C. elegans life span by targeting the insulin/IGF-1 signaling pathway.* Cell Metab, 2011. **14**(2): p. 161-72.
127. Ni, Z., et al., *Two SET domain containing genes link epigenetic changes and aging in Caenorhabditis elegans.* Aging Cell, 2012. **11**(2): p. 315-25.
128. Richards, E.J. and S.C. Elgin, *Epigenetic codes for heterochromatin formation and silencing: rounding up the usual suspects.* Cell, 2002. **108**(4): p. 489-500.
129. Karimi, M.M., et al., *DNA methylation and SETDB1/H3K9me3 regulate predominantly distinct sets of genes, retroelements, and chimeric transcripts in mESCs.* Cell Stem Cell, 2011. **8**(6): p. 676-87.
130. Klenov, M.S., et al., *Separation of stem cell maintenance and transposon silencing functions of Piwi protein.* Proc Natl Acad Sci U S A, 2011. **108**(46): p. 18760-5.
131. Le Thomas, A., et al., *Piwi induces piRNA-guided transcriptional silencing and establishment of a repressive chromatin state.* Genes Dev, 2013. **27**(4): p. 390-9.
132. Matsui, T., et al., *Proviral silencing in embryonic stem cells requires the histone methyltransferase ESET.* Nature, 2010. **464**(7290): p. 927-31.
133. Mikkelsen, T.S., et al., *Genome-wide maps of chromatin state in pluripotent and lineage-committed cells.* Nature, 2007. **448**(7153): p. 553-60.
134. Riddle, N.C., et al., *Plasticity in patterns of histone modifications and chromosomal proteins in Drosophila heterochromatin.* Genome Res, 2011. **21**(2): p. 147-63.
135. Sienski, G., D. Donertas, and J. Brennecke, *Transcriptional silencing of transposons by Piwi and maelstrom and its impact on chromatin state and gene expression.* Cell, 2012. **151**(5): p. 964-80.
136. Frapporti, A., et al., *The Polycomb protein Ezl1 mediates H3K9 and H3K27 methylation to repress transposable elements in Paramecium.* Nat Commun, 2019. **10**(1): p. 2710.
137. Bulut-Karslioglu, A., et al., *Suv39h-dependent H3K9me3 marks intact retrotransposons and silences LINE elements in mouse embryonic stem cells.* Mol Cell, 2014. **55**(2): p. 277-90.
138. Schultz, D.C., et al., *SETDB1: a novel KAP-1-associated histone H3, lysine 9-specific methyltransferase that contributes to HP1-mediated silencing of euchromatic genes by KRAB zinc-finger proteins.* Genes Dev, 2002. **16**(8): p. 919-32.

139. Bannister, A.J., et al., *Selective recognition of methylated lysine 9 on histone H3 by the HP1 chromo domain.* Nature, 2001. **410**(6824): p. 120-4.
140. Lorbeck, M.T., et al., *The histone demethylase Dmel\Kdm4A controls genes required for life span and male-specific sex determination in Drosophila.* Gene, 2010. **450**(1-2): p. 8-17.
141. Djeghloul, D., et al., *Age-Associated Decrease of the Histone Methyltransferase SUV39H1 in HSC Perturbs Heterochromatin and B Lymphoid Differentiation.* Stem Cell Reports, 2016. **6**(6): p. 970-984.
142. Shilatifard, A., *The COMPASS family of histone H3K4 methylases: mechanisms of regulation in development and disease pathogenesis.* Annu Rev Biochem, 2012. **81**: p. 65-95.
143. Miller, T., et al., *COMPASS: a complex of proteins associated with a trithorax-related SET domain protein.* Proc Natl Acad Sci U S A, 2001. **98**(23): p. 12902-7.
144. Mohan, M., et al., *The COMPASS family of H3K4 methylases in Drosophila.* Mol Cell Biol, 2011. **31**(21): p. 4310-8.
145. Greer, E.L., et al., *Members of the H3K4 trimethylation complex regulate lifespan in a germline-dependent manner in C. elegans.* Nature, 2010. **466**(7304): p. 383-7.
146. Li, L., et al., *Essential functions of the histone demethylase lid.* PLoS Genet, 2010. **6**(11): p. e1001221.
147. Sims, R.J., 3rd, et al., *Human but not yeast CHD1 binds directly and selectively to histone H3 methylated at lysine 4 via its tandem chromodomains.* J Biol Chem, 2005. **280**(51): p. 41789-92.
148. Wysocka, J., et al., *A PHD finger of NURF couples histone H3 lysine 4 trimethylation with chromatin remodelling.* Nature, 2006. **442**(7098): p. 86-90.
149. Vermeulen, M., et al., *Selective anchoring of TFIID to nucleosomes by trimethylation of histone H3 lysine 4.* Cell, 2007. **131**(1): p. 58-69.
150. Bian, C., et al., *Sgf29 binds histone H3K4me2/3 and is required for SAGA complex recruitment and histone H3 acetylation.* EMBO J, 2011. **30**(14): p. 2829-42.
151. Zhang, X., et al., *ING4 induces G2/M cell cycle arrest and enhances the chemosensitivity to DNA-damage agents in HepG2 cells.* FEBS Lett, 2004. **570**(1-3): p. 7-12.
152. Xu, C., et al., *The structural basis for selective binding of non-methylated CpG islands by the CFP1 CXXC domain.* Nat Commun, 2011. **2**: p. 227.
153. Coda, D.M., et al., *SMYD1 and G6PD modulation are critical events for miR-206-mediated differentiation of rhabdomyosarcoma.* Cell Cycle, 2015. **14**(9): p. 1389-402.
154. Yuan, H., et al., *Overexpression of SPINDLIN1 induces cellular senescence, multinucleation and apoptosis.* Gene, 2008. **410**(1): p. 67-74.
155. Wang, Z., et al., *PHF23 (plant homeodomain finger protein 23) negatively regulates cell autophagy by promoting ubiquitination and degradation of E3 ligase LRSAM1.* Autophagy, 2014. **10**(12): p. 2158-70.
156. Chi, P., C.D. Allis, and G.G. Wang, *Covalent histone modifications--miswritten, misinterpreted and mis-erased in human cancers.* Nat Rev Cancer, 2010. **10**(7): p. 457-69.
157. Vakoc, C.R., et al., *Histone H3 lysine 9 methylation and HP1gamma are associated with transcription elongation through mammalian chromatin.* Mol Cell, 2005. **19**(3): p. 381-91.

158. Feldman, N., et al., *G9a-mediated irreversible epigenetic inactivation of Oct-3/4 during early embryogenesis.* Nat Cell Biol, 2006. **8**(2): p. 188-94.
159. Ren, C., et al., *Small-molecule modulators of methyl-lysine binding for the CBX7 chromodomain.* Chem Biol, 2015. **22**(2): p. 161-8.
160. Bierne, H., et al., *Human BAHD1 promotes heterochromatic gene silencing.* Proc Natl Acad Sci U S A, 2009. **106**(33): p. 13826-31.
161. Garcia-Carpizo, V., et al., *NSD2 contributes to oncogenic RAS-driven transcription in lung cancer cells through long-range epigenetic activation.* Sci Rep, 2016. **6**: p. 32952.
162. Dhayalan, A., et al., *The Dnmt3a PWWP domain reads histone 3 lysine 36 trimethylation and guides DNA methylation.* J Biol Chem, 2010. **285**(34): p. 26114-20.
163. Pfister, S.X., et al., *SETD2-dependent histone H3K36 trimethylation is required for homologous recombination repair and genome stability.* Cell Rep, 2014. **7**(6): p. 2006-18.
164. Fnu, S., et al., *Methylation of histone H3 lysine 36 enhances DNA repair by nonhomologous end-joining.* Proc Natl Acad Sci U S A, 2011. **108**(2): p. 540-5.
165. Luco, R.F., et al., *Regulation of alternative splicing by histone modifications.* Science, 2010. **327**(5968): p. 996-1000.
166. Guo, R., et al., *BS69/ZMYND11 reads and connects histone H3.3 lysine 36 trimethylation-decorated chromatin to regulated pre-mRNA processing.* Mol Cell, 2014. **56**(2): p. 298-310.
167. Huyen, Y., et al., *Methylated lysine 79 of histone H3 targets 53BP1 to DNA double-strand breaks.* Nature, 2004. **432**(7015): p. 406-11.
168. Botuyan, M.V., et al., *Structural basis for the methylation state-specific recognition of histone H4-K20 by 53BP1 and Crb2 in DNA repair.* Cell, 2006. **127**(7): p. 1361-73.
169. Boccuni, P., et al., *The human L(3)MBT polycomb group protein is a transcriptional repressor and interacts physically and functionally with TEL (ETV6).* J Biol Chem, 2003. **278**(17): p. 15412-20.
170. Kuo, A.J., et al., *The BAH domain of ORC1 links H4K20me2 to DNA replication licensing and Meier-Gorlin syndrome.* Nature, 2012. **484**(7392): p. 115-9.
171. Beck, D.B., et al., *The role of PR-Set7 in replication licensing depends on Suv4-20h.* Genes Dev, 2012. **26**(23): p. 2580-9.
172. Wang, Y., et al., *Regulation of Set9-mediated H4K20 methylation by a PWWP domain protein.* Mol Cell, 2009. **33**(4): p. 428-37.
173. Xu, Y., et al., *WERAM: a database of writers, erasers and readers of histone acetylation and methylation in eukaryotes.* Nucleic Acids Res, 2017. **45**(D1): p. D264-D270.
174. Marmorstein, R. and M.M. Zhou, *Writers and readers of histone acetylation: structure, mechanism, and inhibition.* Cold Spring Harb Perspect Biol, 2014. **6**(7): p. a018762.
175. Dhalluin, C., et al., *Structure and ligand of a histone acetyltransferase bromodomain.* Nature, 1999. **399**(6735): p. 491-6.
176. Lange, M., et al., *Regulation of muscle development by DPF3, a novel histone acetylation and methylation reader of the BAF chromatin remodeling complex.* Genes Dev, 2008. **22**(17): p. 2370-84.
177. Zeng, L., et al., *Mechanism and regulation of acetylated histone binding by the tandem PHD finger of DPF3b.* Nature, 2010. **466**(7303): p. 258-62.

178. Robertson, K.D., *DNA methylation and human disease.* Nat Rev Genet, 2005. **6**(8): p. 597-610.
179. Lister, R., et al., *Human DNA methylomes at base resolution show widespread epigenomic differences.* Nature, 2009. **462**(7271): p. 315-22.
180. Wilson, V.L., et al., *Genomic 5-methyldeoxycytidine decreases with age.* J Biol Chem, 1987. **262**(21): p. 9948-51.
181. Berdyshev, G.D., et al., *[Nucleotide composition of DNA and RNA from somatic tissues of humpback and its changes during spawning].* Biokhimiia, 1967. **32**(5): p. 988-93.
182. Romanov, G.A. and B.F. Vanyushin, *Methylation of reiterated sequences in mammalian DNAs. Effects of the tissue type, age, malignancy and hormonal induction.* Biochim Biophys Acta, 1981. **653**(2): p. 204-18.
183. Bjornsson, H.T., et al., *Intra-individual change over time in DNA methylation with familial clustering.* JAMA, 2008. **299**(24): p. 2877-83.
184. Heyn, H., et al., *Distinct DNA methylomes of newborns and centenarians.* Proc Natl Acad Sci U S A, 2012. **109**(26): p. 10522-7.
185. Issa, J.P., et al., *Methylation of the oestrogen receptor CpG island links ageing and neoplasia in human colon.* Nat Genet, 1994. **7**(4): p. 536-40.
186. Horvath, S., *DNA methylation age of human tissues and cell types.* Genome Biol, 2013. **14**(10): p. R115.
187. Weidner, C.I., et al., *Aging of blood can be tracked by DNA methylation changes at just three CpG sites.* Genome Biol, 2014. **15**(2): p. R24.
188. Balch, W.E., et al., *Adapting proteostasis for disease intervention.* Science, 2008. **319**(5865): p. 916-9.
189. Powers, E.T., et al., *Biological and chemical approaches to diseases of proteostasis deficiency.* Annu Rev Biochem, 2009. **78**: p. 959-91.
190. Walker, G.A. and G.J. Lithgow, *Lifespan extension in C. elegans by a molecular chaperone dependent upon insulin-like signals.* Aging Cell, 2003. **2**(2): p. 131-9.
191. Tatar, M., A.A. Khazaeli, and J.W. Curtsinger, *Chaperoning extended life.* Nature, 1997. **390**(6655): p. 30.
192. Swindell, W.R., et al., *Endocrine regulation of heat shock protein mRNA levels in long-lived dwarf mice.* Mech Ageing Dev, 2009. **130**(6): p. 393-400.
193. Min, J.N., et al., *CHIP deficiency decreases longevity, with accelerated aging phenotypes accompanied by altered protein quality control.* Mol Cell Biol, 2008. **28**(12): p. 4018-25.
194. Klionsky, D.J., *Autophagy revisited: a conversation with Christian de Duve.* Autophagy, 2008. **4**(6): p. 740-3.
195. Mizushima, N. and M. Komatsu, *Autophagy: renovation of cells and tissues.* Cell, 2011. **147**(4): p. 728-41.
196. Kobayashi, S., *Choose Delicately and Reuse Adequately: The Newly Revealed Process of Autophagy.* Biol Pharm Bull, 2015. **38**(8): p. 1098-103.
197. Matecic, M., et al., *A microarray-based genetic screen for yeast chronological aging factors.* PLoS Genet, 2010. **6**(4): p. e1000921.
198. Lee, J.H., et al., *Sestrin as a feedback inhibitor of TOR that prevents age-related pathologies.* Science, 2010. **327**(5970): p. 1223-8.
199. Toth, M.L., et al., *Longevity pathways converge on autophagy genes to regulate life span in Caenorhabditis elegans.* Autophagy, 2008. **4**(3): p. 330-8.

200. Simonsen, A., et al., *Promoting basal levels of autophagy in the nervous system enhances longevity and oxidant resistance in adult Drosophila.* Autophagy, 2008. **4**(2): p. 176-84.
201. Dwivedi, M., H.O. Song, and J. Ahnn, *Autophagy genes mediate the effect of calcineurin on life span in C. elegans.* Autophagy, 2009. **5**(5): p. 604-7.
202. Mathew, R., et al., *Autophagy suppresses tumorigenesis through elimination of p62.* Cell, 2009. **137**(6): p. 1062-75.
203. Komatsu, M., et al., *The selective autophagy substrate p62 activates the stress responsive transcription factor Nrf2 through inactivation of Keap1.* Nat Cell Biol, 2010. **12**(3): p. 213-23.
204. Singh, R., et al., *Autophagy regulates lipid metabolism.* Nature, 2009. **458**(7242): p. 1131-5.
205. Hartleben, B., et al., *Autophagy influences glomerular disease susceptibility and maintains podocyte homeostasis in aging mice.* J Clin Invest, 2010. **120**(4): p. 1084-96.
206. Zhang, C. and A.M. Cuervo, *Restoration of chaperone-mediated autophagy in aging liver improves cellular maintenance and hepatic function.* Nat Med, 2008. **14**(9): p. 959-65.
207. Inuzuka, Y., et al., *Suppression of phosphoinositide 3-kinase prevents cardiac aging in mice.* Circulation, 2009. **120**(17): p. 1695-703.
208. Tonoki, A., et al., *Genetic evidence linking age-dependent attenuation of the 26S proteasome with the aging process.* Mol Cell Biol, 2009. **29**(4): p. 1095-106.
209. Dahlmann, B., *Role of proteasomes in disease.* BMC Biochem, 2007. **8 Suppl 1**: p. S3.
210. Gaczynska, M., P.A. Osmulski, and W.F. Ward, *Caretaker or undertaker? The role of the proteasome in aging.* Mech Ageing Dev, 2001. **122**(3): p. 235-54.
211. Chondrogianni, N. and E.S. Gonos, *Proteasome dysfunction in mammalian aging: steps and factors involved.* Exp Gerontol, 2005. **40**(12): p. 931-8.
212. Sun, N., R.J. Youle, and T. Finkel, *The Mitochondrial Basis of Aging.* Mol Cell, 2016. **61**(5): p. 654-666.
213. Rockstein, M. and K.F. Brandt, *Enzyme changes in flight muscle correlated with aging and flight ability in the male housefly.* Science, 1963. **139**(3559): p. 1049-51.
214. Piko, L., A.J. Hougham, and K.J. Bulpitt, *Studies of sequence heterogeneity of mitochondrial DNA from rat and mouse tissues: evidence for an increased frequency of deletions/additions with aging.* Mech Ageing Dev, 1988. **43**(3): p. 279-93.
215. Trifunovic, A., et al., *Premature ageing in mice expressing defective mitochondrial DNA polymerase.* Nature, 2004. **429**(6990): p. 417-23.
216. Kujoth, G.C., et al., *Mitochondrial DNA mutations, oxidative stress, and apoptosis in mammalian aging.* Science, 2005. **309**(5733): p. 481-4.
217. Cortopassi, G.A. and N. Arnheim, *Detection of a specific mitochondrial DNA deletion in tissues of older humans.* Nucleic Acids Res, 1990. **18**(23): p. 6927-33.
218. Kuilman, T., et al., *The essence of senescence.* Genes Dev, 2010. **24**(22): p. 2463-79.
219. Campisi, J. and F. d'Adda di Fagagna, *Cellular senescence: when bad things happen to good cells.* Nat Rev Mol Cell Biol, 2007. **8**(9): p. 729-40.
220. Collado, M., M.A. Blasco, and M. Serrano, *Cellular senescence in cancer and aging.* Cell, 2007. **130**(2): p. 223-33.
221. Hayflick, L. and P.S. Moorhead, *The serial cultivation of human diploid cell strains.* Exp Cell Res, 1961. **25**: p. 585-621.

222. Hayflick, L., *The Limited in Vitro Lifetime of Human Diploid Cell Strains.* Exp Cell Res, 1965. **37**: p. 614-36.
223. Baker, D.J., et al., *BubR1 insufficiency causes early onset of aging-associated phenotypes and infertility in mice.* Nat Genet, 2004. **36**(7): p. 744-9.
224. Baker, D.J., F. Jin, and J.M. van Deursen, *The yin and yang of the Cdkn2a locus in senescence and aging.* Cell Cycle, 2008. **7**(18): p. 2795-802.
225. Baker, D.J., et al., *Opposing roles for p16Ink4a and p19Arf in senescence and ageing caused by BubR1 insufficiency.* Nat Cell Biol, 2008. **10**(7): p. 825-36.
226. Matheu, A., et al., *Delayed ageing through damage protection by the Arf/p53 pathway.* Nature, 2007. **448**(7151): p. 375-9.
227. Matheu, A., et al., *Anti-aging activity of the Ink4/Arf locus.* Aging Cell, 2009. **8**(2): p. 152-61.
228. Rodier, F. and J. Campisi, *Four faces of cellular senescence.* J Cell Biol, 2011. **192**(4): p. 547-56.
229. Csiszar, A., et al., *Age-associated proinflammatory secretory phenotype in vascular smooth muscle cells from the non-human primate Macaca mulatta: reversal by resveratrol treatment.* J Gerontol A Biol Sci Med Sci, 2012. **67**(8): p. 811-20.
230. Efeyan, A., W.C. Comb, and D.M. Sabatini, *Nutrient-sensing mechanisms and pathways.* Nature, 2015. **517**(7534): p. 302-10.
231. Mico, V., et al., *NutrimiRAging: Micromanaging Nutrient Sensing Pathways through Nutrition to Promote Healthy Aging.* Int J Mol Sci, 2017. **18**(5).
232. Barzilai, N., et al., *The critical role of metabolic pathways in aging.* Diabetes, 2012. **61**(6): p. 1315-22.
233. Fontana, L., L. Partridge, and V.D. Longo, *Extending healthy life span--from yeast to humans.* Science, 2010. **328**(5976): p. 321-6.
234. Kenyon, C.J., *The genetics of ageing.* Nature, 2010. **464**(7288): p. 504-12.
235. Kenyon, C., et al., *A C. elegans mutant that lives twice as long as wild type.* Nature, 1993. **366**(6454): p. 461-4.
236. Kimura, K.D., et al., *daf-2, an insulin receptor-like gene that regulates longevity and diapause in Caenorhabditis elegans.* Science, 1997. **277**(5328): p. 942-6.
237. Tatar, M., et al., *A mutant Drosophila insulin receptor homolog that extends life-span and impairs neuroendocrine function.* Science, 2001. **292**(5514): p. 107-10.
238. Clancy, D.J., et al., *Extension of life-span by loss of CHICO, a Drosophila insulin receptor substrate protein.* Science, 2001. **292**(5514): p. 104-6.
239. Snell, G.D., *Dwarf, a New Mendelian Recessive Character of the House Mouse.* Proc Natl Acad Sci U S A, 1929. **15**(9): p. 733-4.
240. Berryman, D.E., et al., *Role of the GH/IGF-1 axis in lifespan and healthspan: lessons from animal models.* Growth Horm IGF Res, 2008. **18**(6): p. 455-71.
241. Flurkey, K., et al., *Lifespan extension and delayed immune and collagen aging in mutant mice with defects in growth hormone production.* Proc Natl Acad Sci U S A, 2001. **98**(12): p. 6736-41.
242. Brown-Borg, H.M., et al., *Dwarf mice and the ageing process.* Nature, 1996. **384**(6604): p. 33.
243. Sun, L.Y., et al., *Growth hormone-releasing hormone disruption extends lifespan and regulates response to caloric restriction in mice.* Elife, 2013. **2**: p. e01098.
244. Coschigano, K.T., et al., *Assessment of growth parameters and life span of GHR/BP gene-disrupted mice.* Endocrinology, 2000. **141**(7): p. 2608-13.

245. Houtkooper, R.H., R.W. Williams, and J. Auwerx, *Metabolic networks of longevity.* Cell, 2010. **142**(1): p. 9-14.
246. Laplante, M. and D.M. Sabatini, *mTOR signaling in growth control and disease.* Cell, 2012. **149**(2): p. 274-93.
247. Johnson, S.C., P.S. Rabinovitch, and M. Kaeberlein, *mTOR is a key modulator of ageing and age-related disease.* Nature, 2013. **493**(7432): p. 338-45.
248. Lamming, D.W., et al., *Rapamycin-induced insulin resistance is mediated by mTORC2 loss and uncoupled from longevity.* Science, 2012. **335**(6076): p. 1638-43.
249. Selman, C., et al., *Ribosomal protein S6 kinase 1 signaling regulates mammalian life span.* Science, 2009. **326**(5949): p. 140-4.
250. Harrison, D.E., et al., *Rapamycin fed late in life extends lifespan in genetically heterogeneous mice.* Nature, 2009. **460**(7253): p. 392-5.
251. Yang, S.B., et al., *Rapamycin ameliorates age-dependent obesity associated with increased mTOR signaling in hypothalamic POMC neurons.* Neuron, 2012. **75**(3): p. 425-36.
252. Alers, S., et al., *Role of AMPK-mTOR-Ulk1/2 in the regulation of autophagy: cross talk, shortcuts, and feedbacks.* Mol Cell Biol, 2012. **32**(1): p. 2-11.
253. Ulgherait, M., et al., *AMPK modulates tissue and organismal aging in a non-cell-autonomous manner.* Cell Rep, 2014. **8**(6): p. 1767-1780.
254. Apfeld, J., et al., *The AMP-activated protein kinase AAK-2 links energy levels and insulin-like signals to lifespan in C. elegans.* Genes Dev, 2004. **18**(24): p. 3004-9.
255. Dong, M.Q., et al., *Quantitative mass spectrometry identifies insulin signaling targets in C. elegans.* Science, 2007. **317**(5838): p. 660-3.
256. Mair, W., et al., *Lifespan extension induced by AMPK and calcineurin is mediated by CRTC-1 and CREB.* Nature, 2011. **470**(7334): p. 404-8.
257. Ning, Y.C., et al., *Short-term calorie restriction protects against renal senescence of aged rats by increasing autophagic activity and reducing oxidative damage.* Mech Ageing Dev, 2013. **134**(11-12): p. 570-9.
258. Klar, A.J., S. Fogel, and K. Macleod, *MAR1-a Regulator of the HMa and HMalpha Loci in SACCHAROMYCES CEREVISIAE.* Genetics, 1979. **93**(1): p. 37-50.
259. Vaquero, A., *The conserved role of sirtuins in chromatin regulation.* Int J Dev Biol, 2009. **53**(2-3): p. 303-22.
260. Michan, S. and D. Sinclair, *Sirtuins in mammals: insights into their biological function.* Biochem J, 2007. **404**(1): p. 1-13.
261. Kaeberlein, M., M. McVey, and L. Guarente, *The SIR2/3/4 complex and SIR2 alone promote longevity in Saccharomyces cerevisiae by two different mechanisms.* Genes Dev, 1999. **13**(19): p. 2570-80.
262. Rogina, B. and S.L. Helfand, *Sir2 mediates longevity in the fly through a pathway related to calorie restriction.* Proc Natl Acad Sci U S A, 2004. **101**(45): p. 15998-6003.
263. Tissenbaum, H.A. and L. Guarente, *Increased dosage of a sir-2 gene extends lifespan in Caenorhabditis elegans.* Nature, 2001. **410**(6825): p. 227-30.
264. Mostoslavsky, R., et al., *Genomic instability and aging-like phenotype in the absence of mammalian SIRT6.* Cell, 2006. **124**(2): p. 315-29.
265. Kanfi, Y., et al., *The sirtuin SIRT6 regulates lifespan in male mice.* Nature, 2012. **483**(7388): p. 218-21.
266. Price, N.L., et al., *SIRT1 is required for AMPK activation and the beneficial effects of resveratrol on mitochondrial function.* Cell Metab, 2012. **15**(5): p. 675-90.

267. Conboy, I.M. and T.A. Rando, *Heterochronic parabiosis for the study of the effects of aging on stem cells and their niches.* Cell Cycle, 2012. **11**(12): p. 2260-7.
268. Gruber, R., et al., *Fracture healing in the elderly patient.* Exp Gerontol, 2006. **41**(11): p. 1080-93.
269. Molofsky, A.V., et al., *Increasing p16INK4a expression decreases forebrain progenitors and neurogenesis during ageing.* Nature, 2006. **443**(7110): p. 448-52.
270. Schlessinger, D. and G. Van Zant, *Does functional depletion of stem cells drive aging?* Mech Ageing Dev, 2001. **122**(14): p. 1537-53.
271. Shaw, A.C., et al., *Aging of the innate immune system.* Curr Opin Immunol, 2010. **22**(4): p. 507-13.
272. Rossi, D.J., et al., *Deficiencies in DNA damage repair limit the function of haematopoietic stem cells with age.* Nature, 2007. **447**(7145): p. 725-9.
273. Janzen, V., et al., *Stem-cell ageing modified by the cyclin-dependent kinase inhibitor p16INK4a.* Nature, 2006. **443**(7110): p. 421-6.
274. Flores, I., M.L. Cayuela, and M.A. Blasco, *Effects of telomerase and telomere length on epidermal stem cell behavior.* Science, 2005. **309**(5738): p. 1253-6.
275. Sharpless, N.E. and R.A. DePinho, *How stem cells age and why this makes us grow old.* Nat Rev Mol Cell Biol, 2007. **8**(9): p. 703-13.
276. Rando, T.A. and H.Y. Chang, *Aging, rejuvenation, and epigenetic reprogramming: resetting the aging clock.* Cell, 2012. **148**(1-2): p. 46-57.
277. Russell, S.J. and C.R. Kahn, *Endocrine regulation of ageing.* Nat Rev Mol Cell Biol, 2007. **8**(9): p. 681-91.
278. Zhang, G., et al., *Hypothalamic programming of systemic ageing involving IKK-beta, NF-kappaB and GnRH.* Nature, 2013. **497**(7448): p. 211-6.
279. Franceschi, C., et al., *Inflammaging: a new immune-metabolic viewpoint for age-related diseases.* Nat Rev Endocrinol, 2018. **14**(10): p. 576-590.
280. Salminen, A., K. Kaarniranta, and A. Kauppinen, *Inflammaging: disturbed interplay between autophagy and inflammasomes.* Aging (Albany NY), 2012. **4**(3): p. 166-75.
281. Green, D.R., L. Galluzzi, and G. Kroemer, *Mitochondria and the autophagy-inflammation-cell death axis in organismal aging.* Science, 2011. **333**(6046): p. 1109-12.
282. Adler, A.S., et al., *Motif module map reveals enforcement of aging by continual NF-kappaB activity.* Genes Dev, 2007. **21**(24): p. 3244-57.
283. Osorio, F.G., et al., *Nuclear lamina defects cause ATM-dependent NF-kappaB activation and link accelerated aging to a systemic inflammatory response.* Genes Dev, 2012. **26**(20): p. 2311-24.
284. Tilstra, J.S., et al., *NF-kappaB inhibition delays DNA damage-induced senescence and aging in mice.* J Clin Invest, 2012. **122**(7): p. 2601-12.
285. Pont, A.R., et al., *mRNA decay factor AUF1 maintains normal aging, telomere maintenance, and suppression of senescence by activation of telomerase transcription.* Mol Cell, 2012. **47**(1): p. 5-15.
286. Xie, J., X. Zhang, and L. Zhang, *Negative regulation of inflammation by SIRT1.* Pharmacol Res, 2013. **67**(1): p. 60-7.
287. Gillum, M.P., et al., *SirT1 regulates adipose tissue inflammation.* Diabetes, 2011. **60**(12): p. 3235-45.
288. Kawahara, T.L., et al., *SIRT6 links histone H3 lysine 9 deacetylation to NF-kappaB-dependent gene expression and organismal life span.* Cell, 2009. **136**(1): p. 62-74.

289. Tabula Muris, C., *A single-cell transcriptomic atlas characterizes ageing tissues in the mouse.* Nature, 2020. **583**(7817): p. 590-595.
290. Schaum, N., et al., *Ageing hallmarks exhibit organ-specific temporal signatures.* Nature, 2020. **583**(7817): p. 596-602.
291. Tabula Muris, C., et al., *Single-cell transcriptomics of 20 mouse organs creates a Tabula Muris.* Nature, 2018. **562**(7727): p. 367-372.
292. Aging Atlas, C., *Aging Atlas: a multi-omics database for aging biology.* Nucleic Acids Res, 2021. **49**(D1): p. D825-D830.
293. Brink, T.C., et al., *Age-related transcriptional changes in gene expression in different organs of mice support the metabolic stability theory of aging.* Biogerontology, 2009. **10**(5): p. 549-64.
294. Zhuang, J., et al., *Comparison of multi-tissue aging between human and mouse.* Sci Rep, 2019. **9**(1): p. 6220.
295. Palliyaguru, D.L., et al., *Study of Longitudinal Aging in Mice: Presentation of Experimental Techniques.* J Gerontol A Biol Sci Med Sci, 2021. **76**(4): p. 552-560.
296. Tiniakos, D.G., A. Kandilis, and S.A. Geller, *Tityus: a forgotten myth of liver regeneration.* J Hepatol, 2010. **53**(2): p. 357-61.
297. Si-Tayeb, K., F.P. Lemaigre, and S.A. Duncan, *Organogenesis and development of the liver.* Dev Cell, 2010. **18**(2): p. 175-89.
298. Nemeth, E., A.W. Baird, and C. O'Farrelly, *Microanatomy of the liver immune system.* Semin Immunopathol, 2009. **31**(3): p. 333-43.
299. Dienes, H.P. and U. Drebber, *Pathology of immune-mediated liver injury.* Dig Dis, 2010. **28**(1): p. 57-62.
300. Higgins, G.a.R.A., *Experimental pathology of liver: restoration of liver in white rat following partial surgical removal* Arch Pathol, 1931.
301. Duncan, A.W., C. Dorrell, and M. Grompe, *Stem cells and liver regeneration.* Gastroenterology, 2009. **137**(2): p. 466-81.
302. RA., M., *"Lifespan" of Liver Cells: Autoradiographic Study Using Tritiated Thymidine in Normal, Cirrhotic, and Partially Hepatectomized Rats.* Arch Intern Med, 1961: p. 335–343.
303. Magami, Y., et al., *Cell proliferation and renewal of normal hepatocytes and bile duct cells in adult mouse liver.* Liver, 2002. **22**(5): p. 419-25.
304. Floreani, A., *Liver diseases in the elderly: an update.* Dig Dis, 2007. **25**(2): p. 138-43.
305. Amarapurkar, D., et al., *Prevalence of non-alcoholic fatty liver disease: population based study.* Ann Hepatol, 2007. **6**(3): p. 161-3.
306. Sheedfar, F., et al., *Liver diseases and aging: friends or foes?* Aging Cell, 2013. **12**(6): p. 950-4.
307. Schmucker, D.L., *Age-related changes in liver structure and function: Implications for disease ?* Exp Gerontol, 2005. **40**(8-9): p. 650-9.
308. Wynne, H.A., et al., *The effect of age upon liver volume and apparent liver blood flow in healthy man.* Hepatology, 1989. **9**(2): p. 297-301.
309. Iber, F.L., P.A. Murphy, and E.S. Connor, *Age-related changes in the gastrointestinal system. Effects on drug therapy.* Drugs Aging, 1994. **5**(1): p. 34-48.
310. Le Couteur, D.G. and A.J. McLean, *The aging liver. Drug clearance and an oxygen diffusion barrier hypothesis.* Clin Pharmacokinet, 1998. **34**(5): p. 359-73.
311. Zoli, M., et al., *Total and functional hepatic blood flow decrease in parallel with ageing.* Age Ageing, 1999. **28**(1): p. 29-33.

312. Wakabayashi, H., et al., *Evaluation of the effect of age on functioning hepatocyte mass and liver blood flow using liver scintigraphy in preoperative estimations for surgical patients: comparison with CT volumetry.* J Surg Res, 2002. **106**(2): p. 246-53.
313. Tietz, N.W., D.F. Shuey, and D.R. Wekstein, *Laboratory values in fit aging individuals--sexagenarians through centenarians.* Clin Chem, 1992. **38**(6): p. 1167-85.
314. Michalopoulos, G.K., *Hepatostat: Liver regeneration and normal liver tissue maintenance.* Hepatology, 2017. **65**(4): p. 1384-1392.
315. Timchenko, N.A., *Aging and liver regeneration.* Trends Endocrinol Metab, 2009. **20**(4): p. 171-6.
316. Cheng, Y., et al., *Aging-associated oxidative stress inhibits liver progenitor cell activation in mice.* Aging (Albany NY), 2017. **9**(5): p. 1359-1374.
317. Tsuchida, T. and S.L. Friedman, *Mechanisms of hepatic stellate cell activation.* Nat Rev Gastroenterol Hepatol, 2017. **14**(7): p. 397-411.
318. Maeso-Diaz, R., et al., *Effects of aging on liver microcirculatory function and sinusoidal phenotype.* Aging Cell, 2018. **17**(6): p. e12829.
319. Cogger, V.C., et al., *Hepatic sinusoidal pseudocapillarization with aging in the non-human primate.* Exp Gerontol, 2003. **38**(10): p. 1101-7.
320. Marcos, R., et al., *Stereological assessment of sexual dimorphism in the rat liver reveals differences in hepatocytes and Kupffer cells but not hepatic stellate cells.* J Anat, 2016. **228**(6): p. 996-1005.
321. Koliaki, C., et al., *Adaptation of hepatic mitochondrial function in humans with non-alcoholic fatty liver is lost in steatohepatitis.* Cell Metab, 2015. **21**(5): p. 739-46.
322. Cogger, V.C., et al., *Liver aging and pseudocapillarization in a Werner syndrome mouse model.* J Gerontol A Biol Sci Med Sci, 2014. **69**(9): p. 1076-86.
323. Hilmer, S.N., V.C. Cogger, and D.G. Le Couteur, *Basal activity of Kupffer cells increases with old age.* J Gerontol A Biol Sci Med Sci, 2007. **62**(9): p. 973-8.
324. Singh, P., et al., *Lymphoid neogenesis and immune infiltration in aged liver.* Hepatology, 2008. **47**(5): p. 1680-90.
325. Kudriavtsev BN, K.M., Sakuta GA, Shteĭn GI., *The kinetics of the cell population of human liver parenchyma at different periods of life (Kinetika kletochnoĭ populiatsii parenkhimy pecheni cheloveka v raznye periody ego zhizni).* Tsitologiia, 1991: p. 96-109.
326. Si-Tayeb, K., F.P. Lemaigre, and S.A. Duncan, *Organogenesis and development of the liver.* Developmental cell, 2010. **18**(2): p. 175-189.
327. Brodsky, W.Y. and I. Uryvaeva, *Cell polyploidy: its relation to tissue growth and function*, in *International review of cytology*. 1977, Elsevier. p. 275-332.
328. Carriere, R., *Polyploid cell reproduction in normal adult rat liver.* Experimental cell research, 1967. **46**(3): p. 533-540.
329. Nadal, C. and F. Zajdela, *Polyploidy in the rat liver. II. The role of the hypophysis and protein deficiency.* Experimental cell research, 1966. **42**(1): p. 117.
330. Nadal, C. and F. Zajdela, *Hepatic polyploidy in the rat. IV. Experimental changes in the nucleolar volume of liver cells and their mechanisms of regulation.* Experimental cell research, 1967. **48**(3): p. 518.
331. Anatskaya, O.V., A.E. Vinogradov, and B.N. Kudryavtsev, *Hepatocyte polyploidy and metabolism/life-history traits: hypotheses testing.* Journal of theoretical biology, 1994. **168**(2): p. 191-199.

332. Duncan, A.W., et al., *The ploidy conveyor of mature hepatocytes as a source of genetic variation.* Nature, 2010. **467**(7316): p. 707-710.
333. Gandillet, A., et al., *Hepatocyte ploidy in normal young rat.* Comparative Biochemistry and Physiology Part A: Molecular & Integrative Physiology, 2003. **134**(3): p. 665-673.
334. Pandit, S.K., et al., *E2F8 is essential for polyploidization in mammalian cells.* Nature cell biology, 2012. **14**(11): p. 1181-1191.
335. Duncan, A.W., et al., *Frequent aneuploidy among normal human hepatocytes.* Gastroenterology, 2012. **142**(1): p. 25-28.
336. Kudryavtsev, B., et al., *Human hepatocyte polyploidization kinetics in the course of life cycle.* Virchows Archiv B, 1993. **64**(1): p. 387.
337. Toyoda, H., et al., *Changes to hepatocyte ploidy and binuclearity profiles during human chronic viral hepatitis.* Gut, 2005. **54**(2): p. 297-302.
338. Toyoda, H., et al., *Conserved balance of hepatocyte nuclear DNA content in mononuclear and binuclear hepatocyte populations during the course of chronic viral hepatitis.* World Journal of Gastroenterology: WJG, 2006. **12**(28): p. 4546.
339. Gupta, S., *Hepatic polyploidy and liver growth control.* Semin Cancer Biol, 2000. **10**(3): p. 161-71.
340. Guidotti, J.E., et al., *Liver cell polyploidization: a pivotal role for binuclear hepatocytes.* J Biol Chem, 2003. **278**(21): p. 19095-101.
341. Viola-Magni, M.P., *Synthesis and turnover of DNA in hepatocytes of neonatal rats.* J Microsc, 1972. **96**(2): p. 191-203.
342. Wang, M.J., et al., *Reversal of hepatocyte senescence after continuous in vivo cell proliferation.* Hepatology, 2014. **60**(1): p. 349-61.
343. Duncan, A.W., et al., *The ploidy conveyor of mature hepatocytes as a source of genetic variation.* Nature, 2010. **467**(7316): p. 707-10.
344. *Global ageing statistics.*
345. *Why Population Aging Matters: A Global Perspective.* NATIONAL INSTITUTE ON AGING
NATIONAL INSTITUTES OF HEALTH
U.S. DEPARTMENT OF HEALTH AND HUMAN SERVICES
U.S. DEPARTMENT OF STATE, 2007.
346. Malato, Y., et al., *Fate tracing of mature hepatocytes in mouse liver homeostasis and regeneration.* J Clin Invest, 2011. **121**(12): p. 4850-60.
347. Macdonald, R.A., *"Lifespan" of liver cells. Autoradio-graphic study using tritiated thymidine in normal, cirrhotic, and partially hepatectomized rats.* Arch Intern Med, 1961. **107**: p. 335-43.
348. Wood, T.E., et al., *The frequency of polyploid speciation in vascular plants.* Proc Natl Acad Sci U S A, 2009. **106**(33): p. 13875-9.
349. Otto, S.P. and J. Whitton, *Polyploid incidence and evolution.* Annu Rev Genet, 2000. **34**: p. 401-437.
350. Clarke, J.T., G.T. Lloyd, and M. Friedman, *Little evidence for enhanced phenotypic evolution in early teleosts relative to their living fossil sister group.* Proc Natl Acad Sci U S A, 2016. **113**(41): p. 11531-11536.
351. Albertin, W. and P. Marullo, *Polyploidy in fungi: evolution after whole-genome duplication.* Proc Biol Sci, 2012. **279**(1738): p. 2497-509.

352. Hansen, M.T., *Multiplicity of genome equivalents in the radiation-resistant bacterium Micrococcus radiodurans.* J Bacteriol, 1978. **134**(1): p. 71-5.
353. Guc-Scekic, M., et al., *Tetraploidy in a 26-month-old girl (cytogenetic and molecular studies).* Clin Genet, 2002. **61**(1): p. 62-5.
354. Jacobs, P.A., et al., *Human triploidy: relationship between parental origin of the additional haploid complement and development of partial hydatidiform mole.* Ann Hum Genet, 1982. **46**(3): p. 223-31.
355. Wertheim, B., et al., *Polyploidy in Animals: Effects of Gene Expression on Sex Determination, Evolution and Ecology.* Cytogenetic and Genome Research, 2013. **140**(2-4): p. 256-269.
356. Anzi, S., et al., *Postnatal Exocrine Pancreas Growth by Cellular Hypertrophy Correlates with a Shorter Lifespan in Mammals.* Dev Cell, 2018. **45**(6): p. 726-737.e3.
357. Oates, P.S. and R.G. Morgan, *Changes in pancreatic acinar cell nuclear number and DNA content during aging in the rat.* Am J Anat, 1986. **177**(4): p. 547-54.
358. Davoli, T. and T. de Lange, *The causes and consequences of polyploidy in normal development and cancer.* Annu Rev Cell Dev Biol, 2011. **27**: p. 585-610.
359. Pandit, S.K., B. Westendorp, and A. de Bruin, *Physiological significance of polyploidization in mammalian cells.* Trends Cell Biol, 2013. **23**(11): p. 556-66.
360. Jones, K.R.J.L.J.M.Z.M.R., *Roads to polyploidy: The megakaryocyte example.* JOURNAL OF CELLULAR PHYSIOLOGY, 2002. **190** p. 7-20.
361. Donne, R., et al., *Polyploidy in liver development, homeostasis and disease.* Nat Rev Gastroenterol Hepatol, 2020. **17**(7): p. 391-405.
362. Abmayr, S.M. and G.K. Pavlath, *Myoblast fusion: lessons from flies and mice.* Development, 2012. **139**(4): p. 641-56.
363. Duelli, D. and Y. Lazebnik, *Cell-to-cell fusion as a link between viruses and cancer.* Nat Rev Cancer, 2007. **7**(12): p. 968-76.
364. Alvarez-Dolado, M., et al., *Fusion of bone-marrow-derived cells with Purkinje neurons, cardiomyocytes and hepatocytes.* Nature, 2003. **425**(6961): p. 968-73.
365. Rizvi, A.Z., et al., *Bone marrow-derived cells fuse with normal and transformed intestinal stem cells.* Proc Natl Acad Sci U S A, 2006. **103**(16): p. 6321-5.
366. Sanges, D., et al., *Wnt/beta-catenin signaling triggers neuron reprogramming and regeneration in the mouse retina.* Cell Rep, 2013. **4**(2): p. 271-86.
367. Wang, X., et al., *Cell fusion is the principal source of bone-marrow-derived hepatocytes.* Nature, 2003. **422**(6934): p. 897-901.
368. Weimann, J.M., et al., *Stable reprogrammed heterokaryons form spontaneously in Purkinje neurons after bone marrow transplant.* Nat Cell Biol, 2003. **5**(11): p. 959-66.
369. Lee, H.O., J.M. Davidson, and R.J. Duronio, *Endoreplication: polyploidy with purpose.* Genes Dev, 2009. **23**(21): p. 2461-77.
370. Fox, D.T. and R.J. Duronio, *Endoreplication and polyploidy: insights into development and disease.* Development, 2013. **140**(1): p. 3-12.
371. Edgar, B.A. and T.L. Orr-Weaver, *Endoreplication cell cycles: more for less.* Cell, 2001. **105**(3): p. 297-306.
372. Parisi T, B.A., Rougier N, McNeil T, Lucian L, Werb Z, Amati B, *Cyclins E1 and E2 are required for endoreplication in placental trophoblast giant cells.* EMBO J 2003. **2**(22): p. 4794-4803.

373. Zakir Ullah, M.J.K., Rieko Yagi, Lyubomir T. Vassilev, and Melvin L. DePamphilis, *Differentiation of trophoblast stem cells into giant cells is triggered by p57/Kip2 inhibition of CDK1 activity* Genes & Dev. , 2008. **22**: p. 3024-3036.
374. Celton-Morizur, S. and C. Desdouets, *Polyploidization of liver cells*, in *Polyploidization and cancer*. 2010, Springer. p. 123-135.
375. Fortier, M., S. Celton-Morizur, and C. Desdouets, *Incomplete cytokinesis/binucleation in mammals: The powerful system of hepatocytes*, in *Methods in cell biology*. 2017, Elsevier. p. 119-142.
376. Li, F., et al., *Formation of binucleated cardiac myocytes in rat heart: I. Role of actin–myosin contractile ring.* Journal of molecular and cellular cardiology, 1997. **29**(6): p. 1541-1551.
377. Zimmet, J. and K. Ravid, *Polyploidy: occurrence in nature, mechanisms, and significance for the megakaryocyte-platelet system.* Experimental hematology, 2000. **28**(1): p. 3-16.
378. Guidotti JE, B.O., Robert A, Debey P, Brechot C, Desdouets C., *Liver cell polyploidization: a pivotal role for binuclear hepatocytes.* J Biol Chem, 2003 **278**.
379. Lacroix, B. and A.S. Maddox, *Cytokinesis, ploidy and aneuploidy.* The Journal of pathology, 2012. **226**(2): p. 338-351.
380. Mullins, J. and J.J. Biesele, *Terminal phase of cytokinesis in D-98s cells.* The Journal of cell biology, 1977. **73**(3): p. 672-684.
381. Pandit, S.K., et al., *E2F8 is essential for polyploidization in mammalian cells.* Nat Cell Biol, 2012. **14**(11): p. 1181-91.
382. Hsu, S.H., et al., *MicroRNA-122 regulates polyploidization in the murine liver.* Hepatology, 2016. **64**(2): p. 599-615.
383. Margall-Ducos, G., et al., *Liver tetraploidization is controlled by a new process of incomplete cytokinesis.* J Cell Sci, 2007. **120**(Pt 20): p. 3633-9.
384. Wheatley, D.N., *Binucleation in mammalian liver. Studies on the control of cytokinesis in vivo.* Exp Cell Res, 1972. **74**(2): p. 455-65.
385. Girard, J., et al., *Adaptations of glucose and fatty acid metabolism during perinatal period and suckling-weaning transition.* Physiol Rev, 1992. **72**(2): p. 507-62.
386. Kurinna, S., *p53 regulates a mitotic transcription program and determines ploidy in normal mouse liver.* Hepatology, 2013. **57**.
387. Kudryavtsev, B.N., et al., *Human hepatocyte polyploidization kinetics in the course of life cycle.* Virchows Arch B Cell Pathol Incl Mol Pathol, 1993. **64**(6): p. 387-93.
388. Kurinna, S., et al., *p53 regulates a mitotic transcription program and determines ploidy in normal mouse liver.* Hepatology, 2013. **57**(5): p. 2004-13.
389. Mayhew, C.N., et al., *Liver-specific pRB loss results in ectopic cell cycle entry and aberrant ploidy.* Cancer Res, 2005. **65**(11): p. 4568-77.
390. Wang, M.J., et al., *Hepatocyte polyploidization and its association with pathophysiological processes.* Cell Death Dis, 2017. **8**(5): p. e2805.
391. Margall-Ducos, G., et al., *Liver tetraploidization is controlled by a new process of incomplete cytokinesis.* Journal of cell science, 2007. **120**(20): p. 3633-3639.
392. Germain Margall-Ducos, S.C.-M., Dominique Couton, Olivier Brégerie, Chantal Desdouets, *Liver tetraploidization is controlled by a new process of incomplete cytokinesis.* Journal of Cell Science, 2007 **120**: p. 3633-3639.
393. Celton-Morizur, S., et al., *Polyploidy and liver proliferation: central role of insulin signaling.* Cell Cycle, 2010. **9**(3): p. 460-6.

394. Celton-Morizur, S., et al., *Polyploidy and liver proliferation: central role of insulin signaling.* Cell Cycle, 2010. **9**.
395. Celton-Morizur, S., et al., *The insulin/Akt pathway controls a specific cell division program that leads to generation of binucleated tetraploid liver cells in rodents.* J Clin Invest, 2009. **119**(7): p. 1880-7.
396. Wullschleger, S., R. Loewith, and M.N. Hall, *TOR signaling in growth and metabolism.* Cell, 2006. **124**(3): p. 471-484.
397. Celton-Morizur, S., et al., *Polyploidy and liver proliferation: central role of insulin signaling.* Cell Cycle, 2010. **9**(3): p. 460-466.
398. Celton-Morizur, S., et al., *The insulin/Akt pathway controls a specific cell division program that leads to generation of binucleated tetraploid liver cells in rodents.* The Journal of clinical investigation, 2009. **119**(7): p. 1880-1887.
399. Chaussepied, M. and D. Ginsberg, *Transcriptional regulation of AKT activation by E2F.* Mol Cell, 2004. **16**(5): p. 831-7.
400. Li, J., et al., *Synergistic function of E2F7 and E2F8 is essential for cell survival and embryonic development.* Dev Cell, 2008. **14**(1): p. 62-75.
401. Lammens, T., et al., *Atypical E2Fs: new players in the E2F transcription factor family.* Trends Cell Biol, 2009. **19**(3): p. 111-8.
402. Chen, H.Z., et al., *Canonical and atypical E2Fs regulate the mammalian endocycle.* Nat Cell Biol, 2012. **14**(11): p. 1192-202.
403. Wilkinson, P.D., et al., *The Polyploid State Restricts Hepatocyte Proliferation and Liver Regeneration in Mice.* Hepatology, 2019. **69**(3): p. 1242-1258.
404. Wilkinson, P.D., *The polyploid state restricts hepatocyte proliferation and liver regeneration.* Hepatology, 2018. **69**.
405. Pandit, S.K., *E2F8 is essential for polyploidization in mammalian cells.* Nat. Cell Biol., 2012. **14**.
406. Chen, H.Z., *Canonical and atypical E2Fs regulate the mammalian endocycle.* Nat. Cell Biol., 2012. **14**.
407. Diril, M.K., *Cyclin-dependent kinase 1 (Cdk1) is essential for cell division and suppression of DNA re-replication but not for liver regeneration.* Proc. Natl Acad. Sci. USA, 2012. **109**.
408. Sheahan, S., et al., *Additive effect of p53, p21 and Rb deletion in triple knockout primary hepatocytes.* Oncogene, 2004. **23**.
409. Wu, H., *Targeted in vivo expression of the cyclin dependent kinase inhibitor p21 halts hepatocyte cell cycle progression, postnatal liver development and regeneration.* Genes Dev., 1996. **10**.
410. Baena, E., *c-Myc regulates cell size and ploidy but is not essential for postnatal proliferation in liver.* Proc. Natl Acad. Sci. USA, 2005. **102**.
411. Nevzorova, Y.A., *Aberrant cell cycle progression and endoreplication in regenerating livers of mice that lack a single E-type cyclin.* Gastroenterology, 2009. **137**.
412. Li, D., *Hepatic loss of survivin impairs postnatal liver development and promotes expansion of hepatic progenitor cells in mice.* Hepatology, 2013. **58**.
413. Kim, S.H., *Hepatocyte homeostasis for chromosome ploidization and liver function is regulated by Ssu72 protein phosphatase.* Hepatology, 2016. **63**.
414. Zhang, S., *Hippo signaling suppresses cell ploidy and tumorigenesis through skp2.* Cancer Cell, 2017. **31**.

415. Santis Puzzonia, M., *TGFβ induces binucleation/polyploidization in hepatocytes through a Src-dependent cytokinesis failure.* PLOS ONE, 2016. **11**.
416. Mayhew, C.N., *Liver-specific pRB loss results in ectopic cell cycle entry and aberrant ploidy.* Cancer Res., 2005. **65**.
417. Sladky, V.C., et al., *E2F-Family Members Engage the PIDDosome to Limit Hepatocyte Ploidy in Liver Development and Regeneration.* Dev Cell, 2020. **52**(3): p. 335-349 e7.
418. Hsu, S.H., *MicroRNA-122 regulates polyploidization in the murine liver.* Hepatology, 2016. **64**.
419. Anabel Fernández-Iglesias, D.H., Jordi Gracia-Sancho, *Chapter 9 -Oxidative Stress in Liver Diseases,.* Gastrointestinal Tissue, 2017: p. 125-140.
420. Klaunig JE, W.Z., Pu X, Zhou S, *Oxidative stress and oxidative damage in chemical carcinogenesis.* Toxicol Appl Pharmacol. , 2011 p. 86-99.
421. Cheng, K.C., et al., *8-Hydroxyguanine, an abundant form of oxidative DNA damage, causes G----T and A----C substitutions.* J Biol Chem, 1992. **267**(1): p. 166-72.
422. Olga V. Anatskaya, A.E.V., *Genome multiplication as adaptation to tissue survival: Evidence from gene expression in mammalian heart and liver.* Genomics, 2007: p. 70-80.
423. Anatskaya, O.V., Vinogradov, *Somatic polyploidy promotes cell function under stress and energy depletion: evidence from tissue-specific mammal transcriptome.* A.E. Funct Integr Genomics 2010: p. 433–446.
424. !!! INVALID CITATION !!! [304, 389-392].
425. Kudryavtsev, B.N., et al., *Human hepatocyte polyploidization kinetics in the course of life cycle.* Virchows Archiv. B, Cell pathology including molecular pathology, 1993. **64**(6): p. 387-393.
426. Gupta, S. *Hepatic polyploidy and liver growth control*. in *Seminars in cancer biology*. 2000. Elsevier.
427. Gerlyng, P., *Binucleation and polyploidization patterns in developmental and regenerative rat liver growth.* Cell Prolif., 1993. **26**.
428. Sigal, S.H., *Partial hepatectomy-induced polyploidy attenuates hepatocyte replication and activates cell aging events.* Am. J. Physiol., 1999. **276**.
429. Schmucker, D.L., *Do hepatocytes age?* Exp. Gerontol., 1990. **25**.
430. Schmucker, D.L., *Hepatocyte fine structure during maturation and senescence.* J. Electron. Microsc. Tech., 1990. **14**.
431. Asahina, K., *Multiplicative mononuclear small hepatocytes in adult rat liver: their isolation as a homogeneous population and localization to periportal zone.* Biochem. Biophys. Res. Commun., 2006. **342**.
432. Duncan, A.W., *The ploidy conveyor of mature hepatocytes as a source of genetic variation.* Nature, 2010. **467**.
433. Knouse, K.A., et al., *Chromosome segregation fidelity in epithelia requires tissue architecture.* Cell, 2018. **175**.
434. Miyaoka, Y., *Hypertrophy and unconventional cell division of hepatocytes underlie liver regeneration.* Curr. Biol., 2012. **22**.
435. Overturf, K., et al., *The repopulation potential of hepatocyte populations differing in size and prior mitotic expansion.* Am. J. Pathol., 1999. **155**.
436. Ganem, N.J., *Cytokinesis failure triggers hippo tumor suppressor pathway activation.* Cell, 2014. **158**.

437. Wang, M.J., et al., *Hepatocyte polyploidization and its association with pathophysiological processes.* Cell Death Dis., 2017. **8**.
438. Wang, M.J., *Reversal of hepatocyte senescence after continuous in vivo cell proliferation.* Hepatology, 2014. **60**.
439. Lu, P., *Microarray analysis of gene expression of mouse hepatocytes of different ploidy.* Mamm. Genome, 2007. **18**.
440. Kreutz, C., et al., *Hepatocyte Ploidy Is a Diversity Factor for Liver Homeostasis.* Front Physiol, 2017. **8**: p. 862.
441. Eldar, A. and M.B. Elowitz, *Functional roles for noise in genetic circuits.* Nature, 2010. **467**.
442. Bahar Halpern, K., *Bursty gene expression in the intact mammalian liver.* Mol. Cell, 2015. **58**.
443. Bielski, C.M., et al., *Genome doubling shapes the evolution and prognosis of advanced cancers.* Nat Genet, 2018. **50**(8): p. 1189-1195.
444. Zack, T.I., et al., *Pan-cancer patterns of somatic copy number alteration.* Nat Genet, 2013. **45**(10): p. 1134-40.
445. Zhang, S., et al., *The origins and functions of hepatic polyploidy.* Cell Cycle, 2019. **18**(12): p. 1302-1315.
446. Zhang, S., et al., *The Polyploid State Plays a Tumor-Suppressive Role in the Liver.* Dev Cell, 2018. **44**(4): p. 447-459 e5.
447. Schwarze, P.E., et al., *Emergence of a population of small, diploid hepatocytes during hepatocarcinogenesis.* Carcinogenesis, 1984. **5**(10): p. 1267-75.
448. Saeter, G., et al., *The polyploidizing growth pattern of normal rat liver is replaced by divisional, diploid growth in hepatocellular nodules and carcinomas.* Carcinogenesis, 1988. **9**(6): p. 939-45.
449. Kutay, H., et al., *Downregulation of miR-122 in the rodent and human hepatocellular carcinomas.* J Cell Biochem, 2006. **99**(3): p. 671-8.
450. Saeter, G., et al., *Changes in ploidy distributions in human liver carcinogenesis.* J Natl Cancer Inst, 1988. **80**(18): p. 1480-5.
451. Bou-Nader, M., et al., *Polyploidy spectrum: a new marker in HCC classification.* Gut, 2020. **69**(2): p. 355-364.
452. Soltis, P.S. and D.E. Soltis, *The role of genetic and genomic attributes in the success of polyploids.* Proc Natl Acad Sci U S A, 2000. **97**(13): p. 7051-7.
453. Duncan, A.W., *Frequent aneuploidy among normal human hepatocytes.* Gastroenterology, 2012. **142**.
454. Knouse, K.A., et al., *Single cell sequencing reveals low levels of aneuploidy across mammalian tissues.* Proc. Natl Acad. Sci. USA, 2014. **111**.
455. Duncan, A.W., *Aneuploidy, polyploidy and ploidy reversal in the liver.* Semin. Cell Dev. Biol., 2013. **24**.
456. Duncan, A.W., et al., *Aneuploidy as a mechanism for stress-induced liver adaptation.* J Clin Invest, 2012. **122**(9): p. 3307-15.
457. Knouse, K.A., et al., *Single cell sequencing reveals low levels of aneuploidy across mammalian tissues.* Proc Natl Acad Sci U S A, 2014. **111**(37): p. 13409-14.
458. Matsumoto, T., et al., *In Vivo Lineage Tracing of Polyploid Hepatocytes Reveals Extensive Proliferation during Liver Regeneration.* Cell Stem Cell, 2020. **26**(1): p. 34-47 e3.

459. Matsumoto, T., et al., *In vivo lineage tracing of polyploid hepatocytes reveals extensive proliferation during liver regeneration.* Cell Stem Cell, 2019. **26**.
460. Gentric, G., et al., *Oxidative stress promotes pathologic polyploidization in nonalcoholic fatty liver disease.* J Clin Invest, 2015. **125**(3): p. 981-92.
461. Dobin, A., et al., *STAR: ultrafast universal RNA-seq aligner.* Bioinformatics, 2013. **29**(1): p. 15-21.
462. Liao, Y., G.K. Smyth, and W. Shi, *featureCounts: an efficient general purpose program for assigning sequence reads to genomic features.* Bioinformatics, 2014. **30**(7): p. 923-30.
463. Robinson, M.D., D.J. McCarthy, and G.K. Smyth, *edgeR: a Bioconductor package for differential expression analysis of digital gene expression data.* Bioinformatics, 2010. **26**(1): p. 139-40.
464. Risso, D. *EDASeq : Exploratory Data Analysis and Normalization for RNA-Seq*. 2013.
465. Subramanian, A., et al., *Gene set enrichment analysis: a knowledge-based approach for interpreting genome-wide expression profiles.* Proc Natl Acad Sci U S A, 2005. **102**(43): p. 15545-50.
466. Raudvere, U., et al., *g:Profiler: a web server for functional enrichment analysis and conversions of gene lists (2019 update).* Nucleic Acids Res, 2019. **47**(W1): p. W191-W198.
467. Franks, L.M. and J. Payne, *The influence of age on reproductive capacity in C57BL mice.* J Reprod Fertil, 1970. **21**(3): p. 563-5.
468. Jake Lever, M.K.N.A., *Principal component analysis.* Nature Methods, 2017(14): p. 641–642.
469. Jolliffe, I.T., *Principal Component Analysis.* Springer Series in Statistics, Springer, New York, NY, 2002.
470. Ovrebo, J.I. and B.A. Edgar, *Polyploidy in tissue homeostasis and regeneration.* Development, 2018. **145**(14).
471. Orr-Weaver, T.L., *When bigger is better: the role of polyploidy in organogenesis.* Trends Genet, 2015. **31**(6): p. 307-15.
472. Pflaum, J., S. Schlosser, and M. Muller, *p53 Family and Cellular Stress Responses in Cancer.* Front Oncol, 2014. **4**: p. 285.
473. Beg, A.A., et al., *Embryonic lethality and liver degeneration in mice lacking the RelA component of NF-kappa B.* Nature, 1995. **376**(6536): p. 167-70.
474. Xu, Y., et al., *NF-kappaB inactivation converts a hepatocyte cell line TNF-alpha response from proliferation to apoptosis.* Am J Physiol, 1998. **275**(4): p. C1058-66.
475. Kirillova, I., M. Chaisson, and N. Fausto, *Tumor necrosis factor induces DNA replication in hepatic cells through nuclear factor kappaB activation.* Cell Growth Differ, 1999. **10**(12): p. 819-28.
476. Shen, X., Y. Peng, and H. Li, *The Injury-Related Activation of Hedgehog Signaling Pathway Modulates the Repair-Associated Inflammation in Liver Fibrosis.* Front Immunol, 2017. **8**: p. 1450.
477. Machado, M.V. and A.M. Diehl, *Hedgehog signalling in liver pathophysiology.* J Hepatol, 2018. **68**(3): p. 550-562.
478. Omenetti, A., et al., *Hedgehog signaling in the liver.* J Hepatol, 2011. **54**(2): p. 366-73.

479. Seki, E., *HEDGEHOG Signal in hepatocytes mediates macrophage recruitment: A new mechanism and potential therapeutic target for fatty liver disease.* Hepatology, 2016. **63**(4): p. 1071-3.
480. Meng, E., et al., *The Impact of Hedgehog Signaling Pathway on DNA Repair Mechanisms in Human Cancer.* Cancers (Basel), 2015. **7**(3): p. 1333-48.
481. Scheffold, A., et al., *Elevated Hedgehog activity contributes to attenuated DNA damage responses in aged hematopoietic cells.* Leukemia, 2020. **34**(4): p. 1125-1134.
482. Allaire, M., et al., *Autophagy in liver diseases: Time for translation?* J Hepatol, 2019. **70**(5): p. 985-998.
483. Rautou, P.E., et al., *Autophagy in liver diseases.* J Hepatol, 2010. **53**(6): p. 1123-34.
484. Ke, P.Y., *Diverse Functions of Autophagy in Liver Physiology and Liver Diseases.* Int J Mol Sci, 2019. **20**(2).
485. Dudkowska, M., et al., *The role of autophagy in escaping therapy-induced polyploidy/senescence.* Adv Cancer Res, 2021. **150**: p. 209-247.
486. Yang, J., Okabe, H., & Monga, S., *Liver Development, Regeneration, and Stem Cells.* 2014.
487. Ortica, S., et al., *The 4 Notch receptors play distinct and antagonistic roles in the proliferation and hepatocytic differentiation of liver progenitors.* FASEB J, 2014. **28**(2): p. 603-14.
488. Zhou, Z., et al., *Insights into APC/C: from cellular function to diseases and therapeutics.* Cell Div, 2016. **11**: p. 9.
489. Gentric, G. and C. Desdouets, *Polyploidization in liver tissue.* Am J Pathol, 2014. **184**(2): p. 322-31.
490. Engelbert, D., et al., *The ubiquitin ligase APC(Cdh1) is required to maintain genome integrity in primary human cells.* Oncogene, 2008. **27**(7): p. 907-17.
491. Ross, R.J., M.M. Weiner, and H. Lin, *PIWI proteins and PIWI-interacting RNAs in the soma.* Nature, 2014. **505**(7483): p. 353-359.
492. Khurana, J.S., et al., *Distinct functions for the Drosophila piRNA pathway in genome maintenance and telomere protection.* PLoS Genet, 2010. **6**(12): p. e1001246.
493. Matsumura, A., et al., *HGF regulates VEGF expression via the c-Met receptor downstream pathways, PI3K/Akt, MAPK and STAT3, in CT26 murine cells.* Int J Oncol, 2013. **42**(2): p. 535-42.
494. Xiao, G.H., et al., *Anti-apoptotic signaling by hepatocyte growth factor/Met via the phosphatidylinositol 3-kinase/Akt and mitogen-activated protein kinase pathways.* Proc Natl Acad Sci U S A, 2001. **98**(1): p. 247-52.
495. Boccaccio, C., et al., *Induction of epithelial tubules by growth factor HGF depends on the STAT pathway.* Nature, 1998. **391**(6664): p. 285-8.
496. Ponzetto, C., et al., *A novel recognition motif for phosphatidylinositol 3-kinase binding mediates its association with the hepatocyte growth factor/scatter factor receptor.* Mol Cell Biol, 1993. **13**(8): p. 4600-8.
497. Chang, L. and M. Karin, *Mammalian MAP kinase signalling cascades.* Nature, 2001. **410**(6824): p. 37-40.
498. Tsai, S.M., D.W. Liu, and W.P. Wang, *Fibroblast growth factor (Fgf) signaling pathway regulates liver homeostasis in zebrafish.* Transgenic Res, 2013. **22**(2): p. 301-14.
499. Shin, D., et al., *Bmp and Fgf signaling are essential for liver specification in zebrafish.* Development, 2007. **134**(11): p. 2041-50.

500. Glotzer, M., *Animal cell cytokinesis.* Annu Rev Cell Dev Biol, 2001. **17**: p. 351-86.
501. Jordan, S.N. and J.C. Canman, *Rho GTPases in animal cell cytokinesis: an occupation by the one percent.* Cytoskeleton (Hoboken), 2012. **69**(11): p. 919-30.
502. Chircop, M., *Rho GTPases as regulators of mitosis and cytokinesis in mammalian cells.* Small GTPases, 2014. **5**.
503. Berasain, C. and M.A. Avila, *The EGFR signalling system in the liver: from hepatoprotection to hepatocarcinogenesis.* J Gastroenterol, 2014. **49**(1): p. 9-23.
504. Wells, A., *EGF receptor.* The International Journal of Biochemistry & Cell Biology, 1999: p. 637-643.
505. Gusterson BA, H.K., *Should we be surprised at the paucity of response to EGFR inhibitors?* Lancet Oncol, 2009: p. 522-7.
506. Liu, Y., et al., *ERBB4 acts as a suppressor in the development of hepatocellular carcinoma.* Carcinogenesis, 2017. **38**(4): p. 465-473.
507. Scheving, L.A., et al., *Hepatocyte ERBB3 and EGFR are required for maximal CCl4-induced liver fibrosis.* Am J Physiol Gastrointest Liver Physiol, 2016. **311**(5): p. G807-G816.
508. Zhang, X., et al., *Akt, FoxO and regulation of apoptosis.* Biochim Biophys Acta, 2011. **1813**(11): p. 1978-86.
509. K., K., *Aging and the liver: functional aspects. .* Arch Gerontol Geriatr., 1994: p. 145-58.
510. Regev A, S.E., *Liver disease in the elderly.* Gastroenterol Clin North Am, 2001 p. 547-63.
511. Bertolotti, M., et al., *Nonalcoholic fatty liver disease and aging: epidemiology to management.* World J Gastroenterol, 2014. **20**(39): p. 14185-204.
512. White, R.R., et al., *Comprehensive transcriptional landscape of aging mouse liver.* BMC Genomics, 2015. **16**: p. 899.
513. Cao, S.X., et al., *Genomic profiling of short- and long-term caloric restriction effects in the liver of aging mice.* Proc Natl Acad Sci U S A, 2001. **98**(19): p. 10630-5.
514. Niedernhofer, L.J., et al., *A new progeroid syndrome reveals that genotoxic stress suppresses the somatotroph axis.* Nature, 2006. **444**(7122): p. 1038-43.
515. Lebel, M., N.C. de Souza-Pinto, and V.A. Bohr, *Metabolism, genomics, and DNA repair in the mouse aging liver.* Curr Gerontol Geriatr Res, 2011. **2011**: p. 859415.
516. Hill, K.A., et al., *Tissue-specific time courses of spontaneous mutation frequency and deviations in mutation pattern are observed in middle to late adulthood in Big Blue mice.* Environ Mol Mutagen, 2005. **45**(5): p. 442-54.
517. Bochkis, I.M., et al., *Changes in nucleosome occupancy associated with metabolic alterations in aged mammalian liver.* Cell Rep, 2014. **9**(3): p. 996-1006.
518. Chen, Y., et al., *Remodeling of the H3 nucleosomal landscape during mouse aging.* Transl Med Aging, 2020. **4**: p. 22-31.
519. Tvardovskiy, A., et al., *Accumulation of histone variant H3.3 with age is associated with profound changes in the histone methylation landscape.* Nucleic Acids Res, 2017. **45**(16): p. 9272-9289.
520. Sen, P., et al., *Epigenetic Mechanisms of Longevity and Aging.* Cell, 2016. **166**(4): p. 822-839.
521. Bacalini, M.G., et al., *Molecular Aging of Human Liver: An Epigenetic/Transcriptomic Signature.* J Gerontol A Biol Sci Med Sci, 2019. **74**(1): p. 1-8.

522. Chapski, D.J., et al., *Spatial Principles of Chromatin Architecture Associated With Organ-Specific Gene Regulation.* Front Cardiovasc Med, 2018. **5**: p. 186.
523. Vietri Rudan, M., et al., *Comparative Hi-C reveals that CTCF underlies evolution of chromosomal domain architecture.* Cell Rep, 2015. **10**(8): p. 1297-309.
524. Downes, D.J., et al., *High-resolution targeted 3C interrogation of cis-regulatory element organization at genome-wide scale.* Nat Commun, 2021. **12**(1): p. 531.
525. Schmucker, D.L. and H. Sanchez, *Liver regeneration and aging: a current perspective.* Curr Gerontol Geriatr Res, 2011. **2011**: p. 526379.
526. Aravinthan, A., et al., *Hepatocyte senescence predicts progression in non-alcohol-related fatty liver disease.* J Hepatol, 2013. **58**(3): p. 549-56.
527. Noureddin, M., et al., *Clinical and histological determinants of nonalcoholic steatohepatitis and advanced fibrosis in elderly patients.* Hepatology, 2013. **58**(5): p. 1644-54.
528. Jin, J., et al., *Increased expression of enzymes of triglyceride synthesis is essential for the development of hepatic steatosis.* Cell Rep, 2013. **3**(3): p. 831-43.
529. Amir, M. and M.J. Czaja, *Autophagy in nonalcoholic steatohepatitis.* Expert Rev Gastroenterol Hepatol, 2011. **5**(2): p. 159-66.
530. Franceschi, C., et al., *Inflamm-aging. An evolutionary perspective on immunosenescence.* Ann N Y Acad Sci, 2000. **908**: p. 244-54.
531. Kim IH, K.T., Brenner DA., *Aging and liver disease.* Curr Opin Gastroenterol., 2015.
532. Seitz, H.K.a.S., Felix., *Risk factors and mechanisms of hepatocarcinogenesis with special emphasis on alcohol and oxidative stress.* 2006: p. 349-360.
533. Poynard T, B.P., Opolon P., *Natural history of liver fibrosis progression in patients with chronic hepatitis C. The OBSVIRC, METAVIR, CLINIVIR, and DOSVIRC groups. .* Lancet, 1997
534. BJ., M., *Natural history of chronic hepatitis B.* Clin Liver Dis. , 2010
535. Wiley TE, M.M., Breidi L, McCarthy M, Layden TJ., *Impact of alcohol on the histological and clinical progression of hepatitis C infection.* Hepatology, 1998
536. Johan Westin, H.N., Martin Lagging, Gunnar Norkrans, Rune Wejstål,, *Steatosis accelerates fibrosis development over time in hepatitis C virus genotype 3 infected patients.* Journal of Hepatology, 2002.
537. Poynard T, R.V., Charlotte F, Goodman Z, McHutchison J, Albrecht J., *Rates and risk factors of liver fibrosis progression in patients with chronic hepatitis c.* J Hepatol. , 2001.
538. Thabut, D., et al., *Hepatitis C in 6,865 patients 65 yr or older: a severe and neglected curable disease?* Am J Gastroenterol, 2006. **101**(6): p. 1260-7.
539. Ryder, S.D., et al., *Progression of hepatic fibrosis in patients with hepatitis C: a prospective repeat liver biopsy study.* Gut, 2004. **53**(3): p. 451-5.
540. Herwig, R., et al., *Analyzing and interpreting genome data at the network level with ConsensusPathDB.* Nat Protoc, 2016. **11**(10): p. 1889-907.
541. Langmead, B.S., S. L., *Fast gapped-read alignment with Bowtie 2.* Nat Methods, 2012. **9**: p. 357-359.
542. Zhang, Y.e.a., *Model-based analysis of ChIP-Seq (MACS).* Genome Biol 2008. **9**(137).
543. Feng, J., Liu, T., Qin, B., Zhang, Y. & Liu, X. S, *Identifying ChIP-seq enrichment using MACS.* Nat Protoc, 2012. **7**: p. 1728-1740.
544. Ramirez, F.e.a., *deepTools2: a next generation web server for deep-sequencing data analysis.* Nucleic Acids Res, 2016. **44**: p. 160-165.

545. Heinz, S., et al., *Simple combinations of lineage-determining transcription factors prime cis-regulatory elements required for macrophage and B cell identities.* Mol Cell, 2010. **38**(4): p. 576-89.
546. Dekker, J., et al., *Capturing chromosome conformation.* Science, 2002. **295**(5558): p. 1306-11.
547. Naumova, N., et al., *Analysis of long-range chromatin interactions using Chromosome Conformation Capture.* Methods, 2012. **58**(3): p. 192-203.
548. Imakaev, M., et al., *Iterative correction of Hi-C data reveals hallmarks of chromosome organization.* Nat Methods, 2012. **9**(10): p. 999-1003.
549. Langmead, B. and S.L. Salzberg, *Fast gapped-read alignment with Bowtie 2.* Nat Methods, 2012. **9**(4): p. 357-9.
550. Li, H., et al., *The Sequence Alignment/Map format and SAMtools.* Bioinformatics, 2009. **25**(16): p. 2078-9.
551. Hunter, J.D., *Matplotlib: A 2D Graphics Environment.* Computing in Science & Engineering, 2007.
552. Chaturvedi, M.M., and M. S. Kanungo, *Analysis of conformation and function of the chromatin of the brain of young and old rats.* Molecular biology reports, 1985. **10.4**: p. 215-219.
553. Slack, C., et al., *The Ras-Erk-ETS-Signaling Pathway Is a Drug Target for Longevity.* Cell, 2015. **162**(1): p. 72-83.
554. Borras, C., et al., *RasGrf1 deficiency delays aging in mice.* Aging (Albany NY), 2011. **3**(3): p. 262-76.
555. Hsieh, C.-C., and John Papaconstantinou. , *The effect of aging on p38 signaling pathway activity in the mouse liver and in response to ROS generated by 3-nitropropionic acid.* Mechanisms of ageing and development, 2002. **123.11**: p. 1423-1435.
556. Hsieh, C.-C., Judah I. Rosenblatt, and John Papaconstantinou., *Age-associated changes in SAPK/JNK and p38 MAPK signaling in response to the generation of ROS by 3-nitropropionic acid.* Mechanisms of ageing and development 2003. **124.6**: p. 733-746.
557. Bennett, R.G., *Targeting the Relaxin Pathway for Liver Disease Treatment.* Eur Med J Hepatol, 2018. **6**(1): p. 80-87.
558. Henry, B.L., et al., *Relaxin suppresses atrial fibrillation in aged rats by reversing fibrosis and upregulating Na+ channels.* Heart Rhythm, 2016. **13**(4): p. 983-91.
559. Martin, B., Gabris, B., Barakat, A.F. et al., *Relaxin reverses maladaptive remodeling of the aged heart through Wnt-signaling.* Sci Rep, 2019(9): p. 18545
560. Martinez, P., et al., *A genetic interaction between RAP1 and telomerase reveals an unanticipated role for RAP1 in telomere maintenance.* Aging Cell, 2016. **15**(6): p. 1113-1125.
561. Ferrara-Romeo, I., P. Martinez, and M.A. Blasco, *Mice lacking RAP1 show early onset and higher rates of DEN-induced hepatocellular carcinomas in female mice.* PLoS One, 2018. **13**(10): p. e0204909.
562. Hou, L., et al., *Blood telomere length attrition and cancer development in the normative aging study cohort.* EBioMedicine 2015: p. 591-596.
563. T., H., *Educational initiatives in geriatric oncology - Who, why, and how?* J Geriatr Oncol, 2016

564. Zinger, A.e.a., *Cancer and Aging - the Inflammatory Connection.* Aging and disease, 2017. **8,5** p. 611-627.
565. Aunan, J.R.e.a., *The Biology of Aging and Cancer: A Brief Overview of Shared and Divergent Molecular Hallmarks.* Aging and disease, 2017. **8,5**.
566. William B. Ershler, D.L.L., *Aging and Cancer: Issues of Basic and Clinical Science.* JNCI: Journal of the National Cancer Institute, 1997. **Volume 89,** (Issue 20): p. 1489–1497.
567. Hunt, N.J., et al., *Hallmarks of Aging in the Liver.* Comput Struct Biotechnol J, 2019. **17**: p. 1151-1161.
568. Hagen, T.M., et al., *Mitochondrial decay in hepatocytes from old rats: membrane potential declines, heterogeneity and oxidants increase.* Proc Natl Acad Sci U S A, 1997. **94**(7): p. 3064-9.
569. Wallace, D.C., *Mitochondrial genetics: a paradigm for aging and degenerative diseases?* Science, 1992. **256**(5057): p. 628-32.
570. Turturro, A., et al., *Growth curves and survival characteristics of the animals used in the Biomarkers of Aging Program.* J Gerontol A Biol Sci Med Sci, 1999. **54**(11): p. B492-501.
571. Yannarell, A., Dorothy E. Schumm, and Thomas E. Webb., *Age-dependence of nuclear RNA processing.* Mechanisms of ageing and development, 1977. **6** p. 259-264.
572. Holly, A.C., et al., *Changes in splicing factor expression are associated with advancing age in man.* Mechanisms of ageing and development 2013. **134.9**: p. 356-366.
573. Li, H., et al., *Alternative splicing in aging and age-related diseases.* Translational Medicine of Aging, 2017. **1**: p. 32-40.
574. *Human aging is characterized by focused changes in gene expression and deregulation of alternative splicing.*
575. Wauthier, V., R.K. Verbeeck, and P.B. Calderon, *The effect of ageing on cytochrome p450 enzymes: consequences for drug biotransformation in the elderly.* Curr Med Chem, 2007. **14**(7): p. 745-57.
576. Shavlakadze, T., et al., *Age-Related Gene Expression Signature in Rats Demonstrate Early, Late, and Linear Transcriptional Changes from Multiple Tissues.* Cell Rep, 2019. **28**(12): p. 3263-3273 e3.
577. Xu S, H.D., Liu J, Ji L., *Age-associated changes in GSH S-transferase gene/proteins in livers of rats.* Redox Rep., 2018
578. Delgado I, F.O., Iglesias A, Rueda Y, Syn WK, Zubiaga AM, Ochoa B., *A role for transcription factor E2F2 in hepatocyte proliferation and timely liver regeneration.* Am J Physiol Gastrointest Liver Physiol., 2011
579. Iakova P, A.S., Timchenko NA. , *Aging reduces proliferative capacities of liver by switching pathways of C/EBPalpha growth arrest. .* Cell, 2003
580. Frenk, S. and J. Houseley, *Gene expression hallmarks of cellular ageing.* Biogerontology, 2018. **19**(6): p. 547-566.
581. Harries, L.W., et al., *Human aging is characterized by focused changes in gene expression and deregulation of alternative splicing.* Aging Cell, 2011. **10**(5): p. 868-78.
582. Tomasetti, C., et al., *Cell division rates decrease with age, providing a potential explanation for the age-dependent deceleration in cancer incidence.* Proc Natl Acad Sci U S A, 2019. **116**(41): p. 20482-20488.
583. CE., F., *The menopause and aging, a comparative perspective. .* J Steroid Biochem Mol Biol., 2014

584. Fontana L, P.L., Longo VD., *Extending healthy life span--from yeast to humans.* Science, 2010
585. CJ., K., *The genetics of ageing. .* Nature, 2010
586. Kenyon C, C.J., Gensch E, Rudner A, Tabtiang R. A, *C. elegans mutant that lives twice as long as wild type.* Nature, 1993
587. Kimura KD, T.H., Liu Y, Ruvkun G., *daf-2, an insulin receptor-like gene that regulates longevity and diapause in Caenorhabditis elegans.* Science, 1997
588. Nakamura T, S.K., Nakamura T, Matsumoto K., *Hepatocyte growth factor twenty years on: Much more than a growth factor. .* J Gastroenterol Hepatol., 2011
589. Ponzetto C, B.A., Zhen Z, Maina F, dalla Zonca P, Giordano S, Graziani A, Panayotou G, Comoglio PM., *A multifunctional docking site mediates signaling and transformation by the hepatocyte growth factor/scatter factor receptor family. .* Cell, 1994
590. Trusolino, L., Bertotti, A. & Comoglio, P., *MET signalling: principles and functions in development, organ regeneration and cancer. .* Nat Rev Mol Cell Biol, 2010.
591. Fixman ED, F.T., Kamikura DM, Naujokas MA, Park M., *Pathways downstream of Shc and Grb2 are required for cell transformation by the tpr-Met oncoprotein.* J Biol Chem., 1996
592. Paumelle R, T.D., Kherrouche Z, Plaza S, Leroy C, Reveneau S, Vandenbunder B, Fafeur V., *Hepatocyte growth factor/scatter factor activates the ETS1 transcription factor by a RAS-RAF-MEK-ERK signaling pathway. .* Oncogene, 2002
593. Harrison DE, S.R., Sharp ZD, Nelson JF, Astle CM, Flurkey K, Nadon NL, Wilkinson JE, Frenkel K, Carter CS, Pahor M, Javors MA, Fernandez E, Miller RA., *Rapamycin fed late in life extends lifespan in genetically heterogeneous mice.* Nature, 2009
594. Hsieh CC, P.J., *The effect of aging on p38 signaling pathway activity in the mouse liver and in response to ROS generated by 3-nitropropionic acid.* Mech Ageing Dev., 2002
595. Hsieh CC, R.J., Papaconstantinou J., *Age-associated changes in SAPK/JNK and p38 MAPK signaling in response to the generation of ROS by 3-nitropropionic acid. .* Mech Ageing Dev., 2003
596. Mays, P.K., R. McAnulty, and G.J. Laurent, *Age-related changes in total protein and collagen metabolism in rat liver.* Hepatology, 1991. **14**(6): p. 1224-9.
597. Guzelian PS, Q.G., Diegelmann RF., *Collagen synthesis by the hepatocyte: studies in primary cultures of parenchymal cells from adult rat liver.* Coll Relat Res., 1981.
598. Wang, L., et al., *Cdc42 GTPase-activating protein deficiency promotes genomic instability and premature aging-like phenotypes.* Proc Natl Acad Sci U S A, 2007. **104**(4): p. 1248-53.
599. Florian, M.C., et al., *Expression and Activity of the Small RhoGTPase Cdc42 in Blood Cells of Older Adults Are Associated With Age and Cardiovascular Disease.* J Gerontol A Biol Sci Med Sci, 2017. **72**(9): p. 1196-1200.
600. Hu, S.J., et al., *Effects of apoptosis on liver aging.* World J Clin Cases, 2019. **7**(6): p. 691-704.
601. Biel, M., V. Wascholowski, and A. Giannis, *Epigenetics--an epicenter of gene regulation: histones and histone-modifying enzymes.* Angew Chem Int Ed Engl, 2005. **44**(21): p. 3186-216.
602. Pal, S. and J.K. Tyler, *Epigenetics and aging.* Sci Adv, 2016. **2**(7): p. e1600584.

603. Kimura, H., *Histone modifications for human epigenome analysis.* J Hum Genet, 2013. **58**(7): p. 439-45.
604. Mosammaparast, N. and Y. Shi, *Reversal of histone methylation: biochemical and molecular mechanisms of histone demethylases.* Annu Rev Biochem, 2010. **79**: p. 155-79.
605. Ku Hui-Chen, C.C.-F., *Master Regulator Activating Transcription Factor 3 (ATF3) in Metabolic Homeostasis and Cancer* Frontiers in Endocrinology 2020.
606. Zhang C, Z.X., Huang L, Guan Y, Huang X, Tian XL, Zhang L, Tao W., *ATF3 drives senescence by reconstructing accessible chromatin profiles.* Aging Cell., 2021
607. Brantley, D., Cheng, N., Thompson, E. et al. , *Soluble Eph A receptors inhibit tumor angiogenesis and progression in vivo.* Oncogene 2002.
608. Goichberg P, K.R., Cimini M, Bai Y, Sanada F, Sorrentino A, Signore S, Kajstura J, Rota M, Anversa P, Leri A. , *Age-associated defects in EphA2 signaling impair the migration of human cardiac progenitor cells. .* 2013.
609. Irving J, F.J., Wistrom C, Pikaart M, Villeponteau B. , *An altered repertoire of fos/jun (AP-1) at the onset of replicative senescence. .* Exp Cell Res., 1992
610. Tong, L., Toliver-Kinsky, T., Edwards, M., Rassin, D.K., Werrbach-Perez, K. and Perez-Polo, J.R., *Attenuated transcriptional responses to oxidative stress in the aged rat brain. .* J. Neurosci. Res., 2002.
611. Hu, J.W., et al., *Identification of FOS as a Candidate Risk Gene for Liver Cancer by Integrated Bioinformatic Analysis.* Biomed Res Int, 2020. **2020**: p. 6784138.
612. Bakiri, L., et al., *Liver carcinogenesis by FOS-dependent inflammation and cholesterol dysregulation.* J Exp Med, 2017. **214**(5): p. 1387-1409.
613. Delpoux A, M.N., Hess Michelini R, Katayama CD, Allison KA, Glass CK, Quiñones-Parra SM, Murre C, Loh L, Kedzierska K, Lappas M, Hedrick SM, Doedens AL. , *FOXO1 constrains activation and regulates senescence in CD8 T cells. .* Cell Rep. , 2021
614. Rouault, J.P., et al., *Identification of BTG2, an antiproliferative p53-dependent component of the DNA damage cellular response pathway.* Nat Genet, 1996. **14**(4): p. 482-6.
615. Wheaton, K., et al., *BTG2 antagonizes Pin1 in response to mitogens and telomere disruption during replicative senescence.* Aging Cell, 2010. **9**(5): p. 747-60.
616. Lim, I.K., *TIS21 (/BTG2/PC3) as a link between ageing and cancer: cell cycle regulator and endogenous cell death molecule.* J Cancer Res Clin Oncol, 2006. **132**(7): p. 417-26.
617. Paluvai, H., E. Di Giorgio, and C. Brancolini, *The Histone Code of Senescence.* Cells, 2020. **9**(2).
618. Yuan, R., L.L. Peters, and B. Paigen, *Mice as a mammalian model for research on the genetics of aging.* ILAR J, 2011. **52**(1): p. 4-15.
619. Ackert-Bicknell, C.L., et al., *Aging Research Using Mouse Models.* Curr Protoc Mouse Biol, 2015. **5**(2): p. 95-133.
620. Lonnig, W.E. and H. Saedler, *Chromosome rearrangements and transposable elements.* Annu Rev Genet, 2002. **36**: p. 389-410.
621. Vitte, C. and O. Panaud, *LTR retrotransposons and flowering plant genome size: emergence of the increase/decrease model.* Cytogenet Genome Res, 2005. **110**(1-4): p. 91-107.
622. Antonarakis, S.E., et al., *Chromosome 21 and down syndrome: from genomics to pathophysiology.* Nat Rev Genet, 2004. **5**(10): p. 725-38.

623. Winkelmann, M., P. Pfitzer, and W. Schneider, *Significance of polyploidy in megakaryocytes and other cells in health and tumor disease.* Klin Wochenschr, 1987. **65**(23): p. 1115-31.
624. Marguerat, S. and J. Bahler, *Coordinating genome expression with cell size.* Trends Genet, 2012. **28**(11): p. 560-5.
625. Corbel, C., et al., *Unusual chromatin status and organization of the inactive X chromosome in murine trophoblast giant cells.* Development, 2013. **140**(4): p. 861-72.
626. Schoenfelder, K.P. and D.T. Fox, *The expanding implications of polyploidy.* J Cell Biol, 2015. **209**(4): p. 485-91.
627. Bernstein, B.E., et al., *A bivalent chromatin structure marks key developmental genes in embryonic stem cells.* Cell, 2006. **125**(2): p. 315-26.
628. Wang, B., et al., *Self-renewing diploid Axin2(+) cells fuel homeostatic renewal of the liver.* Nature, 2015. **524**(7564): p. 180-5.
629. LeCluyse, E.L., et al., *Organotypic liver culture models: meeting current challenges in toxicity testing.* Crit Rev Toxicol, 2012. **42**(6): p. 501-48.
630. Tanami, S., et al., *Dynamic zonation of liver polyploidy.* Cell Tissue Res, 2017. **368**(2): p. 405-410.
631. Nacarelli, T., P. Liu, and R. Zhang, *Epigenetic Basis of Cellular Senescence and Its Implications in Aging.* Genes (Basel), 2017. **8**(12).
632. Narita, M., et al., *Rb-mediated heterochromatin formation and silencing of E2F target genes during cellular senescence.* Cell, 2003. **113**(6): p. 703-16.
633. Zhang, R., et al., *Formation of MacroH2A-containing senescence-associated heterochromatin foci and senescence driven by ASF1a and HIRA.* Dev Cell, 2005. **8**(1): p. 19-30.
634. Di Micco, R., et al., *Interplay between oncogene-induced DNA damage response and heterochromatin in senescence and cancer.* Nat Cell Biol, 2011. **13**(3): p. 292-302.
635. Freund, A., et al., *Lamin B1 loss is a senescence-associated biomarker.* Mol Biol Cell, 2012. **23**(11): p. 2066-75.
636. Shah, P.P., et al., *Lamin B1 depletion in senescent cells triggers large-scale changes in gene expression and the chromatin landscape.* Genes Dev, 2013. **27**(16): p. 1787-99.
637. Sadaie, M., et al., *Redistribution of the Lamin B1 genomic binding profile affects rearrangement of heterochromatic domains and SAHF formation during senescence.* Genes Dev, 2013. **27**(16): p. 1800-8.
638. Azzu, V. and T.G. Valencak, *Energy Metabolism and Ageing in the Mouse: A Mini-Review.* Gerontology, 2017. **63**(4): p. 327-336.
639. Kotre, J.N.H., Elizabeth, *Seasons of Life: The Dramatic Journey from Birth to Death.* University of Michigan Press., 1997: p. 47–49.
640. Roser, M.O.-O., Esteban; Ritchie, Hannah, *"Life Expectancy". Our World in Data. How did life expectancy change over time?.* 2019.
641. U.N. Department of Economic and Social Affairs, P.D.W.P.P.P., "Life expectancy at birth, total (years) – Data". data.worldbank.org., "Life Expectancy by Country and in the World - Worldometer". www.worldometers.info.
642. Zhang, W., et al., *The ageing epigenome and its rejuvenation.* Nat Rev Mol Cell Biol, 2020. **21**(3): p. 137-150.
643. Fahy, G.M., et al., *Reversal of epigenetic aging and immunosenescent trends in humans.* Aging Cell, 2019. **18**(6): p. e13028.

644. Finkel, T., *The metabolic regulation of aging.* Nat Med, 2015. **21**(12): p. 1416-23.
645. Mattison, J.A., et al., *Caloric restriction improves health and survival of rhesus monkeys.* Nat Commun, 2017. **8**: p. 14063.
646. Enesco, H.E. and J. Samborsky, *Liver polyploidy: influence of age and of dietary restriction.* Exp Gerontol, 1983. **18**(1): p. 79-87.
647. Benjamin, G., *On the nature of the function expressive of the law of human mortality, and on a new mode of determining the value of life contingencies. In a letter to Francis Baily, Esq. F. R. S. &cPhil. Trans. .* R. Soc., 1825: p. 115513–583.
648. Makeham, W., *On the Law of Mortality and the Construction of Annuity Tables.* The Assurance Magazine and Journal of the Institute of Actuaries., 1860 p. 301-310.
649. Gavrilov, L.A.G., Natalia S., *The Biology of Life Span: A Quantitative Approach.* New York: Harwood Academic Publisher, 1991.
650. Ruby, J.G., M. Smith, and R. Buffenstein, *Naked Mole-Rat mortality rates defy gompertzian laws by not increasing with age.* Elife, 2018. **7**.